

Activation of White Phosphorus by Molybdenum- and Uranium *tris*-Amides

by

Frances H. Stephens

B.S. Chemistry
University of St. Thomas
St. Paul, MN
1999

Submitted to the Department of Chemistry
On May 21, 2004 in Partial Fulfillment of the [June 2004]
Requirements for the Degree of

DOCTOR OF PHILOSOPHY
in Chemistry
at the
MASSACHUSETTS INSTITUTE OF TECHNOLOGY

© Massachusetts Institute of Technology, MMIV

Signature of Author _____

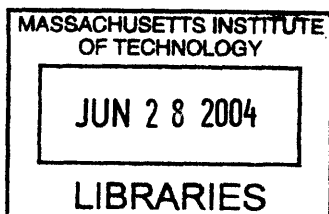
Department of Chemistry
April 20, 2004

Certified by _____

Christopher C. Cummins
Professor of Chemistry
Thesis Supervisor

Accepted by _____

Robert W. Field
Professor of Chemistry
Chairman, Department Committee on Graduate Studies



ARCHIVES

This doctoral thesis has been examined by a Committee of the Department of Chemistry as follows:

Professor Joseph P. Sadighi _____
Professor of Chemistry
Chairman

Professor Christopher C. Cummins _____
Professor of Chemistry
Thesis Supervisor

Professor Richard R. Schrock _____
Professor of Chemistry

for Mom and Dad

Biographical Note

Frances Helen Stephens was born in Fitchburg, Massachusetts on May 1, 1977. On her fourth birthday, she and her parents Ruth and Dennis moved to Niles, Michigan. After a few years in Michigan, and the birth of her younger brother Andrew, the family moved to Circle Pines, Minnesota. Fran completed her secondary schooling in 1995 at Centennial High School as salutatorian. During high school, she was active in many activities including the CHS Speech Team, which she represented at the 1994 and 1995 state tournament in the discussion event. She was an undergraduate at the University of St. Thomas in St. Paul, Minnesota from 1995 to 1999. There she completed several semesters of organic and organometallic research under the guidance of Profs. David C. Boyd and J. Thomas Ippoliti. During her junior year, she chose to study abroad for one semester in Exeter, England. After graduating *summa cum laude* from UST, she began her graduate work at the Massachusetts Institute of Technology under the supervision of Prof. Christopher C. Cummins. After completing her work at MIT in 2004, Fran will be beginning a postdoctoral appointment at Los Alamos National Laboratory in Los Alamos, NM, under the supervision of Dr. R. Thomas Baker where she intends to work on the hydrogenation of B–N unsaturated bonds for hydrogen storage applications.

Table of Contents

Abstract.....	6
Abbreviations used in the text.....	7
Chapter 1: Small-Molecule Activation by Metallaziridine-Hydride Complexes: Mechanistic Sequence of the Small-Molecule Binding and Metallaziridine Ring- Opening Steps.....	9
Chapter 2: Synthesis and Reactivity of a New Terminal Phosphide of Molybdenum Supported by <i>N-iso</i> -Propylanilide Ligands.....	51
Chapter 3: Alcoholysis of Phosphorus-containing Compounds of Mo(N[<i>i</i> -Pr]Ar) ₃	83
Chapter 4: Activation of White Phosphorus by Uranium(III) <i>tris</i> -Amide Complexes.....	112
Appendix 1: Preparation of MoCl ₃ (THF) ₃	127
Appendix 2: X-ray crystallographic data tables.....	128
Appendix 3: Protocol for uranium use in the Cummins group.....	198
Acknowledgements.....	200
<i>Curriculum Vitae</i>	202

Activation of White Phosphorus by Molybdenum- and Uranium *tris*-Amides

by

Frances H. Stephens

Submitted to the Department of Chemistry
May, 2004 in Partial Fulfillment of the
Requirements for the Degree of Doctor of Philosophy in
Chemistry

ABSTRACT

Molybdaziridine-hydride $\text{Mo}(\text{H})(\eta^2\text{-Me}_2\text{C}=\text{NAr})(\text{N}[i\text{-Pr}]\text{Ar})_2$ (**1**, Ar = 3,5- $\text{C}_6\text{H}_3\text{Me}_2$) acts as a source of its three-coordinate isomer $\text{Mo}(\text{N}[i\text{-Pr}]\text{Ar})_3$ (**2**). This relationship has been probed via an investigation of the coordination chemistry of **1** and $\text{Mo}(\text{N}[t\text{-Bu}]\text{Ar})_3$ (**3**), a bulky analog of **2**, with isocyanides RNC (R = 1-adamantyl, *tert*-butyl) and white phosphorus (P_4). A comparison of the rates and activation parameters of these reactions indicates that **2** is not an intermediate on the pathway from **1** to products, but rather than the molybdaziridine-hydride “opens” upon substrate binding in an associative process. Synthesis and characterization of 1:1 and 1:2 isocyanide adducts of **2** and **3**, and bridging and terminal P_n compounds of molybdenum derived from the element P_4 and their alcoholysis products are presented.

The uranium *tris*-amide compounds $(\text{THF})\text{U}(\text{N}[\text{R}]\text{Ar})_3$ (R = *t*-Bu, 1-Ad) reacted with white phosphorus. The unique products contain a square tetraphosphorus moiety characterized formally as the dianion P_4^{2-} . Structural and theoretical analyses are provided for this system.

Thesis Supervisor: Christopher C. Cummins
Title: Professor of Chemistry

Abbreviations Used in the Text

Anal. Calcd.	Calculated elemental analysis values	FTIR	Fourier transform infrared
Å	angstrom (10^{-10} m)	Fc	ferrocene, FeCp_2
A	ampere	fw	formula weight
α	position 1 from the point of connection	F	structure factor
1-Ad	1-adamantyl	g	gram
Ar	3,5-dimethylphenyl	GOF	goodness of fit
Ar ²	2,6-dimethylphenyl	γ	position 3 from the point of connection
atm	atmosphere	h	hours
β	position 2 from the point of connection	η	number of bonds from a metal to a ligand
br	broad	¹ H	proton
CCD	charge coupled devise	² H	deuterium
cm ⁻¹	wavenumber	ΔH^\ddagger	enthalpy of activation
c	concentration	ΔH_{rxn}	enthalpy of reaction
Cp	cyclopentadienyl, $[\text{C}_5\text{H}_5]^-$	Hz	Hertz (s^{-1})
Cp*	pentamethylcyclopentadienyl, $[\text{C}_5\text{Me}_5]^-$	HOMO	highest occupied molecular orbital
12-c-4	12-crown-4 ether	IR	infrared
d	day (24h)	<i>i</i> -Pr	isopropyl
d	doublet	<i>J</i>	coupling constant
d_n	deuterium (n is number of deuteria in molecule)	<i>k</i>	rate constant
D	deuterium	K	degrees in Kelvin
deg	degrees (°)	<i>K</i>	equilibrium constant
δ	delta, chemical shift downfield	L	N[<i>i</i> -Pr]Ar
δ_{iso}	isotropic chemical shift	L ²	N[<i>t</i> -Bu]Ar
equiv	equivalent	λ	wavelength
ϵ	extinction coefficient	LUMO	lowest unoccupied molecular orbital
eu	entropy units, $4.184 \text{ J}\cdot\text{K}^{-1}\cdot\text{mol}^{-1}$	μ_{eff}	effective magnetic moment
		μ_{B}	Bohr magneton

μ	bridging functional group	ppm	parts per million
m	multiplet	ΔS^\ddagger	entropy of activation
M	molarity, mol·L ⁻¹	ΔS_{rxn}	entropy of reaction
Me	methyl, CH ₃	σ	error in bond length or angle
Mes	mesityl, 2,4,6-C ₆ H ₂ Me ₃	s	singlet
min	minute	s	second
mmol	millimole	SOMO	singly occupied molecular orbital
MS	mass spectroscopy	T	temperature
ν	infrared frequency	t	triplet
$\Delta\nu_{1/2}$	peak width at half height	<i>t</i> -Bu	<i>tert</i> -butyl, C(CH ₃) ₃
NMR	nuclear magnetic resonance	THF	tetrahydrofuran, <i>cyclo</i> -O(CH ₂) ₄
Np	neopentyl, CH ₂ C(CH ₃) ₃	UV-Vis	ultraviolet – visible
ORTEP	Oak Ridge Thermal Ellipsoid Plot	V	volts
OTf	triflate, trifluoromethanesulfonate, O ₂ SO ₂ CF ₃	V	volume
Ph	phenyl		

**Small-Molecule Activation by a Molybdaziridine-Hydride Complex:
Mechanistic Sequence of the Small-Molecule Binding and
Molybdaziridine Ring-Opening Steps¹**

Reproduced in part with permission from *Organometallics*, 2004, ASAP.
©2004 American Chemical Society.

Table of Contents

1.1 Introduction.....	11
1.2 Results and Discussion	14
1.2.1 Reaction of Mo(H)(η^2 -Me ₂ C=NAr)(N[<i>i</i> -Pr]Ar) ₂ (1) with <i>N</i> -isopropylidene-3,5-dimethylaniline.....	14
1.2.2 Reaction of Mo(N[<i>t</i> -Bu]Ar) ₃ (3) with bulky isocyanides.....	16
1.2.3 Reaction of Mo(H)(η^2 -Me ₂ C=NAr)(N[<i>i</i> -Pr]Ar) ₂ (1) with bulky isocyanides.....	19
1.3 Stopped-Flow Kinetic Measurements.....	21
1.3.1 Reaction of Mo(N[<i>t</i> -Bu]Ar) ₃ (3) with 1-adamantylisocyanide.....	22
1.3.2 Reaction of Mo(H)(η^2 -Me ₂ C=NAr)(N[<i>i</i> -Pr]Ar) ₂ (1) with 1-adamantylisocyanide.....	24
1.3.3 Reaction between deuterated complex 1-d₃ and AdNC.....	27
1.3.4 Mechanistic considerations.....	27
1.4 Thermochemistry.....	29
1.5 Isocyanide Exchange and Comproportionation Reactions.....	31
1.6 Theoretical Calculations.....	33
1.7 Conclusions.....	37
1.8 Future Directions.....	38
1.9 Experimental Section.....	39
1.9.1 General Considerations: Synthesis and Characterization.....	39
1.9.2 Preparation of Complexes.....	40
1.9.3 Crystallographic Structure Determinations.....	42
1.9.4 General Considerations: Stopped-flow kinetics.....	43
1.9.5 General Considerations: Thermochemistry.....	43
1.9.6 DFT Calculations.....	44
1.10 References.....	45

List of Figures

Figure 1.1: X-ray crystal structure of 2 -(η^2 -imine).	15
Figure 1.2: Reaction of 3 - d_{18} with n equivalents of AdNC ($n = 0, 1, 10$) as monitored by ^2H NMR.	18
Figure 1.3: X-ray crystal structure of 3 - t -BuNC.....	18
Figure 1.4: Reaction of 1 - d_{18} with n equivalents of AdNC ($n = 0, 1, 2, 10$) as monitored by ^2H NMR.	19
Figure 1.5: X-ray crystal structure of 2 -(AdNC) $_2$	21
Figure 1.6: Time-resolved spectral changes and kinetic trace upon mixing 3 and AdNC at $-80\text{ }^\circ\text{C}$	23
Figure 1.7: Dependence of the observed pseudo-first-order rate constant on [AdNC] for the reaction between 3 and AdNC at $-60\text{ }^\circ\text{C}$	24
Figure 1.8: Time-resolved spectral changes and kinetic trace upon mixing 1 and AdNC at $-80\text{ }^\circ\text{C}$	25
Figure 1.9: Dependence of the observed pseudo-first order constants on [AdNC] for the reaction between 1 and AdNC in toluene at different temperatures.....	25
Figure 1.10: Eyring plot for the reactions of 1 and 1 - d_3 with AdNC in toluene.....	26
Figure 1.11: Molecular orbitals of $\text{Mo}(\text{H})(\eta^2\text{-H}_2\text{CNH})(\text{NH}_2)_2$	34
Figure 1.12: Molecular orbitals of $\text{Mo}(\text{NHMe})(\text{NH}_2)_2$	34
Figure 1.13: Calculated molecular orbitals of $\text{Mo}(\text{H})(\eta^2\text{-H}_2\text{C=NH})(\text{NH}_2)_2$ ($\text{Mo}(\text{H})$), $\text{Mo}(\text{NHMe})(\text{NH}_2)_2$ (MoL_3), $(\text{HNC})\text{Mo}(\text{NHMe})(\text{NH}_2)_2$ ($(\text{HNC})\text{MoL}_3$), and $(\text{HNC})_2\text{Mo}(\text{NHMe})(\text{NH}_2)_2$ ($(\text{HNC})_2\text{MoL}_3$). Calculated total bonding energy comparison.....	36
Figure 1.14: Molecular orbitals of $(\eta^1\text{-HNC})\text{Mo}(\text{NHMe})(\text{NH}_2)_2$	34
Figure 1.15: Molecular orbitals of $(\eta^1\text{-HNC})_2\text{Mo}(\text{NHMe})(\text{NH}_2)_2$	35
Figure 1.16: Electrochemical traces of 3 -AdNC, 2 -AdNC, and 2 -(AdNC) $_2$	39

List of Schemes

Scheme 1.1: Insertion or coordination? Reaction of <i>N</i> -Isopropylidene-3,5-dimethylaniline- <i>d</i> ₆ with 1	16
Scheme 1.2: Limiting mechanistic scenarios for reaction of 1 with AdNC	22
Scheme 1.3: Reaction of 3 with AdNC.....	28
Scheme 1.4: Thermochemical cycle for estimation of the enthalpy of oxidative addition of the C–H bond of 2 to form 1	30
Scheme 1.5: Formation of 3-<i>t</i>-BuNC from 3-AdNC via an associative mechanism.....	32
Scheme 1.6: Synthesis of an aminoalkylidyne from 2-AdNC	38

List of Tables

Table 1.1: Selected bond lengths and angles for 2-(η^2-imine)	15
Table 1.2: Selected bond lengths and angles for 3-<i>t</i>-BuNC . Calculated bond lengths and angles for (η^1 -HNC)Mo(NHMe)(NH ₂) ₂ are shown parenthetically.....	18
Table 1.3: Selected bond lengths and angles for 2-(AdNC)₂ . Calculated bond lengths and angles for (η^1 -HNC) ₂ Mo(NHMe)(NH ₂) ₂ are shown parenthetically.....	20
Table 1.4: Activation parameters and reaction enthalpy for reactions of one equivalent of AdNC with 1 and 3	28
Table 1.5: Crystallographic data for 2-(AdNC)₂ , 3-<i>t</i>-BuNC , and 2-(η^2-imine)	42

1.1 Introduction

Elemental nitrogen in the form of N₂ gas is an abundant resource that is currently underutilized in synthesis. In addition to its conversion to ammonia,^{2,3} incorporation of N₂-derived nitrogen atoms into organic molecules is also of interest.^{4,5,6} To this end, we have been developing reactive metal complexes capable of dinitrogen scission according to Equation 1.⁷



Dinitrogen cleavage reactions,⁷⁻⁹ when coupled with N-atom transfer reactivity¹⁰⁻¹⁶ of the product nitrido complexes,^{6,17,18} may yield valuable methods for the synthesis of organonitrogen compounds without requiring the intermediacy of ammonia.

The search for metal complexes capable of effecting the complete six-electron reductive cleavage of N₂ is under way on a variety of fronts.^{5b,7,10} To date, three-coordinate molybdenum(III) complexes such as Mo(N[*t*-Bu]Ar)₃ (**3**, Ar = 3,5-C₆H₃Me₂)⁷ have provided a paradigm for N₂ cleavage (Equation 1) where an open coordination site is available for N₂ binding prior to a bimetallic cleavage process.^{7c} The product nitrido complex N≡Mo(N[*t*-Bu]Ar)₃ (**3-N**) is known from structural studies to be extremely crowded in the vicinity of the molybdenum-nitrogen triple bond,^{*} a circumstance potentially unfavorable with respect to subsequent N-atom transfer processes.

The role of steric and electronic factors in determining reaction chemistry relevant to nitrogen fixation is still evolving.^{5b,19} Recent work by Chirik and coworkers has demonstrated different coordination modes and reactivity when (C₅Me₄R)₂ZrCl₂ (R = H or Me) is treated under nitrogen with sodium amalgam and then with hydrogen.^{20,21} In the case of R = H, a μ²-η²,η²-N₂ complex is formed that reacts at 85 °C with H₂ to generate a zirconium dihydride and ammonia. In contrast, when R = Me, reduction under N₂ of the zirconium dichloride results in a formation of a dimer with a bridging η¹,η¹-N₂ ligand and two terminal η¹-N₂ ligands (one on each Zr).²² This compound does not generate NH₃ when treated with H₂. Apparently, replacement of a single methyl group with a hydrogen on the coordinated Cp* ligand is enough to significantly change the bonding and reactivity picture.

Seeking a sterically less crowded system still capable of dinitrogen scission, we undertook the synthesis of the isopropyl-substituted variant of **3**, Mo(N[*i*-Pr]Ar)₃ (**2**). We found that this system exists not as a three-coordinate molybdenum(III) complex but as the tautomeric molybdaziridine-hydride, Mo(H)(η²-Me₂C=NAr)(N[*i*-Pr]Ar)₂ (**1**).²³ This process is correctly described as either cyclometallation or β-H transfer since the anilide ligand N(*i*-Pr)Ar provides a hydrogen β to the metal. The resultant imine Me₂C=NAr is bound in an η² fashion; at the other extreme of the oxidative addition formalism, this forms a three-membered molybdaziridine ring.²⁴ The molybdaziridine-hydride complex has a single unpaired electron, in contrast to compound **3**, and can be thought of as either Mo(III) or Mo(V) at the two extremes of oxidative addition of the amide ligand. Instead

* The X-ray crystal structure of NMo(N[*t*-Bu]Ph)₃ was determined.⁷

of deactivation due to cyclometallation, the molybdaziridine-hydride complex is active for dinitrogen scission in addition to a host of related small-molecule activation processes.²³⁻²⁶ The molybdaziridine-hydride functional group effectively masks an open coordination site required for small-molecule activation via a reversible cyclometallation process. Small molecule activation by the analogous niobaziridine-hydride $\text{Nb}(\text{H})(\eta^2\text{-}t\text{-Bu}[\text{H}]\text{C}=\text{NAr})(\text{N}[\text{Np}]\text{Ar})_2$ (Np = neopentyl) has also been demonstrated recently.^{27,28}

These and other cyclometallated systems influence both the steric and electronic environment that incoming small molecules encounter.^{21b,23,27a} There are exceedingly few systems where rates of reaction can be compared for both cyclometallated and non-cyclometallated systems for which the crystal structures of both complexes are known. Furthermore, we have recently shown that addition of coordinating bases can serve to accelerate N_2 uptake and cleavage for **1** and **3**.^{7d} NMR data showed evidence for binding of the base to **1** but not to **3** (except in the case of 2,6-dimethylpyrazine), even though an accelerating effect was demonstrated for both. Such results highlight the importance of understanding the mechanism of binding and release of ligands in these complexes. This chapter reports synthetic, kinetic (completed by Drs. Elena Rybak-Akimova and Olga Kryatova at Tufts University), thermodynamic (completed by Dr. Carl Hoff and Eric McDonough at University of Miami), and theoretical investigations aimed at probing differences in rate and energy for binding of isocyanide ligands to **1** and **3**. Fundamental to this quest is a proper description of the sequence of the small-molecule binding and molybdaziridine ring-opening steps in order to determine whether **2** must be generated from **1** as a prerequisite for ligand binding.

1.2 Results and Discussion

1.2.1 Reaction of $\text{Mo}(\text{H})(\eta^2\text{-Me}_2\text{C}=\text{NAr})(\text{N}[i\text{-Pr}]\text{Ar})_2$ (**1**) with *N*-isopropylidene-3,5-dimethylaniline.

Insertion of substrates into the Mo–H bond of molybdaziridine-hydride **1** has never been observed.²⁹ Unsaturated molecules and other substrates that commonly insert into metal-hydride bonds instead appear to coordinate to the 3-coordinate tautomer of **1**, $\text{Mo}(\text{N}[i\text{-Pr}]\text{Ar})_3$ (**2**).²³ For example, benzophenone reacts with **1** to generate the crystallographically characterized $(\eta^2\text{-Ph}_2\text{CO})\text{Mo}(\text{N}[i\text{-Pr}]\text{Ar})_3$ (**2- $\eta^2\text{-OCPh}_2$**).²³ This contrasts with the similar niobaziridine-hydride $\text{Nb}(\text{H})(\eta^2\text{-}t\text{-Bu}[\text{H}]\text{C}=\text{NAr})(\text{N}[\text{Np}]\text{Ar})_2$ for which both coordination and insertion modes of reaction are observed.²⁷ Benzophenone inserts into the Nb–H bond while mesityl nitrile coordinates to form $(\eta^2\text{-MesCN})\text{Nb}(\text{N}[\text{Np}]\text{Ar})_3$.

With the insertable substrate *N*-isopropylidene-3,5-dimethylaniline, it is possible to directly probe this reaction dichotomy. Addition of *N*-isopropylidene-3,5-dimethylaniline- d_6 to molybdaziridine-hydride **1- d_{18}** results in rapid formation of green $(\eta^2\text{-}(\text{D}_3\text{C})_2\text{C}=\text{NAr})\text{Mo}(\text{N}[i\text{-Pr-}d_6]\text{Ar})_3$ (**2- $(\eta^2\text{-imine-}d_{24})$**). This compound crystallizes in the space group $P\bar{1}$, and an X-ray structure determination revealed the expected connectivity (Figure 1.1). It is found that one of the amide ligands (N3) has flipped over

to avoid steric interference with the η^2 -imine moiety. There is an approximate mirror plane passing through the plane containing the imine and the molybdenum; this plane bisects the unique ligand. The dihedral angle defined by the imine and the unique N-C_{aryl} bond is 177.8°. The coordinated imine N-C bond length is 1.376(6) Å, and the C(47)-N(4)-C(41) bond angle is 134.8(4)° (Table 1.1). This N-C bond length is the same (within 3 σ) as that in the naphthyl-1-amide-8- η^2 -imine [η^3 -(Me₂CN)(*i*-PrN)C₁₀H₆]TaCl₂]₂ (1.413(7) Å).^{24g} In contrast with 2-(η^2 -imine), the N-C bond length and C-N-C bond angle of TaCp*Me₂(η^2 -Me₂CNR) (R = 2,6-Me₂C₆H₃) are longer (1.467(7) Å) and more acute (125.8(4)°), respectively.³⁰ This indicates slightly less reduction of the imine in 2-(η^2 -imine) compared to the second example.

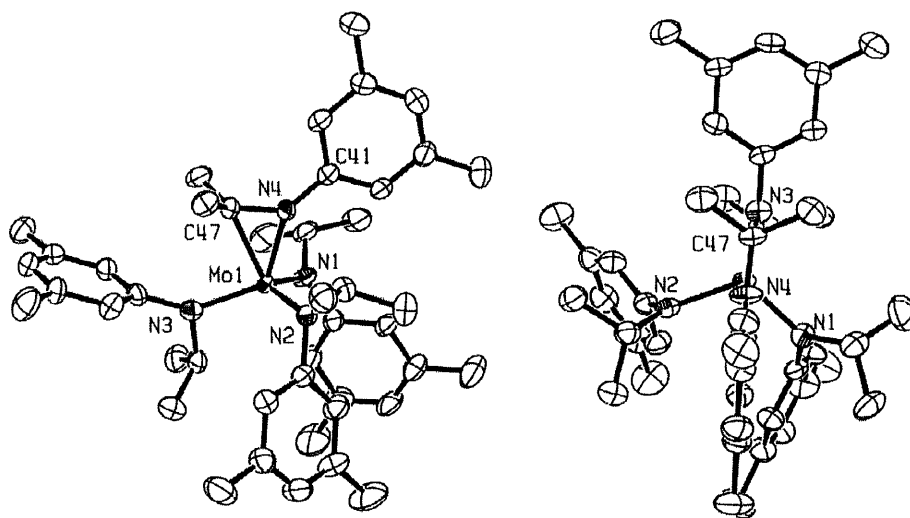


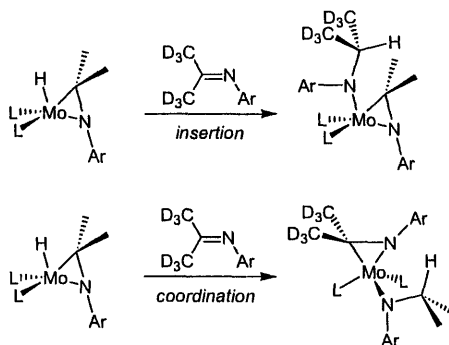
Figure 1.1: X-ray crystal structure of 2-(η^2 -imine). (Left) View showing η^2 coordination of imine. (Right) View showing approximate mirror plane (vertical). Thermal ellipsoids are at the 50% probability level. Hydrogen atoms have been omitted for clarity. Selected bond lengths and angles are listed in Table 1.

<i>Bond Lengths (Å)</i>		<i>Bond Angles (deg)</i>	
Mo-N1	1.973(5)	C47-N4-C41	134.8(4)
Mo-N2	1.961(5)	N4-Mo-N1	91.80(19)
Mo-N3	1.968(5)	N4-Mo-N2	91.3(2)
Mo-N4	1.973(4)	N4-Mo-N3	125.21(18)
Mo-C47	2.187(5)	C47-Mo-N1	113.32(19)
N4-C47	1.376(7)	C47-Mo-N2	107.08(19)
N4-C41	1.370(7)	C47-Mo-N3	87.22(19)

Table 1.1: Selected bond lengths and angles for 2-(η^2 -imine). Calculated bond lengths and angles for (η^1 -HNC)Mo(NHMe)(NH₂)₂ are shown parenthetically.

Because various isotopomers of both **1** and *N*-isopropylidene-3,5-dimethylaniline can be synthesized, ^2H NMR can be used to analyze the paramagnetic product of this reaction (Scheme 1.1), thereby directly probing the insertion *vs.* coordination reaction dichotomy. When d_6 -imine is added to **1**, two scenarios can be envisioned. If insertion occurs, one of the isopropyl groups will consist of an H atom and two CD_3 groups and there will be no deuterons in the imine moiety. In contrast, if the d_6 -imine coordinates there simply will be a η^2 - d_6 -imine and no deuterons in the isopropyl groups of any of the ligands. ^2H NMR can easily distinguish these products. The ^2H NMR shifts of **2**-(η^2 -imine)- d_{24} are $\delta = 2.02$ (*i*-Pr methyl groups) and 1.69 (imine methyl groups) ppm. Analysis of the reaction mixture resulting from addition of $(\text{D}_3\text{C})_2\text{C}=\text{NAr}$ to **1** by ^2H NMR showed only deuteration in the imine portion of the resulting product, **2**-(η^2 -imine)- d_6 , suggesting that no insertion into the Mo–H bond occurs.

Scheme 1.1: *N*-Isopropylidene-3,5-dimethylaniline- d_6 forms an η^2 -imine complex with **2**. This product could be formed via insertion into the Mo–H bond of **1** (deuterium label in amide ligand) or via coordination and metallaziridine ring opening (deuterium label in η^2 -imine).



This reaction was further analyzed by one-electron oxidation of **2**-(η^2 -imine)- d_6 using silver triflate. This results in a diamagnetic, Mo(VI) product that can easily be analyzed by ^1H NMR. If insertion had occurred, one isopropyl group would be composed of a proton (methine position) with two adjacent CD_3 groups. The imine would contain no deuterons, thus the integration of those signals would total six hydrogen atoms. Furthermore, the methine position would be split into 13 lines, as opposed to the septet observed in the fully protio system. In practice, oxidation using silver triflate resulted in formation of orange, diamagnetic [**2**-(η^2 -imine)- d_6][OTf]. No deuteron incorporation into the isopropyl groups was detected by ^1H NMR spectroscopy. Therefore, it can be concluded that insertion is, at least, not a dominant mode of reaction.

1.2.2 Reaction of $\text{Mo}(\text{N}[t\text{-Bu}]\text{Ar})_3$ (**3**) with bulky isocyanides.

On the dinitrogen activation pathway, initial binding of N_2 to molybdenum *tris*-amides⁷ is proposed to happen in an η^1 fashion.^{31,†,‡} In order to probe this step in small

† Most substrates bind η^1 to $\text{Mo}(\text{N}[t\text{-Bu}]\text{Ar})_3$, but dimethylcyanamide is a noteworthy exception.³¹

molecule activation, a simple model substrate was required. 1-Adamantylisocyanide (AdNC), a bulky isocyanide, was selected. Reaction of Mo(N[*t*-Bu]Ar)₃ (**3**) with one or more equivalents of AdNC resulted in rapid formation of a 1:1 adduct (AdNC)Mo(N[*t*-Bu]Ar)₃ (**3-AdNC**). Compound **3-AdNC** is a brown, crystalline solid with a solution magnetic moment $\mu_{\text{eff}} = 1.83 \mu_{\text{B}}$, corresponding to one unpaired electron. This species has a strong infrared CN stretch $\nu_{\text{CN}} = 1762 \text{ cm}^{-1}$. This is similar to Schrock's [N₃N]Mo(CN[*t*-Bu]) ([N₃N]³⁻ = [(Me₃SiNCH₂CH₂)₃N]³⁻), which has an IR band $\nu_{\text{CN}} = 1838 \text{ cm}^{-1}$.³² The strong two-electron π -back bond from the π -basic molybdenum to the isocyanide LUMO results in a reduction of the C–N bond order, explaining the lower energy IR band compared to free AdNC (2130 cm^{-1}).

Binding of a second equivalent of AdNC to **3** was not observed even in the presence of excess isocyanide. ²H NMR was used to monitor the production of paramagnetic products in the reaction of Mo(N[*t*-Bu-*d*₆]Ar)₃ (**3-*d*₁₈**)⁷ with *n* equivalents of AdNC (*n* = 0, 1, 10) in C₆H₆ (Figure 1.2). Unreacted **3-*d*₁₈** has a ²H NMR resonance at $\delta = 65 \text{ ppm}$ (Figure 1.2, bottom; addition of 0 equiv AdNC). When one equivalent of AdNC was added to **3-*d*₁₈**, one new product is formed with a ²H NMR resonance at $\delta = 9.9 \text{ ppm}$ (Figure 1.2, middle). Subsequent addition of an excess of AdNC resulted in no further change of the ²H NMR spectrum (Figure 1.2, top). That only one equivalent of this bulky ligand binds to **3** is consistent with previously published results.^{7c,d}

Reaction of **3** with *tert*-butylisocyanide (*t*-BuNC) led to products analogous to those formed in the AdNC system. X-ray structure determination of (*t*-BuNC)Mo(N[*t*-Bu]Ar)₃ (**3-*t*-BuNC**) (Figure 1.3) revealed a bent conformation of the isocyanide ligand with a C₄₁–N₄–C₄₂ angle of 137.8(7)° (Table 1.2). This C–N–C bond angle is similar to that in (*t*-BuNC)Re[N(CH₂CH₂S)₃] (154.0(10)°)^{33,34} and (*t*-BuCN)W[N₃N_F] ([N₃N_F]³⁻ = [(C₆F₅NCH₂CH₂)₃N]³⁻; 132.2(10)°).³² Deviations from linearity are generally attributed to the degree of backbonding from metal to isocyanide ligand. Backbonding in the *d*³ system **3-*t*-BuNC** is such that the plane perpendicular to the C₄₁–N₄–C₄₂ plane is expected to contain a back bond, while the unpaired electron resides in a molybdenum *d*-orbital lying in the C₄₁–N₄–C₄₂ plane.³⁵ This backbond is reflected in ν_{CN} for **3-*t*-BuNC** (1759 cm^{-1}), at much lower frequency than free *t*-BuNC (2145 cm^{-1}). Furthermore, the Mo–C distance 1.936(6) Å is in the range of a Mo–C double bond.³⁶ The coordinated isocyanide C_α–N distance is 1.184(8) Å.^{§,37} Compound **3-*t*-BuNC** is quite thermally stable, but it began to slowly decompose via *tert*-butyl radical ejection from both the isocyanide moiety and one N[*t*-Bu]Ar ligand at temperatures above 80 °C. This radical ejection resulted in formation of a mixture of (NC)Mo(N[*t*-Bu]Ar)₃³⁸ and (*t*-BuNC)Mo(NAr)(N[*t*-Bu]Ar)₂, respectively.³⁹

† For examples of η^2 bound substrates on the Mo(N[*i*-Pr]Ar)₃ fragment.^{23,26a}

§ Free *t*-BuNC has a NC bond length of between 1.166 and 1.184 Å.³⁷

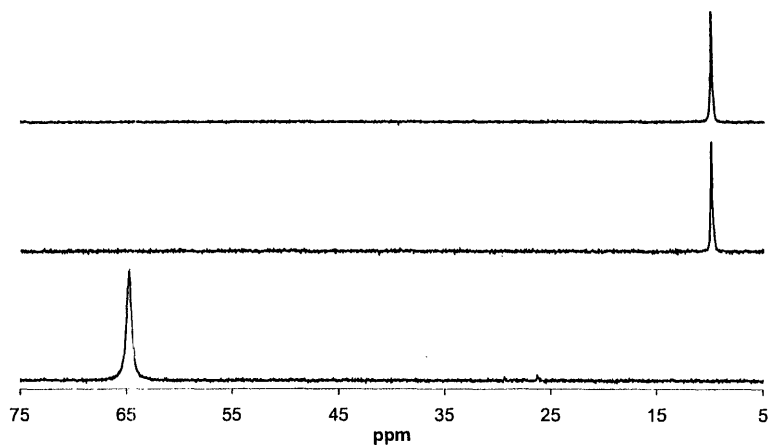


Figure 1.2: Reaction of 3- d_{18} with n equivalents of AdNC ($n = 0, 1, 10$; bottom to top) as monitored by ^2H NMR. Peak at $\delta = 9.9$ ppm ($\nu_{1/2} = 12.8$ Hz) is assigned to 3-AdNC- d_{18} ; peak at $\delta = 65$ ppm is assigned to 3- d_{18} . Compound 3-(AdNC) $_2$ was not observed.

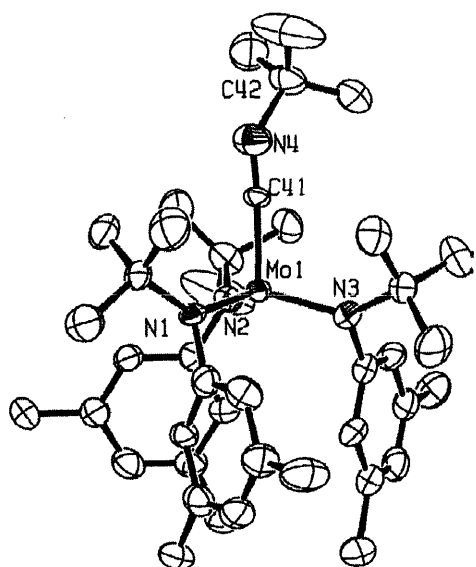


Figure 1.3: X-ray crystal structure of 3- t -BuNC. Thermal ellipsoids are at the 50% probability level. Hydrogen atoms have been omitted for clarity. Selected bond lengths and angles are listed in Table 2.

<i>Bond Lengths (Å)</i>	
Mo(1)-C(41)	1.936(6) (1.918)
Mo(1)-N(1)	1.972(5) (1.975)
Mo(1)-N(2)	1.981(5) (1.959)
Mo(1)-N(3)	1.967(5) (1.941)
C(41)-N(4)	1.184(8) (1.228)
N(4)-C(42)	1.495(9)
<i>Bond Angles (deg)</i>	
C(41)-Mo(1)-N(1)	99.9(2)
C(41)-Mo(1)-N(2)	99.6(2)
C(41)-Mo(1)-N(3)	104.4(2)
Mo(1)-C(41)-N(4)	174.2(5) (169.06)
C(41)-N(4)-C(42)	137.8(7) (136.36)

Table 1.2: Selected bond lengths and angles for 3- t -BuNC. Calculated bond lengths and angles for $(\eta^1\text{-HNC})\text{Mo}(\text{NHMe})(\text{NH}_2)_2$ are shown parenthetically.

1.2.3 Reaction of Mo(H)(η^2 -Me₂C=NAr)(N[*i*-Pr]Ar)₂ (**1**) with bulky isocyanides.

Reaction of Mo(H)(η^2 -Me₂C=NAr)(N[*i*-Pr]Ar)₂ (**1**) with 1 equiv AdNC results in rapid, irreversible formation of a 1:1 adduct, (AdNC)Mo(N[*i*-Pr]Ar)₃ (**2-AdNC**). This compound is a brown, oily solid with an solution infrared band $\nu_{\text{CN}} = 1718 \text{ cm}^{-1}$. This strong IR band is at lower frequency than that observed for **3-AdNC** (*vide supra*), consistent with a more significant backbonding interaction in the less-sterically crowded complex.^{**},⁴⁰

In contrast to **3**, compound **1** is capable of binding a second equivalent of AdNC. Reaction of the deuterated variant Mo(H)(η^2 -(CD₃)₂C=NAr)(N[*i*-Pr-*d*₆]Ar)₂ (**1-*d*₁₈**)⁷ with *n* equivalents (*n* = 0, 1, 2, 10) of AdNC in C₆D₆ was monitored by ²H NMR spectroscopy. After addition of slightly more than one equivalent of AdNC, the broad spectrum of **1-*d*₁₈** (Figure 1.4, bottom) sharpened to a peak at $\delta = 6.2 \text{ ppm}$ ($\Delta\nu_{1/2} = 12.0 \text{ Hz}$). This peak was assigned to **2-AdNC-*d*₁₈**. A small peak began to appear at $\delta = 3.5 \text{ ppm}$ ($\Delta\nu_{1/2} = 11.5 \text{ Hz}$), attributable to (AdNC)₂Mo(N[*i*-Pr]Ar)₃ (**2-(AdNC)₂-*d*₁₈**). This peak continued to grow in upon addition of a second equivalent of AdNC where it reached a maximum. Addition of more than two equivalents of AdNC resulted in no further reaction (Figure 1.4, top). Formation of this 2:1 adduct was anticipated based on previously published results.^{23,31}

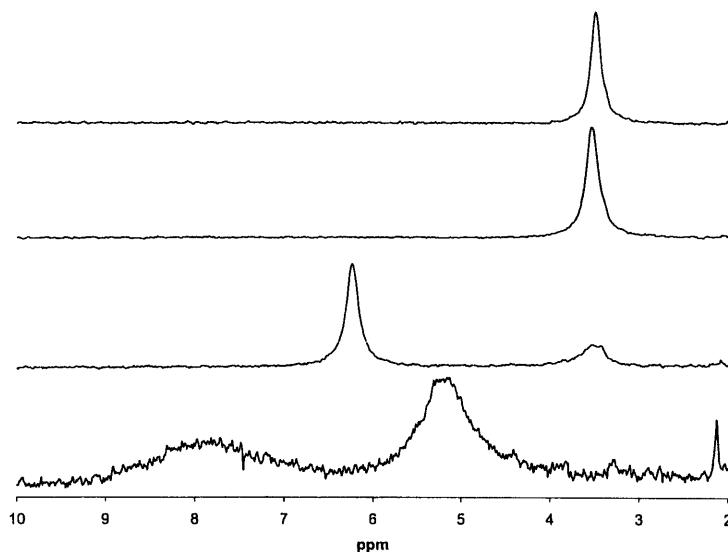


Figure 1.4: Reaction of **1-*d*₁₈** with *n* equivalents of AdNC (*n* = 0, 1, 2, 10; bottom to top) as monitored by ²H NMR. The peak at $\delta = 6.2 \text{ ppm}$ ($\Delta\nu_{1/2} = 12.0 \text{ Hz}$) can be assigned to **2-AdNC-*d*₁₈**; at $\delta = 3.5 \text{ ppm}$ ($\Delta\nu_{1/2} = 11.5 \text{ Hz}$) to **2-(AdNC)₂-*d*₁₈**.

^{**} Compound **3** is electronically very similar to **2**, as can be seen by a comparison of the CO stretching frequencies in compounds **2-CO** (1827 cm^{-1})²⁵ and **3-CO** (1840 cm^{-1}).⁴⁰ Small differences in the IR stretching frequencies may be due to steric differences at the reaction site between the two compounds.

Compound **2**-(AdNC)₂ is a purple, crystalline solid with an infrared band at 2035 cm⁻¹. This agrees well with literature compounds displaying *trans* disposed isocyanide ligands. For example, *trans*-(dppe)₂Mo(CNPh)(CN[*t*-Bu]) exhibits an infrared band at 2010 cm⁻¹ corresponding to the CN stretch of the *tert*-butylisocyanide ligand.⁴¹ The solution magnetic moment (μ_{eff}) of **2**-(AdNC)₂ is 1.76 μ_{B} , corresponding to one unpaired electron. When the second equivalent of isocyanide coordinates, it interacts with the *d*_z² orbital, raising that orbital's energy and accounting for the presence of only one unpaired electron. The other two filled *d* orbitals (*xz* and *yz*) in this adduct participate in a three-center-two-electron bonding interaction, delocalized over Mo, C, and N in a backbonding fashion. When **2**-AdNC was heated at 65 °C for 24 h no substantive change was observed by ¹H NMR spectroscopy. However, heating of **2**-(AdNC)₂ under the same conditions resulted in formation of **2**-AdNC as observed by ¹H NMR spectroscopy with a concomitant color change from purple to brown. These spectral changes imply that the second equivalent of AdNC is more weakly bound than the first. Indeed, a color change from purple to brown and the UV-Vis and FTIR spectral changes can also be observed when dilute solutions of **2**-(AdNC)₂ are prepared (*vide infra*).

An X-ray diffraction study revealed the solid state structure of **2**-(AdNC)₂ (Figure 1.5). The isocyanide ligands adopt a *trans* disposition, and the core geometry is approximately trigonal bipyramidal. The N(*i*-Pr)Ar ligands are arranged in a pseudo-C_s configuration, thus optimizing lone pair donation from two of the amide ligands. The AdNC ligands are close to linear (C–N–C: 173.9(11), 167.1(11)°), implying a reduction in the degree of backbonding compared to **3**-*t*-BuNC. The distances between the molybdenum atom and the coordinated isocyanide ligands' carbons are 2.135(11) and 2.083(11) Å. This is similar to previously reported molybdenum-isocyanide single bond lengths.^{32,41} Furthermore, this Mo–C distance is longer by 0.17 Å than the analogous bond length in **3**-*t*-BuNC, indication a reduction of Mo–C multiple bonding character. The carbon-nitrogen bond lengths of the coordinated isocyanides are 1.153(12) and 1.153(13) Å, which are the same as the C–N distance^{††} in free aliphatic isocyanides within experimental error.^{8,42}

Table 1.3: Selected bond lengths and angles for **2**-(AdNC)₂. Calculated bond lengths and angles for (η¹-HNC)₂Mo(NHMe)(NH₂)₂ are shown parenthetically.

Bond Lengths (Å)		Bond Angles (deg)			
Mo1-N1	2.112(8) (1.988)	N1-Mo1-C41	82.7(3)	Mo1-C41-N4	175.9(9) (171.43)
Mo1-N2	1.983(8) (1.984)	N2-Mo1-C41	90.7(4)	C41-N4-C42	173.9(11)
Mo1-N3	1.990(8) (1.987)	N3-Mo1-C41	91.6(4)	Mo1-C51-N5	176.7(10) (175.36)
Mo1-C41	2.135(11) (2.079)	N1-Mo1-C51	90.7(4)	C51-N5-C52	167.1(11)
Mo1-C51	2.083(11) (2.050)	N2-Mo1-C51	94.7(4)	C51-Mo1-C41	172.8(4) (178.10)
C41-N4	1.153(12) (1.201)	N3-Mo1-C51	90.8(4)		
C51-N5	1.153(13) (1.209)				

^{††} Free MeNC has a NC bond length of 1.167 Å as determined by microwave absorption spectroscopy.⁴²

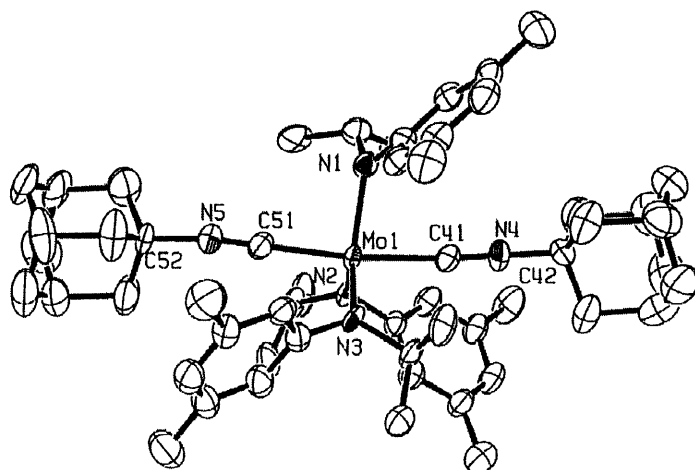


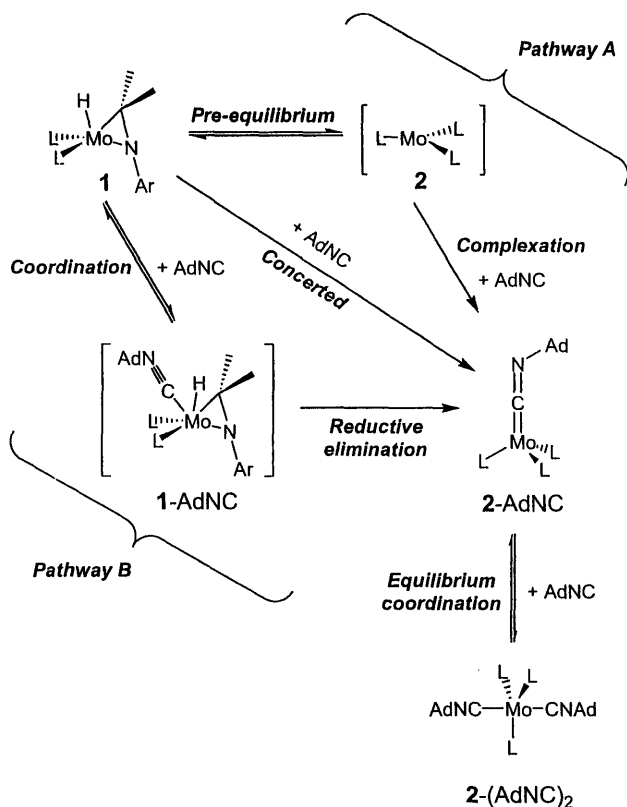
Figure 1.5: X-ray crystal structure of 2-(AdNC)₂. Thermal ellipsoids are at the 50% probability level. Hydrogen atoms and a co-crystallized molecule of *n*-pentane have been omitted for clarity.

1.3 Stopped-Flow Kinetic Measurements

In collaboration with Drs. Elena Rybak-Akimova and Olga Kryatova at Tufts University, stopped-flow UV-Vis spectrometry was utilized to distinguish between the possible mechanistic pathways available for small molecule activation by **1** and **3**. There are several possibilities available for reaction of **1** with AdNC, including a pre-equilibrium pathway (Scheme 1.2, Pathway A), an associative pathway (Scheme 1.2, Pathway B), and a concerted pathway. The pre-equilibrium pathway would proceed with initial formation of **2** from **1** (such that a small population of **2** is present in solution), followed by complexation of AdNC. In contrast, the associative pathway would require initial coordination of AdNC by **1**, with subsequent reductive elimination of the Mo–H bond. Finally, the concerted pathway would involve simultaneous coordination and reductive elimination, perhaps proceeding via an agostic transition state. An additional complexity is that 2-AdNC rapidly and reversibly binds a second equivalent of AdNC forming 2-AdNC₂ as discussed above.

The simpler of the two systems to study is the reaction of **3** with AdNC since no gross ligand rearrangements are expected. This hypothesis is supported by structural studies of **3**⁷ and small molecule activation products of **3** (including 3-*t*-BuNC, *vide supra*),^{7,31,40,43} where the amide ligands maintain their integrity. However a spin change occurs during the reaction from high spin (**3**, three unpaired electrons) to low spin (3-AdNC, one unpaired electron).⁴⁴ In contrast, reaction of **1** (one unpaired electron) must occur with reversible β-H elimination at some time along the reaction coordinate, but does not necessarily require a spin-state change. Outlined herein is a strategy to probe the mechanism by which molybdaziridine-hydride **1** permits access to the *tris*-amide Mo(III) complex **2**. In this strategy, the 1-to-2 dichotomy is investigated by comparison to three-coordinate Mo(N[*t*-Bu]Ar)₃ (**3**), which has no β-hydrogen atoms to eliminate.

Scheme 1.2: Limiting mechanistic scenarios for reaction of $\text{Mo}(\text{H})(\eta^2\text{-Me}_2\text{C}=\text{NAr})(\text{N}[i\text{-Pr}]\text{Ar})_2$ (**1**) with AdNC; L = N[*i*-Pr]Ar.



Reactions between coordinatively unsaturated compounds **1** and **3** with AdNC proved to be rapid (color changes were immediately observed upon mixing the metal species with isocyanide solutions), therefore reaction rates were studied by the stopped-flow method with spectrophotometric registration. The spectral changes observed in the stopped-flow experiments were identical to the spectral changes for these systems observed in quartz cells with a conventional spectrophotometer. In most cases, the reactions at room temperature were too rapid even for the stopped-flow methodology, and accurate measurements of the reaction rates were only possible at low temperature.

1.3.1 Reaction of $\text{Mo}(\text{N}[t\text{-Bu}]\text{Ar})_3$ (**3**) with 1-adamantylisocyanide.

This reaction was studied by rapid scanning spectrometry in toluene solution over the temperature range -80 to 25 °C using a broad concentration range of isocyanide (0.3 – 8 mM). A single process was observed under all studied conditions (Figure 1.6), accompanied by growth of an absorption band with $\lambda_{\text{max}} = 445$ nm ($\epsilon = 5800 \text{ M}^{-1}\text{cm}^{-1}$). These spectral changes are consistent with formation of a 1:1 adduct between **3** and AdNC.

The system containing equal concentrations of **3** and AdNC gave kinetic traces that were fitted to a second order kinetic equation (with mean standard deviation within 3%) (Figure 1.6, inset). In a separate series of experiments, a 10-fold excess of AdNC was used, and kinetic traces (more than 5 half-lives) were fitted with a first-order kinetic equation, suggesting that the reaction is first-order in **3**. Indeed, varying the concentration of **3** while keeping the concentration of AdNC constant yielded identical values of pseudo-first-order rate constant k_{obs} , confirming that k_{obs} is independent of the concentration of **3**, and the reaction rate depends on the first power of [**3**]. A plot of the k_{obs} vs. the initial concentration of AdNC is a straight line with an intercept near zero (Figure 1.7), indicating that the reaction is practically irreversible and is first order in AdNC. Consequently, the reaction between **3** and AdNC is a second-order process (first order in each reactant) in the broad temperature range from $-80\text{ }^{\circ}\text{C}$ to $25\text{ }^{\circ}\text{C}$ (Equation 2).



The rate constants measured at different temperatures under otherwise identical conditions gave linear Arrhenius and Eyring plots.¹ The values of activation parameters calculated from the data obtained under second-order conditions (equal concentrations of both reactants) and pseudo-first order conditions (10 fold excess of AdNC) are in a good agreement: $\Delta H^{\ddagger} = 5.5 \pm 0.5\text{ kcal}\cdot\text{mol}^{-1}$, $\Delta S^{\ddagger} = -15 \pm 4\text{ eu}$. In summary, the formation of a monoadduct of **3** with AdNC was found to be a rapid, low barrier, second order reaction (first order in both reagents).

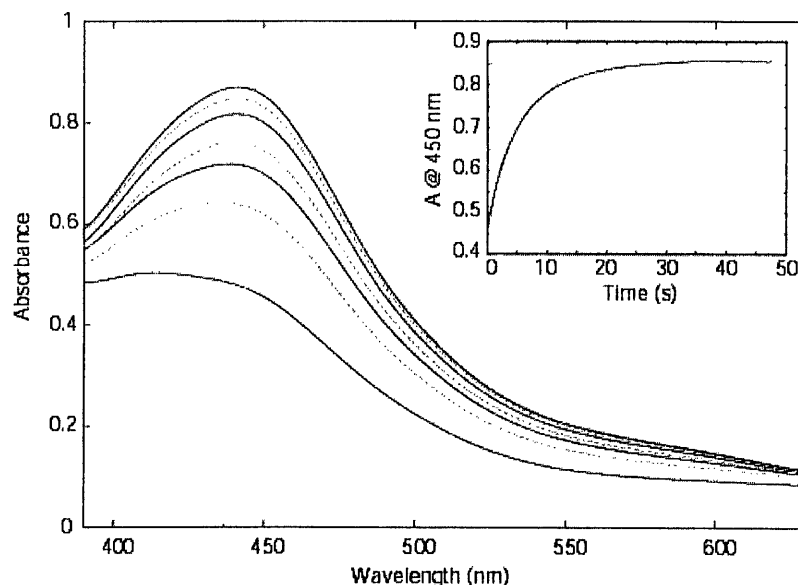


Figure 1.6: Time-resolved (2.5 s intervals) spectral changes and kinetic trace upon mixing 0.3 mM toluene solutions of **3** and AdNC in a 1:1 ratio at $-80\text{ }^{\circ}\text{C}$ observed by stopped-flow spectrophotometry.

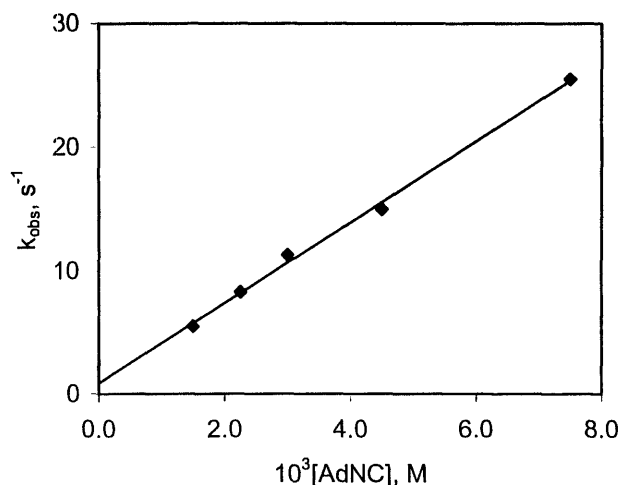


Figure 1.7: Dependence of the observed pseudo-first-order rate constant on [AdNC] for the reaction between $\text{Mo}(\text{N}[\textit{t}\text{-Bu}]\text{Ar})_3$ (**3**) and AdNC in toluene at $-60\text{ }^\circ\text{C}$. The initial concentration of **3** was 0.15 mM (after mixing). A least-squares fit of the data gives an intercept of 0.86 s^{-1} and a slope (corresponding to a second-order rate constant) of $3270\text{ M}^{-1}\text{s}^{-1}$ with $R^2 = 0.997$.

1.3.2 Reaction of $\text{Mo}(\text{H})(\text{Me}_2\text{C}=\text{NAr})(\text{N}[\textit{i}\text{-Pr}]\text{Ar})_2$ (**1**) with 1-adamantylisocyanide.

The reaction between **1** and AdNC is more complex than the analogous reaction with **3**. The observed spectral changes depended upon the concentration of AdNC and on temperature. At low temperature ($-80\text{ }^\circ\text{C}$), an intense absorption band with $\lambda_{\text{max}} = 524\text{ nm}$ ($\epsilon = 6600\text{ M}^{-1}\text{cm}^{-1}$) and a shoulder at *ca.* 575 nm ($\epsilon = 5100\text{ M}^{-1}\text{cm}^{-1}$) appeared (Figure 1.8). This spectrum is substantially different from the spectrum of **3**-AdNC, where a single maximum at 445 nm was observed (Figure 1.6). Stopped-flow “titration” of **1** with AdNC at $-40\text{ }^\circ\text{C}$ showed that absorbance from 525 to 575 nm doubles upon increasing the **1**:AdNC ratio from $1:1$ to $1:2$, and remains unchanged (within experimental error) upon further increase in concentration of AdNC. This result allowed us to estimate the stoichiometry of AdNC addition to **1** and indicated that a *bis*-adduct **2**- $(\text{AdNC})_2$ formed at low temperatures ($-80\text{ }^\circ\text{C}$ to $-20\text{ }^\circ\text{C}$) and/or high concentration of isocyanide. Spectral differences observed at various temperatures for the toluene solution containing 0.15 mM of **1** and 0.3 mM of AdNC suggested reversibility of binding of the second molecule of AdNC to **1**.

The equilibrium of AdNC binding to **1** in toluene was further characterized by conventional, room temperature, spectrophotometric titrations, which showed complete formation of a $1:1$ adduct followed by reversible addition of a second AdNC (Scheme 1.2). The K_{assoc} for the first, nearly irreversible process could be estimated as $K_1 > 3 \times 10^6\text{ M}^{-1}$. The equilibrium constant for the second, reversible coordination was calculated: $K_2 = 4.5 \times 10^3\text{ M}^{-1}$. In concentrated solutions (*ca.* 0.1 M), stoichiometric AdNC (2 equiv) is sufficient for quantitative formation of **2**- $(\text{AdNC})_2$.

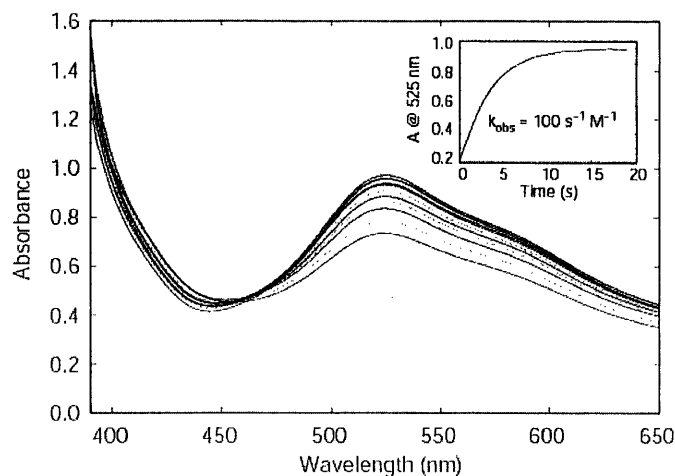


Figure 1.8: Time-resolved (2.5 s intervals) spectral changes and a kinetic trace obtained upon mixing toluene solutions of **1** (0.3 mM) and AdNC (3 mM) in a 1:1 ratio in the stopped-flow apparatus at $-80\text{ }^{\circ}\text{C}$.

Even though the reaction between **1** and AdNC involves two processes, the observed kinetics is fairly similar to the simple 1:1 adduct formation described above for **3**-AdNC. Formation of the adduct from **1** and a 10-fold excess of AdNC can be clearly seen as a pseudo-first order process in the spectral window from 500 to 575 nm (Figure 1.8, inset; small absorbance changes below 500 nm gave rise to noisy kinetic traces).

The adduct formation rate increased substantially with an increase in AdNC concentration. At low temperature ($-80\text{ }^{\circ}\text{C}$ or $-40\text{ }^{\circ}\text{C}$) the plot of the pseudo-first-order rate constant, k_{obs} , vs. the initial concentration of AdNC is a straight line with a small intercept (0.014 at $-80\text{ }^{\circ}\text{C}$ ($\sim 1.5\%$ of rate scale); -0.086 at $-40\text{ }^{\circ}\text{C}$ ($\sim 1\%$ of rate scale)). Similar results were obtained at $24\text{ }^{\circ}\text{C}$ in single-wavelength ($\lambda = 550\text{ nm}$) experiments.¹ These experiments confirmed that the rate limiting step is nearly irreversible and first order in AdNC.

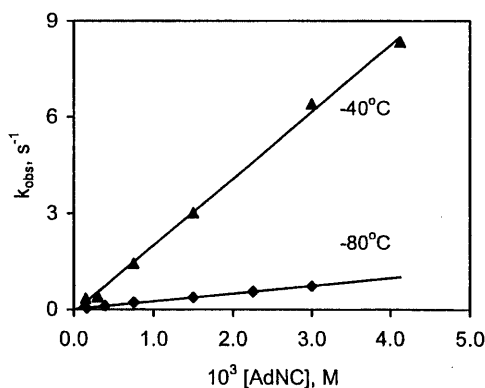


Figure 1.9: Dependence of the observed pseudo-first order constants on $[\text{AdNC}]$ for the reaction between $\text{Mo(H)(Me}_2\text{C=NAr)(N}[i\text{-Pr]Ar)}_2$ (**1**) and AdNC in toluene at different temperatures. In all cases the initial concentration of **1** was 0.15 mM (after mixing). A least-squares fit of the data generated the following intercepts and slopes (corresponding to a second-order rate constant): At $-80\text{ }^{\circ}\text{C}$: 0.014, $240\text{ M}^{-1}\text{s}^{-1}$, $R^2 = 0.998$; At $-40\text{ }^{\circ}\text{C}$: -0.086 , $2080\text{ M}^{-1}\text{s}^{-1}$, $R^2 = 0.998$.

The order in **1** was determined based on results of the dependence of observed pseudo-first order rate constants from concentration of **1** under pseudo-first-order conditions (excess AdNC). The observed pseudo-first order rate constants did not depend on the concentration of **1**. The kinetic data suggest a second-order rate law for the rate-limiting step of the reaction (Equation 3).

$$v = k_{\text{obs}}[\mathbf{1}] = k[\mathbf{1}][\text{AdNC}] \quad (3)$$

The observed rate constants increased with temperature, yielding linear Arrhenius and Eyring plots. The measurements were performed using various concentrations: a 1:1 molar ratio of **1** to AdNC (second-order conditions), and a large excess of AdNC (pseudo-first-order conditions). Virtually identical values for the activation parameters were obtained under all conditions studied: $\Delta H^\ddagger = 4.5 \pm 0.5 \text{ kcal}\cdot\text{mol}^{-1}$, $\Delta S^\ddagger = -24 \pm 4 \text{ eu}$.

The kinetic data, taken together, indicate that the binding of the first equivalent of AdNC (*Concerted* reaction, Scheme 1.2) is the rate-limiting step with the binding of the second equivalent (*Equilibrium coordination*) being faster. The rate-limiting step, an addition of the first AdNC ligand to **1**, is practically irreversible, as evidenced by a zero intercept of the plots of k_{obs} vs. [AdNC]. The rate law and the kinetic parameters (second-order rate constants and activation enthalpies and entropies) do not depend on the stoichiometry of the reaction mixture, also suggesting that the rate-limiting step does not change upon increase in AdNC concentration. The spectral changes, however, are consistent with a *bis*-adduct formation at high concentrations of AdNC. This observation agrees with the observed kinetics if the addition of a second monodentate ligand is a rapid process.

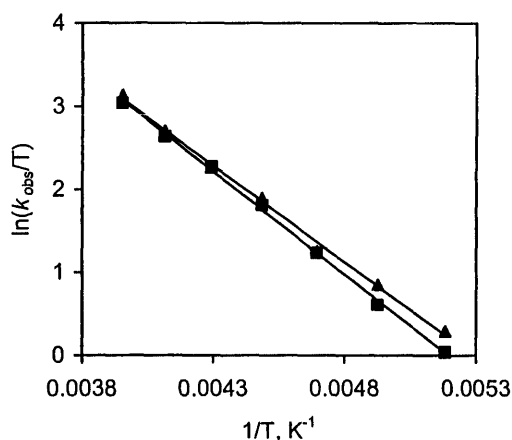


Figure 1.10: Eyring plot for the reaction of $\text{Mo}(\text{H})(\text{Me}_2\text{C}=\text{NAr})(\text{N}[i\text{-Pr}]\text{Ar})_2$ (**1**) (squares) and $\text{Mo}(\text{D})(\text{Me}_2\text{C}=\text{NAr})(\text{N}[i\text{-Pr-}d_1]\text{Ar})_2$ (**1-d₃**) (triangles) with AdNC in toluene. The data were obtained under pseudo-first-order conditions: $c(\mathbf{1}, \mathbf{1-d}_3) = 0.15 \text{ mM}$, $c(\text{AdNC}) = 1.5 \text{ mM}$. Activation parameters for Mo(H) ($\Delta H^\ddagger = +4.5 \pm 0.5 \text{ kcal}\cdot\text{mol}^{-1}$, $\Delta S^\ddagger = -24 \pm 4 \text{ eu}$) agree within experimental error with those for Mo(D) ($\Delta H^\ddagger = 4.6 \pm 0.5 \text{ kcal}\cdot\text{mol}^{-1}$, $\Delta S^\ddagger = -23 \pm 4 \text{ eu}$).

1.3.3 Reaction between deuterated complex 1-*d*₃ and AdNC.

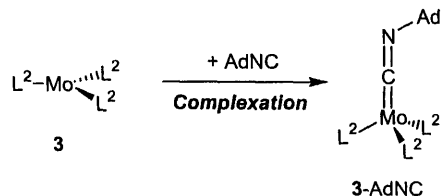
Use of 1-*d*₃, where deuterium atoms have been incorporated into the methine position of the ligand *iso*-propyl group, has allowed us to probe the existence of a kinetic isotope effect. If Mo–H(D) bond breaking were the rate-limiting step in isocyanide coordination, then a primary kinetic isotope effect would be expected when 1-*d*₃ is utilized. The reaction between 1-*d*₃ and excess AdNC was studied by rapid scanning stopped-flow spectrophotometry as a function of temperature (from –80 to 20 °C). The spectral changes observed were identical to those observed previously for the reaction between **1** and AdNC. The rates of the reactions of AdNC with **1** and 1-*d*₃ at the same temperatures were nearly identical (deviations within 8%), and Eyring plots yielded very similar values for the activation parameters (Figure 1.10). Therefore, there is no detectable isotope effect in this system.

1.3.4 Mechanistic considerations.

The major reaction pathways for adding one molecule of AdNC to **1** are depicted in Scheme 2. For complex **3** bearing *tert*-butyl alkyl substituents, molybdaziridine-hydride cannot form, and the reaction scheme simplifies to the reaction depicted in Scheme 1.3. The experimentally observed second-order rate law and activation parameters for this reaction ($\Delta H^\ddagger = 5.5 \pm 0.5 \text{ kcal}\cdot\text{mol}^{-1}$, $\Delta S^\ddagger = -15 \pm 4 \text{ eu}$) are consistent with a bimolecular transition state involving a simple associative addition at a crowded center. These data provide a basis for comparison to the reaction of **1** with AdNC.

For complex **1**, the addition of one molecule of AdNC could occur, as discussed above (Scheme 1.2, Pathway A), by initial rate determining conversion to **2**. The second order rate law dependence on incoming AdNC rules out that possibility. A more plausible scenario would be a rapid pre-equilibrium between **1** and **2** (*Pre-equilibrium*, K_{eq}) followed by slower trapping of **2** by AdNC (*Complexation*, k_3). However, three additional pieces of evidence argue against Pathway A. First, previously reported ²H NMR studies²³ demonstrated that high temperatures (*ca.* 70 °C) were necessary for coalescence of deuterium atoms bound to Mo and those on the isopropyl groups of the amides (methine position). Rapid equilibration at the low temperatures utilized in the stopped flow experiments therefore seems unlikely. Furthermore, such an equilibrium would be expected to display an inverse equilibrium isotope effect,⁴⁵ where the 1-*d*₃ reacted at a faster rate than **1**. However, rates of reaction and activation parameters are identical within experimental error.

Scheme 1.3: Reaction of $\text{Mo}(\text{N}[t\text{-Bu}]\text{Ar})_3$ (**3**) with AdNC; $\text{L}^2 = \text{N}[t\text{-Bu}]\text{Ar}$.



Finally, if rapid pre-equilibrium kinetics were followed, the derived rate law would resemble that shown in Equation 4:

$$v = k_{\text{obs(A)}}[\mathbf{1}][\text{AdNC}], \quad k_{\text{obs(A)}} = K_{\text{eq}}k_3, \quad \Delta H_{\text{obs(A)}}^\ddagger = \Delta H_{\text{eq}}^\circ + \Delta H_3^\ddagger \quad (4)$$

The observed enthalpy of activation would be a sum of the reaction enthalpies for the molybdaziridine-hydride rearrangement ($\Delta H_{\text{eq}}^\circ$) and an activation enthalpy of AdNC addition to the three-coordinate complex **2** (ΔH_3^\ddagger). Comparative activation parameters as well as enthalpies of reaction for reaction of **1** and **3** with AdNC are summarized in Table 1.4. Thermochemical data and theoretical calculations (*vide infra*) indicate that ($\Delta H_{\text{eq}}^\circ$) is expected to be on the order of $5 \text{ kcal}\cdot\text{mol}^{-1}$ for this reaction. This implies a value for ΔH_3^\ddagger near zero, which is not reasonable.

Based on these observations we find no evidence that reaction of **1** with AdNC proceeds via complex **2** as shown in Pathway A of Scheme 1.2, and it can be concluded that reaction occurs via the associative Pathway B. This pathway yields the observed second-order rate law (i.e., for the rate-limiting *Coordination* step, Equation 5).

$$k_{\text{obs(B)}} = k_4, \quad \Delta H_{\text{obs(B)}}^\ddagger = \Delta H_4^\ddagger \quad (5)$$

The lack of kinetic isotope effect and the values of activation and thermodynamic parameters also favor pathway B.^{††}

	1 + AdNC	3 + AdNC
ΔH^\ddagger (kcal·mol ⁻¹)	4.5 ± 0.5	5.5 ± 0.5
ΔS^\ddagger (eu)	-24 ± 4	-15 ± 4
ΔH_{rxn} (kcal·mol ⁻¹)	-24.6 ± 0.5	-29.1 ± 0.5

Table 1.4: Activation parameters and reaction enthalpy for reactions of one equivalent of AdNC with molybdaziridine-hydride (**1**, Scheme 1.2) and $\text{Mo}(\text{N}[t\text{-Bu}]\text{Ar})_3$ (**3**, Scheme 1.3).

^{††} We cannot unambiguously distinguish between the A mechanism (that involves a six-coordinate intermediate) and the I_a (associative interchange) mechanism that proceeds through a six-coordinate transition state.

When comparing the activation parameters in Table 1.4, it can be seen that the reaction of AdNC with **1** has a significantly more negative entropy of activation than does the analogous reaction with **3**. This is consistent with a more precise orientation of the incoming monodentate ligand for its coordination at the sixth available site in molybdaziridine-hydride **1**. The enthalpies of activation are comparable, with that of **3** slightly more negative than that of **1**.

Even though the reactions between **1** or **3** with AdNC are complete within seconds, and their second-order rate constants are high (1.2×10^4 and $3 \times 10^5 \text{ M}^{-1}\text{s}^{-1}$, respectively, at 25 °C), these processes are several orders of magnitude slower than the diffusion limit. In contrast, reactions at sterically unhindered coordination sites that do not require steric or electronic reorganization are much faster. For example, a rate constant of $10^{13} \text{ M}^{-1}\text{s}^{-1}$ was reported for CO addition to $\text{Cr}(\text{CO})_5$ in the gas phase,⁴⁶ and the rate constant for CO addition to $[\text{IrCl}(\text{PPh}_3)_2]$ at room temperature was found to be $2.7 \times 10^8 \text{ M}^{-1}\text{s}^{-1}$ in benzene solution at room temperature.⁴⁷ Similarly, the rate constants for small molecule binding to vacant coordination sites in hemoproteins and their models approach the diffusion limit and often equal to $10^8 - 10^9 \text{ M}^{-1}\text{s}^{-1}$.⁴⁸⁻⁵⁰

1.4 Thermochemistry

In collaboration with Dr. Carl Hoff and Eric McDonough at University of Miami, a thermochemical investigation of the systems outlined herein was completed. The enthalpies of binding of the first mole of AdNC to **1** and to **3** (with all species in toluene solution) are $\Delta H = -24.6 \pm 0.5 \text{ kcal}\cdot\text{mol}^{-1}$ and $\Delta H = -29.1 \pm 0.4 \text{ kcal}\cdot\text{mol}^{-1}$, respectively (Table 1.4), as determined by solution calorimetry. These values correspond to the formal definition of the molybdenum-isocyanide bond strengths for the two complexes. Differences in the enthalpies of binding of AdNC can be used to derive an estimate for the enthalpy of the **2** to **1** tautomerization. The enthalpy of transfer of the isocyanide ligand from **2**-AdNC to **3**, generating **3**-AdNC and **1**, is shown at the bottom of Scheme 1.4 and is calculated from direct measurements (from solid AdNC) to be $-4.5 \pm 0.3 \text{ kcal}\cdot\text{mol}^{-1}$.⁵¹ This will equal the sum of the three steps in the upper cycle of Scheme 4: $\text{BDE}_{2\text{-AdNC}} + \Delta H_{2 \rightarrow 1} - \text{BDE}_{3\text{-AdNC}} = -4.5 \text{ kcal}\cdot\text{mol}^{-1}$ (BDE = bond dissociation energy). Provided $\text{BDE}_{2\text{-AdNC}}$ is approximately equal to $\text{BDE}_{3\text{-AdNC}}$, these two terms cancel and it is reasonable to assign $\Delta H = -4.5 \text{ kcal}\cdot\text{mol}^{-1}$ to the **2** to **1** tautomerization.

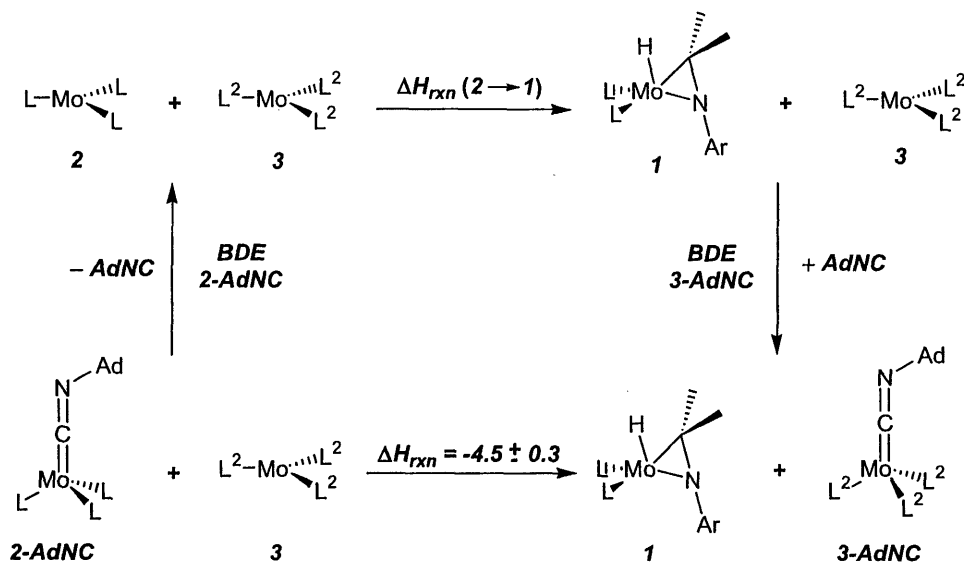
It is possible that oxidative addition of the anilide ligand $\text{N}[i\text{-Pr}]\text{Ar}$ may be slightly more exothermic than this first estimate. The lower CN stretching frequency of **2**-AdNC ($\nu_{\text{CN}} = 1718 \text{ cm}^{-1}$) compared to **3**-AdNC ($\nu_{\text{CN}} = 1762 \text{ cm}^{-1}$) appears to indicate (presumably for steric reasons) that the **2**-AdNC bonding interaction may be slightly stronger than that in **3**-AdNC. There is no simple correlation between this vibration and the relative AdNC–Mo bond strengths; however it is reasonable to conclude that **2** to **1** tautomerization is exothermic by $5 \pm 2 \text{ kcal}\cdot\text{mol}^{-1}$.

That molybdaziridine-hydride **1** is thermodynamically downhill from its tautomer **2** supports kinetic studies preferring Pathway B over A in Scheme 1.2. The observed

activation energy of 4.5 ± 0.4 mol in Table 4 overlaps within experimental error the 5 ± 2 kcal·mol⁻¹ derived ground state enthalpy difference for **1** → **2**. If the reaction proceeded via Pathway A, it would therefore require no barrier to oxidative addition of the C–H bond and no barrier to addition of AdNC to **2**. Neither of these is reasonable and all data (kinetic as well as thermodynamic) support Pathway B of Scheme 1.2.

That **2** is not observed at room temperature²³ is consistent with the value of -5 ± 2 kcal·mol⁻¹ for $\Delta H_{2 \rightarrow 1}$. The exothermic nature of this cyclometallation is in accord with an unfavorable entropic component due to restricted rotation in the molybdaziridine-hydride. Recent theoretical work by Milstein and coworkers⁵² on cycloaddition reactions of C–H and C–C bonds has indicated unfavorable $-T\Delta S$ terms on the order of 2 kcal·mol⁻¹ that must be overcome for cycloadditions. A room temperature estimate of $\Delta G_{1 \rightarrow 2} = 3$ kcal·mol⁻¹ is consistent with the failure to observe **2** directly and with the aforementioned observation of high temperature coalescence in NMR studies.²³ On the other hand if the intramolecular oxidative addition were more exothermic than 5 kcal·mol⁻¹, oxidative addition of external H–H or C–H bonds might be expected to occur if steric factors did not preclude this. Activation of hydrocarbons, for example, does not occur. Therefore, the estimate of the oxidative addition appears reasonable in terms of these observations.

Scheme 1.4: Thermochemical cycle for estimation of the enthalpy of oxidative addition of the C–H bond of **2** to form **1**; L = N[*i*-Pr]Ar, L² = N[*t*-Bu]Ar.



In contrast to rapid and irreversible binding of the first mole of AdNC to **1**, the second mole of AdNC adds rapidly but the reaction is reversible. Direct measurement of the enthalpy of binding of AdNC to **2-AdNC** yielded $\Delta H = -10.3 \pm 0.5$ kcal·mol⁻¹ in toluene solution. In spite of this relatively low value, FTIR data¹ indicate that, at room

temperature and 0.1 to 0.001 M concentration range, there is little dissociation of 2-(AdNC)₂ to 2-AdNC and AdNC. It is estimated based on these data that, at room temperature, K_{eq} for binding of AdNC to 2-AdNC is greater than 5×10^3 , in reasonable agreement with UV-Vis estimates discussed earlier. These data imply that the unfavorable $T\Delta S$ of binding of the second mole of AdNC is at least $-5.3 \text{ kcal}\cdot\text{mol}^{-1}$ at room temperature. This value is not as large as values typically observed for ligand binding reactions ($-10 \text{ kcal}\cdot\text{mol}^{-1}$). This may be due to a more disordered structure of the *bis* adduct 2-(AdNC)₂ compared to the mono adduct 2-AdNC. The low value for the second enthalpy of binding of AdNC to **1** also explains the failure of **3** to bind a second mole of AdNC even in the presence of 10-fold excess. The binding of the second mole of isocyanide occurs not only with increased steric pressure at the binding site, but with a concomitant reduction in the Mo-CNAd bond order of the trans isocyanide.

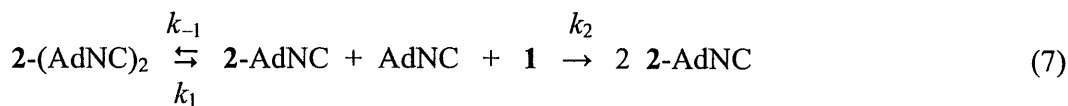
1.5 Isocyanide Exchange and Comproportionation Reactions

The enthalpic preference of *ca.* $5 \text{ kcal}\cdot\text{mol}^{-1}$ for binding of AdNC to **3** compared to **1** prompted investigation of the exchange reaction (Equation 6):



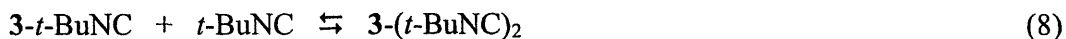
While it was anticipated that the reaction shown in Equation 6 would proceed as shown, the reverse reaction was also attempted. Reactions monitored after several days at room temperature showed no sign of exchange in either direction.¹ Since kinetic data showed that trapping of AdNC by **3** is faster than trapping by **1**, it can be concluded that dissociation of isocyanides from the 1:1 adducts occurs at a negligible rate at room temperature.

In contrast, dissociation of AdNC from the *bis* adduct 2-(AdNC)₂ occurs at a much faster rate. The enthalpy of binding of a second mole of AdNC to 2-AdNC is *ca.* $15 \text{ kcal}\cdot\text{mol}^{-1}$ lower than the first mole, thus, the rate increase can be anticipated. Stopped flow kinetic studies¹ of the comproportionation reaction between 2-AdNC₂ and **1** are interpreted in terms of the mechanism in Equation 7, which is a combination of Pathway B and the *equilibrium coordination* reaction (Scheme 1.2).



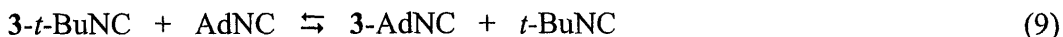
This reaction is rapid at room temperature, and its rate constants (k_1 , k_{-1} , and k_2) could not be unequivocally resolved even at low temperature. Nevertheless, the following semiquantitative observations could be made: (1) Temperature dependence studies revealed an overall enthalpy of activation of *ca.* $9 \text{ kcal}\cdot\text{mol}^{-1}$ indicating that dissociation of AdNC from 2-(AdNC)₂ plays a key role in the mechanism; (2) The rate of binding of AdNC, surprisingly, was roughly equivalent for **1** and for 2-AdNC (i.e. $k_2 \approx k_1$).

The observation of near-quantitative binding of the second mole of AdNC to 2-AdNC at low temperatures led to attempts to determine whether 3-*t*-BuNC would add a second equivalent of isocyanide at low temperature in concentrated solution:



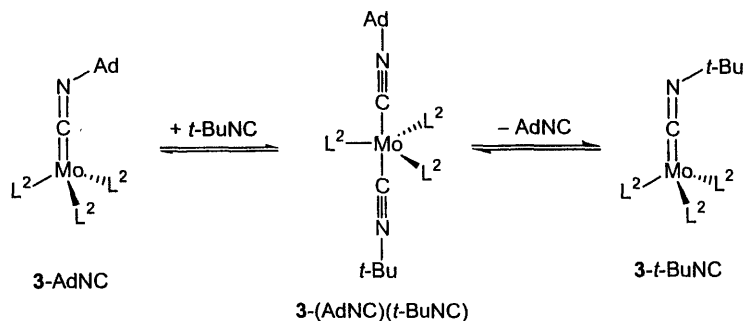
However, even when 3 was dissolved in 3M *t*-BuNC in toluene at *ca.* $-50\text{ }^\circ\text{C}$, no formation of a 2:1 adduct was observed by FT-IR spectroscopy. Isocyanide exchange reactions are observed for 3-AdNC and 3-*t*-BuNC (*vide infra*), and this must be due to thermodynamic instability of the *bis* adduct of 3. Spectroscopic data allow the conservative estimate that K_{eq} for Equation 8 is less than 0.033 M^{-1} at 293 K. The analogous binding of AdNC by 2-AdNC has a K_{eq} of $4,500\text{ M}^{-1}$. The difference in binding constants of five orders of magnitude for the second mole of isocyanide corresponds at room temperature to a free energy difference of $\geq 6\text{ kcal}\cdot\text{mol}^{-1}$. This is a reasonable lower bound for the “steric pressure” that would be generated if the ligands’ isopropyl groups are replaced by *tert*-butyl groups.

In spite of thermodynamic instability, there is kinetic evidence that suggests 3-(AdNC)(*t*-BuNC) is a viable intermediate in isocyanide exchange. Small differences in the FTIR band shapes of 3-AdNC and 3-*t*-BuNC and the free isocyanides AdNC and *t*-BuNC allowed study of the equilibrium reaction shown in Equation 9:



At room temperature and in dilute solution, this equilibrium is established within minutes. The equilibrium constant is approximately 1, and the reaction can be approached from either side.¹ Because bound isocyanide dissociates very slowly from 3-AdNC and 3-*t*-BuNC (*vide supra*), a dissociative exchange mechanism can be excluded and we assume a mechanism similar to that shown in Scheme 1.5.

Scheme 1.5: Formation of 3-*t*-BuNC from 3-AdNC via an associative mechanism.



Quantitative kinetic study of this reaction was not made, but it is several orders of magnitude slower than any of the steps in the comproportionation reaction mechanism shown in Equation 7. The much slower rate of the reaction (Equation 9) is primarily attributed to slower uptake of a second isocyanide to form the five-coordinate

intermediate **3**-(AdNC)(*t*-BuNC), which is estimated to be at least 6 kcal·mol⁻¹ less stable than **2**-(AdNC)₂. This result indicates a reason for the rare observation of η^2 or *bis* compounds of **3**,^{7d,31} implicated in base-catalyzed N₂ cleavage by **1** and **3**.

1.6 Theoretical Calculations

Density functional theory calculations have been effectively used to elucidate bonding in a variety of molybdenum *tris*-amide complexes.^{23,25,31,40,53} Relatively large N(*t*-Bu)Ar ligands were effectively approximated by the much smaller NHMe and NH₂ ligands, and the bulky 1-adamantyl group was simplified to H. Therefore, we investigated computationally the compounds Mo(NHMe)(NH₂)₂, Mo(H)(η^2 -H₂C=NH)(NH₂)₂, (η^1 -HNC)Mo(NH₂)₃, and (η^1 -HNC)₂Mo(NH₂)₃. The spin-unrestricted, all-electron calculations focused on obtaining good agreement between calculated and experimental geometries, and on an investigation of the molecular orbitals and their relative energies with specific concern paid to the spin states of the fragments. Binding of AdNC to **2** or **3** involves spin change from a quartet to a doublet ground electronic state.⁵⁴⁻⁵⁶ In contrast, binding of AdNC to **1** does not involve spin change since both reactant and product have been shown to have doublet ground states. However the latter reaction involves, at some point, conversion of the molybdaziridine hydride form (**1**) to the *tris*-amide form (**2**).

Geometry optimization of the tautomers Mo(H)(η^2 -H₂C=NH)(NH₂)₂ and Mo(NHMe)(NH₂)₂ revealed structural parameters that agree well with X-ray crystallographically determined structures of **1**⁷ and **3**.²³ For molybdaziridine-hydride, the experimentally (theoretically) determined parameters are as follows: Mo–H, 1.69(5) (1.675); Mo–C(imine), 2.18(2) (2.153); Mo–N(imine), 1.93(2) (2.009); Mo–N(amide), 1.93(2) (1.947) and 2.02(2) (1.951) Å. Similarly, for the *tris*-amide species Mo(NHMe)(NH₂)₂, the experimentally (theoretically) determined parameters are as follows: Mo–N(unique), 1.960(7) (1.965); Mo–N, 1.964(7) (1.976) and 1.977(7) (1.978) Å. An orbital energy level diagram is shown in Figure 1.15. For the molybdaziridine-hydride model (Figure 1.15, far left), the three highest energy occupied orbitals are the unpaired electron (SOMO) and the backbond from the metal to the η^2 -imine functionality (HOMO–1, HOMO–2). In three-coordinate Mo(NHMe)(NH₂)₂, the highest-occupied molecular orbitals are three singly occupied d orbitals (d_{xz} , d_{yz} , and d_{z^2}). The HOMO-LUMO gap in the former compound is slightly smaller than that in the latter, but the overall bonding energies indicate that Mo(H)(η^2 -H₂C=NH)(NH₂)₂ is about 1 ± 2 kcal·mol⁻¹ more stable than Mo(NHMe)(NH₂)₂ (Figure 1.15, bottom). This value indicates that the two species are almost isoenergetic. Consequently, the opening of the molybdaziridine-hydride should be a relatively low-energy process, in agreement with experimental results (*vide supra*).

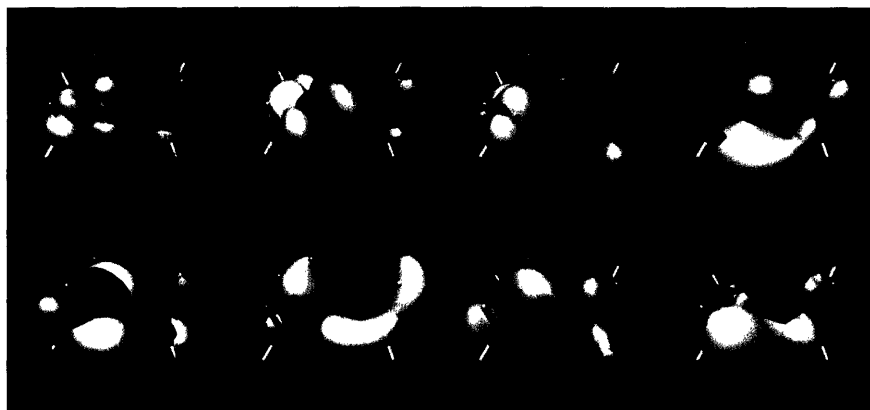


Figure 1.11: One-electron molecular orbitals of $\text{Mo}(\text{H})(\eta^2\text{-H}_2\text{CNH})(\text{NH}_2)_2$. Top, left to right: LUMO+3, LUMO+2, LUMO+1, LUMO. Bottom, left to right: HOMO, HOMO-1, HOMO-2, HOMO-3.

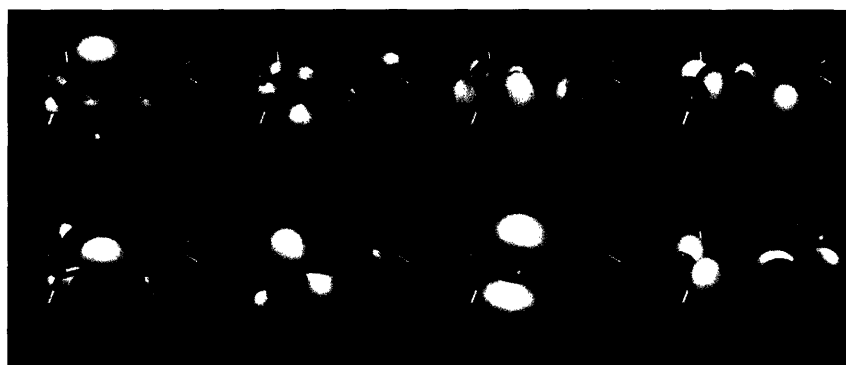


Figure 1.12: One-electron molecular orbitals of $\text{Mo}(\text{NHMe})(\text{NH}_2)_2$. Top, left to right: LUMO+3, LUMO+2, LUMO+1, LUMO. Bottom, left to right: HOMO, HOMO-1, HOMO-2, HOMO-3.



Figure 1.13: One-electron molecular orbitals of $(\eta^1\text{-HNC})\text{Mo}(\text{NHMe})(\text{NH}_2)_2$. Top, left to right: LUMO+3, LUMO+2, LUMO+1, LUMO. Bottom, left to right: HOMO, HOMO-1, HOMO-2, HOMO-3.



Figure 1.14: One-electron molecular orbitals of $(\eta^1\text{-HNC})_2\text{Mo}(\text{NHMe})(\text{NH}_2)_2$. Top, left to right: LUMO+3, LUMO+2, LUMO+1, LUMO. Bottom, left to right: HOMO, HOMO-1, HOMO-4, HOMO-5.

Utilizing the same amido ligand set as discussed above, geometry optimization of $(\eta^1\text{-HNC})\text{Mo}(\text{NHMe})(\text{NH}_2)_2$ was carried out with no symmetry constraints. The Mo–C distance was computed to be 1.918 Å, just slightly longer than a typical Mo–C double bond distance (*ca.* 1.88 Å) in Schrock-type carbene complexes of molybdenum.^{36,57} The calculated value is slightly shorter than the experimentally determined value for the Mo–C distance in 3-*t*-BuNC, 1.936(6) Å (Figure 1.3). This is likely due to the steric constraints imposed by the N(*t*-Bu)Ar ligands in the synthetic system compared to the reduced steric bulk of NH₂ ligands in the computational system. Approximate C–N double bond character is indicated by the bend C–N–H bond angle of 139° (experimental, 137.8(7)°), as well as by the C–N distance of 1.223 Å (experimental, 1.184(8) Å). Subsequently, a spin unrestricted calculation was carried out on the d^1 complex and the orbitals were examined. The conformation of the three amide ligands in the complex is such that two of the lone pairs are directed perpendicular to the Mo–C vector, while one is parallel. That the computed structure corresponds to a minimum on the potential energy surface was confirmed via a frequencies calculation; there were no imaginary frequencies and the most intense vibrational band (ν_{CN}) was predicted to occur at 1802 cm⁻¹. This value agrees well with the experimental values reported above for 2-AdNC (1718 cm⁻¹), 3-AdNC (1762 cm⁻¹), and the *t*-BuNC analogs.

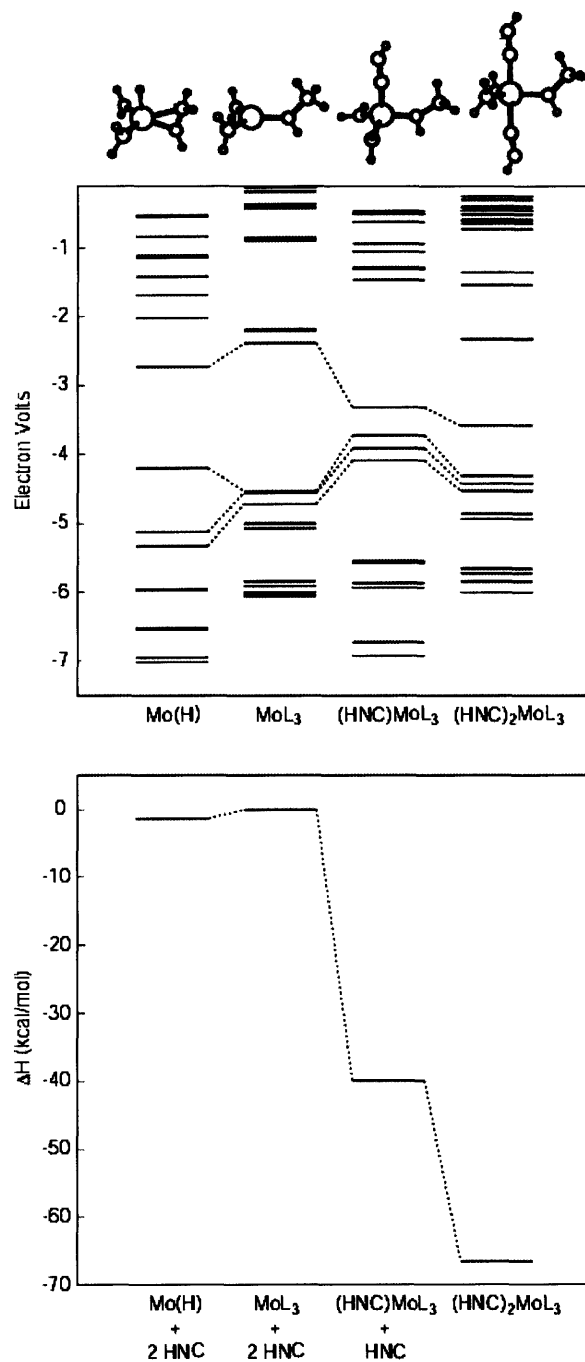


Figure 1.15: (Top) Calculated molecular orbitals of Mo(H)(η^2 -H₂C=NH)(NH₂)₂ (Mo(H)), Mo(NHMe)(NH₂)₂ (MoL₃), (HNC)Mo(NHMe)(NH₂)₂ ((HNC)MoL₃), and (HNC)₂Mo(NHMe)(NH₂)₂ ((HNC)₂MoL₃). Dashed lines connect the LUMOs (top) and the three highest occupied molecular orbitals. (Bottom) Calculated total bonding energy comparison. Each energy level depicts a system with the same formula.

The unpaired electron of $(\eta^1\text{-HNC})\text{Mo}(\text{NHMe})(\text{NH}_2)_2$ lies in the same plane as the nitrogen lone pair p orbital on the unique amide ligand (Figure 1.13). The unpaired electron is, therefore, antibonding with respect to the lone pair of electrons on the unique amide ligand. At the same time, it is weakly back-bonding with respect to the isocyanide LUMO. A two-electron back bond is in place involving the other two formal d electrons and the second component of the isocyanide LUMO. The two-electron back bond is at lower energy than the one-electron back bond because it experiences minimal repulsive effects from amide lone pairs.

Geometry optimization with no symmetry constraints and a spin-unrestricted calculation were completed on $(\eta^1\text{-HNC})_2\text{Mo}(\text{NHMe})(\text{NH}_2)_2$ (Figure 1.14). The calculated bond distances agreed well with the experimentally determined distances (Figure 1.5). For example, the Mo–C distances were computed to be 2.079 and 2.050 Å, while the distances from the X-ray crystal structure are 2.135(11) and 2.083(11) Å. Like in the previously discussed 1:1 adduct, the HOMO represents a backbond to the isocyanide ligands.

1.7 Conclusions

Thermochemical cycles, together with DFT calculations, suggest that tautomerization of molybdaziridine-hydride **1** to three-coordinate $\text{Mo}(\text{N}[i\text{-Pr}]\text{Ar})_3$ (**2**) is identified with a small reaction enthalpy of *ca.* +5 kcal·mol⁻¹. Nonetheless, failure to observe a kinetic isotope effect (either primary or inverse) in reaction of molybdaziridine-deuteride **1-*d*₃** with AdNC, the rate law, and the activation parameters all support associative attack of AdNC on **1** rather than any requirement of prior conversion to **2**.

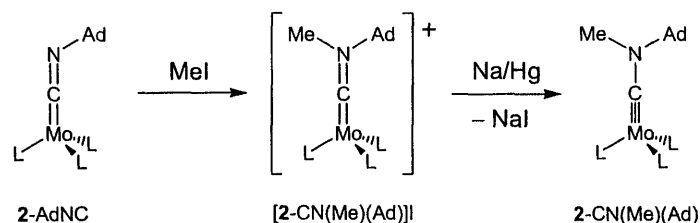
The important role that ancillary ligands can play in determining reactivity was also demonstrated in the fact that **1** reversibly binds a second equivalent of isocyanide whereas **3** could not be observed to do so even in concentrated solution at low temperature. The crystal structures of **3-*t*-BuNC** and **1-(AdNC)₂** reported here, as well as data on enthalpy and entropy of binding of the second mole of AdNC provide a good entry to further understanding of ligand binding in these sterically congested but low-coordinate systems.

Isolable coordinatively unsaturated metal complexes such as **3** have afforded remarkable new small-molecule transformations.^{7,8,10,23,25-†,58} Comparative reactivity and mechanistic studies are making increasingly clear the fact that coordinative unsaturation in a starting metal complex is *not* an absolute requirement for the type of small molecule activation processes exemplified by dinitrogen binding and subsequent scission. On the contrary, reversible intramolecular elements of stabilization, from agostic stabilization⁵⁹ to near-thermoneutral cyclometalation as seen here,⁶⁰ may be employed as design elements in the synthesis of new reactive motifs.²⁷

1.8 Future Directions

As was discovered by Tsai, et al., Mo(VI) alkyldynes supported by *N*-*iso*-propylanilido ligands are valuable precursors to alkyne metathesis catalysts via alcoholysis.²⁶ These alkyldynes are synthesized in several steps. First, trimethylsilylacetylene is added to **1**, to which it coordinates in an η^2 fashion. This is followed by oxidation using iodine, deprotonation using [Li][BHEt₃], and thermolysis at 80 °C for 12 h. A potentially more rapid synthetic route to Mo(VI) alkyldynes supported by *N*-*iso*-propylanilido ligands may be found in this isocyanide chemistry. Initial results indicate that isocyanide adduct **2-AdNC** may be a precursor to desirable aminocarbynes^{61–64} comparable to those molecules mentioned above. Aminoalkyldynes have also been documented to intermolecularly couple to form 1,2-diaminoalkynes, to insert alkynes, and to act as sources of amine.⁶¹

Scheme 1.6: Synthesis of an aminoalkylidyne from 2-AdNC.



This chemistry was hinted at by the electrochemistry of 2-AdNC, 3-AdNC, and 2-(AdNC)₂. Adduct 3-AdNC displayed a quasireversible reduction wave at -1.90 V and a quasireversible oxidation wave at -0.82 V. The electrochemical analysis of the less bulky *iso*-propyl system is not as straightforward due to the significant equilibrium formation of 2-AdNC from 2-(AdNC)₂. However, what can be seen is an easily chemically accessible reduction wave. Accordingly, the 1:1 adduct 2-AdNC is susceptible to reduction via sodium amalgam to form a monoanion [Na(THF)_x][AdN-C≡Mo(N[*i*-Pr]Ar)₃]. This orange-red compound crystallizes from cold diethyl ether. Neutral aminoalkyldynes can also be achieved in a “reverse” method. *N*-Adamantyl-*N*-methylaminomethylidyne is synthesized via addition of methyl iodide to 2-AdNC followed by reduction (Scheme 1.6).

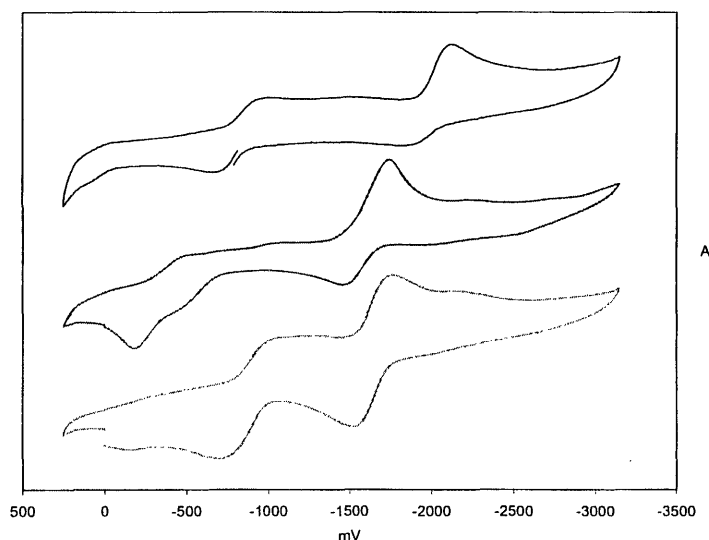


Figure 1.16: Electrochemical traces of 3-AdNC (top), 2-AdNC (middle), and 2-(AdNC)₂ (bottom).

1.9 Experimental Section

1.9.1 General Considerations: Synthesis and Characterization.

Unless stated otherwise, all operations were performed in a Vacuum Atmospheres drybox under an atmosphere of purified nitrogen or using Schlenk techniques under an argon atmosphere. Diethyl ether, toluene, benzene, pentane, and *n*-hexane were dried and deoxygenated by the method of Grubbs.⁶⁵ THF was distilled under nitrogen from purple sodium benzophenone ketyl. Benzene-*d*₆ was purchased from Cambridge Isotope Laboratory, was degassed, and was dried over 4 Å sieves. Alumina, Celite, and 4 Å sieves were dried in vacuo overnight at a temperature above 200 °C. Mo(H)(η²-Me₂C=NAr)(N[*i*-Pr]Ar)₂,²³ Mo(D)(η²-Me₂C=NAr)(N[*i*-Pr-*d*₁]Ar)₂,²³ Mo(H)(η²-(CD₃)₂C=NAr)(N[*i*-Pr-*d*₆]Ar)₂,²³ Mo(N[*t*-Bu]Ar)₃,^{7,§§} Mo(N[*t*-Bu-*d*₆]Ar)₃,⁷ and 1-adamantylisocyanide⁶⁶ were synthesized according to literature procedures. MoCl₃(THF)₃ was synthesized by a newly modified procedure (see Appendix 1). 1-Adamantylisocyanide was sublimed before use. Other chemicals were used as received. Solution infrared spectra were recorded on a Perkin-Elmer 1600 Series FTIR using KBr plates. ¹H and ¹³C NMR spectra were recorded on Varian XL-300, Varian Mercury-300, or Varian INOVA-501 spectrometers at room temperature. Chemical shifts are reported with respect to internal residual benzene (7.15 and 128.38 (t) ppm). C, H, and N analyses were performed by H. Kolbe Mikroanalytisches Laboratorium (Mülheim, Germany).

§§ *N-tert*-Butyl-3,5-dimethylaniline was synthesized via an improved procedure.³¹

1.9.2 Preparation of Complexes

Synthesis of $(\eta^2\text{-}(\text{D}_3\text{C})_2\text{C}=\text{NAr})\text{Mo}(\text{N}[i\text{-Pr-}d_6]\text{Ar})_3$ (2- $(\eta^2\text{-imine-}d_{24})$). To an orange-brown solution of $\text{Mo}(\text{H})(\eta^2\text{-Me}_2\text{C}=\text{NAr})(\text{N}[i\text{-Pr-}d_6]\text{Ar})_3$ (1.262 g, 2.10 mmol) in 6 mL diethyl ether were added 2 mL of a colorless solution of imine $(\text{D}_3\text{C})_2\text{C}=\text{NAr}$ (0.345 g, 2.14 mmol, 1 equiv). Upon mixing, the solution became blue. After stirring for 1 h, the solvent was removed *in vacuo*. The residue was extracted with pentane and the product recrystallized at $-35\text{ }^\circ\text{C}$ (0.718 g, 0.935 mmol, 44.5 %). ^1H NMR (500 MHz, C_6D_6): $\delta = 7.79$ ($\Delta\nu_{1/2} = 1100$ Hz), 4.918 ($\Delta\nu_{1/2} = 290$ Hz), 3.116 ($\Delta\nu_{1/2} = 88$ Hz), 1.191 ($\Delta\nu_{1/2} = 56$ Hz), 0.572 ($\Delta\nu_{1/2} = 317$ Hz) ppm. ^2H NMR (77 MHz, Et_2O): $\delta = 10.69$ ($\Delta\nu_{1/2} = 65$ Hz), 7.46 ($\Delta\nu_{1/2} = 17$ Hz), 5.21 ($\Delta\nu_{1/2} = 9.8$ Hz), *ca.* -19 ppm. Anal. Calcd. for $\text{C}_{44}\text{H}_{39}\text{D}_{24}\text{N}_4\text{Mo}$: C, 68.81; H, 8.27; N, 7.29. Found: C, 69.08; H, 8.51; N, 7.29.

Oxidation of $(\eta^2\text{-Me}_2\text{C}=\text{NAr})\text{Mo}(\text{N}[i\text{-Pr-}d_6]\text{Ar})_3$. A cold ($-35\text{ }^\circ\text{C}$), blue, tetrahydrofuran solution of 2- $(\eta^2\text{-imine-}d_{18})$ (0.145 g, 0.192 mmol) was added to cold, solid silver triflate (0.053 g, 0.205 mmol). The reaction was allowed to stir for 20 minutes and warm to room temperature. At that time, the brown solution was filtered through Celite and the solvent was removed *in vacuo*. The product was recrystallized from a mixture of pentane and tetrahydrofuran. ^1H NMR (C_6D_6 , 300 MHz): $\delta = 6.61$ (s, 1H, imine *para*), 6.56 (s, 3H, *para*), 6.47 (s, 6H, *ortho*), 6.45 (s, 2H, imine *ortho*), 4.38 (br s, 3H, methine), 2.16 (s, 6H, imine aryl methyl), 2.11 (s, 18H, aryl methyl), 1.91 (s, 3H, imine methyl), 1.45 (s, 3H, imine methyl) ppm. ^{19}F NMR (C_6D_6 , 282 MHz): $\delta = -77.2$ ppm.

Synthesis of (1-AdNC)Mo(N[*i*-Pr]Ar)₃ (2-AdNC). To an orange-brown solution of 1.334 g of $\text{Mo}(\text{H})(\eta^2\text{-Me}_2\text{C}=\text{NAr})(\text{N}[i\text{-Pr}]\text{Ar})_2$ (2.289 mmol) in 5 mL Et_2O were added 3 mL of a colorless solution of AdNC (0.369 g, 2.292 mmol, 1 equiv). Upon mixing of the two solutions at $20\text{ }^\circ\text{C}$, the reaction mixture became green-brown. After stirring for 1 h, the solvent was removed *in vacuo* to yield an oily brown product. ^1H NMR (500 MHz, C_6D_6): $\delta = 18.14$, 12.12 (*i*-Pr methyl), 6.65, 1.96, 1.66, 1.42, -8.68 ppm. ^2H NMR (77 MHz, Et_2O): $\delta = 6.21$ ppm. IR (Et_2O , KBr): 1718 cm^{-1} .

Synthesis of (1-AdNC)₂Mo(N[*i*-Pr]Ar)₃ (2-(AdNC)₂). To an orange-brown solution of 2.775 g $\text{Mo}(\text{H})(\eta^2\text{-Me}_2\text{C}=\text{NAr})(\text{N}[i\text{-Pr}]\text{Ar})_2$ (4.759 mmol) in 20 mL Et_2O were added 5 mL of a colorless solution of AdNC (1.530 g, 9.501 mmol, 2 equiv). Upon mixing of the two solutions at $20\text{ }^\circ\text{C}$, the reaction mixture became purple. After 1 h, the solvent was removed *in vacuo* and the resulting solid was recrystallized from cold Et_2O to yield 3.4271 g of purple crystals (79.7%). ^1H NMR (500 MHz, C_6D_6): $\delta = 18.00$, 6.9, 4.14, 2.07, 1.74, -0.12 , -2.23 , -8.59 , -11.76 ppm. ^2H NMR (77 MHz, Et_2O): $\delta = 3.5$ ppm ($\Delta\nu_{1/2} = 11.5$ Hz). $\mu_{\text{eff}} = 1.59\ \mu_{\text{B}}$ (Evans' Method, C_6D_6 , $20\text{ }^\circ\text{C}$). IR (Et_2O , KBr): 2035 cm^{-1} . Anal. Calcd. for $\text{C}_{55}\text{H}_{78}\text{N}_5\text{Mo}$: C, 72.98; H, 8.68; N, 7.73. Found: C, 72.73; H, 8.82; N, 7.65.

Synthesis of (1-AdNC)Mo(N[*t*-Bu]Ar)₃ (3-AdNC). To an orange solution of 1.566 g of $\text{Mo}(\text{N}[t\text{-Bu}]\text{Ar})_3$ (2.505 mmol) in 10 mL Et_2O were added 5 mL of a colorless Et_2O solution of AdNC (0.404 g, 2.507 mmol, 1 equiv). The brown-orange reaction mixture was stirred at $20\text{ }^\circ\text{C}$ for 90 min, and then the solvent was removed *in vacuo*.

Crystallization from cold Et₂O yielded red-brown needles (1.229 g, 62.4 %). ¹H NMR (500 MHz, C₆D₆): δ = 28.42, 16.75, 10.42, 3.40, 1.63, -7.64, -7.93, -18.50 ppm. ²H NMR (77 MHz, Et₂O): δ = 9.9 ppm (Δν_{1/2} = 12.8 Hz). IR (Et₂O, KBr): 1762 cm⁻¹. μ_{eff} = 1.83 μ_B (Evans' method, C₆D₆, 20 °C). Anal. Calcd. for C₄₇H₆₉N₄Mo: C, 71.81; H, 8.84; N, 7.12. Found: C, 70.94; H, 8.68; N, 7.00.

Synthesis of (*t*-BuNC)Mo(N[*t*-Bu]Ar)₃ (3-*t*-BuNC). To an orange-brown solution of 2.732 g of Mo(N[*t*-Bu]Ar)₃ (4.371 mmol) in 10 mL of pentane was added a solution of *t*-BuNC (0.375 g, 4.371 mmol, 1.0 equiv) in 5 mL of pentane. The solution was stirred for one hour at room temperature, at which time the reaction mixture was filtered through a fine frit and 1.926 g of spectroscopically pure brown powder was isolated. The filtrate was dried *in vacuo*, redissolved in approximately 10 mL of pentane, and a second crop of orange-brown, crystalline product was recrystallized at -35 °C (2.676 g (overall), 3.780 mmol, 86.4 %). ¹H NMR (C₆D₆, 500 MHz): δ = 11.43 (9H, isocyanide *tert*-butyl), 10.91 (27H, *tert*-butyl), 3.54 (6H, *ortho*), 3.19 (3H, *para*), 1.72 (18H, aryl methyl) ppm. IR (KBr, pentane): 1759, 1727 cm⁻¹. Anal. Calcd. for C₄₁H₆₃N₄Mo: C, 69.56; H, 8.97; N, 7.91. Found: C, 69.10; H, 8.98; N, 7.99.

Thermolysis of (*t*-BuNC)Mo(N[*t*-Bu]Ar)₃. Approximately 20 mg of 3-*t*-BuNC were dissolved in 0.7 mL toluene-*d*₈, and the solution was placed into a NMR tube that was subsequently sealed with a Teflon stopcock. This solution was heated at approximately 40 °C for 12 h, after which time no change was observed by ¹H NMR spectroscopy. The sample was then heated at 80 °C for 2 d, during which time a modest amount of *tert*-butyl radical ejection occurred from the isocyanide moiety forming (NC)Mo(N[*t*-Bu]Ar)₃ and radical ejection from the ligand to form (*t*-BuNC)Mo(NAr)(N[*t*-Bu]Ar)₂.

Synthesis of (*t*-BuNC)Mo(N[*i*-Pr]Ar)₃-*d*₁₈ (2-*t*-BuNC-*d*₁₈). To a brown solution of 1.519 g of Mo(H)(η²-Me₂C=NAr)(N[*i*-Pr]Ar)₂-*d*₁₈ (2.527 mmol) was added a pentane solution of *t*-BuNC (0.209 g, 1.0 equiv, 2.524 mmol). The solution was stirred for one hour at room temperature, at which time the solvent was removed *in vacuo*. The orange-brown residue was oily, and pure solid was not obtained by recrystallization from cold pentane (-35 °C). IR (KBr, pentane): 1751, 1718 cm⁻¹. ²H NMR (77 MHz, Et₂O): δ = 7.1 ppm (Δν_{1/2} = 9.2 Hz).

Synthesis of (*t*-BuNC)₂Mo(N[*i*-Pr]Ar)₃ (2-(*t*-BuNC)₂). To a brown solution of 0.127 g of Mo(H)(η²-Me₂C=NAr)(N[*i*-Pr]Ar)₂-*d*₁₈ (0.211 mmol) was added a diethyl ether solution of *t*-BuNC (0.036 g, 2.05 equiv, 0.433 mmol). The reaction mixture became purple upon mixing and was stirred for one hour at room temperature. ¹H NMR (C₆D₆, 500 MHz): δ = 4.31, 1.61, -2.24, -11.92 (v br) ppm. IR (KBr, pentane): 2019 cm⁻¹. ²H NMR (77 MHz, Et₂O): δ = 3.9 ppm (Δν_{1/2} = 14.6 Hz). Anal. Calcd. for C₄₃H₆₆N₅Mo: C, 68.96; H, 8.88; N, 9.35. Found: C, 67.58; H, 8.86; N, 9.10.

Synthesis of [Na(THF)_x][(AdNC)Mo(N[*i*-Pr]Ar)₃]. 1-Adamantyl isocyanide (0.124 g, 0.770 mmol, 0.91 equiv) was added to a THF solution of Mo(H)(η²-Me₂C=NAr)(N[*i*-Pr]Ar)₂ (0.496 g, 0.850 mmol, 1 equiv) and the solution was stirred for 30 min. Subsequently, 4.65 equiv of 0.5 % sodium amalgam (0.091 g Na, 3.96 mmol; 18.3 g Hg) was added, resulting in a gradual color change to red-orange over 2 h. At this time, the

supernatant solution was decanted away from the amalgam, filtered through Celite, and the solvent was removed *in vacuo*. The residue was extracted with pentane and recrystallized at $-35\text{ }^{\circ}\text{C}$. ^1H NMR (500 MHz, pyridine- d_5): $\delta = 6.88$ (ortho, s, 6H), 6.54 (para, s, 3H), 4.82 (methine, septet, 3H), 2.26 (aryl methyl, s, 18H), 2.01 (Ad, s, 3H), 1.82 (Ad, br d, 6H), 1.63 (*i*-Pr methyl, d, 18H), 1.61 (Ad, br d, 6H) ppm. ^{13}C NMR (125 MHz, pyridine- d_5): $\delta = 266.34$ (MoC), 157.96 (ipso), 137.23 (meta), 123.35 (para), 122.15 (ortho), 59.25 (methine), 56.13 (Ad), 48.17 (Ad), 37.72 (Ad), 31.62 (Ad), 26.20 (aryl methyl), 22.04 (*i*-Pr methyl) ppm.

1.9.3 Crystallographic Structure Determinations.

	2-(η^2 -imine)	3- <i>t</i> -BuNC	2-(AdNC) ₂
formula	C ₄₄ H ₆₃ MoN ₄	C ₄₁ H ₆₃ N ₄ Mo	C ₆₀ H ₉₀ N ₅ Mo
fw	743.92	707.89	977.31
space group	<i>P</i> $\bar{1}$	<i>P</i> 2 ₁ / <i>n</i>	<i>P</i> $\bar{1}$
a, Å	11.1241(15)	15.1350(14)	10.6383(11)
b, Å	12.0233(15)	13.5623(12)	10.9340(11)
c, Å	16.837(2)	19.6178(18)	24.980(3)
α , deg	78.988(3)	90	91.598(2)
β , deg	79.148(2)	91.1720(10)	101.624(2)
γ , deg	72.990(3)	90	101.257(2)
V, Å ³	2092.7(5)	4026.0(6)	2784.4(5)
Z	2	4	2
cryst description	green block	orange prism	purple cube
D _{calcd} , g·cm ⁻³	1.181	1.168	1.166
μ (Mo K α), mm ⁻¹	0.346	0.357	0.276
F(000)	794	1516	1054
GOF on F ²	1.088	1.143	1.219
<i>R</i> (<i>F</i>), % ^a	0.0898	0.0647	0.1077
<i>R</i> _w (<i>F</i>), % ^a	0.1712	0.1563	0.2495

^a Quantity minimized = $R_w(F^2) = \sum[w(F_o^2 - F_c^2)^2] / \sum[(wF_o^2)^2]^{1/2}$; $R = \sum\Delta / \sum(F_o)$, $\Delta = |(F_o - F_c)|$, $w = 1/[\sigma^2(F_o^2) + (aP)^2 + bP]$, $P = [2F_c^2 + \text{Max}(F_o, 0)]/3$.

Table 1.5: Crystallographic data for 2-(η^2 -imine), 3-*t*-BuNC, and 2-(AdNC)₂.

The X-ray data collections were carried out on a Siemens Platform three-circle diffractometer (Mo K α , $\lambda = 0.71073\text{ }^{\circ}\text{Å}$) mounted with a CCD detector and outfitted with a low-temperature, nitrogen-stream aperture (189 K). The structures were solved by direct methods, in conjunction with standard difference Fourier techniques and refined by full-matrix least-squares procedures. Selected bond lengths and angles are supplied in Table 1, Table 2, and Table 3. A summary of crystallographic data is given in Table 5, with full details found in Appendix 2. The systematic absences in the diffraction data are uniquely consistent with the assigned space group of *P*2₁/*n* for 3-*t*-BuNC. No space

group symmetry higher than triclinic was indicated in the diffraction data for **2**-(AdNC)₂ and **2**-(η^2 -imine). These choices led to chemically sensible and computationally stable refinements. An empirical absorption correction (ψ -scans) was applied to all data sets. All software for diffraction data processing and crystal-structure solution and refinement are contained in the SHELXTL (v5.10) program suite (G. Sheldrick, Siemens XRD, Madison, WI).

1.9.4 General Considerations: Stopped-flow kinetics.

Toluene (anhydrous, 99.8%, Acros) was purified further by the method of Grubbs.⁶⁵ Toluene solutions of **1**, **1-d₃**, **3**, and AdNC were prepared in a Vacuum Atmospheres glovebox filled with argon. Kinetic measurements were performed at temperatures from -80 to 25 °C using a Hi-Tech Scientific (Salisbury, Wiltshire, UK) SF-43 Multi-Mixing CryoStopped-Flow Instrument in diode array and single wavelength modes. The stopped-flow instrument was equipped with stainless steel plumbing, a stainless steel mixing cell with sapphire windows, and an anaerobic gas-flashing kit. The instrument was connected to an IBM computer with IS-2 Rapid Kinetic software (Hi-Tech Scientific). The temperature in the mixing cell was maintained to ± 0.1 K, and the mixing time was 2 ms. The driving syringe compartment and the cooling bath filled with heptane (Fisher) were flushed with argon before and during the experiments, using anaerobic kit flush lines. All flow lines of the SF-43 instrument were extensively washed with degassed, anhydrous toluene before charging the driving syringes with reactant solutions. The experiments were performed in a single-mixing mode of the instrument, with solutions of two reagents mixed in a 1:1 (v/v) ratio.

1.9.5 General Considerations: Thermochemistry.

Infrared data were recorded on a Perkin-Elmer System 2000 FTIR in sealed solution cells obtained from Harrick Scientific. Solvents used, toluene, C₆D₆, and heptane were all distilled from Na/benzophenone under argon prior to use. Enthalpies of reaction were measured in a Setaram C-80 Calvet calorimeter that was loaded in the glove box in an argon atmosphere. In a typical procedure a stock solution of approximately 0.2 g of **1** was dissolved in 7 ml of toluene that had been freshly distilled from sodium benzophenone ketyl. The solution was filtered and 5 mL were loaded into the calorimeter containing an ampoule of AdNC (0.0176 g). (The remaining solution was used to obtain an FTIR spectrum of the stock solution.) The calorimeter cell was subsequently sealed, taken from the glove box, loaded in calorimeter, and allowed to thermally equilibrate for two hours. Rotation of the calorimeter prior to breaking the ampoule gave a small exothermic reaction due to trace contaminants inside the cell. A second such rotation showed no thermal signal and the reaction was initiated by breaking the ampoule. Upon completion of the reaction and thermal equilibration, the cell was taken back into the glove box, an aliquot loaded into an FTIR cell for product observation, and the entire apparatus cleaned with dried and degassed toluene. The cell was stored in an evacuated container inside the glove box between calorimetric runs.

1.9.6 DFT Calculations.

Calculations were performed with version 2002.02 of the Amsterdam DFT program package, ADF.⁶⁷⁻⁶⁹ Atomic coordinates from the X-ray diffraction study of **1**,²³ **3**,⁷ **3-*t*-BuNC**, and **2-(AdNC)₂** were employed. The calculation was carried out with all the electrons considered explicitly, i.e., no frozen core approximation was utilized. The atomic basis sets employed were the ZORA/TZ2P bases supplied with the program, and accordingly, scalar relativistic effects were included with the ZORA treatment.⁷⁰ The calculations were carried out in spin-unrestricted mode. The local density approximation functional used was that of Vosko, Wilk, and Nusair, while the functionals for the generalized gradient approximations took the form of Becke (exchange) and Perdew (correlation).⁷¹⁻⁷³

1.10 References

1. Stephens, F. H.; Figueroa, J. S.; Cummins, C. C.; Kryatova, O. P.; Kryatov, S. V.; Rybak-Akimova, E. V.; McDonough, J. E.; Hoff, C. D. *Organometallics*, **2004**, in press.
2. (a) Yandulov, D. V.; Schrock, R. R. *J. Am. Chem. Soc.* **2002**, *124*, 6252. (b) Yandulov, D. V.; Schrock, R. R.; Rheingold, A. L.; Ceccarelli, C.; Davis, W. M. *Inorg. Chem.* **2003**, *42*, 796. (c) Yandulov, D. V.; Schrock, R. R. *Science* **2003**, *301*, 76. (d) Schrock, R. R.; Kolodziej, R. M.; Liu, A. H.; Davis, W. M.; Vale, M. G. *J. Am. Chem. Soc.* **1990**, *112*, 4338.
3. (a) Nishibayashi, Y.; Iwai, S.; Hidai, M. *Science* **1998**, *279*, 540. (b) Nishibayashi, Y.; Takemoto, S.; Iwai, S.; Hidai, M. *Inorg. Chem.* **2000**, *39*, 5946. (c) Ishino, H.; Nagano, T.; Kuwata, S.; Yokobayashi, Y.; Ishii, Y.; Hidai, M.; Mizobe, Y. *Organometallics* **2001**, *20*, 188. (d) Nishibayashi, Y.; Wakiji, I.; Hirata, K.; Du Bois, M. R.; Hidai, M. *Inorg. Chem.* **2001**, *40*, 578. (e) Hidai, M. *Coord. Chem. Rev.* **1999**, *185-186*, 99.
4. (a) Mori, M. *J. Heterocycl. Chem.* **2000**, *37*, 623. (b) Hori, M.; Mori, M. *J. Org. Chem.* **1995**, *60*, 1480. (c) Mori, M.; Kawaguchi, M.; Hori, M.; Hamaoka, S. *Heterocycles* **1994**, *39*, 729.
5. For reviews of dinitrogen-derived organonitrogen compounds, see the following reviews and references therein: (a) Fryzuk, M. D. *Chem. Record* **2003**, *3*, 2. (b) Fryzuk, M. D.; Johnson, S. A. *Coord. Chem. Rev.* **2000**, *200-202*, 379. (c) Hidai, M.; Yasushi, M. *Topics Organomet. Chem.* **1999**, *3*, 227. (d) Hidai, M.; Mizobe, Y. *Chem. Rev.* **1995**, *95*, 1115. (e) Mizobe, Y.; Ishii, Y.; Hidai, M. *Coord. Chem. Rev.* **1995**, *139*, 281. (f) George, T. A.; DeBord, J. R. D. *ACS Symp. Series* **1993**, *535*, 363.
6. Henderickx, H.; Kwakkenbos, G.; Peters, A.; van der Spoel, J.; de Vries, K. *Chem. Commun.* **2003**, 2050.
7. (a) Laplaza, C. E.; Cummins, C. C. *Science* **1995**, *268*, 861. (b) Laplaza, C. E.; Odom, A. L.; Davis, W. M.; Cummins, C. C. *J. Am. Chem. Soc.* **1995**, *117*, 4999. (c) Laplaza, C. E.; Johnson, M. J. A.; Peters, J. C.; Odom, A. L.; Kim, E.; Cummins, C. C.; George, G. N.; Pickering, I. J. *J. Am. Chem. Soc.* **1996**, *118*, 8623. (d) Tsai, Y.-C.; Cummins, C. C. *Inorg. Chim. Acta* **2003**, *345*, 63.
8. (a) Mindiola, D. J.; Meyer, K.; Cherry, J.-P. F.; Baker, T. A.; Cummins, C. C. *Organometallics* **2000**, *19*, 1622. (b) Caselli, A.; Solari, E.; Scopelliti, R.; Floriani, C.; Re, N.; Rizzoli, C.; Chiesi-Villa, A. *J. Am. Chem. Soc.* **2000**, *122*, 3652.

9. (a) Clentsmith, G. K. B.; Bates, V. M. E.; Hitchcock, P. B.; Cloke, F. G. N. *J. Am. Chem. Soc.* **1999**, *121*, 10444. (b) Fryzuk, M. D.; Kozak, C. M.; Bowdridge, M. R.; Patrick, B. O.; Rettig, S. J. *J. Am. Chem. Soc.* **2002**, *124*, 8389.
10. (a) Laplaza, C. E.; Davis, W. M.; Cummins, C. C. *Angew. Chem. Int. Ed. Engl.* **1995**, *34*, 2042. (b) Laplaza, C. E.; Johnson, A. R.; Cummins, C. C. *J. Am. Chem. Soc.* **1996**, *118*, 709. (c) Johnson, M. J. A.; Lee, P. M.; Odom, A. L.; Davis, W. M.; Cummins, C. C. *Angew. Chem. Int. Ed. Engl.* **1997**, *36*, 87. (d) Agapie, T.; Odom, A. L.; Cummins, C. C. *Inorg. Chem.* **2000**, *39*, 174.
11. (a) Woo, L. K.; Goll, J. G. *J. Am. Chem. Soc.* **1989**, *111*, 3755. (b) Woo, L. K.; Goll, J. G.; Czaplá, D. J.; Hays, J. A. *J. Am. Chem. Soc.* **1991**, *113*, 8478.
12. (a) Bottomley, L. A.; Neely, F. L. *J. Am. Chem. Soc.* **1989**, *111*, 5955. (b) Neely, F. L.; Bottomley, L. A. *Inorg. Chim. Acta* **1992**, *192*, 147. (c) Neely, F. L.; Bottomley, L. A. *Inorg. Chem.* **1997**, *36*, 5432. (d) Bottomley, L. A.; Neely, F. L. *Inorg. Chem.* **1997**, *36*, 5435.
13. Chang, C. J.; Low, D. W.; Gray, H. B. *Inorg. Chem.* **1997**, *36*, 270.
14. (a) Demadis, K. D.; Bakir, M.; Kleszczewski, B. G.; Williams, D. S.; White, P. S.; Meyer, T. J. *Inorg. Chim. Acta* **1998**, *270*, 511. (b) Wong, T.-W.; Lau, T.-C.; Wong, W.-T. *Inorg. Chem.* **1999**, *38*, 6181.
15. McCarthy, M. R.; Crevier, T. J.; Bennett, B.; Dehestani, A.; Meyer, J. M. *J. Am. Chem. Soc.* **2000**, *122*, 12391.
16. Clough, C. R.; Greco, J. B.; Figueroa, J. S.; Cummins, C. C. *J. Am. Chem. Soc.* **2004**, in press.
17. (a) Tomooka, C. S.; Carreira, E. M. *Helv. Chim. Acta* **2002**, *85*, 3773. (b) Carreira, E. M.; Hong, J.; Du Bois, J.; Tomooka, C. S. *Pure Appl. Chem.* **1998**, *70*, 1097. (c) Du Bois, J.; Tomooka, C. S.; Hong, J.; Carreira, E. M. *Acc. Chem. Res.* **1997**, *30*, 364. (d) Du Bois, J.; Tomooka, C. S.; Hong, J.; Carreira, E. M. *Angew. Chem. Int. Ed. Engl.* **1997**, *36*, 1645. (e) Du Bois, J.; Hong, J.; Carreira, E. M.; Day, M. W. *J. Am. Chem. Soc.* **1996**, *118*, 915.
18. (a) Nishimura, M.; Minakata, S.; Takahashi, T.; Oderaotoshi, Y.; Komatsu, M. *J. Org. Chem.* **2002**, *67*, 2101. (b) Minakata, S.; Nishimura, M.; Takahashi, T.; Oderaotoshi, Y.; Komatsu, M. *Tetrahedron Lett.* **2001**, *42*, 9019. (c) Nishimura, M.; Minakata, S.; Thongchant, S.; Ryu, I.; Komatsu, M. *Tetrahedron Lett.* **2000**, *41*, 7089. (d) Ho, C.-M.; Lau, T.-C.; Kwong, H.-L.; Wong, W.-T. *J. Chem. Soc., Dalton Trans.* **1999**, 2411. (e) Svenstrup, N.; Bogevig, A.; Hazell, R. G.; Jorgensen, K. A. *J. Chem. Soc., Perkin Trans. 1* **1999**, 1559.

19. (a) Hahn, J.; Landis, C. R.; Nasluzov, V. A.; Neyman, K. M.; Roesch, N. *Inorg. Chem.* **1997**, *36*, 3947. (b) Christian, G.; Driver, J.; Stranger, R. *Faraday Disc.* **2003**, *124*, 331. (c) Holland, P. L. *Comprehensive Coord. Chem. II* **2004**, *8*, 569.
20. Pool, J. A.; Lobkovsky, E.; Chirik, P. J. *Nature* **2004**, *427*, 527.
21. (a) Pool, J. A.; Lobkovsky, E.; Chirik, P. J. *Organometallics* **2003**, *22*, 2797. (b) Pool, J. A.; Lobkovsky, E.; Chirik, P. J. *J. Am. Chem. Soc.* **2003**, *125*, 2241.
22. Manriquez, J. M.; McAlister, D. R.; Rosenberg, E.; Shiller, A. M.; Williamson, K. L.; Chan, S. I.; Bercaw, J. E. *J. Am. Chem. Soc.* **1978**, *100*, 3078.
23. Tsai, Y.-C.; Johnson, M. J. A.; Mindiola, D. J.; Cummins, C. C.; Klooster, W. T.; Koetzle, T. F. *J. Am. Chem. Soc.* **1999**, *121*, 10426.
24. For other examples of β -H elimination from organoamide ligands, see the following: (a) Mayer, J. M.; Curtis, C. J.; Bercaw, J. E. *J. Am. Chem. Soc.* **1983**, *105*, 2651. (b) Bryndza, H. E.; Tam, W. *Chem. Rev.* **1988**, *88*, 1163. (c) Fryzuk, M. D.; Montgomery, C. D. *Coord. Chem. Rev.* **1989**, *95*, 1. (d) Berno, P.; Gambarotta, S. *Organometallics* **1995**, *14*, 2159. (e) Driver, M. S.; Hartwig, J. F. *J. Am. Chem. Soc.* **1996**, *118*, 4206. (f) Hartwig, J. F. *J. Am. Chem. Soc.* **1996**, *118*, 7010. (g) Bazinet, P.; Yap, G. P. A.; Richeson, D. S. *Organometallics* **2001**, *20*, 4129. (h) Cai, H.; Chen, T.; Wang, X.; Schultz, A. J.; Koetzle, T. F.; Xue, Z. *Chem. Commun.* **2002**, 230.
25. Cherry, J.-P. F.; Stephens, F. H.; Johnson, M. J. A.; Diaconescu, P. L.; Cummins, C. C. *Inorg. Chem.* **2001**, *40*, 6860.
26. (a) Tsai, Y.-C.; Diaconescu, P. L.; Cummins, C. C. *Organometallics* **2000**, *19*, 5260. (b) Blackwell, J. B.; Figueroa, J. S.; Stephens, F. H.; Cummins, C. C. *Organometallics* **2003**, *22*, 3351.
27. (a) Figueroa, J. S.; Cummins, C. C. *J. Am. Chem. Soc.* **2003**, *125*, 4020. (b) Mindiola, D. J.; Cummins, C. C. *Organometallics* **2001**, *20*, 3626.
28. Figueroa, J. S.; Cummins, C. C. *Angew. Chem. Int. Ed.* **2004**, *43*, 984.
29. (a) Johnson, M. J. A. Ph. D. Thesis, Massachusetts Institute of Technology, 1998. (b) Tsai, Y.-C. Ph. D. Thesis, Massachusetts Institute of Technology, 2002.
30. Galakhov, M. V.; Gomez, M.; Jimenez, G.; Royo, P.; Pellinghelli, M. A.; Tiripicchio, A. *Organometallics* **1995**, *14*, 1901.
31. Tsai, Y.-C.; Stephens, F. H.; Meyer, K.; Mendiratta, A.; Gheorghiu, M. D.; Cummins, C. C. *Organometallics* **2003**, *22*, 2902.

32. Greco, G. E.; O'Donoghue, M. B.; Seidel, S. W.; Davis, W. M.; Schrock, R. R. *Organometallics* **2000**, *19*, 1132.
33. Glaser, M.; Spiers, H.; Lugger, T.; Hahn, F. E. *J. Organomet. Chem.* **1995**, *503*, C32.
34. Spiers, H.; Glaser, M.; Pietzsch, H.-J.; Hahn, F. E.; Lugger, T. *Inorg. Chim. Acta* **1995**, *240*, 465.
35. Leigh, G. J.; Winterton, N. *Modern Coordination Chemistry: The Legacy of Joseph Chatt*; Royal Society of Chemistry: Cambridge, 2002.
36. Nugent, W. A.; Mayer, J. M. *Metal-Ligand Multiple Bonds*; Wiley: New York, 1988.
37. Bak, B.; Hansen-Nygaard, L.; Rastrup-Andersen, J. *J. Mol. Spectrosc.* **1958**, *2*, 54.
38. Peters, J. C.; Baraldo, L. M.; Baker, T. A.; Johnson, A. R.; Cummins, C. C. *J. Organomet. Chem.* **1999**, *591*, 24.
39. Johnson, A. R.; Davis, W. M.; Cummins, C. C.; Serron, S.; Nolan, S. P.; Musaev, D. G.; Morokuma, K. *J. Am. Chem. Soc.* **1998**, *120*, 2071.
40. Greco, J. B.; Peters, J. C.; Baker, T. A.; Davis, W. M.; Cummins, C. C.; Wu, G. *J. Am. Chem. Soc.* **2001**, *123*, 5003.
41. Seino, H.; Arita, C.; Nonokawa, D.; Nakamura, G.; Harada, Y.; Mizobe, Y.; Hidai, M. *Organometallics* **1999**, *18*, 4165.
42. Kessler, M.; Ring, H.; Trambarudo, R.; Gordy, W. *Phys. Rev.* **1950**, *79*, 54.
43. Laplaza, C. E.; Davis, W. M.; Cummins, C. C. *Angew. Chem., Int. Ed. Engl.* **1995**, *34*, 2042.
44. For other examples of spin state changes upon coordination, see the following: (a) Fukuzumi, S.; Satoh, N.; Okamoto, T.; Yasui, K.; Suenobu, T.; Seko, Y.; Fujitsuka, M.; Ito, O. *J. Am. Chem. Soc.* **2001**, *123*, 7756. (b) Smith, K. M.; Poli, R.; Harvey, J. N. *New J. Chem.* **2000**, *24*, 77. (c) Ray, M.; Golombek, A.; Hendrich, M. P.; Young, V. G.; Borovik, A. S. *J. Am. Chem. Soc.* **1996**, *118*, 6084.
45. (a) Jones, W. D. *Acc. Chem. Res.* **2003**, *36*, 140. (b) Labinger, J. A.; Bercaw, J. E. *Nature* **2002**, *417*, 507.
46. Seder, T. A.; Church, S. P.; Ouder Kirk, A. J.; Weitz, E. *J. Am. Chem. Soc.* **1985**, *107*, 1432.
47. Wink, D. A.; Ford, P. C. *J. Am. Chem. Soc.* **1987**, *109*, 436.

48. Wilkins, R. G. *Oxygen Complexes and Oxygen Activation by Transition Metals*; Plenum Press: New York, 1987.
49. Momenteau, M.; Reed, C. A. *Chem. Rev.* **1994**, *94*, 659.
50. Warburton, P. R.; Busch, D. H. *Perspectives on Bioinorganic Chemistry*, Vol. 2; JAI Press Ltd.: London, 1993.
51. Nolan, S. P.; Lopez de la Vega, R.; Hoff, C. D. *Organometallics* **1986**, *5*, 2529.
52. Rybtchinski, B.; Oevers, S.; Montag, M.; Vigalok, A.; Rozenberg, H.; Martin, J. M. L.; Milstein, D. *J. Am. Chem. Soc.* **2001**, *123*, 9064.
53. (a) Mindiola, D. J.; Tsai, Y.-C.; Hara, R.; Chen, Q.; Meyer, K.; Cummins, C. C. *Chem. Commun.* **2001**, 125. (b) Agapie, T.; Diaconescu, P. L.; Cummins, C. C. *J. Am. Chem. Soc.* **2002**, *124*, 2412.
54. (a) Harvey, J. N.; Poli, R.; Smith, K. M. *Coord. Chem. Rev.* **2003**, *238-239*, 347. (b) Poli, R.; Harvey, J. N. *Chem. Soc. Rev.* **2003**, *32*, 1. (c) Poli, R. *Acc. Chem. Res.* **1997**, *30*, 494. (d) Poli, R. *Chem. Rev.* **1996**, *96*, 2135.
55. (a) Hess, J. S.; Leelasubcharoen, S.; Rheingold, A. L.; Doren, D. J.; Theopold, K. H. *J. Am. Chem. Soc.* **2002**, *124*, 2454. (b) Detrich, J. L.; Reinaud, O. M.; Rheingold, A. L.; Theopold, K. H. *J. Am. Chem. Soc.* **1995**, *117*, 11745.
56. Schröder, D.; Shaik, S.; Schwarz, H. *Acc. Chem. Res.* **2000**, *33*, 139.
57. Schrock, R. R. *Chem. Rev.* **2002**, *102*, 145.
58. (a) Veige, A. S.; Slaughter, L. M.; Lobkovsky, E. B.; Wolczanski, P. T.; Matsunaga, N.; Decker, S. A.; Cundari, T. R. *Inorg. Chem.* **2003**, *42*, 6204. (b) Veige, A. S.; Slaughter, L. M.; Wolczanski, P. T.; Matsunaga, N.; Decker, S. A.; Cundari, T. R. *J. Am. Chem. Soc.* **2001**, *123*, 6419. (c) Wolczanski, P. T. *Polyhedron* **1995**, *14*, 3335.
59. (a) King, W. A.; Scott, B. L.; Eckert, J.; Kubas, G. J. *Inorg. Chem.* **1999**, *38*, 1069. (b) King, W. A.; Luo, X.-L.; Scott, B. L.; Kubas, G. J.; Zilm, K. W. *J. Am. Chem. Soc.* **1996**, *118*, 6782. (c) Luo, X.-L.; Kubas, G. J.; Bryan, J. C.; Burns, C. J.; Unkefer, C. J. *J. Am. Chem. Soc.* **1994**, *116*, 10312.
60. Bercaw, J. E. *J. Am. Chem. Soc.* **1974**, *96*, 5087.
61. Pombeiro, A. J. L.; Guedes da Silva, M. F. C.; Michelin, R. A. *Coord. Chem. Rev.* **2001**, *218*, 43.
62. Gamble, A. S.; White, P. S.; Templeton, J. L. *Organometallics* **1991**, *10*, 693.

63. Luo, X.-L.; Kubas, G. J.; Burns, C. J.; Buixher, R. J. *Organometallics* **1995**, *14*, 3370.
64. (a) Filippou, A. C.; Hofmann, P.; Kiprof, P.; Schmid, H. R.; Wagner, C. *J. Organomet. Chem.* **1993**, *459*, 233. (b) Filippou, A. C.; Wagner, C.; Fischer, E. O.; Völkl, C. *J. Organomet. Chem.* **1992**, *438*, C15. (c) Filippou, A. C.; Grünleitner, W.; Fischer, E. O. *J. Organomet. Chem.* **1992**, *428*, C37. (d) Filippou, A. C.; Grünleitner, W.; Fischer, E. O., Imhof, W.; Huttner, G. *J. Organomet. Chem.* **1991**, *413*, 165. (e) Filippou, A. C.; Grünleitner, W.; Fischer, E. O. *J. Organomet. Chem.* **1991**, *411*, C21. (f) Filippou, A. C.; Grünleitner, W. *J. Organomet. Chem.* **1991**, *407*, 61. (g) Filippou, A. C.; Grünleitner, W.; Fischer, E. O. *J. Organomet. Chem.* **1991**, *401*, C37. (h) Filippou, A. C.; Fischer, E. O.; Grünleitner, W. *J. Organomet. Chem.* **1990**, *386*, 333.
65. Pangborn, A. B.; Giardello, M. A.; Grubbs, R. H.; Rosen, R. K.; Timmers, F. J. *Organometallics* **1996**, *15*, 1518.
66. Sasaki, T.; Nakanishi, A.; Ohno, M. *J. Org. Chem.* **1981**, *46*, 5445.
67. te Velde, G.; Bickelhaupt, F. M.; van Gisbergen, S. J. A.; Fonseca Guerra, C.; Baerends, E. J.; Snijders, J. G.; Ziegler, T. *J. Comput. Chem.* **2001**, *22*, 931.
68. Fonseca Guerra, C.; Snijders, J. G.; te Velde, G.; Baerends, E. J. *J. Theor. Chem. Acc.* **1998**, *99*, 391.
69. ADF2002.02, SCM, Theoretical Chemistry, Vrije Universiteit, Amsterdam, The Netherlands, <http://www.scm.com>.
70. (a) van Lenthe, E.; Baerends, E. J.; Snijders, J. G. *J. Chem. Phys.* **1993**, *99*, 4597. (b) van Leeuwen, R.; van Lenthe, E.; Baerends, E. J.; Snijders, J. G. *J. Chem. Phys.* **1994**, *101*, 1272. (c) van Lenthe, E.; Baerends, E. J.; Snijders, J. G. *J. Chem. Phys.* **1994**, *101*, 9783. (d) Sadlej, A. J.; Snijders, J. G.; van Lenthe, E.; Baerends, E. J. *J. Chem. Phys.* **1995**, *102*, 1758.
71. Baerends, E. J.; Ellis, D. E.; Ros, P. *Chem. Phys.* **1973**, *2*, 41.
72. Versluis, L.; Ziegler, T. *J. Chem. Phys.* **1988**, *88*, 322.
73. te Velde, G.; Baerends, E. J. *J. Comput. Phys.* **1992**, *99*, 84.

**Synthesis and Reactivity of a New Terminal Phosphide of Molybdenum Supported
by *N*-iso-Propylanilide Ligands¹**

Reproduced in part with permission from *Inorganic Chemistry*, 2001, 40(27), 6860.
©2001 American Chemical Society.

Table of Contents

2.1 Introduction.....	54
2.2 Results and Discussion	55
2.2.1 Synthesis of a symmetrically bridging μ -phosphide, its anion, and its cation.....	55
2.2.2 Synthesis of a new terminal phosphide of molybdenum.....	58
2.2.3 Reactions of $\text{PMo}(\text{N}[i\text{-Pr]Ar})_3$ (2-P).....	60
2.2.4 Synthesis and reactivity of $(\eta^3\text{-P}_3)\text{Mo}(\text{N}[i\text{-Pr]Ar})_3$ (2- $\eta^3\text{-P}_3$).....	61
2.3 Theoretical Section	62
2.4 Mechanistic Section.....	66
2.5 Conclusions.....	71
2.6 Future Directions	72
2.7 Experimental Section.....	73
2.7.1 General Considerations: Synthesis and Characterization.....	73
2.7.2 Preparation of compounds.....	73
2.7.3 Electrochemical Measurements.....	76
2.7.4 Crystallographic Structure Determinations.....	76
2.7.5 General Considerations: Stopped-flow kinetics	77
2.7.6 Theoretical Calculations.....	78
2.8 References.....	79

List of Figures

Figure 2.1: Molecular structure of [Na(THF)][2 ₂ -μ-P]	57
Figure 2.2: Electrochemical trace for 2 ₂ -μ-P	58
Figure 2.3: Molecular structure of 2-P	59
Figure 2.4: Selected molecular orbitals of [Na(THF)][2 ₂ -μ-P]	62
Figure 2.5: Selected molecular orbitals of PMo(NMe ₂) ₃	64
Figure 2.6: Selected molecular orbitals of (η ³ -P ₃)Mo(NMe ₂) ₃	65
Figure 2.7: UV-Vis spectra of 2 ₂ -μ-P, 1 , 2-P, and 2-η ³ -P ₃	66
Figure 2.8: Eyring plot of Reactions 1 through 5	68
Figure 2.9: Dependence of the observed pseudo-first-order rate constant on [P ₄] for Reaction 5	70

List of Schemes

Scheme 2.1: Cleavage modes of μ-phosphide 2 ₂ -μ-P.	56
Scheme 2.2: Reaction of 2-P with the “carbene” 2-CCPh	61
Scheme 2.3: Reactions of phosphorus and phosphorus-containing compounds with 1 and 3	67
Scheme 2.4: Proposed mechanism for reaction of P ₄ with molybdaziridine-hydride 1	71
Scheme 2.5: Thermochemical cycle for reaction of white phosphorus (P ₄) with molybdaziridine-hydride 1	72

List of Tables

Table 2.1: Selected bond distances and angles for [Na(THF)][2 ₂ -μ-P]	57
Table 2.2: Selected bond lengths and angles for 2-P	59
Table 2.3: Activation parameters for Reactions 1 through 5	69
Table 2.4: Crystallographic parameters for [Na(THF)][2 ₂ -μ-P] and 2-P.	77

2.1 Introduction

The reaction of $W_2(ONp)_6(HNMe_2)_2$ with white phosphorus yields two products, $(cyclo-\eta^3-P_3)W(ONp)_3(HNMe_2)$ and $W_3(\mu_3-P)(ONp)_9$ (Np = neopentyl).² Chisholm *et al.* proposed that the latter compound forms via the reaction of the starting material $W_2(ONp)_6(HNMe_2)_2$ with a transient terminal phosphide $PW(ONp)_3$, which was not observed spectroscopically. A “chop-chop” reaction of *tert*-butylphosphaalkyne (*t*-BuCP) with a mixture of $W(CO)_5(THF)$ and $W_2(O-t-Bu)_6$ resulted in formation of an asymmetric bridging phosphide, $[(t-Bu-O)_3W](\mu-P)[W(CO)_5]$.³ Again, the presence of a terminal phosphide was implicated in the reaction mechanism. This claim was supported by observation of a uniquely downfield ³¹P NMR spectroscopic signal assigned to $PW(O-t-Bu)_3$.

In 1995, back-to-back publications in *Angewandte Chemie, International Edition in English* revealed the first authentic examples of terminal phosphides including their structural characterization.^{4,5} Two of these novel terminal phosphides were synthesized by Zanetti *et al.* and were supported on molybdenum or tungsten by a bulky triamidoamine (tren, $[(Me_3SiNCH_2CH_2)_3N]^{3-}$) ligand.⁴ The structurally characterized molecule $PW(tren)^*$ was synthesized via addition of two equivalents of LiPPhH to $ClW(tren)$ followed by heating at 80 °C for 48 h.⁶ Laplaza *et al.* synthesized the other reported terminal phosphide by addition of 0.25 equiv white phosphorus (P_4) to the three-coordinate $Mo(N[t-Bu]Ar)_3$ (**3**) at room temperature (or lower) over the course of approximately 1 h.⁵ The latter example was an interesting and rare example of the activation of the element P_4 .

Isolation of these molecules permitted the subsequent synthesis of several derivatives of the terminal phosphide moiety. In the case of $PW(tren)$, derivatives include Lewis acid adducts of the lone pair on the terminal phosphide.^{6,7} Particularly, transition metal carbonyl compounds and gallium(III) chloride formed adducts with $PW(tren)$. In contrast, new element-element multiple-bond-forming reactions were achieved with $PMo(N[t-Bu]Ar)_3$ (**3-P**).⁸ Dimethyldioxirane, a potent oxygen-atom transfer reagent reacted with **3-P** forming the first example of a terminal phosphoryl **3-PO**.⁹ Sulfur or cyclohexene sulfide reacted with **3-P** forming a similar thiophosphoryl **3-PS**, and mesityl azide reacted with **3-P** forming a phosphinimine **3-PNMes**.⁵ Despite these interesting developments, neither $PM(tren)$ ($M = Mo, W$) or **3-P** were observed to undergo side-on $M-P$ bond activation.

For several years, these molecules were the only known examples of transition metal terminal phosphides.^{†,10,11} However, once molybdaziridine-hydride $Mo(H)(\eta^2-Me_2C=NAr)(N[i-Pr]Ar)_2$ (**1**) was developed as a masked form of the less-bulky $Mo(N[i-Pr]Ar)_3$ (**2**),¹² the synthesis of a less-sterically crowded terminal phosphide became an attractive goal. Potentially, this change in the ligand periphery would permit access to the $Mo-P$ bond and result in the ability to incorporate the phosphorus atom into organic

* This molecule was also synthesized using 2 equiv $LiP(SiMe_3)_2$.⁶

† White phosphorus also reacts with the molybdenum *tris*-amide $Mo(N[2-Ad]Ar)_3$, analogous to but bulkier than **3**, to form the corresponding terminal phosphide, $PMo(N[2-Ad]Ar)_3$.¹⁰

molecules via side-on reactivity and subsequent atom transfer. The synthesis of $\text{PMo}(\text{N}[i\text{-Pr}]\text{Ar})_3$ (**2-P**) proved to be less straightforward than the synthesis of **3-P**, but the terminal phosphide was still ultimately derived from the element. Herein is reported synthesis of **2-P** via reductive and oxidative cleavage pathways.

2.2 Results and Discussion

2.2.1 Synthesis of a symmetrically bridging μ -phosphide, its anion, and its cation.

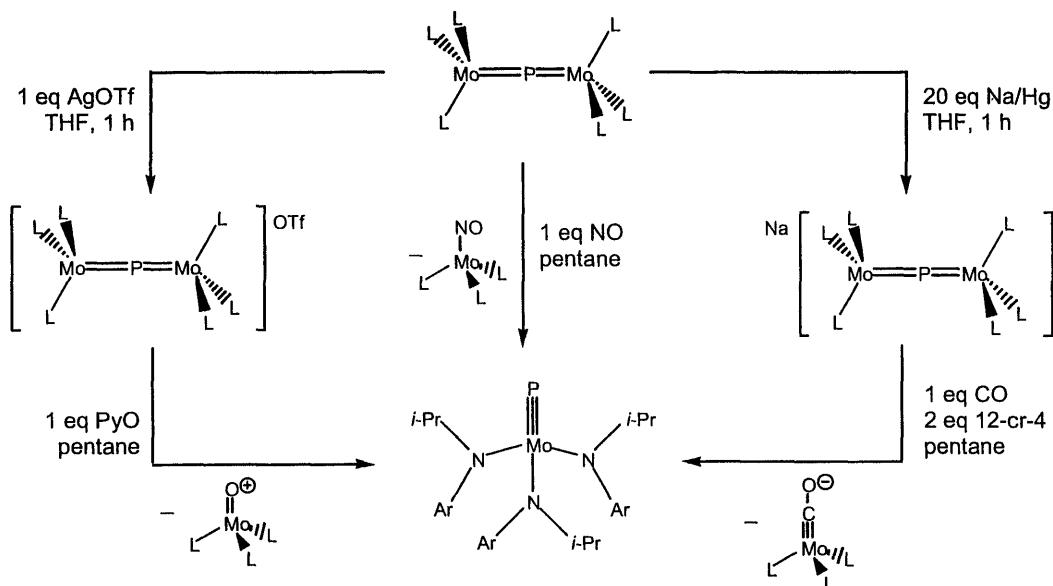
Reaction at room temperature of white phosphorus (P_4) with the bulky, three-coordinate molybdenum compound $\text{Mo}(\text{N}[t\text{-Bu}]\text{Ar})_3$ (**3**, $\text{Ar} = 3,5\text{-C}_6\text{H}_3\text{Me}_2$) has given rise exclusively to the terminal phosphide functionality $\text{PMo}(\text{N}[t\text{-Bu}]\text{Ar})_3$ (**3-P**).⁵ In contrast, slow addition of P_4 to molybdaziridine-hydride $\text{Mo}(\text{H})(\eta^2\text{-Me}_2\text{C}=\text{NAr})(\text{N}[i\text{-Pr}]\text{Ar})_2$ (**1**) in cold diethyl ether leads to a red-purple phosphide-bridged product $(\mu\text{-P})[\text{Mo}(\text{N}[i\text{-Pr}]\text{Ar})_3]_2$ (**2₂- μ -P**) in 74 % yield.^{1,12b,13} This compound is paramagnetic, with a solution magnetic moment $\mu_{\text{eff}} = 1.92 \mu_{\text{B}}$ corresponding to one unpaired electron.

Few symmetrically bridged P_1 compounds have been reported. Existing examples include the red, paramagnetic compound $(\mu\text{-P})[\text{W}(\text{tren}')_2]$ ($\text{tren}' = [(i\text{-PrNCH}_2\text{CH}_2)_3\text{N}]^{3-}$). This compound was synthesized from $\text{ClW}(\text{tren}')$ and two equivalents of $\text{LiP}(\text{SiMe}_3)_2$ at 100 °C for 48 h and was isolated in 43 % yield.^{13a} The $\mu\text{-P}$ functionality was proposed to result from P–Si bond cleavage. Another example of a symmetrically bridged P_1 compound is the paramagnetic species $(\text{Cp}^*_2\text{Zr})_2(\mu\text{-P})$, which was synthesized over several hours from $\text{Cp}^*_2\text{ZrCl}_2$, excess KH, and phosphine in THF.^{13c} This compound resulted from P–C bond cleavage and was isolated in 10% yield.

In contrast to the P–X bond cleavage routes to $(\mu\text{-P})[\text{W}(\text{tren}')_2]$ and $(\text{Cp}^*_2\text{Zr})_2(\mu\text{-P})$,^{13a,c} facile combination of $\text{PMo}(\text{N}[i\text{-Pr}]\text{Ar})_3$ (**2-P**) with reactive **1** could account for formation of **2₂- μ -P** (*vide infra*). This supposition seems reasonable since the symmetrically bridged, purple $(\mu\text{-P})[\text{Mo}(\text{N}[t\text{-Bu}]\text{Ar})_3]_2$ (**3₂- μ -P**) was formed at low temperature when **3-P** and **3** were combined.^{13b} Consequently, in order to isolate **2-P** and explore its reactivity compared to **3-P**, it must be synthesized in the absence of **1**. For this reason, a method was sought for splitting dinuclear **2₂- μ -P**.

Dr. Marc Johnson initially discovered that nitric oxide (NO) was able to effect quantitative bridge cleavage to give equimolar amounts of the desired terminal phosphide **2-P** and byproduct nitrosyl $(\text{ON})\text{Mo}(\text{N}[i\text{-Pr}]\text{Ar})_3$ (**2-NO**) (Scheme 2.1, middle).^{1,12b} Full characterization and reactivity studies of **2-P** were precluded, however, because similar solubility properties made separation from **2-NO** difficult. An alternative method for isolation of **2-P** was envisioned based on the isoelectronic character of the anion $[(\text{OC})\text{Mo}(\text{N}[i\text{-Pr}]\text{Ar})_3]^-$ (**[2-CO]⁻**) and the neutral species **2-NO**. In this case, the byproduct **[2-CO]⁻** should be separable from **2-P** in hydrocarbon solvents due to its monoanionic charge. Therefore, one electron reduction and subsequent carbonylation of **2₂- μ -P** were investigated (Scheme 2.1, right).

Scheme 2.1: Cleavage modes of μ -phosphide 2_2 - μ -P; L = N[*i*-Pr]Ar, Ar = 3,5-dimethylphenyl.



Excess sodium amalgam (0.5 % w/w) in THF under a nitrogen atmosphere proved an effective regimen for high-yield isolation of the anion $[\text{Na}(\text{THF})][(\mu\text{-P})\text{Mo}_2(\text{N}[i\text{-Pr}]\text{Ar})_6]$ ($[\text{Na}(\text{THF})][2_2\text{-}\mu\text{-P}]$) (Scheme 2.1, right). The red-purple contact ion pair $[\text{Na}(\text{THF})][2_2\text{-}\mu\text{-P}]$ crystallized in space group $P2_1/c$ as large blocks from pentane. In order to stabilize the sodium cation in the solid state, one aryl group flipped to interact in a π -fashion with the alkali metal (Figure 1).¹⁴ The Mo–P–Mo bridge was thereby desymmetrized, resulting in modestly different Mo–P distances (2.183(2) and 2.197(2) Å). The Mo–P bond distances in the neutral and anionic species are similar. In the solid-state structure of neutral $2_2\text{-}\mu\text{-P}$, the phosphorus atom lies on a crystallographic inversion center making the Mo–P distances identical (2.2164(4) Å).^{1,12b} The bond length similarity is expected, since the electron introduced upon reduction occupies a primarily non-bonding orbital (rather than a Mo–P–Mo bonding orbital) (Figure 2.4). In both $2_2\text{-}\mu\text{-P}$ and $[\text{Na}(\text{THF})][2_2\text{-}\mu\text{-P}]$, the Mo–P distances are shorter than those observed for $3_2\text{-}\mu\text{-P}$ (2.2430(6) Å),^{13b} attributable to steric considerations.

Interestingly, encapsulation of the sodium counteranion by addition of 2 equiv of the crown ether 12-c-4 to $[\text{Na}(\text{THF})][2_2\text{-}\mu\text{-P}]$ resulted in oxidation of the molecule and formation of sodium metal; neutral $2_2\text{-}\mu\text{-P}$ was observed by ^1H NMR spectroscopy. This behavior is reminiscent of bridging- N_1 compounds of **2** that spontaneously oxidize (forming sodium metal) when solvent is removed.¹⁵ Presumably, in the case of nitrogen, the aromatic periphery of the ligands cannot accommodate the intimate presence of the alkali metal cation due to the smaller size of the bridging atom and the anion is not stable

when the cation is separated. Cation-anion separation[‡] may be achieved by using a different cation.¹⁶ For example, cesium more readily gives up its electron (lower first ionization energy) than sodium. Therefore, Cs⁺ should not be as readily reduced to cesium metal with formation of neutral 2₂-μ-P. Furthermore, in the inorganic electride literature, it has been noted that cryptands are more able to stabilize the cation-anion separation than crown ethers since they are not as easily reduced.¹⁶

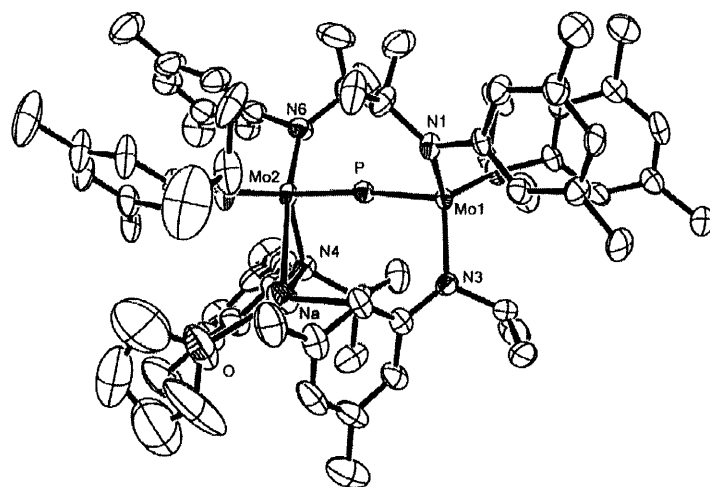


Figure 2.1: Molecular structure of [Na(THF)][2₂-μ-P] (35% thermal ellipsoids). Hydrogen atoms are omitted for clarity. Selected bond distances and angles are listed in Table 1.

<i>Bond Lengths (Å)</i>		<i>Bond Angles (deg)</i>	
Mo1-P	2.183(2)	Mo1-P-Mo2	173.87(10)
Mo2-P	2.197(2)	P-Mo1-N1	100.6(2)
Mo1-N1	2.051(6)	P-Mo1-N2	101.5(2)
Mo1-N2	2.017(5)	P-Mo1-N3	100.6(2)
Mo1-N3	1.970(6)	P-Mo2-N4	101.5(2)
Mo2-N4	2.059(6)	P-Mo2-N5	94.7(2)
Mo2-N5	2.059(6)	P-Mo2-N6	97.9(2)
Mo2-N6	1.959(6)	O-Na-N4	93.6(3)
N4-Na	2.908(8)	O-Na-N5	111.6(3)
N5-Na	2.702(7)	P-Mo1-Na	110.51(9)
Na-O	2.252(8)	P-Mo2-Na	65.66(8)

Table 2.1: Selected bond lengths and angles for [Na(THF)][2₂-μ-P].

[‡] Examples of this can be found in the literature of alkali metal electrides.¹⁶

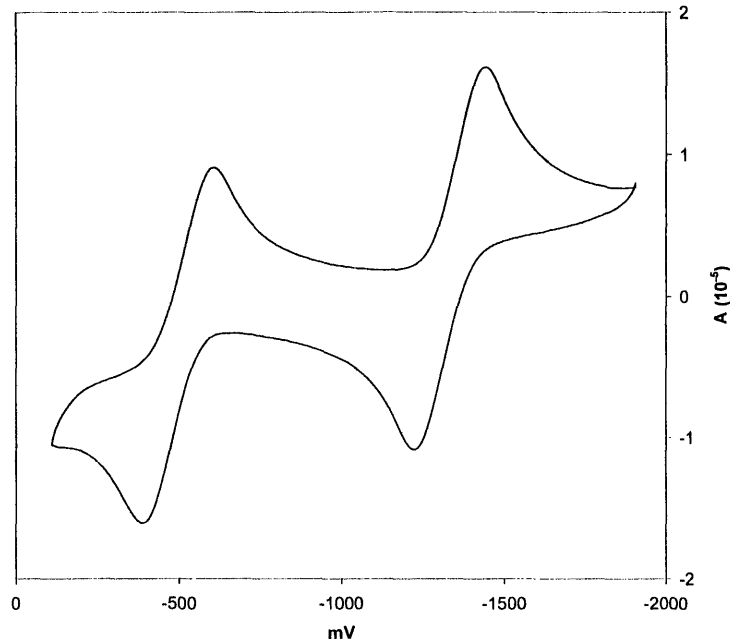


Figure 2.2: Electrochemical trace for $2_2\text{-}\mu\text{-P}$. Data were collected in THF solution with 0.5 M NBu_4PF_6 electrolyte with reference to ferrocene-ferrocenium ($\text{Fc}/\text{Fc}^+ = 0$ V).

The bridging phosphide $2_2\text{-}\mu\text{-P}$ is also susceptible to one electron oxidation, creating another pathway for the synthesis of the desired terminal phosphide 2-P . Electrochemical investigation of neutral $2\text{-}\mu\text{-P}$ (Figure 2.2) revealed a clean, reversible reduction wave ($E^{\circ'} = -1.33$ V vs. Fc/Fc^+) and a clean, reversible oxidation wave ($E^{\circ'} = -0.50$ V). In contrast, $(\mu\text{-P})[\text{W}(\text{tren}')_2]$ is not susceptible to reversible oxidation electrochemically or chemically (using ferrocenium tetrafluoroborate).^{13a} The observed oxidation wave for $2_2\text{-}\mu\text{-P}$ indicated that the use of the oxidizing agent silver triflate (AgOTf)¹⁷ would be sufficient to form the product $[(\mu\text{-P})\text{Mo}_2(\text{N}[i\text{-Pr}]\text{Ar})_6][\text{OTf}]$ ($[2\text{-}\mu\text{-P}][\text{OTf}]$) (Scheme 2.1, left). Experimentally, reaction of $2\text{-}\mu\text{-P}$ with AgOTf in THF indeed resulted in the desired product, $[2_2\text{-}\mu\text{-P}][\text{OTf}]$, with concomitant formation of silver(0).

2.2.2 Synthesis of a new terminal phosphide of molybdenum.

Addition of stoichiometric carbon monoxide to a red-purple THF solution of $[\text{Na}(\text{THF})][2_2\text{-}\mu\text{-P}]$ at 25 °C resulted in quantitative cleavage of the phosphide bridge and formation of a yellow solution. Because of the ionic nature of the byproduct $[2\text{-CO}]^-$, it was easily separated from the desired terminal phosphide $\text{PMo}(\text{N}[i\text{-Pr}]\text{Ar})_3$ (2-P). This was done by fractional crystallization from cold pentane, whereby orange $[\text{Na}(\text{THF})_x][2\text{-CO}]$ crystallized from cold pentane before 2-P did. Separation was more reliably achieved via precipitation and subsequent filtration after the addition of 12-c-4 (2 equiv

based on Na) to produce yellow-brown $[\text{Na}(12\text{-c-4})_2][2\text{-CO}]$.^{1,15} This molecule was independently synthesized by addition of one atmosphere of CO to **1** followed by reduction using sodium amalgam, using a method established for synthesis of $[3\text{-CO}]^-$.¹⁸

Following this series, where CO was used to cleave $[\text{Na}(\text{THF})][2\text{-}\mu\text{-P}]$ and NO was used to cleave **2-}\mu\text{-P}**, O₂ or an O₂-surrogate was chosen to cleave the oxidized μ -phosphide $[2_2\text{-}\mu\text{-P}][\text{OTf}]$ (Scheme 2.1, left). In practice, pyridine-*N*-oxide provided the cleanest cleavage reaction, forming **2-P** and the cation $[2\text{-O}][\text{OTf}]$. Compound **2-O** was investigated electrochemically, and the voltammogram displayed a reversible oxidation wave at -0.66 V. Hence, compound $[2\text{-O}][\text{OTf}]$ was synthesized independently by addition of pyridine-*N*-oxide to **1**, followed by oxidation using silver triflate. This method is similar to that employed for the synthesis of $[3\text{-O}][\text{OTf}]$.¹⁹ Overall, this oxidative route to **2-P** is not as clean as the reductive pathway, and the latter method is used preparatively.

X-ray quality yellow blocks of **2-P** were found to crystallize from pentane in the space group $P2_12_12_1$ (Figure 2.3). Two independent molecules were found in the unit cell with identical bond lengths and angles (within 3σ). The Mo–P vector generally points into the aromatic portion of the next molecule’s ligand periphery in a head-to-tail fashion with a P–Mo distance of greater than 8.5 Å. This packing mode is similar to that found in $\text{PMo}(\text{N}[t\text{-Bu}]\text{Ar})_3$ (**3-P**). The Mo–P distance of $2.116(3)$ Å (Table 2.2) is in close agreement with those observed for previously reported **3-P** ($2.119(4)$ Å),⁵ $\text{PMo}(\text{N}[2\text{-Ad}]\text{Ar})_3$ ($2.107(3)$ Å),[†] and $\text{PW}(\text{tren})$ ($2.162(4)$ Å).⁴ This seems to indicate that the electronic contributions from the fragments $\text{Mo}(\text{N}[i\text{-Pr}]\text{Ar})_3$ (**2**), $\text{Mo}(\text{N}[t\text{-Bu}]\text{Ar})_3$ (**3**), and $\text{Mo}(\text{N}[2\text{-Ad}]\text{Ar})_3$ are approximately equal despite the slight variation of the ligands’ aliphatic groups.

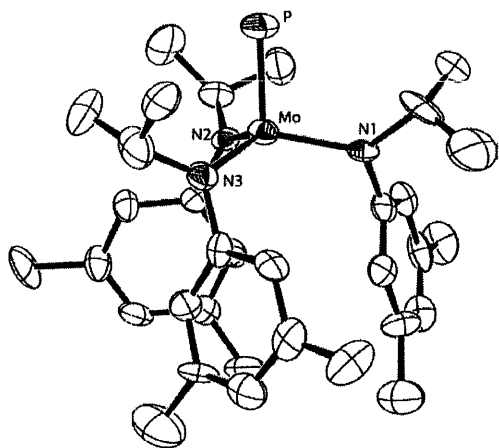


Figure 2.3: (Left) Molecular structure of **2-P** (35% thermal ellipsoids). One of two independent molecules is shown. The bond lengths and angles in the second molecule are identical within 3σ . Hydrogen atoms are omitted for clarity.

<i>Bond Lengths (Å)</i>		<i>Bond Angles (deg)</i>	
Mo–P	2.116(3)	N1–Mo–P	104.1(3)
Mo–N1	1.935(9)	N2–Mo–P	102.0(3)
Mo–N2	1.978(10)	N3–Mo–P	105.1(3)
Mo–N3	1.971(10)		

Table 2.2: Selected bond lengths and angles for **2-P**.

The ³¹P NMR resonance at $\delta = 1256$ ppm for **2-P** is similar to the values of $\delta = 1216$ and 1346 ppm, respectively, for the aforementioned compounds $\text{PMo}(\text{N}[t\text{-Bu}]\text{Ar})_3$ and $\text{PW}(\text{tren})$. A ³¹P NMR shift calculation on the model compound $\text{PMo}(\text{NMe}_2)_3$

revealed a similar value, $\delta_{\text{iso}} = 1250$ ppm ($\delta_{11} = 1841$ ppm, $\delta_{22} = 1841$ ppm, $\delta_{33} = 70$ ppm). The large downfield shift results from large paramagnetic contributions to δ_{11} and δ_{22} .[§] These are derived from rotational mixing in the presence of an applied field of HOMO-2 (σ bond, P p_z - Mo d_z^2) with the degenerate LUMO (π^* , P p_x - Mo d_{xz} and P p_y - Mo d_{yz}) (see Theoretical Section).^{20,21}

2.2.3 Reactions of $\text{PMo}(\text{N}[i\text{-Pr}]\text{Ar})_3$ (2-P).

As proposed earlier, terminal phosphide 2-P rapidly reacts with molybdaziridine-hydride 1 to form $2_2\text{-}\mu\text{-P}$. Similarly, 2-P reacts with bulky $\text{Mo}(\text{N}[t\text{-Bu}]\text{Ar})_3$ (3) to form the asymmetrically bridged $(\text{Ar}[i\text{-Pr}]\text{N})_3\text{Mo}(\mu\text{-P})\text{Mo}(\text{N}[t\text{-Bu}]\text{Ar})_3$ (2-P-3). This compound is red-purple, similar to the symmetrically bridged $2_2\text{-}\mu\text{-P}$; the two compounds have comparable UV-Vis spectra ($2_2\text{-}\mu\text{-P}$: $\lambda = 340, 500$ nm; 2-P-3: $\lambda = 350, 520$ nm). Also like $2_2\text{-}\mu\text{-P}$, compound 2-P-3 reacts with NO. Addition of 1 atm of NO to a solution of 2-P-3 resulted in exclusive formation of 2-NO and 3-P in a 1:1 ratio. In other words, the phosphorus atom is effectively transferred from 2-P to 3 in a manner controlled by the steric accessibility of the two molybdenum atoms; it can be asserted that the molybdenum center supported by $\text{N}[i\text{-Pr}]\text{Ar}$ ligands is more easily accessed by an incoming molecule of NO than the molybdenum center supported by $\text{N}[t\text{-Bu}]\text{Ar}$ ligands. Compound 2-P-3 differs significantly from $3_2\text{-}\mu\text{-P}$, in that the latter is only stable at very low temperatures. An X-ray crystallographic structural study of red-purple crystals of 2-P-3 grown from cold pentane revealed an end-over-end disorder. This made determination of the two Mo-P bond distances impossible; the phosphorus atom occupied a position between the two molybdenum atoms at a distance (2.2297 Å) that is the average of the corresponding distance in $2_2\text{-}\mu\text{-P}$ and $3_2\text{-}\mu\text{-P}$.

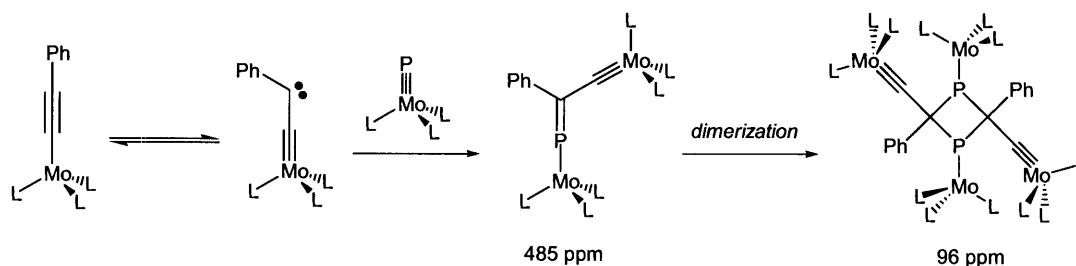
Other reactivity of 2-P was discovered to be limited despite the decrease in the steric protection of the Mo-P triple bond. Dr. Marc Johnson had previously discovered that 2-P (contaminated with a significant amount of 2-NO) does not react with internal alkynes.¹² Now that 2-P can be isolated in pure form, this conclusion was verified; 2-P does not react with internal alkynes even at elevated temperature and/or in neat alkyne solution. Additionally, 2-P is not susceptible to one-electron reduction by sodium amalgam or $\text{Ti}(\text{N}[t\text{-Bu}]\text{Ar})_3$ ²² or two-electron reduction by $\text{V}(\text{N}[\text{R}]\text{Ar})_3$ ($\text{R} = i\text{-Pr}, t\text{-Bu}$).²³ Terminal phosphide 2-P is also not reactive toward mild oxidizing agents such as thallium(I) triflate, carbon dioxide, and diphenyl disulfide.

Functionalization of the nitrile carbon of benzonitrile in the coordination sphere of 3 has recently been achieved.²⁴ The η^2 -benzonitrile adduct²⁵ of 3 reacted with compounds such as diphenyl disulfide to form a thiobenzimidate. This product could also result from the addition of carbene $\text{C}(\text{Ph})(\text{SPh})$ to the terminal nitride $\text{NMo}(\text{N}[t\text{-Bu}]\text{Ar})_3$ (3-N). Addition of carbenes to terminal phosphides has not been documented, although it has been investigated for a variety of P(V) compounds.²⁶

[§] This is comparable to the computed contributions for 3-N.²⁰

It also has recently been reported that the deprotonation of $[(\eta^2\text{-PhCCH})\text{Mo}(\text{N}[\textit{i}\text{-Pr}]\text{Ar})_3]\text{I}$ using sodium hexamethyldisilazide results in a carbon-carbon bond forming reaction via reductive coupling of $(\text{PhCC})\text{Mo}(\text{N}[\textit{i}\text{-Pr}]\text{Ar})_3$ (**2-CCPh**).²⁷ Although acetylide **2-CCPh** contains a linear $\text{C}_\alpha\text{-C}_\beta\text{-C}_{\text{Ph}}$ bond angle in the solid state,²⁸ its dimerization is proposed to proceed as a consequence of carbene-like character at the β carbon. This bulky “carbene” has been trapped by PMe_3 .²⁸ It does not react with bulky **3-P**, but reacts in minutes with **2-P** to form a green compound (Scheme 2.2). Attempts to isolate this compound have not yet succeeded, but structural information was gleaned from the ^{31}P NMR spectrum. Monitoring a C_6D_6 solution of **2-P** and **2-CCPh** by ^{31}P NMR spectroscopy revealed several new features after 10 min. Some unreacted starting material ($\delta = 1256$ ppm) was joined by a prominent peak at $\delta = 485$ ppm and a smaller peak at $\delta = 96$ ppm. After 4 h, the peak at 485 ppm had disappeared and only the peak at 96 ppm remained. (A small amount of unreacted **2-P** was present after all **2-CCPh** was consumed. The dimer of **2-CCPh** was observed by ^1H NMR, thereby accounting for the unreacted **2-P**.) The observed ^{31}P NMR shifts are comparable to that observed for $\text{Ph}_2\text{C}=\text{P-}t\text{-Bu}$ (289.6 ppm) and its dimer, the corresponding 1,3-diphosphetane (30.1 ppm).²⁹ This indicates that the signals observed during the reaction of **2-P** and **2-CCPh** likely correspond to the carbene addition product (485 ppm) and its dimer (96 ppm). Potentially, dimerization could be precluded by judicious variation of the acetylide’s phenyl group substitution. Synthesis of the *ortho*-tolyl derivative is currently underway.

Scheme 2.2: Reaction of **2-P** with the “carbene” **2-CCPh**.



2.2.4 Synthesis and reactivity of $(\eta^3\text{-P}_3)\text{Mo}(\text{N}[\textit{i}\text{-Pr}]\text{Ar})_3$ (**2- $\eta^3\text{-P}_3$**).

Another important product in the reaction of molybdaziridine-hydride **1** with P_4 is $(\eta^3\text{-P}_3)\text{Mo}(\text{N}[\textit{i}\text{-Pr}]\text{Ar})_3$ (**2- $\eta^3\text{-P}_3$**).^{12b} This yellow, flaky compound was synthesized when a toluene solution of **1** was added slowly to a toluene solution of P_4 . When the reaction mixture was concentrated and chilled, the product was filtered away. Compound **2- $\eta^3\text{-P}_3$** is only sparingly soluble in pentane so the simultaneously-formed **2- $\mu\text{-P}$** can be washed away with minimal product loss. Compound **2- $\eta^3\text{-P}_3$** reacts with 5 equiv of molybdaziridine-hydride **1** to generate 3 equiv of **2- $\mu\text{-P}$** .^{12b} Probing compound **2- $\eta^3\text{-P}_3$** by cyclic voltammetry revealed a reversible reduction wave at -2.03 V. However, **2- $\eta^3\text{-P}_3$** is not even susceptible to reduction by strong reducing agents (e.g. KC_8) to form **2-P**.

Reaction of $2-\eta^3\text{-P}_3$ with 2 equiv $\text{Mo}(\text{N}[t\text{-Bu}]\text{Ar})_3$ (**3**) resulted in some formation of the bulky terminal phosphide **3-P**, but the major product was the mixed bridging- P_1 compound (**2-P-3**) mentioned previously. Extremely slow addition of **3** to $2-\eta^3\text{-P}_3$ ideally would result in formation of a 1:2 mixture of **2-P** and **3-P**. However, the presence of excess **3** when **2-P** is generated will quickly result in the mixed μ -phosphide **2-P-3**.

Interestingly, addition of the sulfur-atom transfer agents S_8 , cyclohexene sulfide, and ethylene sulfide to **2-P** resulted in some formation of $2-\eta^3\text{-P}_3$ (which does not react with S_8). This contrasts with the bulky terminal phosphide **3-P**, which reacted with these reagents to form an unprecedented terminal PS moiety.⁵

2.3 Theoretical Section

The frontier orbitals of $2_2\text{-}\mu\text{-P}$ and **2-P-3** are certainly similar in composition to those in $3_2\text{-}\mu\text{-P}$.^{13b} In $3_2\text{-}\mu\text{-P}$, there is a delocalization of electron density over the phosphide bridge. The orbitals contributing to this include the d_{xz} and d_{yz} orbitals of both molybdenum atoms and the p_x and p_y orbitals of phosphorus. The major difference in the orbitals of $2_2\text{-}\mu\text{-P}$ is the greater extent of orbital overlap due to closer approach of the two molybdenum centers. The same is can be said for **2-P-3**, but the orbital contributions also can be expected to be slightly skewed due to the asymmetric nature of the bridge.

All-electron density functional theory calculations on the crystallographic parameters of $[\text{Na}(\text{THF})][2_2\text{-}\mu\text{-P}]$ showed that the molecule's HOMO and nearly degenerate HOMO-1 are mostly localized on the molybdenum atoms (Figure 2.4). The electrons are contained in either d_{xz} and d_{yz} orbitals, rendering a rather symmetrical electronic distribution. The LUMO is based on the d_{z^2} orbitals from both molybdenum atoms, with some mixing from the molybdenum p orbitals. Negligible contributions from phosphorus are observed for these frontier molecular orbitals.



Figure 2.4: Molecular orbitals of the anion $[\text{Na}(\text{THF})][2_2\text{-}\mu\text{-P}]$ calculated using full electronic configuration of all atoms on X-ray crystallographic coordinates. Left, HOMO; right, HOMO-1.

The frontier molecular orbitals of the model compound $\text{PMo}(\text{NH}_2)_3$ have been discussed.²¹ This model system was calculated using the GAUSSIAN94 package, the B3LYP3 functional, and the lanl2dz+f and 6-311G** basis sets. It was found that the HOMO-1 was a $\text{P}(p_z)\text{-Mo}(d_z^2)$ σ orbital, the HOMO was a set of degenerate $\text{P}(p_x, p_y)\text{-Mo}(d_{xz}, d_{yz})$ π orbitals, and the LUMO was a set of degenerate $\text{P}(p_x, p_y)\text{-Mo}(d_{xz}, d_{yz})$ π^* orbitals. Slightly different results were obtained when the model compound $\text{PMo}(\text{NMe}_2)_3$ was investigated using *ADF2002.02* using ZORA(V) basis sets (see Experimental Section for details). In this case, the HOMO is a set of amide lone pairs, $\text{N}(p_x, p_y)$. The HOMO-1 represents a degenerate set of π orbitals, $\text{P}(p_x, p_y)\text{-Mo}(d_{xz}, d_{yz})$, and the HOMO-2 is the P-Mo σ bond, $\text{P}(p_z)\text{-Mo}(d_z^2)$ (Figure 2.5). Like in the simpler model system, the LUMO is a degenerate set of π^* orbitals, $\text{P}(p_x, p_y)\text{-Mo}(d_{xz}, d_{yz})$.

An investigation of the frontier orbitals $2\text{-}\eta^3\text{-P}_3$ was also completed using density functional theory. The calculation utilized simplified ligands (i.e., NMe_2), and it was completed in C_{3v} symmetry. The HOMO is primarily amide lone pairs and the LUMO is the d_z^2 orbital of molybdenum. LUMO+1 represents mainly the degenerate $d_{x^2-y^2}$ and d_{xy} orbitals interacting with small components of P-P antibonding character. HOMO-1 is a set of degenerate orbitals reflecting a backbonding interaction from the metal to the *cyclo*- P_3 ligand. The perpendicular d_{xz} and d_{yz} orbitals interact with the compatible P_3^+ orbitals that have one node (Figure 2.6). HOMO-4 and HOMO-5 are the aromatic P_3^+ orbitals. This orbital analysis is similar to one derived by a Fenske-Hall molecular orbital calculation of $(\eta^3\text{-P}_3)\text{W}(\text{ONp})_3(\text{HNMe}_2)$ presented by Chisholm *et al.*³⁰ In that case, the tungsten d_z^2 , d_{xz} , and d_{yz} orbitals interacted with the P_3^+ frontier orbitals. There is no evidence for mixing in of the P-based s orbitals in the frontier orbital framework for $2\text{-}\eta^3\text{-P}_3$.³¹ This orbital analysis of $2\text{-}\eta^3\text{-P}_3$ indicates why very little reactivity is observed from the *cyclo*- P_3 portion of this compound, since neither the most acidic nor most basic portions of the molecule include P-P bonding (Figure 2.6).

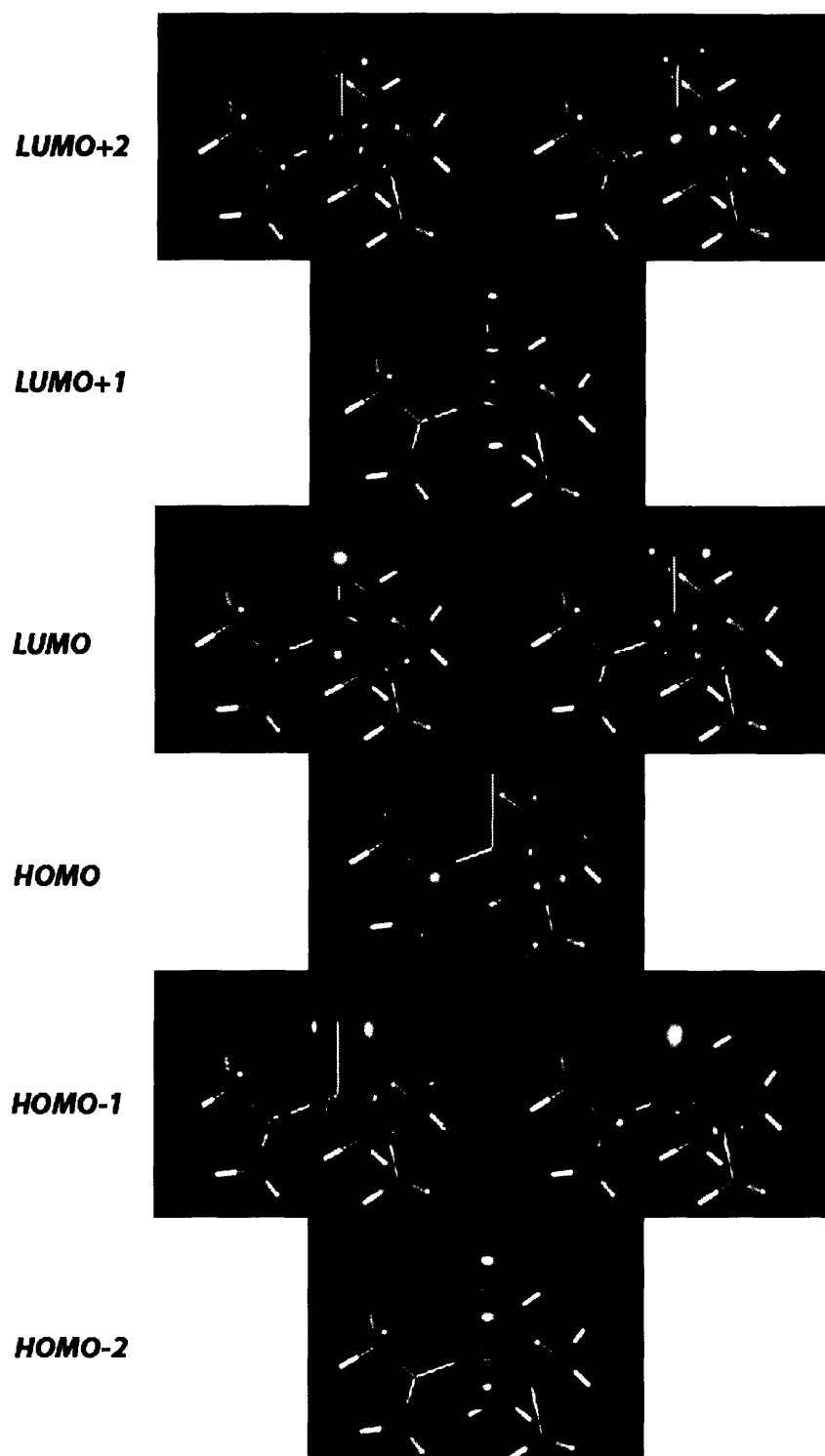


Figure 2.5: Selected molecular orbitals of $\text{PMo}(\text{NMe}_2)_3$ calculated in C_{3v} symmetry.

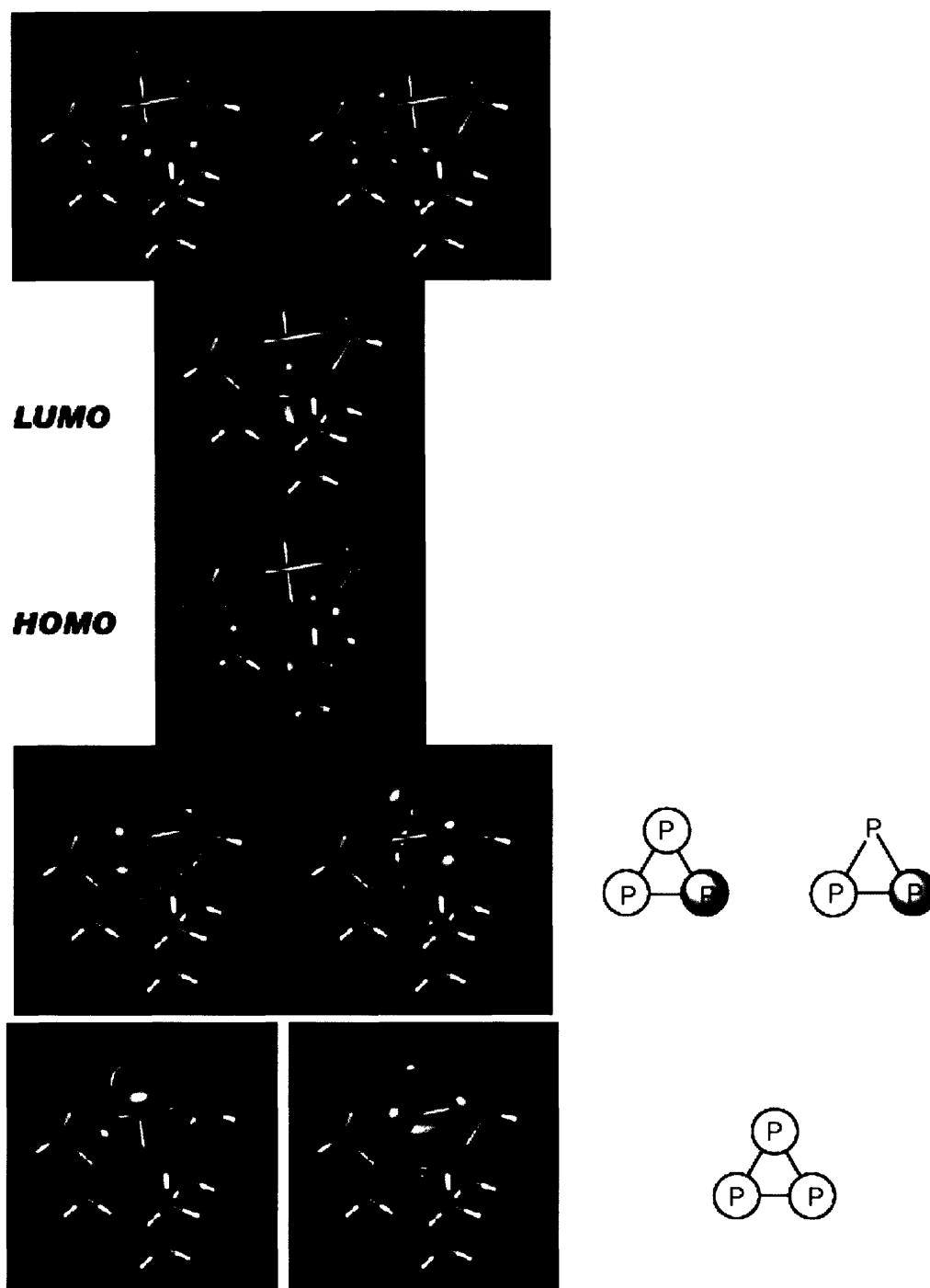


Figure 2.6: Selected molecular orbitals of $(\eta^3\text{-P}_3)\text{Mo}(\text{NMe}_2)_3$ calculated in C_{3v} symmetry. (Top) Degenerate LUMO+1, LUMO, HOMO, degenerate HOMO-1, HOMO-4 (bottom left), and HOMO-5 (bottom right). Representations of the frontier molecular orbitals of the P_3^+ π -system are depicted on the far right.

2.4 Mechanistic Section³²

Transition metal complexes have been documented to both coordinate intact P₄ tetrahedra and cleave one or more of the substrate's P–P bonds.³³ In the cases where bond cleavage occurs, the extent of activation depends on the number of electrons provided by the incoming metal complex. For example, one phosphorus-phosphorus bond of P₄ oxidatively adds to the fragment [Cp*Co(CO)] under thermolytic conditions to form (η²-P₄)Co(CO)Cp*.³⁴ The η²-P₄ moiety results from two-electron reduction of white phosphorus.³⁵ Successive two-electron reductions cleave more of the P–P bonds; three such reductions can lead to P₃ and P₁ fragments. An interesting example of a system that is arrested along the pathway to P₃/P₁ generation is [{Cp*Ni}(η^{3:1}-P₄){Cp*Ni(CO)}{Cr(CO)₅}₃].³⁶ In this compound, two sides of the P₄ tetrahedron have been cleaved. Three of the P atoms were coordinated to one NiCp* unit while the remaining P atom was coordinated by Cp*Ni(CO). When this compound was photolyzed, two products were formed, one containing a (η³-P₃)NiCp* moiety and the other containing a Ni₂P₂ pseudo-tetrahedral moiety. The latter compound was proposed to form via dimerization of an unobserved [(OC)₅Cr]←P≡NiCp* intermediate.^{**37}

There are very few examples of this P₃/P₁ unsymmetrical cleavage of white phosphorus. Here, the activation of P₄ by molybdaziridine-hydride **1**, with its formation of 2₂-μ-P and 2-η³-P₃, serves to considerably enhance this area of the chemical literature. Furthermore, few examples of mechanistic investigations of reactions of white phosphorus have been reported.^{33,38} As in Chapter 1,³⁹ the rapid reactions of interest (Scheme 2.3) were probed using stopped-flow UV-Vis spectrometry kinetic measurements by Drs. Elena Rybak-Akimova and Olga Kryatova at Tufts University. The reactions listed below were monitored at 500 nm, where the spectral changes were expected to be maximal (Figure 2.7).

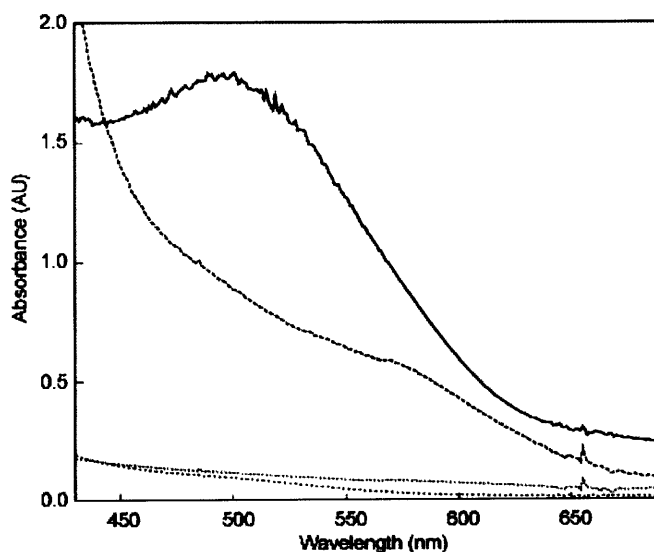
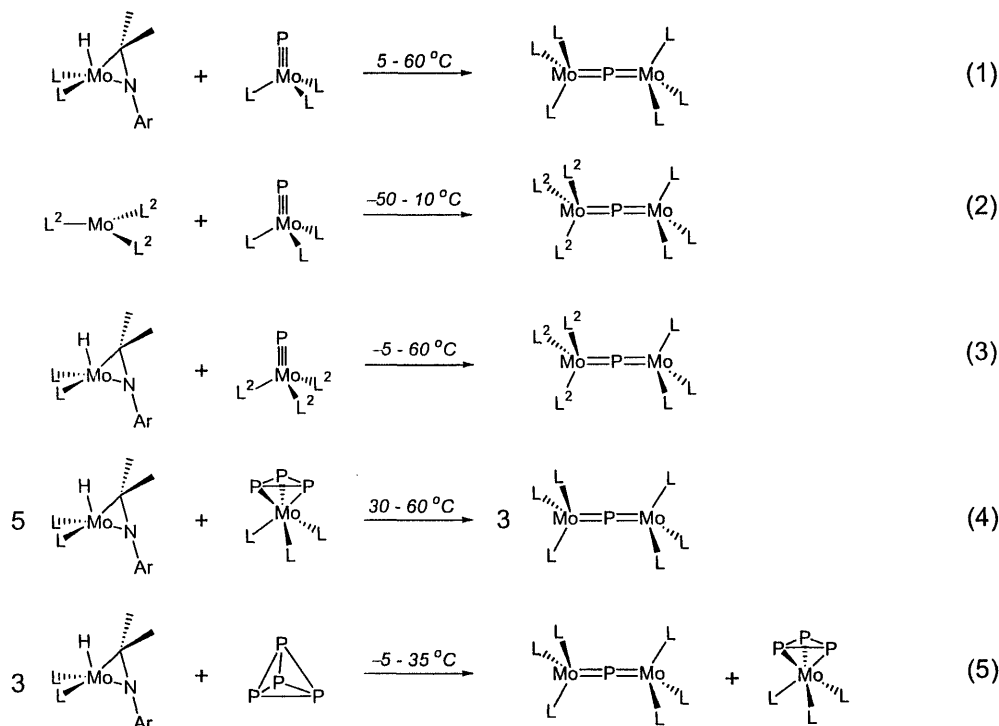


Figure 2.7: UV-Vis spectra of 2₂-μ-P (top), **1**, 2-P, and 2-η³-P₃ (bottom); 0.3 mM solutions in toluene.

** See Chapter 3 for examples of authentic terminal phosphide dimerization.³⁷

Scheme 2.3: Balanced reactions of phosphorus and phosphorus-containing compounds with **1** and **3**. The temperature range over which each reaction was studied is indicated over the arrow. L = N[*i*-Pr]Ar; L² = N[*t*-Bu]Ar.



The synthesis of symmetrically bridged $2_2\text{-}\mu\text{-P}$ from molybdaziridine-hydride **1** and terminal phosphide **2-P** is shown in Scheme 2.3, Reaction 1. This reaction was mentioned above as a possible route to the formation of $2_2\text{-}\mu\text{-P}$ during the reaction of white phosphorus with **1**. This reaction was studied from 10 to 60 °C in toluene under second order conditions ($[\mathbf{1}] = [\mathbf{2-P}] = 0.15 \text{ mM}$ after mixing in the stopped flow cell). Upon mixing the solutions of **1** and **2-P**, increasing absorbance was observed in the entire spectrum with a maximum at 500nm. The same spectral changes were observed at all studied temperatures. The reaction was clean, kinetic traces were best fit to a second-order process, and no intermediates were observed. Rate constants were measured at several temperatures (Table 2.3) and activation parameters were calculated from an Eyring plot (Figure 2.8). The rate limiting step was determined to be a bimolecular process with a moderately positive activation enthalpy ($\Delta H^\ddagger = 10.5 \pm 0.5 \text{ kcal}\cdot\text{mol}^{-1}$) and a modestly negative activation entropy ($\Delta S^\ddagger = -11 \pm 2 \text{ eu}$). This may be consistent with an associative transition state. However, the associative transition state unambiguously proposed for the reaction of **1** with AdNC (Chapter 1)³⁹ has a lower activation enthalpy ($\Delta H^\ddagger = +4.5 \pm 0.5 \text{ kcal}\cdot\text{mol}^{-1}$) and a more negative activation entropy ($\Delta S^\ddagger = -24 \pm 4 \text{ eu}$) than Reaction 1. The significantly less negative ΔS^\ddagger in the case of Reaction 1 might be explained by simultaneous binding of substrate and molybdaziridine-hydride ring-opening reaction (i.e., associative interchange).

Reaction between terminal phosphide **2-P** and bulky *tris*-amide **3** (Reaction 2) has a second-order process as its rate limiting step. Over all temperatures intervals studied from -50 to 10 °C, a maximum absorbance was observed at *ca.* 500 nm. Reaction 2 is characterized by a low activation enthalpy ($\Delta H^\ddagger = 2.7 \pm 0.4$ kcal·mol $^{-1}$) and large negative entropy of activation ($\Delta S^\ddagger = -33 \pm 4$ eu, Table 2.3). The rate of Reaction 2 and its activation parameters are very similar to those in the reaction of **3** with diphenyl ditelluride ($\Delta H^\ddagger = 2.8$ kcal·mol $^{-1}$; $\Delta S^\ddagger = -34$ eu), and it has bimolecular activation of substrate as its rate-limiting step.²⁴ This implies that the rate-limiting step of Reaction 2 is coordination of **2-P**. It is interesting to note that formation of the asymmetrical **2-P-3** according to Reaction 2 is significantly faster (approximately 15 times faster at 25 °C, Table 2.3) than formation of symmetric **2₂- μ -P** complex (Reaction 1). As suggested previously, from this we can assume that ring opening of the molybdaziridine-hydride impedes the reaction.³⁹

Kinetic studies on formation of **2-P-3** were also performed starting from **3-P** and **1** (Reaction 3). Spectral changes observed upon mixing of the reagents are similar to those for the reaction between **2-P** and **3** (Reaction 2). This reaction is also a clean, second-order process, but, surprisingly, it is slower than Reactions 1 and 2 (Table 2.3). The activation enthalpy is 2 kcal·mol $^{-1}$ smaller than that for the reaction between **2-P** and **1** (Reaction 1), and the activation entropy is significantly more negative (-22 vs. -11 eu). The difference in activation entropy may have arisen from steric congestion in the transition state due to the bulkier terminal phosphide **3-P**.

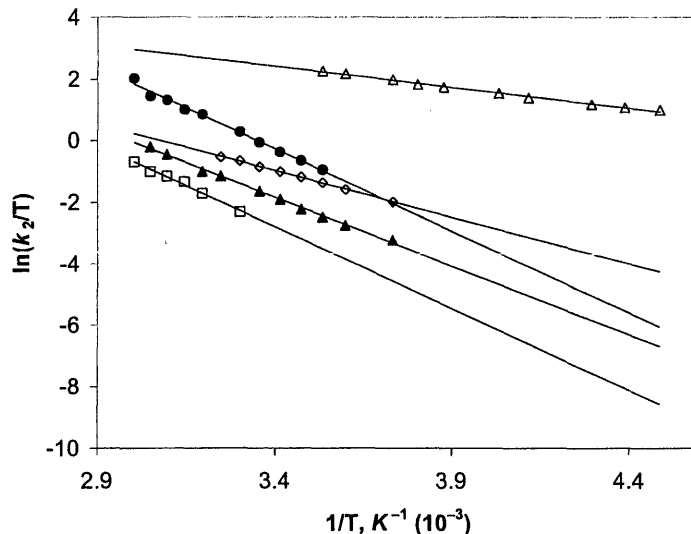


Figure 2.8: Eyring plot of Reactions 1 (black circle), 2 (open triangle), 3 (black triangle), 4 (open square), and 5 (open diamond).

Table 2.3: Activation parameters for Reactions 1 through 5. The rate constants that were calculated from Eyring plots are italicized, and those that were measured directly are in standard font.

	<i>Reaction 1</i>	<i>Reaction 2</i>	<i>Reaction 3</i>	<i>Reaction 4</i>	<i>Reaction 5</i>
E_a (kcal·mol ⁻¹)	11.2 ± 0.5	3.2 ± 0.4	9.5 ± 0.5	11.2 ± 0.5	6.7 ± 0.5
ΔH^\ddagger (kcal·mol ⁻¹)	10.5 ± 0.5	2.7 ± 0.4	8.7 ± 0.5	10.5 ± 0.5	6.0 ± 0.5
ΔS^\ddagger (eu)	-11 ± 2	-33 ± 4	-22 ± 4	-17 ± 2	-30 ± 4
k_2 , s ⁻¹ M ⁻¹ , 60 °C	2533.3	<i>6623</i>	400	166.7	<i>415.4</i>
k_2 , s ⁻¹ M ⁻¹ , 25 °C	280	3733.3	57.8	23	126.7
k_2 , s ⁻¹ M ⁻¹ , 5 °C	73.7	2444.4	17.8	5.9	57
k_2 , s ⁻¹ M ⁻¹ , -5 °C	34.8	1955.6	10.7	2.8	36.7

Compound $2-\eta^3-P_3$ reacted with molybdaziridine-hydride **1** to form of $2_2-\mu-P$ (Scheme 2.3, Reaction 4). Between 30 and 60 °C under second-order conditions, data fit a second-order kinetic equation. Reaction 4 is the slowest of the reactions depicted in Scheme 2.3; it is about 10 times slower than formation of symmetrical $2_2-\mu-P$ according to Reaction 1. The activation enthalpies of Reactions 1 and 4 are identical ($\Delta H^\ddagger = 10.5 \pm 0.5$ kcal·mol⁻¹, Table 2.3). However, the activation entropy for Reaction 4 is significantly more negative ($\Delta S^\ddagger = -17 \pm 2$ eu) indicating a more ordered transition state for this bimolecular reaction's rate-limiting step. The mechanism of Reaction 4 must include several steps to proceed to final products. However, these steps occurred significantly faster than the rate-limiting step, and they were not seen during the stopped-flow experiments.

It is known from synthetic experiments that reaction of **1** with P_4 (Reaction 5) in toluene gives two products, $2_2-\mu-P$ and $2-\eta^3-P_3$, but the yield of these products strongly depends on experimental conditions. Consequently, before studying the kinetics of Reaction 5 by stopped-flow UV-vis spectrometry, the reaction was preliminarily studied using a conventional UV-Vis spectrometer to estimate the reaction rate and to find the conditions for formation of $2_2-\mu-P$ and $2-\eta^3-P_3$. Surprisingly, in dilute solutions using any concentration of P_4 , the formation of $2_2-\mu-P$ species takes place. This does not mean that $2_2-\mu-P$ is the only product formed; formation of $2-\eta^3-P_3$ also might occur, decreasing the absorbance change, but this did not change the rate of formation of $2_2-\mu-P$.

Kinetic studies of Reaction 5 were performed over the temperature range -5 to 40 °C using a wide range of concentrations of both reagents ($[1] = 0.15 - 0.6$ mM; $[P_4] = 0.0375 - 3$ mM). Second-order conditions and a significant concentration of **1** (≤ 0.6 mM), revealed a reaction that was too slow to be followed by stopped flow technique ($t_{1/2} > 500$ s). Instead, Reaction 5 was studied under pseudo-first-order conditions with P_4 in a 10- to 40-fold excess. The reaction was followed in a single wavelength mode (500 nm, 550 nm, 460 nm), and concentration dependence experiments were done at 25 °C and -5 °C. Under pseudo-first-order conditions, the kinetic data were fit to a first-order kinetic equation, suggesting that Reaction 5 is first-order in **1**. Indeed, varying the concentration of **1** while keeping the concentration of P_4 large and constant yielded identical values of

pseudo-first-order rate constant k_{obs} . This confirmed that the reaction rate depended on the first power of $[1]$. A plot of k_{obs} vs. the initial concentration of P_4 at 25 °C was a straight line with a small intercept (~5%) (Figure 2.9), indicating that the reaction is practically irreversible and is first order in $[P_4]$. Consequently, Reaction 5 is a second-order process with the rate law shown in Equation 1:

$$v = k_{\text{obs}5}[1] = k_2[1][P_4] \quad (1)$$

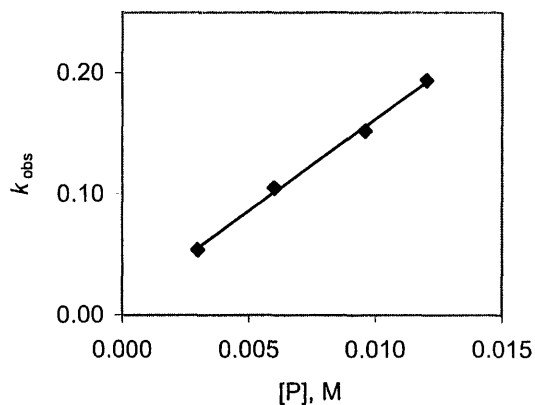
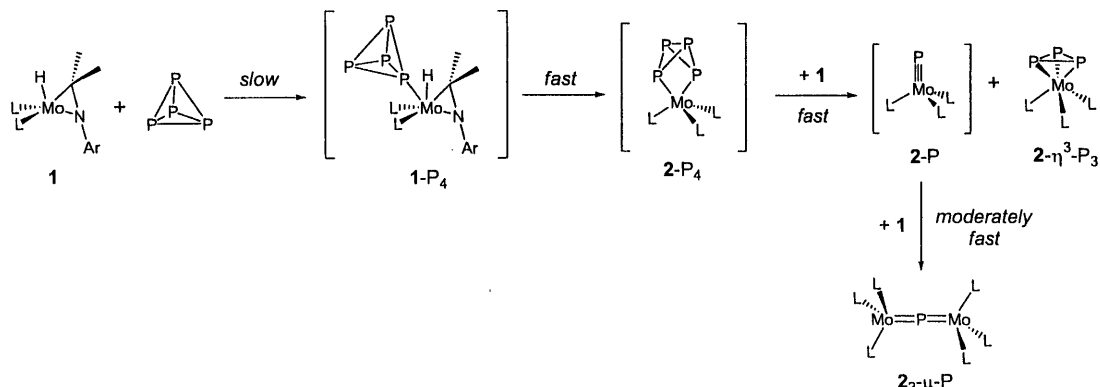


Figure 2.9: Dependence of the observed pseudo-first-order rate constant on $[P_4]$ for Reaction 5 (toluene, 25 °C). The initial concentration of **1** was 0.3 mM (after mixing).

Reaction 5 is faster than Reaction 4, immediately eliminating $2-\eta^3-P_3$ as a possible intermediate in the formation of $2_2-\mu-P$ during the reaction between **1** and P_4 . The second-order rates for Reactions 1 and 5 are comparable. Therefore, if terminal phosphide **2-P** was an intermediate in white phosphorus activation by **1**, higher-order kinetics would be observed for Reaction 5. This was not observed.

To further verify that **2-P** was not an intermediate in the reaction of **1** with P_4 (Reaction 5), the following NMR experiment was performed. An equimolar mixture of P_4 and **2-P** was prepared in benzene- d_6 and spiked with one equivalent of an integration standard (PPh_3) known not to react with molybdaziridine-hydride **1**. Subsequently, this solution was added to a solution of one equivalent of **1**. The reaction mixture became the red-purple color of $2_2-\mu-P$ upon mixing, but it was allowed to stir for *ca.* 3 h. At this time, the composition of the reaction mixture was evaluated by 1H NMR. Integration of data collected during a single-pulse experiment with a long acquisition time revealed a nearly equimolar ratio of **2-P** and the integration standard PPh_3 . This implied that very little of the terminal phosphide **2-P** was consumed, and that P_4 reacted more quickly than **2-P** with molybdaziridine-hydride **1**.

Scheme 2.4: Possible pathway for reaction of P₄ with molybdaziridine-hydride **1** to form 2₂-μ-P and 2-η³-P₃; L = N[*i*-Pr]Ar.

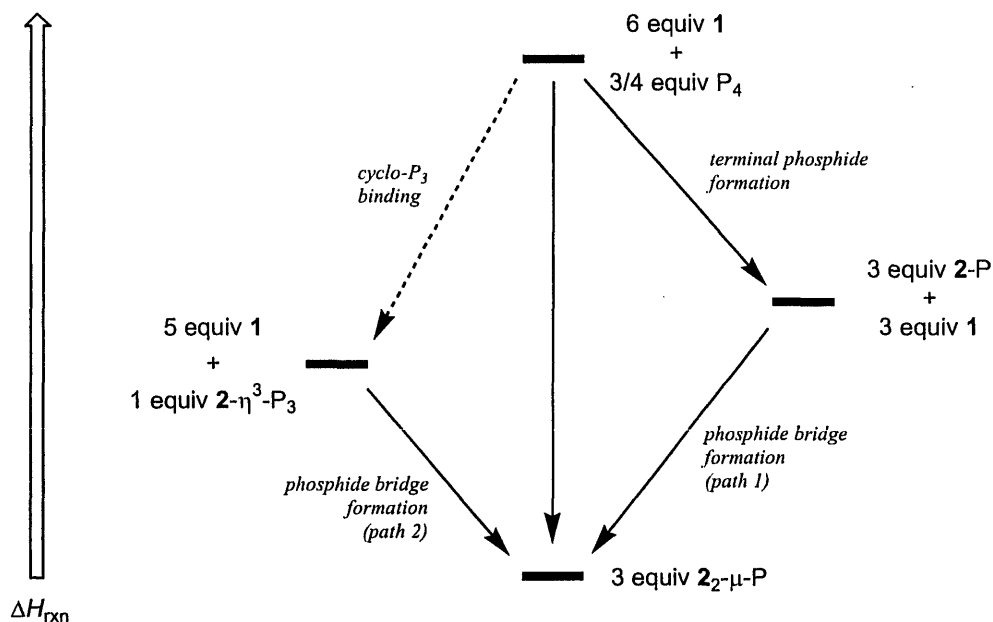


No evidence for reversibility of Reactions 1, 2, or 3 was observed by stopped-flow UV-Vis spectrometry up to 60 °C. This observation, combined with the activation parameters derived for Reactions 1 through 5, permitted a mechanistic hypothesis to be formulated for the reaction of molybdaziridine-hydride **1** with P₄ (Scheme 2.4). The slow step of the reaction is binding of P₄ by molybdaziridine-hydride **1**. This is followed by several fast steps, initiated by molybdaziridine ring opening to form (η²-P₄)Mo(N[*i*-Pr]Ar)₃ (**2-P₄**).^{34,35} As mentioned previously, number of bonds cleaved in the P₄ tetrahedron depends on how many electrons are available from the transition metal. Therefore, compound **2-P₄** probably can be characterized as a η²-P₄ complex where one edge of the tetrahedron has been cleaved by the electrons available from **2**.³³ This is followed by binding of a second equivalent of **1** to **2-P₄** with concomitant bond cleavage to generate terminal phosphide **2-P** and 2-η³-P₃. While it may not be possible to make any conclusive statements about this unobserved, post-rate-determining step, several pathways can be envisioned for this P₃/P₁ cleavage. Perhaps terminal phosphide **2-P** acts as a leaving group, generating the radical ·P₃.⁴⁰ This possibility cannot be ruled out, but it seems unlikely based upon the following experiment. The chromium(III) compound Cr(N[*i*-Pr]₂)₃⁴¹ is known to rapidly react with the radical NO but not with P₄ or **1**. Because ·P₃ is isolobal with NO, Cr(N[*i*-Pr]₂)₃ was utilized as a radical trap during the reaction of P₄ with **1**. However, no species including a Cr-P bond were observed by ³¹P NMR spectroscopy. The ¹H NMR spectrum of the reaction mixture indicated formation of 2-η³-P₃ and 2₂-μ-P while Cr(N[*i*-Pr]₂)₃ was left unreacted. Another mechanistic possibility is that the second equivalent of **1** binds to form a dimolybdenum-tetraphosphorus complex, 2₂-(μ₂-η^{1:1}-P₄). This compound could have a butterfly-P₄ structure, for which there are many examples in the P₄-activation literature.⁴² This compound could subsequently cleave to generate **2-P** and 2-η³-P₃. Regardless of the method of formation, the final step of the reaction occurs after **2-P** and 2-η³-P₃ are generated and P₄ is depleted. This final step is a relatively fast one where **2-P** is trapped by molybdaziridine-hydride **1** takes place to form 2₂-μ-P.

2.5 Conclusions

In summary, the associative, bimolecular reaction of molybdaziridine-hydride **1** with elemental phosphorus generates both the symmetrically bridged compound $2_{2-\mu}\text{-P}$ and the *cyclo*- P_3 compound $2-\eta^3\text{-P}_3$. The former undergoes smooth 1e reduction or oxidation, which can be followed by bridge cleavage upon treatment with carbon monoxide or pyridine-*N*-oxide, respectively. These methods afford synthetic access to terminal phosphide moieties that are sterically less hindered than previously possible. The new multiply bonded species presage new manifolds of chemistry because the relatively unhindered *N*-*iso*-propylanilide ligands are protolytically replaceable as will be discussed in Chapter 3.

Scheme 2.5: Thermochemical cycle for reaction of white phosphorus (P_4) with molybdaziridine-hydride **1**. Pathways depicted with solid arrows indicate reactions that can be observed directly. (In the case of *terminal phosphide formation*, the bulky compound **3** will be substituted for **1** to simplify the reaction.) The dashed arrow represents a quantity to be calculated.



2.6 Future Directions

To complement the synthetic and kinetic work detailed above, a thermochemical cycle has been developed (Scheme 2.5). Determination of the thermodynamic values for several of the reactions detailed above will permit us to probe the thermodynamic values for another reaction we cannot directly observe: the clean formation of $2-\eta^3\text{-P}_3$. No thermodynamic information has been previously reported for the activation of white phosphorus by organometallic compounds to form unique P_n functional groups.

The portions of Scheme 2.5 that can be directly measured include the phosphide bridge formation reaction (path 1) between molybdaziridine-hydride **1** and the terminal phosphide **2-P**. The kinetic parameters of this reaction were determined above (Scheme 2.3, Reaction 1). Similarly, the phosphide bridge formation reaction (path 2) of **1** with *cyclo*-P₃ compound **2- η^3 -P₃** was investigated kinetically (Scheme 2.3, Reaction 2). The terminal phosphide formation reaction cannot be observed for the reaction of P₄ with **1**, but the bulky *tris*-amide Mo(N[*t*-Bu]Ar)₃ (**3**) could be substituted for **1** here. In Chapter 1, it was demonstrated that this **3-for-1** substitution is a valid one for simplification of the reaction products.³⁹

2.7 Experimental Section

2.7.1 General Considerations: Synthesis and Characterization.

Unless stated otherwise, all operations were performed in a Vacuum Atmospheres drybox under an atmosphere of purified nitrogen or using Schlenk techniques under an argon atmosphere. Mo(H)(η^2 -Me₂C=NAr)(N[*i*-Pr]Ar)₂ was prepared as previously published.^{12a} White phosphorus (Aldrich) was purified by crystallizing from toluene. 12-Crown-4 ether was passed through alumina before use. Carbon monoxide (BOC Gases) was used without further purification. Diethyl ether, pentane, dichloromethane, and toluene were dried and deoxygenated by the method of Grubbs.⁴³ THF was distilled from purple sodium benzophenone ketyl and collected under nitrogen. Benzene-*d*₆, dichloromethane-*d*₂, and acetonitrile-*d*₃ were degassed and dried over 4 Å molecular sieves. Other chemicals were purified and dried by standard procedures or were used as received. Celite, alumina and 4 Å molecular sieves were dried in vacuo overnight at a temperature above 200 °C. ¹H, ²H, ¹³C, and ³¹P NMR spectra were recorded on Varian Unity-300, Varian Mercury-300 or Varian INOVA-500 spectrometers. ¹H and ¹³C chemical shifts are reported with respect to internal solvent (C₆D₆, 7.16 and 128.39; CD₃CN, 1.94 and 118.69). ²H NMR spectra are referenced to an external reference (C₆D₆ in Et₂O, 7.16 ppm). ³¹P chemical shifts are reported with respect to external reference (85% H₃PO₄, 0.0 ppm). Infrared spectra were recorded on a Bio-Rad 135 Series FTIR spectrometer. The X-ray data collections were carried out on a Siemens Platform three-circle goniometer with a CCD detector using Mo-K α radiation λ = 0.71073 Å. The data were processed utilizing the program SAINT supplied by Siemens Industrial Automation, Inc. C, H, and N elemental analysis were performed by H. Kolbe Mikroanalytisches Laboratorium, Mülheim an der Ruhr, Germany.

2.7.2 Preparation of compounds.

Synthesis of (μ -P)[Mo(N[*i*-Pr]Ar)₃]₂.^{1,12b} A solution of Mo(H)(η^2 -Me₂C=NAr)(N[*i*-Pr]Ar)₂ (0.504 g, 0.860 mmol, 1.00 equiv) in ether (50 mL) was prepared. To the stirring solution, solid P₄ (26 mg, 0.210 mmol, 0.25 equiv) was added. The solution was stirred for 2 h at room temperature, at which point a deep red suspension was obtained. The red-purple precipitate was isolated by vacuum filtration of the ethereal solution over a sintered glass frit. The desired product (0.382 g, 0.320 mmol, 74%) was washed with

cold ether and dried in vacuo. $\mu_{\text{eff}}(\text{C}_6\text{D}_6) = 1.92 \mu_{\text{B}}$. ^1H NMR (Fully protiated compound, 300 MHz, C_6D_6): $\delta = 11.98$ (12H, ortho), 5.37 (6H, methine), 4.66 (6H, para), 4.01 (36H, *i*-Pr methyl), 2.06 (36H, aryl methyl) ppm. ^2H NMR (D_{36} product, toluene): $\delta = 4.82$ ppm (*i*-Pr methyl, $\Delta\nu_{1/2} = 12$ Hz) ppm. UV-Vis (toluene, 0.3 mM): *ca.* 340 ($\epsilon = \text{ca. } 12200 \text{ M}^{-1}$), 500 ($\epsilon = 5960 \text{ M}^{-1}$) nm. Anal. Calcd. for $\text{C}_{66}\text{H}_{60}\text{D}_{36}\text{N}_6\text{Mo}_2\text{P}$: C, 64.31; H, 7.85; N, 6.82. Found: C, 64.66; H, 7.97; N, 6.90. Note: Synthesis reported here uses fully protiated compound. Deuterated starting materials may be used with no change in product behavior or yield. Elemental analysis is reported here for D_{36} product.

Synthesis of $\{\text{Na}(\text{THF})\}\{(\mu\text{-P})[\text{Mo}(\text{N}[i\text{-Pr}]\text{Ar})_3]_2\}$. A THF solution of $(\mu\text{-P})[\text{Mo}(\text{N}[i\text{-Pr}]\text{Ar})_3]_2$ (0.804 g, 0.63 mmol, 1.0 equiv) was prepared. Twenty equivalents of 1% w/w sodium amalgam (0.300 g Na, 30 g Hg) were added quickly to the rapidly stirring solution. The solution was stirred for 1 h and then decanted away from the amalgam. The reaction mixture was filtered through Celite, and the solvent was removed in vacuo. The product was subsequently recrystallized at -35 °C from pentane (0.756 g, 0.588 mmol, 94%). ^1H NMR (500 MHz, C_6D_6): $\delta = 6.38$ (6H, para), 6.34 (12H, ortho), 5.15 (6H, methine), 3.56 (4H, THF), 2.02 (36 H, aryl methyl), 1.68 (36H, *i*-Pr methyl), 1.41 (4H, THF) ppm. ^{13}C NMR (125 Hz, C_6D_6): $\delta = 154.10$ (ipso), 137.44 (meta), 124.97 (ortho), 124.22 (para), 68.23 (methine), 26.14 ($\text{CH}(\text{CH}_3)_2$), 21.98 (Ar-CH_3) ppm. ^{31}P NMR (200 MHz, C_6D_6): $\delta = 794$ ($\Delta\nu_{1/2} = 120$ Hz) ppm. Anal. Calcd. for $\text{C}_{70}\text{H}_{98}\text{N}_6\text{Mo}_2\text{NaOP}$: C, 65.10; H, 8.11; N, 6.51. Found: C, 65.26; H, 8.15; N, 6.43. Note: $\{\text{Na}(\text{THF})\}\{(\mu\text{-P})[\text{Mo}(\text{N}[i\text{-Pr}]\text{Ar})_3]_2\}$ need not be isolated from THF solution. Instead, the solution can be decanted away from the amalgam, filtered over Celite and placed into a flask for the synthesis of $\text{PMo}(\text{N}[i\text{-Pr}]\text{Ar})_3$.

Synthesis of $\text{PMo}(\text{N}[i\text{-Pr}]\text{Ar})_3$. A 250 mL Schlenk flask was charged with a THF solution (25 mL) of $\{\text{Na}(\text{THF})\}\{(\mu\text{-P})[\text{Mo}(\text{N}[i\text{-Pr}]\text{Ar})_3]_2\}$ (2.19 g, 1.70 mmol). The flask was placed under static vacuum and CO (45.0 mL, 1.84 mmol, 1.1 equiv, 22 °C) was added via a syringe. The solution was stirred for 30 min at room temperature during which time the color changed from purple-red to yellow-brown. The THF solvent was removed in vacuo and the solid was dissolved in pentane (50 mL). A pentane solution (10 mL) of 12-crown-4 ether (0.596 g, 3.39 mmol, 2 equiv) was added to the reaction mixture while stirring. Immediately a yellow-brown precipitate formed, $[\text{Na}(12\text{-c-}4)_2][(\text{OC})\text{Mo}(\text{N}[i\text{-Pr}]\text{Ar})_3]$, which was filtered away from the product by vacuum. The orange filtrate was then reduced in volume and the product crystallized at -35 °C (0.462 g, 84% yield). ^1H NMR (300 MHz, C_6D_6): $\delta = 6.55$ (3H, para), 6.34 (6H, ortho), 4.55 (3H, methine), 2.04 (18H, aryl methyl), 1.54 (18H, *i*-Pr methyl) ppm. ^{13}C NMR (75 MHz, C_6D_6): $\delta = 153.0$ (ipso), 137.9 (meta), 127.0 (para), 126.8 (ortho), 68.1 (methine), 25.9 ($\text{CH}(\text{CH}_3)_2$), 21.7 (Ar-CH_3) ppm. ^{31}P NMR (120 MHz, C_6D_6): $\delta = 1256$ ppm. Anal. Calcd. for $\text{MoC}_{33}\text{H}_{48}\text{N}_3\text{P}$: C, 64.59; H, 7.88; N, 6.85. Found: C, 63.85; H, 8.06; N, 6.88.

Reaction between $\text{PMo}(\text{N}[i\text{-Pr}]\text{Ar})_3$ and $\text{Mo}(\text{H})(\eta^2\text{-Me}_2\text{C}=\text{NAr})(\text{N}[i\text{-Pr}]\text{Ar})_2$. In an NMR tube, yellow $\text{PMo}(\text{N}[i\text{-Pr}]\text{Ar})_3$ (0.012 g, 0.018 mmol, 1 equiv) and orange-brown $\text{Mo}(\text{H})(\eta^2\text{-Me}_2\text{C}=\text{NAr})(\text{N}[i\text{-Pr}]\text{Ar})_2$ (0.010 g, 0.017 mmol, 0.94 equiv) were dissolved in C_6D_6 (*ca.* 1 mL). Immediately upon the addition of solvent, a red-purple solution formed. ^1H NMR verified the formation of $(\mu\text{-P})[\text{Mo}(\text{N}[i\text{-Pr}]\text{Ar})_3]_2$.

Synthesis of $[(\mu\text{-P})\text{Mo}_2(\text{N}[i\text{-Pr}]\text{Ar})_6][\text{OTf}]$. Solid silver triflate was added to a THF solution of $2_2\text{-}\mu\text{-P}$ and the reaction mixture was stirred at 22 °C. During this time, solid silver plated out onto the reaction vessel. After 1 h, the reaction mixture was filtered through Celite to remove Ag(0) and the solvent was removed *in vacuo*. The product was recrystallized from cold (−35 °C) diethyl ether. ^1H NMR (500 MHz, CD_3CN): δ = 6.91 (s, 6H, para), 6.29 (s, 12H, ortho), 4.36 (septet, 6H, methine), 2.20 (s, 36H, aryl methyl), 1.13 (d, 36H, *i*-Pr methyl) ppm. ^{13}C NMR (125 MHz, CD_3CN): δ = 149.15 (ipso), 139.83 (meta), 130.19 (para), 126.43 (ortho), 64.03 (methine), 25.93 (*i*-Pr methyl), 22.61 (triflate, d, J_{CF} = 192 Hz), 21.744 (aryl methyl) ppm. ^{19}F NMR (CD_3CN): −78.5 ppm. Anal. Calcd. for $\text{C}_{65}\text{H}_{90}\text{N}_6\text{F}_3\text{Mo}_2\text{O}_3\text{PS}$: C, 59.81; H, 7.19; N, 6.25. Found: C, 59.89; H, 7.53; N, 6.39.

Synthesis of $[\text{OMo}(\text{N}[i\text{-Pr}]\text{Ar})_3][\text{OTf}]$. To a solution of $\text{Mo}(\text{H})(\eta^2\text{-Me}_2\text{C}=\text{NAr})(\text{N}[i\text{-Pr}]\text{Ar})_2$ in THF was added 1 equiv pyridine-*N*-oxide. Subsequently, a suspension of silver triflate was added. Silver metal plated out onto the walls of the reaction vessel. ^1H NMR (300 MHz, C_6D_6): δ = 6.45 (3H, para), 6.34 (6H, ortho), 4.78 (3H, methine), 1.99 (18H, aryl methyl), 1.18 (d, 18H, isopropyl methyl) ppm. ^{19}F NMR (300 MHz, THF): δ = −78.8 ppm. ^{13}C NMR (125 MHz, C_6D_6): 149.54 (ipso), 138.70 (meta), 129.81 (para), 124.90 (ortho), 65.94 (methine), 22.02 (triflate, J_{CF} = 105 Hz), 1.76 (methyl) ppm. Anal. Calcd. for $\text{C}_{34}\text{H}_{48}\text{F}_3\text{MoN}_3\text{O}_4\text{S}$: C, 66.20; H, 8.08; N, 7.02. Found: C, 65.82; H, 8.59; N, 6.76.

Reaction of $\text{PMo}(\text{N}[i\text{-Pr}]\text{Ar})_3$ with sulfur. A pentane solution of $\text{PMo}(\text{N}[i\text{-Pr}]\text{Ar})_3$ (0.081 g, 0.125 mmol) was chilled to −35 °C. To this cold solution, excess solid S_8 was added. The reaction mixture was stirred for 2 h and was allowed to warm to room temperature. ^1H NMR indicates an incomplete consumption of the starting material and formation of two new products: $(\eta^3\text{-P}_3)\text{Mo}(\text{N}[i\text{-Pr}]\text{Ar})_3$ and a paramagnetic compound.

Reaction of $\text{PMo}(\text{N}[i\text{-Pr}]\text{Ar})_3$ with thallium triflate. There is no reaction of $\text{PMo}(\text{N}[i\text{-Pr}]\text{Ar})_3$ with TlOTf (1 equiv) in tetrahydrofuran after 8 h at 22 °C.

Reaction of $\text{PMo}(\text{N}[i\text{-Pr}]\text{Ar})_3$ with carbon dioxide. $\text{PMo}(\text{N}[i\text{-Pr}]\text{Ar})_3$ does not react with 1 atm CO_2 in diethyl ether after 24 h at 22 °C.

Reaction of $\text{PMo}(\text{N}[i\text{-Pr}]\text{Ar})_3$ with diphenyldisulfide. $\text{PMo}(\text{N}[i\text{-Pr}]\text{Ar})_3$ does not react with 0.5 equiv PhSSPh after 24 h at 22 °C.

Reaction of $\text{PMo}(\text{N}[i\text{-Pr}]\text{Ar})_3$ with triphenylboron. A pentane solution of $\text{PMo}(\text{N}[i\text{-Pr}]\text{Ar})_3$ and BPh_3 displays no reaction after 23 h at 22 °C.

Synthesis of $[(\text{Ar}[i\text{-Pr}]\text{N})_3\text{Mo}](\mu\text{-P})[\text{Mo}(\text{N}[t\text{-Bu}]\text{Ar})_3]$ (2-P-3). Addition of an orange-brown Et_2O solution of $\text{Mo}(\text{N}[t\text{-Bu}]\text{Ar})_3$ (3) to a yellow Et_2O solution of $\text{PMo}(\text{N}[i\text{-Pr}]\text{Ar})_3$ (2-P) results in a color change to red-purple upon mixing. After 30 minutes the solvent was removed *in vacuo*, and the product was recrystallized from Et_2O at −35 °C. μ_{eff} (C_6D_6) = 2.08 μ_{B} . ^1H NMR (500 MHz, C_6D_6): δ = 7.81 ($\Delta\nu_{1/2}$ = 1370 Hz), 7.00, 6.75 ($\Delta\nu_{1/2}$ = 20 Hz), 6.53 (27H, *tert*-butyl, $\Delta\nu_{1/2}$ = 86 Hz), 5.90 ($\Delta\nu_{1/2}$ = 28 Hz), 2.73 (18H, aryl methyl, $\Delta\nu_{1/2}$ = 19 Hz), 2.68 ($\Delta\nu_{1/2}$ = 105 Hz), 2.58 (18H, aryl methyl, $\Delta\nu_{1/2}$ = 10 Hz) ppm.

^2H NMR (77 MHz, C_6H_6) (using $1-d_{18}$): 2.54 ($\Delta\nu_{1/2} = 15$ Hz) ppm. UV-Vis (toluene, 0.3 mM): 350 ($\epsilon = 7360 \text{ M}^{-1}$), 520 ($\epsilon = 5150 \text{ M}^{-1}$) nm.

Reaction of $\text{PMo}(\text{N}[i\text{-Pr}]\text{Ar})_3$ with $(\text{PhCC})\text{Mo}(\text{N}[i\text{-Pr}]\text{Ar})_3$. Upon mixing C_6D_6 solutions, the reaction mixture turns green. Monitoring reaction by ^{31}P NMR reveals a reaction. After 10 minutes, ^{31}P NMR shows some unreacted starting material, and two new peaks: $\delta = 485, 96$ ppm. After 4 h, the peak at $\delta = 485$ ppm has disappeared, leaving only the peak at $\delta = 96$ ppm. When all $(\text{PhCC})\text{Mo}(\text{N}[i\text{-Pr}]\text{Ar})_3$ is consumed, some $\text{PMo}(\text{N}[i\text{-Pr}]\text{Ar})_3$ remains.

Reaction of $\text{PMo}(\text{N}[t\text{-Bu}]\text{Ar})_3$ with $(\text{PhCC})\text{Mo}(\text{N}[i\text{-Pr}]\text{Ar})_3$. No reaction of $\text{PMo}(\text{N}[t\text{-Bu}]\text{Ar})_3$ with $(\text{PhCC})\text{Mo}(\text{N}[i\text{-Pr}]\text{Ar})_3$ occurs over 48 h at 22°C in C_6D_6 .

Competition experiment: Reaction of $\text{PMo}(\text{N}[i\text{-Pr}]\text{Ar})_3$ and P_4 with $\text{Mo}(\text{H})(\eta^2\text{-Me}_2\text{C}=\text{NAr})(\text{N}[i\text{-Pr}]\text{Ar})_2$ in the presence of PPh_3 . A benzene- d_6 solution (*ca.* 1 mL) of P_4 (0.012 g, 0.096 mmol) and $\text{PMo}(\text{N}[i\text{-Pr}]\text{Ar})_3$ (0.062 g, 0.095 mmol, 0.99 equiv) was prepared. To this solution was added a benzene- d_6 solution (*ca.* 1 mL) of $\text{Mo}(\text{H})(\eta^2\text{-Me}_2\text{C}=\text{NAr})(\text{N}[i\text{-Pr}]\text{Ar})_2$ (0.056 g, 0.096 mmol, 1 equiv) and an integration standard, PPh_3 (0.025 g, 0.096 mmol, 1 equiv). After the solutions were combined at 22°C , they were allowed to stir for *ca.* 3 h. Upon mixing a color change from yellow-brown to red-purple was observed. Examination of the reaction mixture after 3 h by ^1H NMR revealed a nearly equimolar mixture of $\text{PMo}(\text{N}[i\text{-Pr}]\text{Ar})_3$ (para, 3H) and PPh_3 (ortho, 6.12H) and presence of $(\mu\text{-P})[\text{Mo}(\text{N}[i\text{-Pr}]\text{Ar})_3]_2$.

2.7.3 Electrochemical Measurements.

Electrochemical measurements were performed in THF solution containing the desired compounds and 0.5 M $[(n\text{-Bu})_4\text{N}][\text{PF}_6]$. In a typical procedure, 5 mg of the complex was dissolved in 0.75 mL of THF. To the solution was added 0.75 mL of a saturated THF solution of $[(n\text{-Bu})_4\text{N}][\text{PF}_6]$. A platinum disk (1.6 mm diameter, Bioanalytical Systems), a platinum wire and a silver wire were employed as the working, auxiliary, and reference electrodes, respectively. The electrochemical response was collected with the assistance of an Eco-Chemie Autolab potentiostat (pgstat20) and the GPES 4.3 software. An IR correction drop was always employed due to the high resistance of the solutions. A typical resistance value measured with the positive feedback technique for these solutions was 975Ω . All of the potentials are reported with respect to the ferrocene/ferrocenium couple measured externally.

2.7.4 Crystallographic Structure Determinations.

The X-ray data collections were carried out on a Siemens Platform three-circle diffractometer (Mo $\text{K}\alpha$, $\lambda = 0.71073 \text{ \AA}$) mounted with a CCD detector and outfitted with a low-temperature, nitrogen-stream aperture (189 K). The structures were solved by direct methods, in conjunction with standard difference Fourier techniques and refined by full-matrix least-squares procedures. Selected bond distances and angles are supplied in

Tables 2.1 and 2.2. A summary of crystallographic data is given in Table 2.4, with full details found in Appendix 2. The systematic absences in the diffraction data are uniquely consistent with the assigned space group of $P2_1/c$ for $[\text{Na}(\text{THF})][2_2\text{-}\mu\text{-P}]$ and $P2_12_12_1$ for 2-P. These choices led to chemically sensible and computationally stable refinements. An empirical absorption correction (ψ -scans) was applied to all data sets. All software for diffraction data processing and crystal-structure solution and refinement are contained in the SHELXTL (v5.10) program suite (G. Sheldrick, Siemens XRD, Madison, WI).

Table 2.4: Crystallographic parameters for $[\text{Na}(\text{THF})][2_2\text{-}\mu\text{-P}]$ and 2-P.

	$[\text{Na}(\text{THF})][2_2\text{-}\mu\text{-P}]$	2-P
formula	$\text{C}_{70}\text{H}_{104}\text{N}_6\text{Mo}_2\text{PNaO}$	$\text{C}_{33}\text{H}_{48}\text{N}_3\text{MoP}$
fw	1291.46	613.67
space group	$P2_1/c$	$P2_12_12_1$
a, Å	17.724(4)	10.493(4)
b, Å	17.853(4)	10.985(4)
c, Å	22.301(5)	58.45(2)
α , deg	90	90
β , deg	96.392(5)	90
γ , deg	90	90
V, Å ³	7013(3)	6737(4)
Z	4	8
cryst description	red-purple block	yellow block
D_{calcd} , g·cm ⁻³	1.223	1.210
μ (Mo K α), mm ⁻¹		
F(000)	2736	2592
GOF on F ²	1.213	1.325
$R(F)$, % ^a	0.1061	0.0909
$R_w(F)$, % ^a	0.1745	0.2070

^a Quantity minimized = $R_w(F^2) = \sum[w(F_o^2 - F_c^2)^2] / \sum[(wF_o^2)^2]^{1/2}$; $R = \sum\Delta / \sum(F_o)$, $\Delta = |(F_o - F_c)|$, $w = 1/[\sigma^2(F_o^2) + (aP)^2 + bP]$, $P = [2F_c^2 + \text{Max}(F_o, 0)]/3$.

2.7.5 General Considerations: Stopped-flow kinetics.

Toluene (anhydrous, 99.8%, Acros) was purified further by the method of Grubbs.⁴³ Toluene solutions of the reagents were prepared in a Vacuum Atmospheres glovebox filled with argon. Kinetic measurements were performed at temperatures from -80 to 25 °C using a Hi-Tech Scientific (Salisbury, Wiltshire, UK) SF-43 Multi-Mixing CryoStopped-Flow Instrument in diode array and single wavelength modes. The stopped-flow instrument was equipped with stainless steel plumbing, a stainless steel mixing cell with sapphire windows, and an anaerobic gas-flashing kit. The instrument was connected to an IBM computer with IS-2 Rapid Kinetic software (Hi-Tech

Scientific). The temperature in the mixing cell was maintained to ± 0.1 K, and the mixing time was 2 ms. The driving syringe compartment and the cooling bath filled with heptane (Fisher) were flushed with argon before and during the experiments, using anaerobic kit flush lines. All flow lines of the SF-43 instrument were extensively washed with degassed, anhydrous toluene before charging the driving syringes with reactant solutions. The experiments were performed in a single-mixing mode of the instrument, with solutions of two reagents mixed in a 1:1 (v/v) ratio.

2.7.6 Theoretical Calculations.

The Amsterdam Density Functional package (version *ADF2000.02*)⁴⁴ was used to derive the molecular orbitals for $[\text{Na}(\text{THF})][\text{2}_2\text{-}\mu\text{-P}]$ by means of a single point calculation on the crystallographically-determined structural parameters of the entire molecule. Full electronic configuration was used for all atoms. Basis sets Zora(III) – H, C, N, O, and Na – and Zora(IV) – P and Mo – were used as implemented in the ADF suite. Relativistic effects were included by virtue of the zero order regular approximation (ZORA).⁴⁵ The local density approximation (LDA) by Vosko, Wilk and Nusair (VWN)⁴⁶ was used together with the exchange and correlation corrections published by Becke⁴⁷ and Perdew,⁴⁸ respectively. All other calculations were completed (*ADF2002.02*) on simplified model compounds containing NMe_2 ligands. These calculations employed full electronic configuration for all atoms using basis set Zora(V). As above, the local density approximation (LDA) by Vosko, Wilk and Nusair (VWN)⁴⁶ was used together with the exchange and correlation corrections published by Becke⁴⁷ and Perdew,⁴⁸ respectively.

2.8 References

1. Cherry, J.-P. F.; Stephens, F. H.; Johnson, M. J. A.; Diaconescu, P. L.; Cummins, C. C. *Inorg. Chem.* **2001**, *40*, 6860.
2. Chisholm, M. H.; Folting, K.; Pasterczyk, J. W. *Inorg. Chem.* **1988**, *27*, 3057.
3. Scheer, M.; Schuster, K.; Budzichowski, T. A.; Chisholm, M. H.; Streib, W. E. *Chem. Commun.* **1995**, 1671.
4. Zanetti, N. C.; Schrock, R. R.; Davis, W. M. *Angew. Chem. Int. Ed. Engl.* **1995**, *34*, 2044.
5. Laplaza, C. E.; Davis, W. M.; Cummins, C. C. *Angew. Chem., Int. Ed. Engl.* **1995**, *34*, 2042.
6. Scheer, M.; Müller, J.; Häser, M. *Angew. Chem. Int. Ed. Engl.* **1996**, *35*, 2492.
7. Scheer, M.; Müller, J.; Baum, G.; Häser, M. *Chem. Commun.* **1998**, 1051.
8. Cummins, C. C. *Chem. Commun.* **1998**, 1777.
9. Johnson, M. J. A.; Odom, A. L.; Cummins, C. C. *Chem. Commun.* **1997**, 1523.
10. (a) Johnson, A. R. Thesis, Massachusetts Institute of Technology, 1998. (b) Cherry, J.-P. F.; Johnson, A. R.; Baraldo, L. M.; Tsai, Y.-C.; Cummins, C. C.; Kryatov, S. V.; Rybak-Akimova, E. V.; Capps, K. B.; Hoff, C. D.; Haar, C. M.; Nolan, S. P. *J. Am. Chem. Soc.* **2001**, *123*, 7271.
11. Johnson, B. P.; Balazs, G.; Scheer, M. *Top. Curr. Chem.* **2004**, *232*, 1.
12. (a) Tsai, Y.-C.; Johnson, M. J. A.; Mindiola, D. J.; Cummins, C. C.; Klooster, W. T.; Koetzle, T. F. *J. Am. Chem. Soc.* **1999**, *121*, 10426. (b) Johnson, M. J. A. Thesis, Massachusetts Institute of Technology, 1998.
13. Other symmetrical μ_2 -P₁ compounds: (a) Scheer, M.; Müller, J.; Schiffer, M.; Baum, G.; Winter, R. *Chem.-Eur. J.* **2000**, *6*, 1252. (b) Johnson, M. J. A.; Lee, P. M.; Odom, A. L.; Davis, W. M.; Cummins, C. C. *Angew. Chem., Int. Ed. Engl.* **1997**, *36*, 87. (c) Fermin, M. C.; Ho, J.; Stephan, D. W. *J. Am. Chem. Soc.* **1994**, *116*, 6033. (d) Strube, A.; Heuser, J.; Huttner, G.; Lang, H. *J. Organomet. Chem.* **1988**, *356*, C9.
14. Weiss, E. *Angew. Chem., Int. Ed. Engl.* **1993**, *32*, 1501.
15. Cherry, J.-P. F. Thesis, Massachusetts Institute of Technology, 2001.
16. (a) Dye, J. L. *Inorg. Chem.* **1997**, *36*, 3816. (b) Dye, J. L. *Science* **2003**, *301*, 607.
17. Connelly, N. G.; Geiger, W. E. *Chem. Rev.* **1996**, *96*, 877.

18. Greco, J. B.; Peters, J. C.; Baker, T. A.; Davis, W. M.; Cummins, C. C.; Wu, G. *J. Am. Chem. Soc.* **2001**, *123*, 5003.
19. Johnson, A. R.; Davis, W. M.; Cummins, C. C.; Serron, S.; Nolan, S. P.; Musaev, D. G.; Morokuma, K. *J. Am. Chem. Soc.* **1998**, *120*, 2071.
20. Sceats, E. L.; Figueroa, J. S.; Cummins, C. C.; Loening, N. M.; Van der Wel, P.; Griffen, R. G. *Polyhedron* **2004**, submitted.
21. Wu, G.; Rovnyak, D.; Johnson, M. J. A.; Zanetti, N. C.; Musaev, D. G.; Morokuma, K.; Schrock, R. R.; Griffin, R. G.; Cummins, C. C. *J. Am. Chem. Soc.* **1996**, *118*, 10654.
22. (a) Wanandi, P. W.; Davis, W. M.; Cummins, C. C.; Russell, M. A.; Wilcox, D. E. *J. Am. Chem. Soc.* **1995**, *117*, 2110. (b) Peters, J. C.; Johnson, A. R.; Odom, A. L.; Wanandi, P. W.; Davis, W. M.; Cummins, C. C. *J. Am. Chem. Soc.* **1996**, *118*, 10175. (c) Johnson, A. R.; Davis, W. M.; Cummins, C. C. *Organometallics* **1996**, *15*, 3825.
23. (a) Fickes, M. G. Ph. D. Thesis, Massachusetts Institute of Technology, 1997. (b) Brask, J. K.; Fickes, M. G.; Sangtrirutnugul, P.; Dura Vila, V.; Odom, A. L.; Cummins, C. C. *Chem. Commun.* **2001**, 1676. (c) Brask, J. K.; Dura Vila, V.; Diaconescu, P. L.; Cummins, C. C. *Chem. Commun.* **2002**, 902.
24. Mendiratta, A.; Cummins, C. C.; Kryatova, O. P.; Rybak-Akimova, E. V.; McDonough, J. E.; Hoff, C. D. *Inorg. Chem.* **2003**, *42*, 8621.
25. Tsai, Y.-C.; Stephens, F. H.; Meyer, K.; Mendiratta, A.; Gheorghiu, M. D.; Cummins, C. C. *Organometallics* **2003**, *22*, 2902.
26. (a) Alberti, A.; Griller, D.; Nazran, A. S.; Pedulli, G. F. *J. Org. Chem.* **1986**, *51*, 3959. (b) Arduengo, A. J., III; Krafczyk, R.; Marshall, W. J.; Schmutzler, R. *J. Am. Chem. Soc.* **1997**, *119*, 3381. (c) Griffiths, D. V.; Harris, J. E.; Whitehead, B. J. *Perkin Trans. 1* **1997**, 2545. (d) Kuhn, N.; Fahl, J.; Blaser, D.; Böse, R. *Z. Anorg. Allg. Chem.* **1999**, *625*, 729.
27. Blackwell, J. M.; Figueroa, J. S.; Stephens, F. H.; Cummins, C. C. *Organometallics* **2003**, *2003*, 3351.
28. Blackwell, J. M. Personal communication.
29. (a) Grützmacher, H.; Pritzkow, H. *Angew. Chem.* **1992**, *104*, 92. (b) Grützmacher, H.; Pritzkow, H. *Angew. Chem. Int. Ed. Engl.* **1992**, *31*, 99.
30. Chisholm, M. H.; Huffman, J. C.; Pasterczyk, J. W. *Inorg. Chim. Acta* **1987**, *133*, 17.
31. Mealli, C.; Costanzo, F.; Ienco, A.; Peruzzini, M.; Perez-Carreño, E. *Inorg. Chim. Acta* **1998**, *275-276*, 366.

32. Stephens, F. H.; Johnson, M. J. A.; Diaconescu, P. L.; Figueroa, J. S.; Cummins, C. C.; Kryatova, O. P.; Rybak-Akimova, E. V.; McDonough, J. E.; Hoff, C. D. Manuscript in preparation.
33. Ehses, M.; Romerosa, A.; Peruzzini, M. *Top. Curr. Chem.* **2002**, *220*, 107.
34. Scherer, O. J.; Swarowsky, M.; Swarowsky, H.; Wolmershäuser, G. *Organometallics* **1989**, *8*, 841.
35. Other examples of η^2 -P₄ complexes where one bond of the tetrahedron has been cleaved: (a) Akbayeva, D. N.; Scherer, O. J. *Z. Anorg. Allg. Chem.* **2001**, *627*, 1429. (b) Peruzzini, M.; Ramirez, J. A.; Vizza, F. *Angew. Chem., Int. Ed.* **1998**, *37*, 2255. (c) Weber, L.; Sonnenberg, U. *Chem. Ber.* **1991**, *124*, 725. (d) Scherer, O. J.; Swarowsky, M.; Swarowsky, H.; Wolmershäuser, G. *Angew. Chem.* **1988**, *100*, 738.
36. Scheer, M.; Becker, U. *Chem. Ber.* **1996**, *129*, 1307.
37. Stephens, F. H.; Figueroa, J. S.; Diaconescu, P. L.; Cummins, C. C. *J. Am. Chem. Soc.* **2003**, *125*, 9264.
38. Barton, D. H. R.; Vonder Embse, R. A. *Tetrahedron* **1998**, *54*, 12475.
39. Stephens, F. H.; Figueroa, J. S.; Cummins, C. C.; Kryatova, O. P.; Kryatov, S. V.; Rybak-Akimova, E. V.; McDonough, J. E.; Hoff, C. D. *Organometallics* **2004**, in press.
40. Van Zee, R. J.; Weltner, Jr., W. *Chem. Phys. Lett.* **1999**, *300*, 243.
41. (a) Alyea, E. C.; Basi, J. S.; Bradley, D. C.; Chisholm, M. H. *Chem. Commun.* **1968**, 495. (b) Bradley, D. C.; Hursthouse, M. B.; Newing, C. W. *Chem. Commun.* **1971**, 411.
42. For examples of bridging *exo/exo*-butterfly μ_2 - $\eta^{1:1}$ -P₄ compounds, see the following: (a) Scherer, O. J.; Hilt, T.; Wolmershäuser, G. *Angew. Chem., Int. Ed.* **2000**, *39*, 1426. (b) Scherer, O. J.; Hilt, T.; Wolmershäuser, G. *Organometallics* **1998**, *17*, 4110. (c) Jutzi, P.; Brusdeilins, N.; Stammler, H. G.; Neumann, B. *Chem. Ber.* **1994**, *127*, 997.
43. Pangborn, A. B.; Giardello, M. A.; Grubbs, R. H.; Rosen, R. K.; Timmers, F. J. *Organometallics* **1996**, *15*, 1518.
44. (a) Baerends, E. J.; Ellis, D. E.; Ros, P. *Chem. Phys.* **1973**, *2*, 41. (b) Versluis, L.; Ziegler, T. *J. Chem. Phys.* **1988**, *322*, 88. (c) te Velde, G.; Baerends, E. J.; *J. Comput. Phys.* **1992**, *99*, 84. (d) Fonseca Guerra, C.; Snijders, J. G.; te Velde, G.; Baerends, E. J. *Theor. Chem. Acc.* **1998**, *99*, 391.
45. (a) Snijders, J. G.; Baerends, E. J.; Ros, P. *Mol. Phys.* **1979**, *38*, 1909. (b) Ziegler, T.; Tschinke, V.; Baerends, E. J.; Snijders, J. G.; Ravenek, W. J. *J. Phys. Chem.*

1989, 93, 3050. (c) van Lenthe, E.; Baerends, E. J.; Snijders, J. G. *J. Chem. Phys.*
1993, 99, 4597.

46. Vosko, S. H.; Wilk, L.; Nusair, M. *Can. J. Phys.* 1980, 58, 1200.

47. Becke, A. D. *Phys. Rev. A* 1988, 38, 3098.

48. Perdew, J. P. *Phys. Rev. B* 1986, 33, 8822.

Alcoholysis of Phosphorus-containing Compounds of Mo(N[*i*-Pr]Ar)₃¹

Reproduced in part with permission from the *Journal of the American Chemical Society*,
2003, 125(31), 9264. ©2003 American Chemical Society

Table of Contents

3.1 Introduction.....	86
3.2 Results and Discussion	87
3.2.1 Reaction of PMo(N[<i>i</i> -Pr]Ar) ₃ (2-P) with bulky alcohols.....	87
3.2.2 Reactions of PMo(N[<i>i</i> -Pr]Ar) ₃ (2-P) with other acidic reagents.....	91
3.2.3 Reactivity of the Mo–P triple bond of 5-P	92
3.2.4 Reaction of (η^3 -P ₃)Mo(N[<i>i</i> -Pr]Ar) ₃ (2-η^3-P₃) with alcohols.....	93
3.2.5 Reaction of Mo(H)(η^2 -Me ₂ C=NAr)(N[<i>i</i> -Pr]Ar) ₂ (1) with bulky alcohols.....	95
3.3 Theoretical Section	97
3.4 Conclusions.....	100
3.5 Experimental Section.....	102
3.5.1 General Considerations.....	102
3.5.2 Crystallographic Structure Determinations.....	106
3.5.3 Theoretical Calculations.....	107
3.6 Mass Spectrum.....	107
3.7 References.....	109

List of Figures

Figure 3.1: X-ray crystal structure of (6-P) ₂	88
Figure 3.2: X-ray crystal structure of 4-P	89
Figure 3.3: Unit cell packing diagram of 4-P	90
Figure 3.4: Mass spectrum of 4-P and simulation.....	90
Figure 3.5: X-ray crystal structure of (η^3 -P ₃)Mo(OCy) ₃ (HN[<i>i</i> -Pr]Ar).....	94
Figure 3.6: X-ray crystal structure of Mo ₂ (OCy) ₃ (N[<i>i</i> -Pr]Ar) ₃	96
Figure 3.7: Graphical representation of the calculated ³¹ P isotropic chemical shifts (δ_{iso}) for 2-P-<i>m</i> , PMo(NMe ₂) ₂ (OMe), PMo(NMe ₂)(OMe) ₂ , and 4-P-<i>m</i>	98

Figure 3.8: Molecular orbital energies (eV) of 2-P-<i>m</i> , PMo(NMe₂)₂(OMe) , PMo(NMe₂)(OMe)₂ , and 4-P-<i>m</i>	99
Figure 3.9: Theoretically determined ΔH_{rxn} for the metathesis of 2-butyne with PMo(OMe)₃ to form methylphosphaalkyne and MeCMo(OMe)₃	100

List of Schemes

Scheme 3.1: Reaction of 2-P with 2,6-dimethylphenol.	87
Scheme 3.2: Reaction of 2-P with 1-methylcyclohexanol.....	89
Scheme 3.3: Reaction of 2-P with bulky carboxylic acids.	92
Scheme 3.4: Alcoholysis of molybdaziridine-hydride 1 with a secondary alcohol.....	95

List of Tables

Table 3.1: Selected bond lengths and angles for (6-P)₂	88
Table 3.2: Selected bonds lengths and angles of 4-P	89
Table 3.3: Selected bond lengths and angles for 2-η^3-P₃	94
Table 3.4: Selected bond lengths and angles of 1,1,2-Mo₂(OCy)₃(N[<i>i</i>-Pr]Ar)₃	96
Table 3.5: Calculated principal components of the ³¹ P chemical shift tensor for the model compounds PMo(NMe₂)_{<i>m</i>}(OMe)_{<i>n</i>} (<i>m</i> + <i>n</i> = 3)	98
Table 3.6: ³¹ P NMR shifts for protonolysis products of 2-P with the listed reagents.	101
Table 3.7: Crystallographic parameters for (6-P)₂ , 4-P , 7-P₃-HN[<i>i</i>-Pr]Ar , and Mo₂(OCy)₃(N[<i>i</i>-Pr]Ar)₃	106
Table 3.8: Simulated fragmentation pattern of the mass spectrum of 4-P	107

3.1 Introduction

Since the 1995 discovery of kinetically stable terminal phosphide complexes $\text{PMo}(\text{N}[\text{R}]\text{Ar})_3$ (3-P, $\text{R} = \text{C}(\text{CD}_3)_2\text{CH}_3$; $\text{Ar} = \text{C}_6\text{H}_3\text{Me}_2$)² and $\text{PM}(\text{Me}_3\text{SiNCH}_2\text{CH}_2)_3\text{N}$ ($\text{M} = \text{Mo}, \text{W}$; $[(\text{Me}_3\text{SiNCH}_2\text{CH}_2)_3\text{N}]^{3-} = \text{tren}$)³ it has been of interest to determine the extent to which sterically demanding amido ligands are *required* for terminal M–P ($\text{M} = \text{Mo}, \text{W}$) triple bond protection. Prior to 1995, attempts to generate and observe terminal phosphide complexes had primarily focused on ancillary alkoxide ligation. In Chisholm's 1988 paper describing P_4 addition to $\text{W}_2(\text{ONp})_6(\text{HNMe}_2)_2$ the intermediacy of $\text{PW}(\text{ONp})_3$ is postulated but not observed.⁴ In 1999, reinvestigating prior work of Becker,^{5–7} Scheer and co-workers used low-temperature, solution ^{31}P NMR to probe the metathesis reaction of $\text{W}_2(\text{O}-t\text{-Bu})_6$ with phosphalkyne $\text{PC}-t\text{-Bu}$. A singlet at $\delta = 845$ ppm ($^1J_{\text{WP}} = 176$ Hz) flanked by tungsten satellites was attributed to the reactive intermediate, $\text{PW}(\text{O}-t\text{-Bu})_3$.⁸ While the terminal tungsten phosphide could not be isolated, its stabilization was achieved by the *in situ* $\text{M}(\text{CO})_5$ ($\text{M} = \text{Cr}, \text{W}$) capping of the terminal phosphide. Following this strategy the asymmetric μ -phosphide complex $(t\text{-BuO})_3\text{W}(\mu\text{-P})\text{W}(\text{CO})_5$ was isolated and structurally characterized. Scheer has extended this methodology to include the synthesis of $(\text{THF})(\text{Ar}^2\text{O})_3\text{W}(\mu\text{-P})\text{M}(\text{CO})_5$ ($\text{M} = \text{Cr}, \text{Mo}$, and $\text{Ar}^2 = 2,6\text{-C}_6\text{H}_3\text{Me}_2$).⁹ However, to date, kinetically stable terminal phosphide complexes of the type $\text{PM}(\text{OR})_3$ have remained elusive.¹

Molybdenum alkylidyne complexes such as $\text{Me}_3\text{SiCH}_2\text{CMo}(\text{OAd})_3$ ($\text{Ad} = 1\text{-adamantyl}, 5\text{-C}^{\text{Si}}$) are well-defined initiators of alkyne metathesis. An efficient synthesis of these complexes was devised recently via facile alcoholysis of the amido ligands belonging to precursor $\text{Me}_3\text{SiCH}_2\text{CMo}(\text{N}[i\text{-Pr}]\text{Ar})_3$ (2-C^{Si}).¹⁰ Prior to development of 5-C^{Si} , it was shown that 2-C^{Si} did not react with alkynes. After alcoholysis, the reduced steric constraints about the metal and the increased Lewis acidity of the metal contribute to the ability of 5-C^{Si} to be an efficient catalyst. Considering the diagonal relationship between carbon and phosphorus, and the fact that 2-C^{Si} and $\text{PMo}(\text{N}[i\text{-Pr}]\text{Ar})_3$ (2-P) are isolobal, replacement of the amide ligands of 2-P may permit transfer of the phosphorus atom into an organic molecule via metathesis. Therefore, the same alcoholysis strategy that was applied to 2-C^{Si} was adapted to the synthesis of the first kinetically persistent terminal phosphide complex supported solely by alkoxide ancillary ligation as reported here.¹

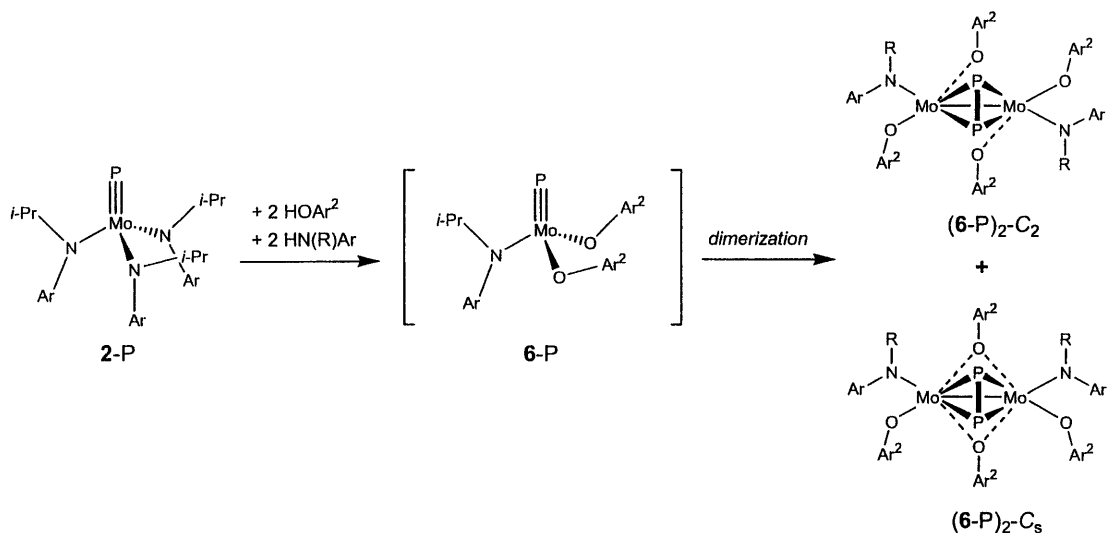
As addressed in Chapter 2, treatment of molybdaziridine-hydride $\text{Mo}(\text{H})(\eta^2\text{-Me}_2\text{CNAr})(\text{N}[i\text{-Pr}]\text{Ar})_2$ (**1**),¹¹ a synthon for the reactive molybdenum(III) *tris*-amide $\text{Mo}(\text{N}[i\text{-Pr}]\text{Ar})_3$ (**2**),¹² with P_4 provides the phosphide-bridged species $(\mu\text{-P})\text{Mo}_2(\text{N}[i\text{-Pr}]\text{Ar})_6$ ($2_2\text{-}\mu\text{-P}$). Reductive carbonylation of $2_2\text{-}\mu\text{-P}$ enabled cleavage of the phosphide bridge to produce the salt $[\text{Na}(12\text{-crown-4})_2][(\text{OC})\text{Mo}(\text{N}[i\text{-Pr}]\text{Ar})_3]$ ($[\text{Na}(12\text{-c-4})_2][2\text{-CO}]$) along with neutral, 4-coordinate terminal phosphide 2-P in gram quantities and 83% yield.¹³ Complex 2-P has a characteristic extremely downfield ^{31}P NMR chemical shift of 1256 ppm, and has been the subject of an X-ray crystal structure investigation.¹³ Theoretical predictions of the properties of alcoholysis products will be discussed below, in conjunction with a detailed discussion of the compounds resulting from protolytic replacement of the amide ligands of terminal phosphide 2-P , *cyclo*- P_3 compound $2\text{-}\eta^3\text{-P}_3$, and molybdaziridine-hydride **1**.

3.2 Results and Discussion

3.2.1 Reaction of $\text{PMo}(\text{N}[i\text{-Pr}]\text{Ar})_3$ (**2-P**) with bulky alcohols.

The terminal phosphide $\text{PMo}(\text{N}[t\text{-Bu}]\text{Ar})_3$ (**3-P**) does not react with alcohols even under forcing conditions and extended reaction times. This is presumably due to the steric protection of the metal afforded by the bulky $\text{N}[t\text{-Bu}]\text{Ar}$ ligands. In contrast, $\text{PMo}(\text{N}[i\text{-Pr}]\text{Ar})_3$ (**2-P**) reacts quite readily with many commercially available alcohols. ^{31}P NMR spectroscopy was used to assess the consequences of **2-P** alcoholysis for more than 20 different alcohols and related acidic substrates.

Scheme 3.1: Reaction of $\text{PMo}(\text{N}[i\text{-Pr}]\text{Ar})_3$ (**2-P**) with 2,6-dimethylphenol. The reaction yielded both C_2 - and C_s -symmetric products.



Addition of three equivalents 2,6-dimethylphenol to a yellow-orange solution of **2-P** (20 mM) resulted in rapid formation of a green-brown product. Alcoholysis was incomplete and $[\text{PMo}(\text{N}[i\text{-Pr}]\text{Ar})(\text{OAr}^2)_2]_2$ was isolated in 51% yield ($(\text{6-P})_2$, Scheme 1). The remaining amide ligands were not replaced when several additional equivalents of 2,6-dimethylphenol were added to a solution of purified $(\text{6-P})_2$ followed by extended heating at 45 °C for 2 d. An X-ray diffraction study revealed a structure of the C_2 -symmetric isomer of $(\text{6-P})_2$. The structure contains a slightly skewed tetrahedral Mo_2P_2 core ($\text{Mo}-\text{P}$, 2.4951(12) Å; $\text{Mo}-\text{P}'$, 2.3926(12) Å) (Figure 3.1, Table 3.1).¹⁴⁻¹⁶ The $\text{P}-\text{P}$ distance (2.086(2) Å) is shorter than that in elemental P_4 (2.21 Å) and that in Chisholm's similar tungsten compound $\text{W}_2(\text{O}-i\text{-Pr})_6(\text{py})(\mu\text{-P}_2)$ (2.154(4) Å),¹⁵ but it is slightly longer than that in Scherer's compound $[\text{Mo}_2\text{Cp}_2(\text{CO})_4(\mu\text{-P}_2)]$ (2.079(2) Å).¹⁶ ^{31}P NMR spectra of $(\text{6-P})_2$ in C_6D_6 showed a mixture of C_s and C_2 isomers in solution. A singlet at $\delta = 235$ ppm was assigned to the $(\text{6-P})_2\text{-}C_2$ isomer where both phosphorus atoms are magnetically equivalent and a pair of doublets centered at $\delta = 248$ and 238 ppm ($J_{\text{PP}} = 366$ Hz) was

assigned to the (6-P)₂-C_s isomer where the phosphorus atoms are magnetically distinct. No attempt was made to study the possible interconversion of the C₂ and C_s isomers.

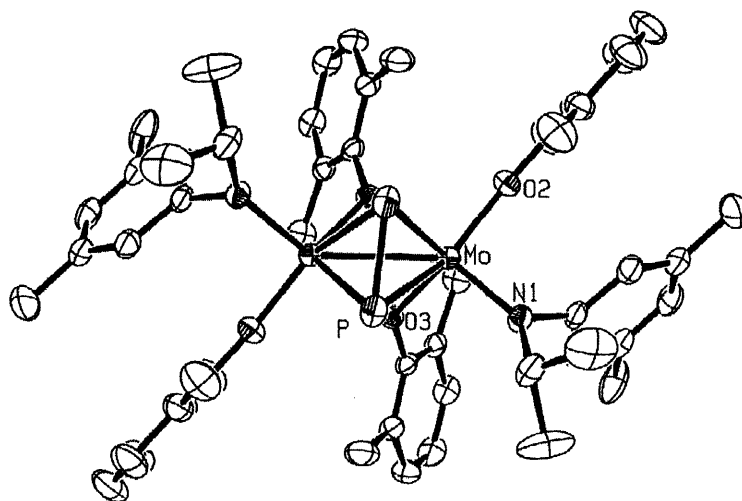


Figure 3.1: X-ray crystal structure of (6-P)₂ with ellipsoids at the 50% probability level.

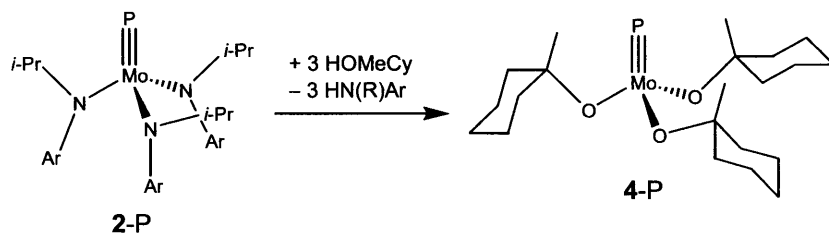
<i>Bond Lengths (Å)</i>				<i>Bond Angles (deg)</i>			
Mo-P	2.4951(12)	Mo-O2	1.930(3)	P-Mo-P'	50.49(6)	P-Mo-N1	84.96(10)
Mo-P'	2.3926(12)	Mo-O3	2.005(3)	P-Mo-Mo'	54.65(3)	P-Mo-O2	142.05(9)
P-P'	2.086(2)	Mo-O3'	2.339(3)	Mo-P-Mo'	67.08(3)	P-Mo-O3	80.81(8)
Mo-N1	1.940(3)						

Table 3.1: Selected bond lengths and angles for (6-P)₂.

Alcoholysis of 2-P using a bulkier alcohol, 1-adamantanol, led to isolation of beige, terminal phosphide PMo(OAd)₃ (5-P) that slowly dimerized to form brown [PMo(OAd)₃]₂ ((5-P)₂). Isolation of the long-lived (*t*_{1/2} = *ca.* 6 h at 20 °C, toluene, *ca.* 15 mM) terminal phosphide 5-P was accomplished by precipitation from the *n*-pentane reaction mixture followed by filtration. When the alcoholysis was performed in more polar solvents, it was very difficult to separate the desired product from the protonolysis product HN[*i*-Pr]Ar (3 equiv). Compound 5-P has a characteristic ³¹P NMR shift at δ = 1124 ppm. This value is intermediate between the ³¹P NMR shift observed for 2-P¹³ and transient PW(O-*t*-Bu)₃.⁸ Over approximately 1 day in toluene solution, 5-P cleanly dimerized to (5-P)₂ with concomitant appearance of a new ³¹P NMR signal at δ = 188 ppm.

In the case of 1-methylcyclohexanol, alcoholysis of 2-P provided the kinetically persistent, monomeric, 4-coordinate terminal phosphide complex PMo(OR)₃ (4-P, R = 1-methylcyclohexyl, Scheme 3.2). Complex 4-P displays a singlet in the ³¹P NMR at δ = 1130 ppm and was isolated in 57% yield by recrystallization (pentane, -35 °C) as a yellow crystalline solid. A single-crystal X-ray diffraction study of 4-P revealed the molecule's structure as depicted in Figure 3.2.

Scheme 3.2: Reaction of 2-P with 1-methylcyclohexanol.



Important structural parameters for complex 4-P include the bond distances (Å) Mo1–P1 = 2.1144(16) and Mo1–O1 = 1.857(2), and the bond angles (°) P1–Mo–O1 = 107.79(6) and Mo–O1–C11 = 141.92(16). In the crystal, 4-P exhibits C_3 symmetry, its Mo–P triple bond vector being coincident with a 3-fold axis of the $R\bar{3}c$ space group. Interestingly, the Mo–P triple bond distance for 4-P is not significantly different than distances observed for corresponding phosphides stabilized by bulky amide ligands.^{2,3} In this respect the Mo–P triple bond functionality retains its identity independent of the nature of ancillary ligands. The closest contact from the phosphorus atom of one molecule to the molybdenum atom of another molecule is 6.887 Å, revealing a structure that is not polymeric in the solid state (Figure 3.3). This is unlike the solid state structure of $\text{NMo}(\text{O}-t\text{-Bu})_3$, which has close contacts (2.844 Å) between the nitrogen from one molecule and the molybdenum of the next.¹⁷ Further verification of the identity of 4-P was provided by EI mass spectrometry, where the observed parent ion ($M^+ = 468.1668 \text{ g}\cdot\text{mol}^{-1}$) corresponds to the intact 4-P monomer (Figure 3.4).

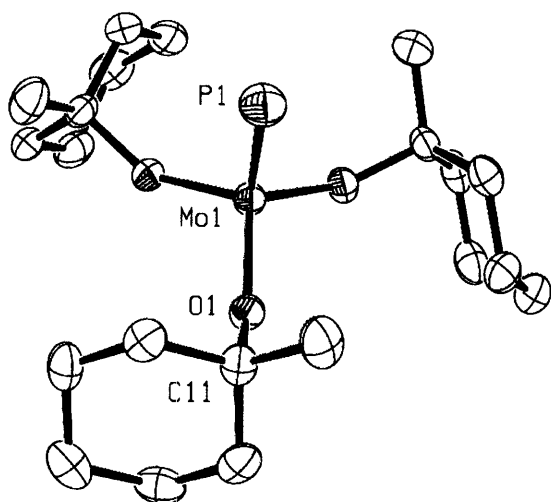


Table 3.2: Selected bonds and angles of 4-P.

<i>Bond Lengths (Å)</i>		<i>Bond Angles (deg)</i>	
Mo1–P1	2.1144(16)	P1–Mo1–O1	107.79(6)
Mo1–O1	1.857(2)	Mo1–O1–C11	141.92(16)
O1–C11	1.456(3)		

Figure 3.2: (Left) X-ray crystal structure of 4-P with ellipsoids at the 50% probability level. Hydrogen atoms have been removed for clarity.

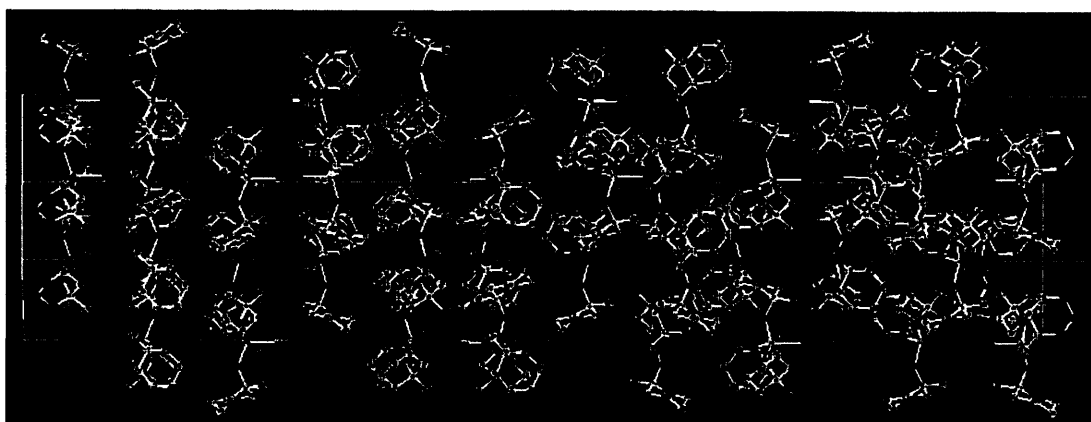


Figure 3.3: Unit cell packing diagram of $\text{PMo}(\text{OMeCy})_3$ (4-P) in the solid state. View is perpendicular to the z-axis. The Mo of one molecule and the P of the next are clearly separate.

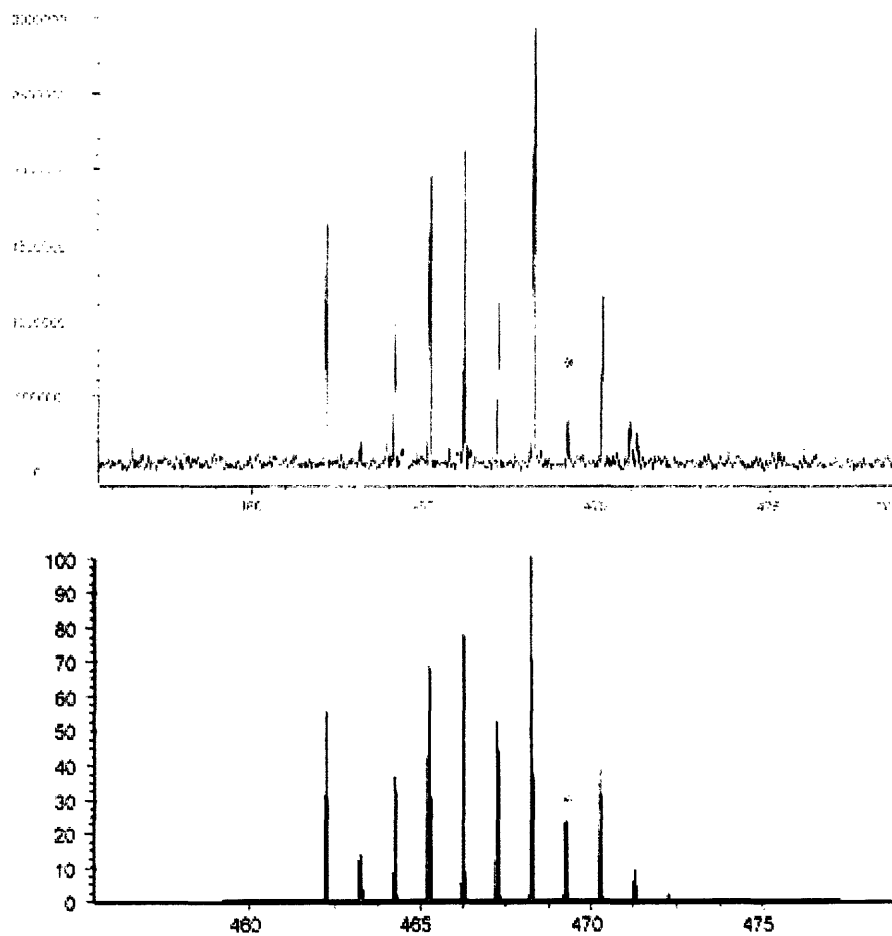


Figure 3.4: Mass spectrum of 4-P (top) and simulation¹⁸ (bottom). Asterisk (*) indicates M^+ ; $M^+ = 468.1668$ (468.16955) $\text{g}\cdot\text{mol}^{-1}$.

Steric bulk appears to be an important factor in the kinetic stabilization of new terminal phosphides. Alcoholysis using triphenylmethanol (Ph_3COH), diphenylethanol (Ph_2MeCOH), and benzhydrol (Ph_2HCOH) in *ca.* 0.1 M solutions enabled a comparison of the kinetic stability of the resulting terminal phosphides with respect to a progressive reduction in the steric bulk of the ancillary ligand set. The very bulky triphenylmethanol reacted slowly with **2-P** (*ca.* 5% conversion after 24 h at 22 °C). The product has a ^{31}P NMR shift at $\delta = 1238$ ppm and a methine peak integrating to 2H in the ^1H NMR spectrum, likely indicating a single protolytic substitution has occurred. Three equivalents of diphenylethanol reacted with **2-P** completely within *ca.* 3 h at 22 °C resulting in a new terminal phosphide with $\delta = 1172$ ppm. This new phosphide is the fully substituted $\text{PMo}(\text{OCMePh}_2)_3$, which slowly dimerized ($t_{1/2} \geq 3$ h) to a product $[\text{PMo}(\text{OCMePh}_2)_3]_2$ with $\delta = 246$ ppm. Finally, benzhydrol (or diphenylmethanol) reacted with **2-P** upon mixing to generate exclusively the dimer, characterized by a ^{31}P NMR shift at 228 ppm.

A comparison of **4-P**, **5-P** and **(5-P)₂**, and **(6-P)₂** and the three additional alcohols discussed in the previous paragraph revealed three possible outcomes of alcoholysis of **2-P**. (1) Incomplete alcoholysis results in a new terminal phosphide, $\text{PMo}(\text{N}[\text{i-Pr}]\text{Ar})_m(\text{OR})_n$. (2) Complete alcoholysis (or possibly incomplete alcoholysis, as seen in **(6-P)₂**) leads to a metastable terminal phosphide that dimerizes. (3) Complete alcoholysis results in a stable terminal phosphide.

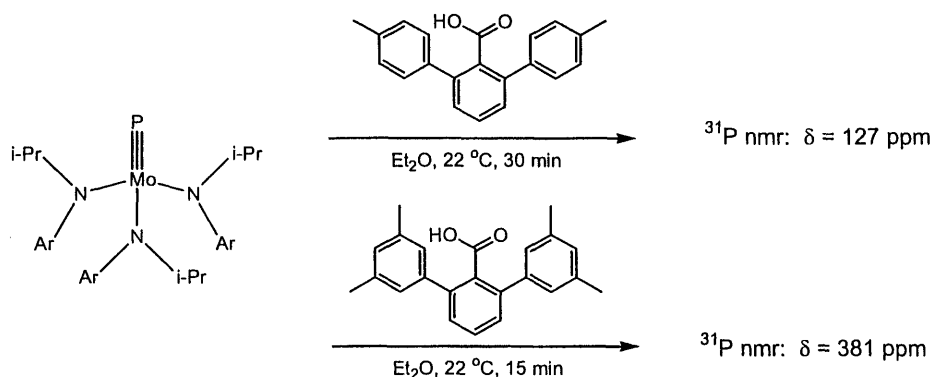
Although the steric issue seems to be simple, subtle differences in ligand size can result in drastically different product composition. This is exemplified by *tert*-butanol, 1-adamantanol, and 1-methylcyclohexanol. These three alcohols are similar in size from the perspective of the metal. As mentioned above, alcoholysis with 1-methylcyclohexanol generated a crystalline, kinetically stable terminal phosphide **4-P** ($\delta = 1130$ ppm) that dimerized only very slowly in solution at room temperature to generate **(4-P)₂** (detected spectroscopically, $\delta = 193$ ppm, $t_{1/2} = \text{ca.}$ 12 h at 45 °C). Similarly, alcoholysis using 1-adamantanol resulted in an isolable terminal phosphide **5-P** ($\delta = 1124$ ppm) that dimerized overnight in toluene to the product **(5-P)₂** ($\delta = 188$ ppm). In contrast to these examples, reaction with *tert*-butanol resulted in dimerization within minutes of mixing. From this comparison, it can be concluded that steric protection of the Mo–P triple bond by the ligand *periphery* is important to preclude dimerization. Formation of the Mo_2P_2 core via terminal phosphide dimerization is a process of great interest as well as potential mechanistic complexity. Chisholm's recent theoretical study of a related process involving breakup of isolobal $\text{M}_2(\text{CH})_2$ (M = Mo, W) alkoxides-supported cores may be consulted for additional insight.¹⁹

3.2.2 Reactions of $\text{PMo}(\text{N}[\text{i-Pr}]\text{Ar})_3$ (**2-P**) with other acidic reagents.

Reagents other than alcohols will react with **2-P** to replace the amide ligands. For example, benzoic acids ($\text{p}K_a = \text{ca.}$ 11) will react with **2-P** to generate dimeric species (Scheme 3.3). In the specific case of the parent benzoic acid $\text{C}_6\text{H}_5\text{COOH}$, reaction occurs upon mixing 3 equivalents of the acid with **2-P**. A brown reaction mixture is

observed and the product has a ^{31}P NMR shift at 123 ppm. The bulky carboxylic acid *bis*-2,6-*p*-tolylbenzoic acid also reacted with 2-P quickly, generating a dimeric product with a ^{31}P NMR shift at 127 ppm. Finally, reaction of 2-P with 3 equivalents of *bis*-2,6-(3,5-dimethylphenyl)benzoic acid resulted in a new product with a ^{31}P NMR shift at 381 ppm. The product of this latter reaction has a more downfield ^{31}P NMR signal than the product of the former reaction due to incomplete substitution of the amide ligands.

Scheme 3.3: Reaction of 2-P with bulky carboxylic acids leads to dimerization of the MoP unit.



In addition to benzoic acids, triphenylsilanol (Ph_3SiOH) and 1-adamantylthiol (1-AdSH) react with 2-P. These two reactions result in formation of new terminal phosphides, but both products resisted isolation from the greasy mixture of hydrocarbon solvent of crystallization and the three equivalents of free amine $\text{HN}[i\text{-Pr}]\text{Ar}$ produced during alcoholysis. In all protonolysis reactions attempted, isolation of the product molecule was challenging due to the presence of $\text{HN}[i\text{-Pr}]\text{Ar}$. A general protocol for isolation involved using pentane as the reaction solvent followed by precipitation or crystallization from the minimum amount of cold pentane.

While no data has been obtained to directly probe the reaction mechanism of these protonolysis reactions, it can be suggested that the protolytic agents must coordinate to 2-P before the amide ligands are replaced. Since no reaction with alcohols was observed for sterically crowded 3-P, this suggestion appears to have merit. This hypothesis was verified when the reaction with cyclopentadiene (CpH) was attempted. The $\text{p}K_a$ of CpH is approximately 16. This is intermediate between aryl alcohols ($\text{p}K_a = 9 - 11$), thiols ($\text{p}K_a = \text{ca. } 12$) and aliphatic alcohols ($\text{p}K_a = 17 - 20$). However, with no electronegative heteroatoms to coordinate CpH to the metal, the acidic proton does not transfer even after extended reaction time at elevated temperature.

3.2.3 Reactivity of the Mo–P triple bond of 5-P.

As mentioned in the introduction, activation of the Mo–P triple bond by replacement of the amide ligands of 2-P by alkoxides is a highly desired goal. This reactivity could permit, for example, access to straightforward, metathetical generation of phosphalkynes. Conventional methods for phosphalkyne production involve harsh

reducing conditions (NaK) precluding the generation of products containing sensitive functional groups.²⁰ In contrast, metathesis is a relatively mild mode of reactivity that should permit synthesis of previously unobserved phosphalkynes.²¹

One equivalent of 3-hexyne was added to a benzene-*d*₆ solution of PMo(OAd)₃ (**5-P**), and the reaction mixture was monitored over one day using ¹H and ³¹P NMR spectroscopy. During this time, no change was observed in the alkyne while **5-P** underwent dimerization to form (**5-P**)₂. Subsequently, **5-P** was dissolved in neat 3-hexyne and the reaction mixture was stirred for approximately 12 h. After this time, ³¹P NMR showed exclusive formation of (**5-P**)₂ with no activation of the alkyne. Other unsaturated substrates were investigated (see list below), but no reactivity was observed.²²

2-butyne	phenyl acetylene	mesityl azide	<i>tert</i> -butyl nitrile
3-hexyne	<i>tert</i> -butyl isocyanide	trimethylsilyl azide	acetonitrile

Other unsaturated substrates which might be of interest include group 6 nitrides and phosphides such as NMo(O-*t*-Bu)₃ and **2-P**. Reaction of **5-P** with these compounds would potentially result in dimers like that which results when the phosphide itself dimerizes. These would be of special interest when nitrides are chosen as the substrate, as the product would contain a P≡N unit suspended between the two metal units. Unfortunately, these compounds also do not demonstrate any reaction with **5-P**. In the future, it may be interesting to use more reactive metal nitrides such as NW(N[*i*-Pr]Ar)₃²³ or NW(O-*t*-Bu)₃,²⁴ since these compounds are known to have less covalent M–N bonds (with some δ⁻ on the nitride ligand) than the corresponding molybdenum complexes.²⁵

While no metathetical reactions were observed, PMo(OMeCy)₃ (**4-P**) did react with Mo(H)(η²-Me₂CNAr)(N[*i*-Pr]Ar)₂ (**1**) and Mo(N[*t*-Bu]Ar)₃ (**3**). In both cases, an asymmetric μ-phosphide was generated. The product of the reaction between **1** and **4-P** is (Ar[*i*-Pr]N)₃Mo(μ-P)Mo(OMeCy)₃ (**2-P-4**). Compound **2-P-4** is red-purple, and it appears to be kinetically stable at temperatures at or below 25 °C. In contrast, the product of the reaction between **3** and **4-P**, (Ar[*t*-Bu]N)₃Mo(μ-P)Mo(OMeCy)₃ (**3-P-4**), gradually decomposed at 25 °C to PMo(N[*t*-Bu]Ar)₃ (**3-P**) and unidentified molybdenum alkoxide products. Behavior as a phosphorus-atom transfer reagent is similar to that seen for NMo(O-*t*-Bu)₃, which was observed to transfer a nitrogen atom to **3**.²⁶

3.2.4 Reaction of (η³-P₃)Mo(N[*i*-Pr]Ar)₃ (**2-η³-P₃**) with alcohols.

As was introduced in Dr. Marc Johnson's thesis²² and elaborated upon in Chapter 2 of this thesis, a cyclo-P₃ compound (**2-η³-P₃**) can be synthesized when molybdaziridine-hydride **1** is slowly added to a toluene solution of white phosphorus. While this compound is not particularly susceptible to reactions at its *cyclo*-P₃ moiety, it reacts with small- and medium-sized alcohols to replace its amide ligands. This is readily understood when the frontier molecular orbitals of **2-η³-P₃** are investigated (Chapter 2,

Figure 2.6). The HOMO is primarily composed of the lone pairs on the amide ligands, which are the most basic locations of the molecule. Hence, the acidic proton of an alcohol reacts at the amide ligands.

Three equivalents of cyclohexanol reacted with $2-\eta^3\text{-P}_3$ in toluene at $75\text{ }^\circ\text{C}$ after approximately 20 h. Characteristic yellow-orange, fibrous $2-\eta^3\text{-P}_3$ was replaced by a significantly more hydrocarbon soluble, orange, crystalline product, $(\eta^3\text{-P}_3)\text{Mo}(\text{OCy})_3(\text{HN}[i\text{-Pr]Ar})$ ($7\text{-P}_3\text{-HN}[i\text{-Pr]Ar}$). This compound was characterized by ^1H and ^{31}P NMR; from ^1H NMR spectroscopy it was evident that complete substitution had occurred, and the presence of a ^{31}P NMR shift at $\delta = -185$ ppm suggested that the *cyclo*- P_3 moiety was intact. The structure was definitively characterized by single-crystal X-ray diffraction (Figure 3.5, Table 3.4). The *cyclo*- P_3 moiety is an equilateral triangle with P–Mo bond lengths of approximately 2.14 Å. The cyclohexanoxide ligands are oriented toward the *cyclo*- P_3 unit, leaving a pocket in which the amine molecule $\text{HN}[i\text{-Pr]Ar}$ coordinates. Compound $7\text{-P}_3\text{-HN}[i\text{-Pr]Ar}$ is structurally very similar to a compound presented by Chisholm *et al.*, $(\eta^3\text{-P}_3)\text{W}(\text{ONp})_3(\text{HN}[i\text{-Pr}]_2)$.²⁷ In this compound, the P–P bond lengths are 2.155(4) Å and the P–W distances are 2.4930(25) Å. Both values are the same, within 3σ , as those in compound $7\text{-P}_3\text{-HN}[i\text{-Pr]Ar}$.

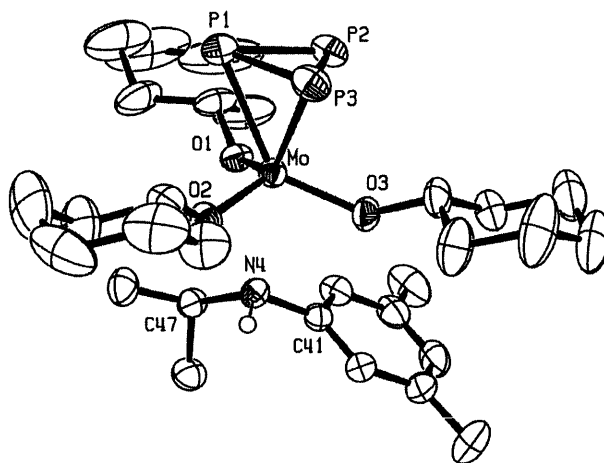


Figure 3.5: X-ray crystal structure of $(\eta^3\text{-P}_3)\text{Mo}(\text{OCy})_3(\text{HN}[i\text{-Pr]Ar})$ with ellipsoids at the 50% probability level. Hydrogen atoms have been removed for clarity, except for the amine hydrogen, which is placed in a calculated position.

<i>Bond Lengths (Å)</i>				<i>Bond Angles (deg)</i>			
P1–P2	2.145(2)	P2–Mo	2.4868(14)	P1–P2–P3	59.83(6)	P1–Mo–O2	89.31(10)
P2–P3	2.138(2)	P3–Mo	2.5028(14)	P2–P3–P1	60.25(6)	P1–Mo–O3	133.03(10)
P3–P1	2.136(2)	Mo–O1	1.903(3)	P3–P1–P2	59.92(6)	O1–Mo–N4	75.54(12)
Mo–N4	2.467(3)	Mo–O2	1.900(3)	P1–P2–Mo	64.84(5)	O2–Mo–N4	76.30(12)
P1–Mo	2.5002(14)	Mo–O3	1.888(3)	P1–Mo–O1	87.41(10)	O3–Mo–N4	77.68(12)

Table 3.3: Selected bond lengths and angles for $(\eta^3\text{-P}_3)\text{Mo}(\text{OCy})_3(\text{HN}[i\text{-Pr]Ar})$.

The long bond (2.467(3) Å) between the amine nitrogen and molybdenum is at the limit of being considered a single bond. This distance exceeds the sum of the covalent radii of the two atoms (2.20 Å). Corresponding to what appears to be a weak bond in the solid state, a solution phase ^1H NMR spectrum of this compound in C_6D_6 was consistent with complete dissociation of the base. The spectrum did not reflect any shift in the resonances assigned to $\text{HN}[i\text{-Pr}]\text{Ar}$ due to coordination as compared to the values observed for the free amine.

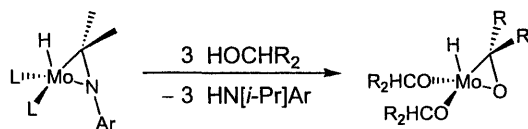
Attempts to synthesize base-free 7-P_3 were unsuccessful. For example, addition of excess methyl iodide did not quaternize the amine of $7\text{-P}_3\text{-HN}[i\text{-Pr}]\text{Ar}$. More strongly coordinating bases displaced $\text{HN}[i\text{-Pr}]\text{Ar}$ from $7\text{-P}_3\text{-HN}[i\text{-Pr}]\text{Ar}$. For example, triethylenediamine (DABCO, $\text{C}_6\text{H}_{12}\text{N}_2$), a cage-shaped base with nitrogen atoms at opposite ends, reacted with $7\text{-P}_3\text{-HN}[i\text{-Pr}]\text{Ar}$ to form the yellow, crystalline, dimeric product $(\eta^3\text{-P}_3)\text{Mo}(\text{OCy})_3(\text{NC}_6\text{H}_{12}\text{N})(\text{OCy})_3\text{Mo}(\eta^3\text{-P}_3)$ ($(7\text{-P}_3)_2\text{-DABCO}$).

3.2.5 Reaction of $\text{Mo}(\text{H})(\eta^2\text{-Me}_2\text{C}=\text{NAr})(\text{N}[i\text{-Pr}]\text{Ar})_2$ with bulky alcohols.

There are no known examples of three-coordinate group 6 metal complexes supported by alkoxide ligands. Attempts to synthesize this genre of molecule from $\text{MoCl}_3(\text{THF})_3$ and lithium alkoxides have only resulted in formation of dinuclear compounds containing molybdenum-molybdenum triple bonds. However, using our metallaziridine-hydride masking strategy, reactive, low-valent compounds of this sort may be attainable.

Synthesis of molybdaziridine-hydride **1** is only possible when a lithium amide containing a secondary alkyl substituent is added to $\text{MoCl}_3(\text{THF})_3$. β -Elimination from one of the amide ligands results in the $\text{Mo}(\text{V})$ product. In contrast, even when secondary alcohols are added to $\text{MoCl}_3(\text{THF})_3$, the dinuclear compound $\text{Mo}_2(\text{OR})_6$ results. Following the alcoholysis strategy presented above, addition of secondary alcohols to molybdaziridine hydride **1** could result in formation of the molybdaoxirane-hydride $\text{Mo}(\text{H})(\eta^2\text{-O}=\text{CR}_2)(\text{OR})_2$ (**8**) (Scheme 3.4). Isolation of this compound could permit direct synthesis of alkoxide-supported terminal phosphides and their dimers from P_4 .

Scheme 3.4: Alcoholysis of molybdaziridine-hydride **1** with a secondary alcohol (HOCHR_2); $\text{L} = \text{N}[i\text{-Pr}]\text{Ar}$.



Addition of three equivalents of the secondary alcohol cyclohexanol to a solution of molybdaziridine-hydride **1** in diethyl ether resulted in formation of a product with the

formula $1,1,2\text{-Mo}_2(\text{OCy})_3(\text{N}[i\text{-Pr}]\text{Ar})_3$ containing a molybdenum-molybdenum bond (Figure 3.6). X-ray crystallography revealed a Mo–Mo bond length of 2.2315(4) Å, consistent with a triple bond. The amide and alkoxide ligands are positioned in a *gauche* (staggered) conformation.^{28,29} The N1–Mo1–Mo2–O6 dihedral angle is 177.7°, the N2–Mo1–Mo2–N4 dihedral angle is 178.2°, and the O3–Mo1–Mo2–O5 dihedral angle is 178.0°. Two of the alkoxide ligands (O3 and O5) are *anti* to one another, and the corresponding Mo–O bond lengths are both 1.924 Å (Table 3.4). Similarly, two of the amide ligands (N2 and N4) are *anti* to one another, with Mo–N bond lengths of 1.944 Å. The remaining two ligands, alkoxide O6 and amide N1, are *anti* to one another making their bonds to molybdenum different lengths than the ligands already discussed by virtue of a through-bond *trans* effect. The Mo2–O6 bond length is 1.888(2) Å, somewhat shortened from the other two molybdenum-alkoxide bond lengths. In contrast, the Mo1–N1 bond length is 1.998(3) Å, a longer bond than the other molybdenum-amides here.

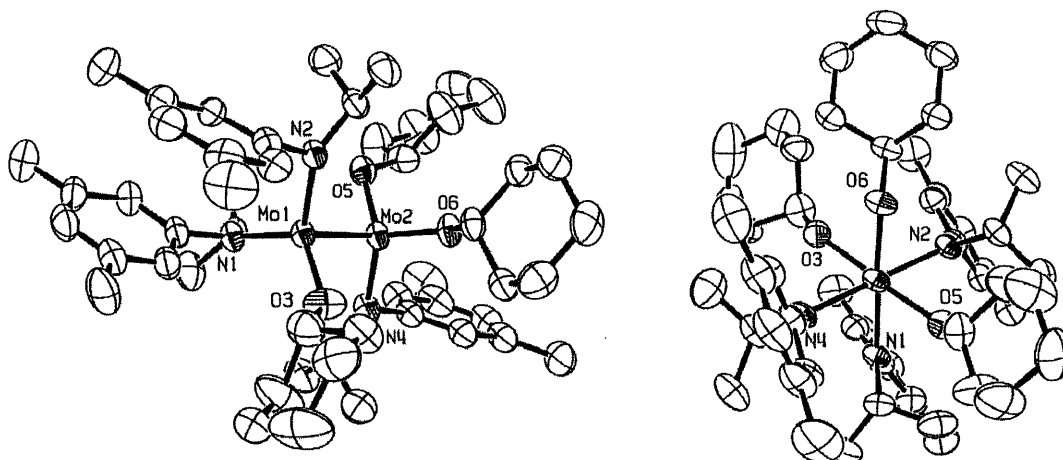


Figure 3.6: X-ray crystal structure of $\text{Mo}_2(\text{OCy})_3(\text{N}[i\text{-Pr}]\text{Ar})_3$ with ellipsoids at the 50% probability level. Hydrogen atoms have been removed for clarity. (Left) View approximately perpendicular to Mo–Mo bond; (right) view parallel to Mo–Mo bond.

Table 3.4: Selected bond lengths and angles of $1,1,2\text{-Mo}_2(\text{OCy})_3(\text{N}[i\text{-Pr}]\text{Ar})_3$.

<i>Bond Lengths (Å)</i>		<i>Bond Angles (deg)</i>	
Mo1–Mo2	2.2315(4)	Mo1–Mo2–N4	102.41(7)
Mo1–N1	1.998(3)	Mo1–Mo2–O5	103.42(6)
Mo1–N2	1.946(2)	Mo1–Mo2–O6	105.89(6)
Mo1–O3	1.923(2)	Mo2–Mo1–N1	102.83(7)
Mo2–N4	1.943(2)	Mo2–Mo1–N2	100.99(7)
Mo2–O5	1.925(2)	Mo2–Mo1–O3	98.52(8)
Mo2–O6	1.888(2)		

While a similar molecule, 1,1,2-Mo₂(O-1,2-C₆H₃Ph₂)₃(NMe₂)₃, has been reported by Rothwell *et al.*,²⁸ no examples of 1,1,2-Mo₂(OR)₃(NR₂)₃ have been crystallographically characterized. However, the compound is generally similar to other Mo₂(OR)₆ and Mo₂(NR₂)₆ compounds,³⁰ and the bond lengths and angles are unremarkable. The closest structural comparison would be to the compound 1,2-Mo₂(NMe₂)₂(O-2,6-C₆H₃Me₂)₄, which has a staggered arrangement of ligands with the amides *anti* to one another.³¹ The Mo–Mo bond length in this species is 2.227(1) Å, which is slightly shorter than the corresponding distance in 1,1,2-Mo₂(OCy)₃(N[*i*-Pr]Ar)₃. Presumably, this is due to both electronic and steric contributions from the three amide ligands. The Mo–O bond lengths, 1.926(3) Å and 1.961(3) Å, are similar to the alkoxide ligands *anti* to one another. The Mo–N bond length is 1.908(4) Å, somewhat shorter than the molybdenum-amide bond lengths observed for 1,1,2-Mo₂(OCy)₃(N[*i*-Pr]Ar)₃ attributable to steric pressure.

3.3 Theoretical Section

³¹P NMR chemical shift calculations (*ADF2002.02*)³² were carried out on several model systems including PMo(NMe₂)₃ (**2-P-m**), PMo(OMe)₃ (**4-P-m**) and [PMo(μ-OH)(OH)(NH₂)₂]₂ ((**6-P**)_{2-m}) whose geometries were optimized based upon X-ray structural parameters of **2-P**, **4-P** and (**6-P**)₂.³³ The details of the calculation on **2-P-m** were reported in Chapter 2; the calculated ³¹P NMR shift was δ = 1250 ppm. We obtained for terminal phosphide model compound **4-P-m** a calculated chemical shift of δ = 1141 ppm, while for the dimer (**6-P**)_{2-m} the calculated chemical shift is δ = 203 ppm.¹ These values are in good agreement with data for the experimental systems reported herein.

Density functional theory was further utilized to probe the change in ³¹P NMR shift with successive protolytic substitutions of the amide ligands of terminal phosphide **2-P**. Again, the simplified molecule **2-P-m** was used to approximate **2-P**, while **4-P-m** was used to approximate the corresponding alcoholysis product **4-P**. The ³¹P NMR shifts for the intermediate substitution products PMo(NMe₂)₂(OMe) and PMo(NMe₂)(OMe)₂ were also calculated (Figure 3.7). In most cases of **2-P** alcoholysis, incompletely substituted monomers were not observed. Nonetheless, these results could provide product confirmation in the cases where incomplete alcoholysis was suspected based on ¹H NMR spectroscopic observations, but where definitive structural characterization was not possible. Furthermore, these calculated ³¹P NMR shifts may prove to be a helpful predictive tool in future chemistry.

In all model compounds, the Mo–P bond vector was defined as the *z*-axis, with the *x*- and *y*-axes perpendicular. This standard permitted an analysis of the components of the isotropic shift (δ_{iso}). The three-fold symmetry of both PMo(NMe₂)₃ and PMo(OMe)₃ was reflected by the equivalency of the calculated shift tensors δ₁₁ and δ₂₂ and their strong paramagnetic deshielding. Shift tensor δ₃₃ is aligned with the P–Mo triple bond and the system's *z*-axis along which the paramagnetic shielding approaches zero (in linear molecules). The value is small due to little paramagnetic shielding.³⁴ The

isotropic shift and shift tensors were calculated for the four model compounds and the results are tabulated below (Table 3.1).

For the approximately C_3 symmetric $\text{PMo}(\text{NMe}_2)_3$ and $\text{PMo}(\text{OMe})_3$, the values of δ_{11} and δ_{22} are nearly equal indicating an axially symmetric chemical shielding tensor. These are derived from rotational mixing in the presence of an applied field of HOMO-2 (2-P- m) or HOMO-1 (4-P- m) (σ bond, P p_z - Mo d_z^2) with the degenerate LUMO (π^* , P p_x - Mo d_{xz} and P p_y - Mo d_{yz}). In contrast, the compounds $\text{PMo}(\text{NMe}_2)_2(\text{OMe})$ and $\text{PMo}(\text{NMe}_2)(\text{OMe})_2$ have significantly different values for δ_{11} and δ_{22} ($\Delta\delta = ca. 120$ ppm) due to the lower symmetry of the systems. For these compounds, δ_{11} is derived from the HOMO-3 (σ , P p_z - Mo d_z^2) to LUMO +1 (π^* , P p_x - Mo d_{xz} or P p_y - Mo d_{yz}) transition. The shift tensors δ_{22} are derived from rotational mixing in the presence of an applied field of HOMO-1 (π , P p_x - Mo d_{xz} or P p_y - Mo d_{yz}) with the LUMO (π^* , P p_x - Mo d_{xz} or P p_y - Mo d_{yz}).

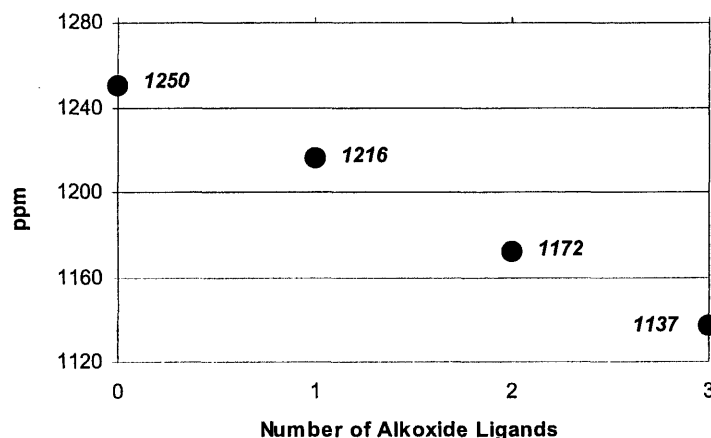


Figure 3.7: Graphical representation of the calculated ^{31}P isotropic chemical shifts (δ_{iso}) for 2-P- m , $\text{PMo}(\text{NMe}_2)_2(\text{OMe})$, $\text{PMo}(\text{NMe}_2)(\text{OMe})_2$, and 4-P- m (left to right).

Table 3.5: Calculated principal components of the ^{31}P chemical shift tensor for the model compounds $\text{PMo}(\text{NMe}_2)_m(\text{OMe})_n$ ($m + n = 3$). The chemical shift tensor component δ_{33} is aligned with the Mo-P vector and is coincident with the z-axis.

	δ_{iso}	δ_{11}	δ_{22}	δ_{33}
$\text{PMo}(\text{NMe}_2)_3$	1250	1841	1841	70
$\text{PMo}(\text{NMe}_2)_2(\text{OMe})$	1216	1919	1809	-81
$\text{PMo}(\text{NMe}_2)(\text{OMe})_2$	1172	1933	1801	-218
$\text{PMo}(\text{OMe})_3$	1137	1867	1852	-311

The relationships among the frontier molecular orbitals of 2-P-*m*, PMo(NMe₂)₂(OMe), PMo(NMe₂)(OMe)₂, and 4-P-*m* are depicted below (Figure 3.8). Each energy level below *ca.* -4 eV represents an orbital containing two electrons. The four compounds have similar HOMO-LUMO gaps, but they are significantly different electronically. Overall, the alkoxide-substituted compounds are lower in energy than 2-P-*m*. The HOMO-1 of 2-P-*m* and the HOMO of 4-P-*m* are degenerate π orbitals composed of P p_x , p_y overlap with Mo d_{xz} , d_{yz} . However, because of the loss of C_{3v} symmetry in the intermediate substitution models, the degeneracy of the corresponding π orbitals of PMo(NMe₂)₂(OMe) and PMo(NMe₂)(OMe)₂ has been broken. The π^* orbitals are split similarly. Importantly, the ligand lone pairs are at sequentially lower energies with successive alcoholyses. This corresponds to the electronegativity difference, and corresponding Lewis basicity difference, between nitrogen and oxygen.

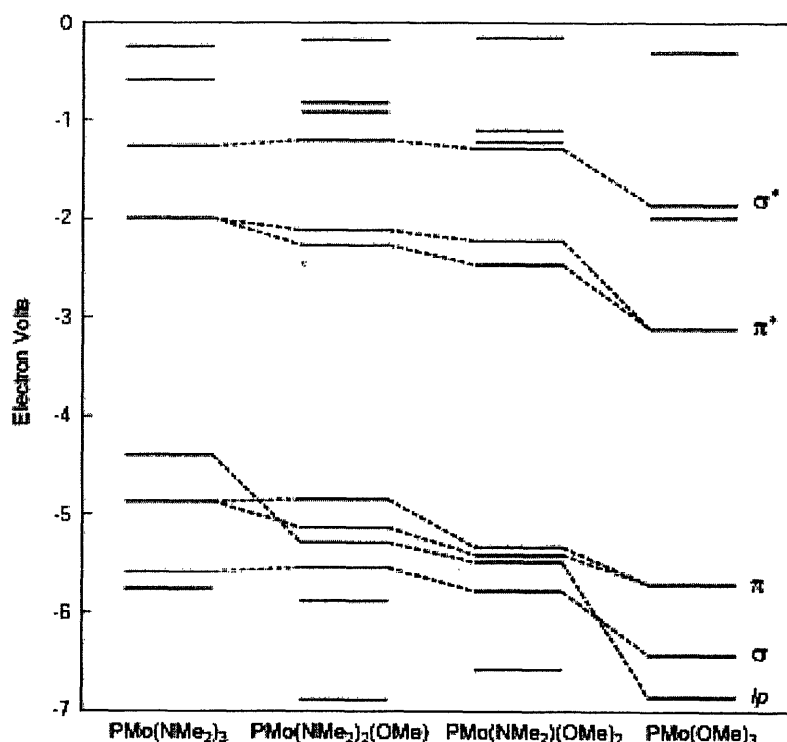


Figure 3.8: Molecular orbital energies (eV) of 2-P-*m*, PMo(NMe₂)₂(OMe), PMo(NMe₂)(OMe)₂, and 4-P-*m*. Dashed lines connect orbitals of the same type: σ^* (P p_z - Mo d_z^2), π^* (P p_x , p_y - Mo d_{xz} , d_{yz}), π (P p_x , p_y - Mo d_{xz} , d_{yz}), σ (P p_z - Mo d_z^2), and ligand lone pairs (*lp*, N p_x , p_y or O p_x , p_y).

As mentioned above, PMo(OAd)₃ (5-P) did not react with internal alkynes that the alkylidyne 5-C^{Si} metathesized. This was somewhat surprising since the HOMO and LUMO of 4-P-*m* are orbitals of appropriate symmetry to react with an alkyne. Geometry optimization of three additional compounds, MeCMo(OMe)₃, 2-butyne, and methylphosphaalkyne, permitted a determination of the energy of the metathesis reaction

(ΔH_{rxn}). Calculated with *ADF2000.02*, the metathetical reaction with alkynes is uphill by approximately $19 \text{ kcal}\cdot\text{mol}^{-1}$, thus giving an explanation for lack of observation of this reaction.

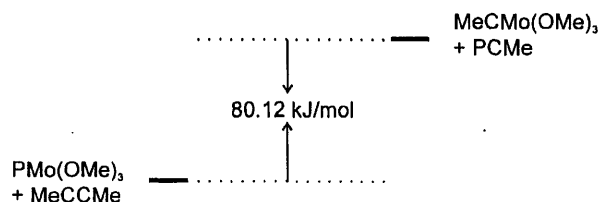


Figure 3.9: Theoretically determined ΔH_{rxn} for the metathesis of 2-butyne with $\text{PMo}(\text{OMe})_3$ to form methylphosphaalkyne and $\text{MeCMo}(\text{OMe})_3$. The reaction is approximately $19 \text{ kcal}\cdot\text{mol}^{-1}$ uphill.

3.4 Conclusions

Addition of protic reagents to terminal phosphide 3-P did not result in a reaction due to the steric congestion at both molybdenum and the amide nitrogens. In contrast, addition of the same reagents to 2-P resulted in formation of two new types of molecules. Simple replacement of the amide ligands by alkoxides, using alcohols as the proton source, allowed the isolation and characterization of two new terminal phosphides of molybdenum, $\text{PMo}(\text{OMeCy})_3$ (4-P) and $\text{PMo}(\text{OAd})_3$ (5-P). Addition of less bulky alcohols generally resulted in dimerization of the Mo–P moiety, leading to a Mo_2P_2 pseudo-tetrahedrane structure, for example $[\text{PMo}(\text{OAr}^2)_2(\text{N}[i\text{-Pr}]\text{Ar})]_2$ ((6-P)₂). A summary of these reactions and other reactions with acidic reagents not discussed here are presented in Table 6.

Although terminal phosphides like 4-P were proposed to have enhanced reactivity (compared to amide supported systems like 2-P) toward unsaturated substrates like alkynes, no reaction was observed. The molybdenum in 4-P is more Lewis acidic than that in 2-P due to a significant reduction in π donation from the ancillary ligands, and it is sterically more accessible. However, a theoretical calculation showed metathesis of alkynes by 4-P to form phosphalkynes is significantly energetically uphill.

Table 3.6: ^{31}P NMR shifts (δ , ppm) for protonolysis products of 2-P with the listed reagents. ^{31}P NMR shifts for the dimerized products of kinetically metastable terminal phosphides are shown parenthetically.

Acidic Reagent	^{31}P NMR shift	n	m	Characterization
2,6-dimethylphenol	248 (d, $J = 366$ Hz) 238 (d, $J = 366$ Hz) 235	2	4	incompletely substituted dimer
1-adamantanol	1124 (188)	0	3	metastable monomer
1-methylcyclohexanol	1130 (193)	0	3	monomer
triphenylmethanol	1238	2	1	incompletely substituted monomer
1,1-diphenylethanol	1172 (246)	0	3	metastable monomer
benzhydrol	228	0	3	dimer
2,6-diphenylphenol	1336 1301	2 1	1 2	incompletely substituted monomer incompletely substituted monomer
2,6-diisopropylphenol	1320 1277 1273	2 1 0	1 2 3	incompletely substituted monomer incompletely substituted monomer monomer
2- <i>tert</i> -butyl-6-methylphenol	1276	1	2	incompletely substituted monomer
2-phenylphenol	265	0	3	dimer
2- <i>tert</i> -butylphenol	240	0	3	dimer
2-methoxyphenol	216	0	3	dimer
2-adamantanol	180	0	3	dimer
cyclohexanol	7 – 392	0	3	dimer(s)
cycloheptanol	0 – 400	0	3	dimer(s)
<i>sec</i> -phenethyl alcohol	189	0	3	dimer
<i>exo</i> -norborneol	0 – 280	0	3	dimer(s)
menthol	221	0	3	dimer
triphenylsilanol	1209 (327)	0	3	metastable monomer
1-adamantyl thiol	1240	0	3	monomer
benzoic acid	123	0	3	dimer
<i>bis</i> -2,6- <i>p</i> -tolylbenzoic acid	127	0	3	dimer
<i>bis</i> -2,6-(3,5-dimethylphenyl)-benzoic acid	381	1	2	dimer
cyclopentadiene	—	—	—	no reaction

3.5 Experimental Section

3.5.1 General Considerations.

Unless stated otherwise, all operations were performed in a Vacuum Atmospheres drybox under an atmosphere of purified nitrogen or using Schlenk techniques under an argon atmosphere. $\text{PMo}(\text{N}[i\text{-Pr}]\text{Ar})_3$ was prepared as previously described.¹³ Diethyl ether, *n*-pentane, and toluene were dried and deoxygenated by the method of Grubbs.³⁵ THF was distilled from purple Na/benzophenone and collected under nitrogen. C_6D_6 was degassed and dried over 4 Å molecular sieves. All alcohols were purchased from Aldrich, dissolved in anhydrous THF, and passed through activated alumina three times before use or were vacuum distilled from sodium. Bulky benzoic acids were received as a gift from the S. J. Lippard group, and were recrystallized from anhydrous diethyl ether. Other chemicals were purified and dried by standard procedures or were used as received. Celite, alumina and 4 Å molecular sieves were dried *in vacuo* overnight at a temperature above 200 °C. ^1H , ^{13}C , and ^{31}P NMR spectra were recorded on Varian Mercury-300 or Varian INOVA-500 spectrometers. ^1H and ^{13}C chemical shifts are reported with respect to internal solvent (C_6D_6 , 7.16 and 128.39 ppm, respectively). ^{31}P chemical shifts are reported with respect to external reference (85% H_3PO_4 , 0.0 ppm). X-ray data collections were carried out on a Siemens Platform three-circle goniometer with a CCD detector using Mo-K_α radiation, $\lambda = 0.71073$ Å. The data were processed utilizing the program SAINT, supplied by Siemens Industrial Automation, Inc. C, H, and N elemental analyses were performed by H. Kolbe Mikroanalytisches Laboratorium, Mülheim an der Ruhr, Germany.

Reaction of $\text{PMo}(\text{N}[t\text{-Bu}]\text{Ar})_3$ with cyclohexanol. A toluene solution of 0.130 g (0.192 mmol) $\text{PMo}(\text{N}[t\text{-Bu}]\text{Ar})_3$ and 0.061 g cyclohexanol (3.1 equiv, 0.611 mmol) was sealed in a Schlenk flask. The headspace was evacuated and the reaction mixture was heated at 66 °C for 12 h. No reaction was observed, assayed by ^1H and ^{31}P NMR spectroscopies.

Synthesis of $[\text{PMo}(\text{N}[i\text{-Pr}]\text{Ar})(\text{O}-2,6\text{-C}_6\text{H}_3\text{Me}_2)_2]_2$. To a diethyl ether solution (5 mL) of 1.396 g $\text{PMo}(\text{N}[i\text{-Pr}]\text{Ar})_3$ (1.396 g, 0.214 mmol) was added 2 equiv 2,6-dimethylphenol (0.055 g, 0.452 mmol) in Et_2O (5 mL). After stirring for 1 h at 20 °C, the solvent was removed *in vacuo*. The oily brown residue was extracted with the minimum amount of Et_2O and the product was crystallized at -35 °C to give green-brown needles (0.059 g, 0.055 mmol, 51%). ^1H NMR (500 MHz, C_6D_6): The ^1H NMR spectrum of $[\text{PMo}(\text{N}[i\text{-Pr}]\text{Ar})(\text{O}-2,6\text{-C}_6\text{H}_3\text{Me}_2)_2]_2$ is very broadened. All peaks occur between approximately 8 ppm and 0 ppm. ^{31}P NMR (202 MHz, C_6D_6): $\delta = 242.9$ (dd, $J = 366$ Hz), 235 (s) ppm. Anal. Calcd. for $\text{C}_{54}\text{H}_{68}\text{N}_2\text{Mo}_2\text{O}_4\text{P}_2$: C, 61.01; H, 6.44; N, 2.63. Found: C, 60.86; H, 6.36; N, 2.35.

Synthesis of $\text{PMo}(\text{OAd})_3$. To an orange, *n*-pentane solution (150 mL) of $\text{PMo}(\text{N}[i\text{-Pr}]\text{Ar})_3$ (1.705 g, 2.62 mmol) was added a *n*-pentane suspension of 1-adamantanol (1.212 g, 7.87 mmol, 3 equiv). After stirring for one hour, the reaction mixture had become brown. The reaction mixture was cooled to -35 °C and the sparingly soluble product was isolated by vacuum filtration as a beige powder (0.5821 g, 1.00 mmol, 38%). ^1H NMR (500 MHz, C_6D_6): $\delta = 2.24$ (18H, d, $J = 2.5$ Hz), 2.14 (9H, s), 1.57 (18H, dd, $J = 32.5$

Hz, $J = 11.5$ Hz) ppm. ^{13}C NMR (75 MHz, C_6D_6): $\delta = 78.47$ (quaternary), 45.80 (CH_2), 36.79 (CH_2), 32.09 (CH) ppm. ^{31}P NMR (121 MHz, C_6D_6): $\delta = 1124$ ppm.

Synthesis of $[\text{PMo}(\text{OAd})_3]_2$. A solution (*ca.* 15 mM) of beige $\text{PMo}(\text{OAd})_3$ in toluene was prepared and allowed to stir at 22 °C overnight. After this time, ^1H and ^{31}P NMR spectroscopies indicated complete conversion of the terminal phosphide to the desired brown, dimeric product $[\text{PMo}(\text{OAd})_3]_2$. This compound exhibits increased solubility in hydrocarbon solvents (e.g. *n*-pentane) when compared to the starting material $\text{PMo}(\text{OAd})_3$. ^1H NMR (300 MHz, C_6D_6): $\delta = 2.37$ (18H, d, $J = 2.1$ Hz), 2.19 (9H, s), 1.62 (18H, dd, $J = 39.2$ Hz, $J = 11.7$ Hz) ppm. ^{13}C NMR (75 MHz, C_6D_6): $\delta = 83.82$ (quaternary), 46.46 (CH_2), 37.12 (CH_2), 32.21 (CH) ppm. ^{31}P NMR (202 MHz, C_6D_6): $\delta = 188$ ppm. Anal. Calcd. for $\text{C}_{60}\text{H}_{90}\text{Mo}_2\text{O}_6\text{P}_2$: C, 62.06; H, 7.81. Found: C, 63.10; H, 7.78.

Synthesis of $\text{PMo}(\text{OMeCy})_3$. To an orange, *n*-pentane solution of $\text{PMo}(\text{N}[i\text{-Pr}]\text{Ar})_3$ (1.156 g in 8 mL *n*-pentane, 1.77 mmol, 1 equiv) was added 2 mL of a *n*-pentane solution of 3 equivalents of 1-methylcyclohexanol (0.606 g, 5.32 mmol). The reaction mixture was stirred for 1 h, during which time a gradual color change from orange to brown was noted. After the designated reaction time, the solvent was removed *in vacuo*. The oily brown residue was extracted with 2 mL *n*-pentane and the yellow product was recrystallized at -35 °C (0.477 g, 1.02 mmol, 57.6%). ^1H NMR (500 MHz, C_6D_6): $\delta = 2.20$ (6H, m, α to quaternary), 1.64 (6H, m, α to quaternary), 1.63 (9H, methyl), 1.49 (3H, m, γ to quaternary), 1.42 (12H, m, β to quaternary), 1.21 (3H, m, γ to quaternary) ppm. ^{13}C NMR (125 MHz, C_6D_6): $\delta = 80.76$ (s, quaternary), 39.63 (t, α to quaternary), 30.69 (q, methyl), 26.33 (t, γ to quaternary), 23.43 (t, β to quaternary) ppm. ^{31}P NMR (121 MHz, C_6D_6): $\delta = 1130$ ppm. Anal. Calcd. for $\text{C}_{21}\text{H}_{39}\text{MoO}_3\text{P}$: C, 54.07; H, 8.43. Found: C, 54.85; H, 8.80. EI-MS M^+ calcd (found): 468.1691 (468.1664) g/mol.

Dimerization of $\text{PMo}(\text{OMeCy})_3$ to generate $[\text{PMo}(\text{OMeCy})_3]_2$. Stirring a C_6D_6 solution of $\text{PMo}(\text{OMeCy})_3$ overnight at 20 °C resulted in partial conversion (*ca.* 25%) to the dimer $[\text{PMo}(\text{OMeCy})_3]_2$. Compound $[\text{PMo}(\text{OMeCy})_3]_2$ decomposes slowly at 45 °C. ^{31}P NMR (121 Hz, C_6D_6): $\delta = 193$ (s) ppm.

Reaction of $\text{PMo}(\text{N}[i\text{-Pr}]\text{Ar})_3$ with cyclopentadiene. A C_6H_6 solution of $\text{PMo}(\text{N}[i\text{-Pr}]\text{Ar})_3$ (0.030 g, 0.046 mmol) and cyclopentadiene (1 mL, 12.1 mmol, approx. 260 equiv.) was prepared. A portion of this solution (0.4 mL) was placed into an NMR tube, which was subsequently sealed. No change in the spectrum was observed when the reaction mixture was observed by ^{31}P NMR at 22 °C for 11.5 h.

Reaction of $\text{PMo}(\text{N}[i\text{-Pr}]\text{Ar})_3$ with 1,1-diphenylethanol. A diethyl ether solution (2 mL) of $\text{PMo}(\text{N}[i\text{-Pr}]\text{Ar})_3$ (0.254 g, 0.391 mmol) was mixed with a diethyl solution (2 mL) of 1,1-diphenylethanol (0.236 g, 1.19 mmol, 3.05 equiv). The reaction mixture was stirred at 22 °C for 6 h, at which point the solvent was removed *in vacuo*. ^{31}P NMR (C_6D_6 , 22 °C): 1172, 246 ppm.

Reaction of $\text{PMo}(\text{N}[i\text{-Pr}]\text{Ar})_3$ with benzhydrol. A tetrahydrofuran solution of $\text{PMo}(\text{N}[i\text{-Pr}]\text{Ar})_3$ (0.077 g, 0.117 mmol) was quickly added to a tetrahydrofuran solution

of benzhydrol (0.064 g, 0.350 mmol, 2.98 equiv). Upon mixing, the yellow solution darkened. After 2 h, solvent was removed *in vacuo*. ^{31}P NMR (C_6D_6 , 22 °C): 228 ppm.

Reaction of $\text{PMo}(\text{N}[i\text{-Pr}]\text{Ar})_3$ with 2-*tert*-butyl-6-methylphenol. Diethyl ether solutions of $\text{PMo}(\text{N}[i\text{-Pr}]\text{Ar})_3$ and 2-*tert*-butyl-6-methylphenol were combined, and the reaction mixture was stirred for 4 h at room temperature. At this time, the reaction mixture was yellow-brown and the solvent was removed *in vacuo*. ^{31}P NMR (C_6D_6 , 22 °C): 1276 ppm.

Reaction of $\text{PMo}(\text{N}[i\text{-Pr}]\text{Ar})_3$ with benzoic acid. A tetrahydrofuran solution of benzoic acid (0.066 g, 0.541 mmol, 2.97 equiv) was prepared and to it a tetrahydrofuran solution of $\text{PMo}(\text{N}[i\text{-Pr}]\text{Ar})_3$ (0.119 g, 0.182 mmol) was added. Upon mixing, a rapid color change from yellow to brown was observed. After 2.5 h, the solvent was removed *in vacuo*. ^{31}P NMR (C_6D_6 , 22 °C): 123 ppm.

Reaction of $\text{PMo}(\text{N}[i\text{-Pr}]\text{Ar})_3$ with 2,6-*bis*-(*p*-tolyl)benzoic acid. A diethyl ether solution of 2,6-*bis*-(*p*-tolyl)benzoic acid (0.089 g, 0.293 mmol, 2.85 equiv) was added to a diethyl ether solution of $\text{PMo}(\text{N}[i\text{-Pr}]\text{Ar})_3$ (0.067 g, 0.103 mmol, 1 equiv) at 22 °C. Upon mixing, the solution changed color from yellow to brown. After 2 h, the solvent was removed *in vacuo* from the reaction mixture. The residue was extracted with pentane and the product was crystallized at -35 °C. ^1H NMR (C_6D_6 , 500 MHz): δ = 7.33 (d, J = 4.5 Hz, 24H, tolyl), 7.31 (d, J = 5 Hz, 24H, tolyl), 7.15 (t, J = 7.5 Hz, 6H, para), 6.90 (d, J = 7.5 Hz, 12H, meta), 2.07 (s, 36H, methyl) ppm. ^{13}C NMR (C_6D_6 , 125 MHz): δ = 176.75 (carboxylate), 144.65 (ortho), 140.19 (tolyl ipso), 136.51 (tolyl para), 131.54 (para), 130.47 (tolyl meta), 129.21 (tolyl ortho), 21.51 (methyl) ppm. ^{31}P NMR (C_6D_6 , 22 °C): δ = 127 ppm.

Reaction of $\text{PMo}(\text{N}[i\text{-Pr}]\text{Ar})_3$ with 2,6-(3,5-dimethylphenyl)benzoic acid. Diethyl ether solutions of $\text{PMo}(\text{N}[i\text{-Pr}]\text{Ar})_3$ (0.018 g, 0.027 mmol) and 2,6-(3,5-dimethylphenyl)benzoic acid (0.022 g, 0.068 mmol, 2.45 equiv) were combined at 22 °C. Over approximately five minutes, the solution changed color from yellow to green-brown. After 20 minutes, vacuum was applied to remove the solvent. ^{31}P NMR (C_6D_6 , 22 °C): 382 (s), 286 (dd, J = 9043, 457) ppm.

Reaction of $\text{PMo}(\text{N}[i\text{-Pr}]\text{Ar})_3$ with 1-adamantylthiol. Cold pentane solutions of $\text{PMo}(\text{N}[i\text{-Pr}]\text{Ar})_3$ and 1-adamantylthiol were combined and allowed to warm to room temperature while stirring rapidly. After 4.5 h, the reaction mixture was brown and the solvent was removed *in vacuo*. The residue is oily, and the NMR spectra show incomplete conversion. ^{31}P NMR (C_6D_6 , 22 °C): 1240 ppm.

Reaction of $\text{PMo}(\text{OMeCy})_3$ with lithium cyclopentadienide. A tetrahydrofuran reaction mixture of $\text{PMo}(\text{OMeCy})_3$ (0.036 g, 0.078 mmol) and lithium cyclopentadienide (0.006 g, 0.077 mmol, 0.99 equiv) was allowed to stir at 22 °C for 24 h. ^{31}P NMR reveals unreacted starting material and homodimer only.

Reaction of $\text{PMo}(\text{OMeCy})_3$ with molybdaziridine-hydride. Diethyl ether solutions of $\text{PMo}(\text{OMeCy})_3$ (0.101 g, 0.216 mmol) and $\text{Mo}(\text{H})(\eta^2\text{-Me}_2\text{C}=\text{NAr})(\text{N}[i\text{-Pr}]\text{Ar})_2$ (0.127 g, 0.219 mmol, 1.01 equiv) were rapidly combined and stirred at 22 °C under nitrogen. ^1H

NMR (C₆D₆, 500 MHz): δ = 13.0, 10.7, 9.5, 8.57, 6.38, 5.53, 4.66, 4.16, 3.2, 2.87, 2.35, 1.91, 0.58, 0.22 ppm.

Reaction of PMo(OMeCy)₃ with Mo(N[*t*-Bu]Ar)₃. Diethyl ether solutions of PMo(OMeCy)₃ (0.077 g, 0.167 mmol) and Mo(N[*t*-Bu]Ar)₃ (0.105 g, 0.167 mmol, 1 equiv) were rapidly combined and stirred at 22 °C under nitrogen. Upon mixing, a color change from brown-orange to pink-purple was observed. ¹H and ³¹P NMR confirmed the generation of PMo(N[*t*-Bu]Ar)₃. Also see a paramagnetic product: δ = 28.38, 24.17, 6.92, 4.19, 3.97, 2.58, 0.78, -1.46, -5.08, -7.63, -9.78, -18.3 ppm.

Reaction of PMo(OMeCy)₃ with 3-hexyne. PMo(OMeCy)₃ (0.025 g) was dissolved in neat 3-hexyne (approx. 0.8 mL) and was placed in a sealed NMR tube. The reaction mixture was heated at 57 °C for 18 h. After this time, only [PMo(OMeCy)₃]₂ was observed by ³¹P NMR. The reaction mixture appears to contain a polymer that formed upon decomposition of a small amount of PMo(OMeCy)₃.

Reaction of PMo(OMeCy)₃ with (PhCC)Mo(N[*i*-Pr]Ar)₃. A C₆D₆ solution containing PMo(OMeCy)₃ (0.021 g, 0.044 mmol, 0.98 equiv) and (PhCC)Mo(N[*i*-Pr]Ar)₃ (0.031 g, 0.045 mmol, 1 equiv) was prepared. After 40 min, ¹H NMR primarily showed unreacted PMo(OMeCy)₃ and unreacted (PhCC)Mo(N[*i*-Pr]Ar)₃. Three new methine peaks are also present in an approximately 1:1:1 ratio: δ = 5.84, 5.13, 4.42 ppm. ³¹P NMR showed some unreacted starting material and a new, broad peak at δ = 116 ppm.

Reaction of (η^3 -P₃)Mo(N[*i*-Pr]Ar)₃ with 1-adamantanol. No reaction is observed between (η^3 -P₃)Mo(N[*i*-Pr]Ar)₃ and three equiv 1-adamantanol at 55 °C for 14 h.

Reaction of (η^3 -P₃)Mo(N[*i*-Pr]Ar)₃ with cyclohexanol (7-P₃-HN[*i*-Pr]Ar). Using 50 mL of toluene, a solution of 2- η^3 -P₃ (0.190 g, 0.260 mmol) and cyclohexanol (0.086 g, 0.855 mmol, 3.3 equiv) was prepared. The solution was heated to 60 °C overnight. The reaction mixture was filtered and the solvent was removed *in vacuo*. The residue was extracted with pentane and the product was crystallized at -35 °C (0.070 g, 0.107 mmol, 41 %). ¹H NMR (300 MHz, C₆D₆): δ = 6.42 (s, 1H, para), 6.17 (s, 2H, ortho), 4.79 (septet, 3H, cyclohexyl quaternary), 3.42 (septet, 1H methine), 2.95 (br d, 1H, amine), 2.23 (s, 6H, aryl methyl), 1.90 (br, cyclohexyl), 1.58 (br, cyclohexyl), 1.50 (br, cyclohexyl), 1.22 (br, cyclohexyl), 0.95 (d, 6H, *i*-Pr methyl) ppm. ³¹P NMR (121 MHz, C₆D₆): δ = -185 ppm. Anal. Calcd. for C₂₉H₅₀MoNO₃P₃: C, 53.62; H, 7.76; N, 2.15. Found: C, 49.38; H, 8.76; N, 1.92.

Synthesis of [(η^3 -P₃)Mo(OCy)₃]₂(DABCO) ((7-P₃)₂-DABCO). To a pentane solution of (η^3 -P₃)Mo(OCy)₃(HN[*i*-Pr]Ar) (0.130 g, 0.200 mmol) was added a pentane solution of triethylenediamine (DABCO, 0.016 g, 0.143 mmol, 0.7 equiv). As the latter solution was added to the former, the color lightened from a yellow-orange to yellow. After 15 min, the reaction mixture was filtered through a frit and a yellow powder was isolated. The powder was recrystallized from cold dichloromethane (*ca.* 2 mL at -35 °C). Yellow microcrystalline solid was isolated (0.061 g, 0.055 mmol, 28 %). ¹H NMR (500 MHz, CD₂Cl₂): δ = 4.545 (septet, 6H, quaternary cyclohexyl), 3.09 (s, 12H, DABCO), 1.84 (overlapping q, 12H, Cy α), 1.71 (overlapping q, 12H, Cy α), 1.57 (overlapping t, 6H, Cy

γ), 1.4 (m, 12H, Cy β), 1.25 (m, 18H, Cy $\beta + \gamma$) ppm. ^{13}C NMR (126 MHz, CD_2Cl_2): $\delta = 86.50$ (DABCO), 46.56 (Cy quaternary), 37.02 (Cy α), 26.25 (Cy γ), 25.13 (Cy β) ppm. ^{31}P NMR (121 MHz, C_6D_6): $\delta = -150$ ppm. Anal. Calcd. for $\text{C}_{42}\text{H}_{78}\text{Mo}_2\text{N}_2\text{O}_6\text{P}_6$: C, 47.66; H, 7.09; N, 2.53. Found: C, 46.67; H, 7.01; N, 2.45.

Synthesis of 1,1,2-Mo₂(OCy)₃(N[*i*-Pr]Ar)₃-*d*₁₈. A diethyl ether solution of cyclohexanol (0.180 g, 1.80 mmol, 1.98 equiv) was added to a diethyl ether solution of 1-*d*₁₈ (0.546 g, 0.91 mmol). The reaction mixture was stirred for 1 h and then was filtered through Celite. The resulting brown, ethereal solution was layered with pentane and placed in the freezer at -35 °C. After 1 week, 0.167 g (0.17 mmol, 19 %) of yellow microcrystalline product was isolated by decanting away the mother liquor and washing with cold pentane.

3.5.2 Crystallographic Structure Determinations.

Table 3.7: Crystallographic parameters for (6-P)₂, 4-P, 7-P₃-HN[*i*-Pr]Ar, and Mo₂(OCy)₃(N[*i*-Pr]Ar)₃.

	(6-P) ₂	4-P	7-P ₃ -HN[<i>i</i> -Pr]Ar	Mo ₂ (OCy) ₃ (N[<i>i</i> -Pr]Ar) ₃
formula	C ₅₉ H ₇₅ Mo ₂ N ₂ O ₄ P ₂	C ₂₁ H ₃₉ MoO ₃ P	C ₂₉ H ₄₉ MoNO ₃ P ₃	C ₅₆ H ₉₃ Mo ₂ N ₃ O ₃
fw	1130.07	466.45	648.57	1048.24
space group	<i>Pccn</i>	<i>R3-c</i>	<i>P2₁/n</i>	<i>P</i> $\bar{1}$
a, Å	18.7073(8)	10.8130(4)	11.087(2)	13.2354(14)
b, Å	16.8765(7)	10.8130(4)	15.273(3)	15.5273(16)
c, Å	18.0139(7)	69.271(3)	19.948(4)	16.2423(17)
α , deg	90	90	90	90.147(2)
β , deg	90	90	97.973(3)	100.121(2)
γ , deg	90	120	90	109.650(2)
V, Å ³	5687.2(4)	7014.2(5)	3345.5(11)	3087.8(6)
Z	4	12	2	2
cryst description	green needle	yellow block	yellow block	yellow block
D_{calcd} , g·cm ⁻³	1.320	1.325	1.288	1.127
F(000)	2356	2952	1364	1116
GOF on F ²	1.046	1.092	1.344	1.039
$R(F)$, % ^a	0.0400	0.0357	0.0555	0.0405
$R_w(F)$, % ^a	0.0895	0.0958	0.1022	0.1171

^a Quantity minimized = $R_w(F^2) = \sum[w(F_o^2 - F_c^2)^2] / \sum[(wF_o^2)^2]^{1/2}$; $R = \sum\Delta / \sum(F_o)$, $\Delta = |(F_o - F_c)|$, $w = 1 / [\sigma^2(F_o^2) + (aP)^2 + bP]$, $P = [2F_c^2 + \text{Max}(F_o, 0)] / 3$.

The X-ray data collections were carried out on a Siemens Platform three-circle diffractometer (Mo $K\alpha$, $\lambda = 0.71073$ Å) mounted with a CCD detector and outfitted with a low-temperature, nitrogen-stream aperture (189 K). The structures were solved by

direct methods, in conjunction with standard difference Fourier techniques and refined by full-matrix least-squares procedures. Selected bond distances and angles are supplied in Tables 3.1, 3.2, 3.3 and 3.4. A summary of crystallographic data is given in Table 3.7, with full details found in Appendix 2. The systematic absences in the diffraction data are uniquely consistent with the assigned space group of *Pccn* for (6-P)₂, *R3-c* for 4-P, *P2₁/n* for 7-P₃-HN[*i*-Pr]Ar, and *P1̄* for Mo₂(OCy)₃(N[*i*-Pr]Ar)₃. These choices led to chemically sensible and computationally stable refinements. An empirical absorption correction (ψ -scans) was applied to all data sets. All software for diffraction data processing and crystal-structure solution and refinement are contained in the SHELXTL (v5.10) program suite (G. Sheldrick, Siemens XRD, Madison, WI).

3.5.3 Theoretical Calculations.

The Amsterdam Density Functional package (version *ADF2000.02*)³² was used to derive the molecular orbitals for the compounds discussed herein by means of an optimization and calculation. Full electronic configuration was used for all atoms. Basis set ZORA(V) was used as implemented in the ADF suite. Relativistic effects were included by virtue of the zero order regular approximation (ZORA).³⁶ The local density approximation (LDA) by Vosko, Wilk and Nusair (VWN)³⁷ was used together with the exchange and correlation corrections published by Becke³⁸ and Perdew,³⁹ respectively.

3.6 Mass Spectrum

Table 3.8: Simulated fragmentation pattern of the mass spectrum of 4-P.

m/z	Abundance	Spread	Multiplicity
466.44540	0.999873	12.01162	108
462.17047	0.1161140	0.00000	1
463.17390	0.0279397	0.00282	3
464.16916	0.0762817	0.01126	5
465.16986	0.1423805	0.01384	9
466.16929	0.1629380	0.01836	10
467.17053	0.1105685	0.01509	14
468.16955	0.2116145	0.01331	14
469.17274	0.0484154	0.01331	14
470.17151	0.0819828	0.01343	14
471.17471	0.0187958	0.00815	10
472.17757	0.0025678	0.00990	7
473.18037	0.0002623	0.00526	6
474.18210	0.0000118	0.00000	1

Mass spectral analysis of 4-P was completed by Li Li at the Massachusetts Institute of Technology Department of Chemistry Mass Spectrometry facility. A Bruker

Daltonics APEXII 3 Tesla Fourier Transform mass spectrometer was utilized. An electron impact method was chosen since the compound is moisture sensitive and could not be easily ionized by dissolution. The simulation of the mass spectrum was completed with the IsoPro program.¹⁸ A list of the simulated fragmentation pattern is presented in Table 3.8.

3.7 References

1. Stephens, F. H.; Figueroa, J. S.; Diaconescu, P. L.; Cummins, C. C. *J. Am. Chem. Soc.* **2003**, *125*, 9264.
2. Laplaza, C. E.; Davis, W. M.; Cummins, C. C. *Angew. Chem., Int. Ed. Engl.* **1995**, *34*, 2042.
3. Zanetti, N. C.; Schrock, R. R.; Davis, W. M. *Angew. Chem., Int. Ed. Engl.* **1995**, *34*, 2044.
4. Chisholm, M. H.; Folting, K.; Pasterczyk, J. W. *Inorg. Chem.* **1988**, *27*, 3057.
5. Becker, G.; Becker, W.; Knebl, R.; Schmidt, H.; Weeber, U.; Westerhausen, M. *Nova Acta Leopoldina* **1985**, *59*, 55.
6. Becker, G.; Becker, W.; Knebl, R.; Schmidt, H.; Hildenbrand, U.; Westerhausen, M. *Phosphorus Sulfur Relat. Elem.* **1987**, *30*, 349.
7. Binger, P. In *Multiple Bonds and Low Coordination in Phosphorus Chemistry*; Regitz, M., Scherer, O. J., Eds.; Thieme Verlag: Stuttgart, 1990; p 100.
8. Scheer, M.; Kramkowski, P.; Schuster, K. *Organometallics* **1999**, *18*, 2874.
9. Kramkowski, P.; Baum, G.; Radius, U.; Kaupp, M.; Scheer, M. *Chem. Eur. J.* **1999**, *5*, 2890.
10. Tsai, Y.-C.; Diaconescu, P. L.; Cummins, C. C. *Organometallics* **2000**, *19*, 5260.
11. Tsai, Y.-C.; Johnson, M. J. A.; Mindiola, D. J.; Cummins, C. C.; Klooster, W. T.; Koetzle, T. F. *J. Am. Chem. Soc.* **1999**, *121*, 10426.
12. Stephens, F. H.; Figueroa, J. S.; Cummins, C. C.; Kryatova, O. P.; Kryatov, S. V.; Rybak-Akimova, E. V.; McDonough, J. E.; Hoff, C. D. *Organometallics* **2004**, in press.
13. Cherry, J.-P. F.; Stephens, F. H.; Johnson, M. J. A.; Diaconescu, P. L.; Cummins, C. C. *Inorg. Chem.* **2001**, *40*, 6860.
14. Examples of M_2P_2 frameworks with otherwise unsupported phosphorus atoms: (a) Davies, J. E.; Feeder, N.; Mays, M. J.; Tompkin, P. K.; Woods, A. D. *Organometallics* **2000**, *19*, 984. (b) Davies, J. E.; Klunduk, M. C.; Mays, M. J.; Raithby, P. R.; Shields, G. P.; Tompkin, P. K. *Dalton* **2000**, 1925. (c) Scheer, M.; Müller, J.; Baum, G.; Häser, M. *Chem. Commun.* **1998**, 1051. (d) Scherer, O. J.; Braun, J.; Walther, P.; Heckmann, G.; Wolmershauser, G. *Angew. Chem.* **1991**, *103*, 861. (e) Goh, L. Y.; Chu, C. K.; Wong, R. C. S.; Hambley, T. W. *Dalton* **1989**, 1951. (f) Scherer, O. J.; Sitzmann, H.; Wolmershauser, G. *Angew. Chem.* **1985**, *97*, 358. (g) Vizi-Orosz, A.; Galamb, V.; Palyi, G.; Marko, L. *J. Organomet. Chem.* **1981**, *216*, 105.

15. Chisholm, M. H.; Folting, K.; Huffman, J. C.; Koh, J. J. *Polyhedron* **1985**, *4*, 893.
16. Scherer, O. J.; Sitzmann, H.; Wolmershäuser, G. *J. Organomet. Chem.* **1984**, *268*, C9.
17. Chan, D. M.-T.; Chisholm, M. H.; Felting, K.; Huffman, J. C.; Marchant, N. S. *Inorg. Chem.* **1986**, *25*, 4170.
18. Senko, M. *IsoPro v3.0*, <http://members.aol.com/msmssoft/>.
19. Chisholm, M. H.; Davidson, E. R.; Quinlan, K. B. *J. Am. Chem. Soc.* **2002**, *124*, 15351.
20. (a) Nixon, J. F. *Chem. Soc. Rev.* **1995**, *24*, 319. (b) Markovskii, L. N.; Romanenko, V. D. *Tetrahedron* **1989**, *45*, 6019. (c) Regitz, M. *Chem. Rev.* **1990**, *90*, 191. (d) Kroto, H. W.; Nixon, J. F. *ACS Symp. Ser.* **1981**, *171*, 383.
21. A niobium phosphide anion has been developed that reacts with acyl chlorides to generate a variety of previously unobserved phosphalkynes. Figueroa, J. S.; Cummins, C. C. Manuscript in preparation.
22. Johnson, M. J. A. Ph.D. Thesis, Massachusetts Institute of Technology, 1998.
23. (a) Greco, J. B. Ph.D. Thesis, Massachusetts Institute of Technology, 2001. (b) Clough, C. R.; Greco, J. B.; Figueroa, J. S.; Diaconescu, P. L.; Cummins, C. C. *J. Am. Chem. Soc.* **2004**, in press.
24. (a) Schrock, R. R.; Listemann, M. L.; Sturgeooff, L. G. *J. Am. Chem. Soc.* **1982**, *104*, 4291. (b) Chisholm, M. H.; Huffman, J. C.; Marchant, N. L. *J. Am. Chem. Soc.* **1983**, *105*, 6162. (c) Chisholm, M. H.; Delbridge, E. E.; Kidwell, A. R.; Quinlan, K. B. *Chem. Commun.* **2003**, 126.
25. Chan, D. M. T.; Chisholm, M. H.; Folting, K.; Huffman, J. C.; Marchant, N. S. *Inorg. Chem.* **1986**, *25*, 4170.
26. Laplaza, C. E.; Johnson, A. R.; Cummins, C. C. *J. Am. Chem. Soc.* **1996**, *118*, 709.
27. Chisholm, M. H.; Huffman, J. C.; Pasterczyk, J. W. *Inorg. Chim. Acta* **1987**, *133*, 17.
28. Coffindaffer, T. W.; Westler, W. M.; Rothwell, I. P. *Inorg. Chem.* **1985**, *24*, 4565.
29. Chisholm, M. H. *Faraday Symp.* **1980**, *14*, 194.
30. (a) Chisholm, M. H. *J. Organomet. Chem.* **1990**, *400*, 235. (b) Chisholm, M. H. *Acc. Chem. Res.* **1990**, *23*, 419. (c) Chisholm, M. H. *Angew. Chem.* **1986**, *98*, 21. (d) Chisholm, M. H. *J. Organomet. Chem.* **1982**, *239*, 79. (e) Bradley, D. C.; Chisholm, M. H. *Acc. Chem. Res.* **1976**, *9*, 273.

31. Coffindaffer, T. W.; Rothwell, I. P.; Huffman, J. C. *Inorg. Chem.* **1984**, *23*, 1433.
32. (a) Baerends, E.J.; Ellis, D.E.; Ros, P. *Chem. Phys.* **1973**, *2*, 41. (b) Versluis, L.; Ziegler, T. *J. Chem. Phys.* **1988**, *322*, 88. (c) te Velde, G.; Baerends, E.J.; *J. Comput. Phys.* **1992**, *99*, 84. (d) Fonseca Guerra, C.; Snijders, J.G.; te Velde, G.; Baerends, E.J. *Theor. Chem. Acc.* **1998**, *99*, 391.
33. Calculations were carried out with ADF version 2002.03. For an introduction to ADF see: te Velde, G.; Bickelhaupt, F. M.; Baerends, E. J.; Fonseca Guerra, C.; Van Gisbergen, S. J. A.; Snijders, J. G.; Ziegler, T. *J. Comput. Chem.* **2001**, *22*, 931-967. The ³¹P NMR shielding calculations derived from an all-electron ADF run that included the effects of spin-orbit coupling.
34. Wu, G.; Rovnyak, D.; Johnson, M. J. A.; Zanetti, N. C.; Musaev, D. G.; Morokuma, K.; Schrock, R. R.; Griffen, R. G.; Cummins, C. C. *J. Am. Chem. Soc.* **1996**, *118*, 10654.
35. Pangborn, A.B.; Giardello, M.A.; Grubbs, R.H.; Rosen, R.K.; Timmers, F.J. *Organometallics* **1996**, *15*, 1518.
36. (a) Snijders, J.G.; Baerends, E.J.; Ros, P. *Mol. Phys.* **1979**, *38*, 1909. (b) Ziegler, T.; Tschinke, V.; Baerends, E.J.; Snijders, J.G.; Ravenek, W.J. *Phys. Chem.* **1989**, *93*, 3050. (c) van Lenthe, E.; Baerends, E.J.; Snijders, J.G. *J. Chem. Phys.* **1993**, *99*, 4597.
37. Vosko, S.H.; Wilk, L.; Nusair, M. *Can. J. Phys.* **1980**, *58*, 1200.
38. Becke, A.D. *Phys. Rev. A* **1988**, *38*, 3098.
39. Perdew, J.P. *Phys. Rev. B* **1986**, *33*, 8822.

Activation of White Phosphorus by Uranium(III) *tris*-Amide Complexes¹

Table of Contents

4.1 Introduction.....	114
4.2 Results and Discussion	114
4.3 Theoretical Section	118
4.4 Future Work.....	120
4.5 Experimental Section.....	121
4.5.1 General Considerations: Synthesis and Characterization.....	121
4.6 References.....	124

List of Figures

Figure 4.1: Molecular structure of $(\mu\text{-}\eta^4, \eta^4\text{-P}_4)[\text{U}(\text{N}[t\text{-Bu}]\text{Ar})_3]_2$	116
Figure 4.2: Molecular structure of $(\mu\text{-}\eta^4, \eta^4\text{-P}_4)[\text{U}(\text{N}[1\text{-Ad}]\text{Ar})_3]_2$	117
Figure 4.3: Orbital pictures for model compound $(\mu\text{-}\eta^4, \eta^4\text{-P}_4)[\text{U}(\text{NH}_2)_3]_2$	119

List of Schemes

Scheme 4.1: Reaction of 8 -THF with white phosphorus.....	115
Scheme 4.2: Reaction of silyl triflates with 8 ₂ -P ₄ or 9 ₂ -P ₄	120

List of Tables

Table 4.1: Selected bond lengths and angles for 8 ₂ -P ₄	116
Table 4.2: Selected bond lengths and angles for 9 ₂ -P ₄	117
Table 4.3: Crystallographic parameters for 8 ₂ -P ₄ and 9 ₂ -P ₄	123

4.1 Introduction

Synthesis of reactive organometallic and inorganometallic uranium compounds has facilitated a tremendous leap forward in the understanding of actinide coordination chemistry and the use of *f* orbitals in bonding.² The number of accessible oxidation states available on uranium has led chemists to call this element a “big transition metal.” However, the larger number of valence orbitals, their symmetry, and the larger radius of the metal should permit the synthesis of a wide variety of uranium complexes that do not have transition metal analogs.

As reported by the Cummins group,^{3–5} δ -backbonding from uranium to arenes was one of these important breakthroughs in organoactinide chemistry. The complexes synthesized include the amide-supported (μ -arene)[U(N[R]Ar)₂]₂ (R = *t*-Bu, 1-Ad; arene = benzene, toluene)³ and the ketimide-supported (μ -arene)[U(N=C(*t*-Bu)(Mes))₃]₂ (Mes = 2,4,6-C₆H₂Me₃; arene = naphthalene, cyclooctatetraene).⁴ The arenes were incorporated into these compounds via reduction of a uranium(IV) halide precursor in the presence of the desired arene. For example, the U(IV) compound IU(N[*t*-Bu]Ar)₃ (**8-I**)⁶ was reduced using potassium graphite in toluene solvent forming (μ -C₆H₅Me)[U(N[*t*-Bu]Ar)₂]₂ (**8₂-toluene**). In this molecule, each uranium fragment can be considered in the oxidation state +2 while the bridging arene is formally neutral. The two, strong δ -backbonds are from filled uranium 6*d* and 5*f* orbitals into the doubly-degenerate arene LUMO having δ symmetry. These conclusions were verified structurally and computationally.

There are few examples of white phosphorus activation by transition metals and actinides resulting in dinuclear, bridging μ -P_{*n*} species. Examples of several μ -P₁ compounds have been given in this thesis.^{7,8} Sacconi *et al.* have reported a variety of (μ - $\eta^{3:3}$ -P₃)M₂(triphos)₂ (M = Rh, Co, Ni) compounds.⁹ Scherer *et al.* have also reported a wide variety of white phosphorus activation products including an interesting thorium compound with a bridging P₃ moiety, Cp'₂Th(μ -P₃)ThCp'₂Cl.¹⁰ There are exceedingly few bridging P₄ compounds reported where each phosphorus atom is two coordinate (only considering P–P interactions),¹¹ and none of these contains a square tetraphosphorus moiety.

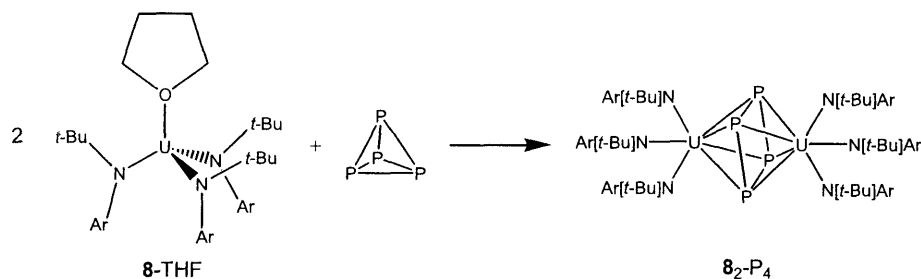
Here is reported the first example of a square tetraphosphorus moiety bridging two metals. Spectroscopic and X-ray crystallographic evidence is provided for this structural assignment. Density functional theory calculations are also presented, and an analysis of this compound's electronic structure is provided.

4.2 Results and Discussion

White phosphorus (P₄) does not react with U(IV) species of the type IU(N[*t*-Bu]Ar)₃ (**8-I**) after 24 h in toluene. Inspired by the synthesis of **8₂-toluene**, compound **8-I** was subjected to sodium amalgam reduction in the presence of one equivalent of P₄. However, this reaction resulted primarily in formation of red phosphorus (polymeric P_{*n*})¹² and U(N[*t*-Bu]Ar)₄. Therefore, isolation and use of the more reactive U(III) compound

(THF)U(N[*t*-Bu]Ar)₃ (**8**-THF) was deemed necessary for activation of white phosphorus. As previously reported, this reactive uranium(III) species has opened the door to a wealth of low-valent uranium chemistry, including the formation of new imido,¹³ μ -oxo,¹³ methyl,¹⁴ silyl,¹⁴ and heterobimetallic bridging N₂ species.⁶ Compound **8**-THF was prepared by reduction of **8**-I using sodium amalgam in tetrahydrofuran.⁶ This compound was synthesized in 500 mg batches, and was isolated as black crystals from cold pentane.

Scheme 4.1: Reaction of **8**-THF with white phosphorus.



First discovered by Drs. Polly Arnold and Aaron Odom, reaction of 0.5 equivalents of white phosphorus with **8**-THF resulted in formation of an orange-brown compound (Scheme 1) with a ³¹P NMR shift at $\delta = 794$ ppm. Use of less than 0.5 equiv P₄ resulted in formation of the same orange-brown product, leaving behind unreacted **8**-THF. Use of more than 0.5 equiv P₄ resulted in formation of the same product with unreacted P₄ (as assayed by ³¹P NMR spectroscopy). X-ray crystal structure determination revealed the identity of this product, $(\mu\text{-}\eta^{4:4}\text{-P}_4)[\text{U}(\text{N}[\textit{t}\text{-Bu}]\text{Ar})_3]_2$ (**8**₂-P₄), a compound with a square P₄ moiety bridging two uranium *tris*-amide fragments (Figure 4.1). Compound **8**₂-P₄ crystallized in the space group $\text{P}\bar{1}$, and the two halves of the molecule are related by an inversion center located at the P₄-square centroid. Within 3 σ , the P–P bond lengths are 2.160 Å and the P–P–P bond angles are 90°. The U–N interatomic distances are approximately 2.23 Å, approximately the same as those in the uranium(IV) compound ((Me₃Si)₃Si)U(N[*t*-Bu]Ar)₃ (**8**-Si(SiMe₃)₃; U–N, 2.210(5) Å).¹⁴

The square tetraphosphorus bridge in compound **8**₂-P₄ represents the formal two-electron reduction of P₄, with concomitant formation of two U(IV) fragments. This structural motif is unique in organometallic chemistry. Square tetrapnictide clusters are known in solid state chemistry for bismuth,¹⁵ antimony,^{16,17} arsenic,^{17,18} and phosphorus.^{17,19} These clusters have a formal 2– charge, which is balanced by alkali metal cations. The recently published phosphorus system Cs₂P₄·2NH₃ was prepared by treatment of P₂H₄ with cesium metal at –78 °C followed by crystallization from anhydrous ammonia at –40 °C. Crystallographic characterization of this yellow compound revealed P–P bond lengths of 2.146(1) and 2.1484(9) Å. These lengths are only slightly shorter than the corresponding distances in **8**₂-P₄. This small lengthening is consistent with a δ -backbonding interaction from uranium into the LUMO of P₄^{2–}.

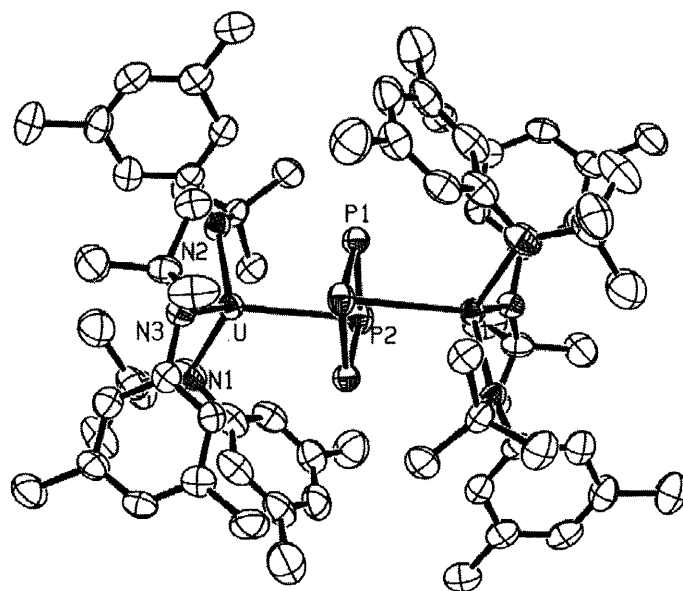


Figure 4.1: Molecular structure of $(\mu\text{-}\eta^4,\eta^4\text{-P}_4)[\text{U}(\text{N}[t\text{-Bu}]\text{Ar})_3]_2$ (35% thermal ellipsoids). Hydrogen atoms and a co-crystallized molecule of pentane are omitted for clarity.

Table 4.1: Selected bond lengths and angles for $\mathbf{8}_2\text{-P}_4$.

<i>Bond Lengths (Å)</i>		<i>Bond Angles (deg)</i>	
P1–P2	2.162(2)	P2–P1–P2′	89.48(9)
P1–P1′	2.157(2)	P1–P2–P1′	90.52(8)
P1–P2′	2.156(2)	U–P2–P1	71.61(6)
U–P1	3.158(2)	U–P1–P2′	70.14(6)
U–P2	3.084(2)	U–P1–P2	67.89(6)
U–P1′	3.101(2)	U–P1–U′	121.32(5)
U–P2′	3.162(2)	U–P2–U′	121.77(5)

Compound $\mathbf{8}_2\text{-P}_4$ has a complicated ^1H NMR spectrum at 20 °C in benzene- d_6 .²⁰ If all of the ligands in $\mathbf{8}_2\text{-P}_4$ were equivalent in solution, four peaks would be seen. These would correspond to the *tert*-butyl and aryl methyl groups, and to the *ortho* and *para* protons. However, there are thirteen obvious peaks in the room temperature ^1H NMR spectrum! To aid in the assignment of this spectrum, deuterated variants $(\mu\text{-}\eta^4,\eta^4\text{-P}_4)[\text{U}(\text{N}[\text{C}(\text{CH}_3)(\text{CD}_3)_2]\text{Ar})_3]_2$ ($\mathbf{8}_2\text{-P}_4\text{-}d_{36}$) and $(\mu\text{-}\eta^4,\eta^4\text{-P}_4)[\text{U}(\text{N}[\text{C}(\text{CH}_3)(\text{CD}_3)_2][3,5\text{-C}_6\text{Me}_2\text{D}_3]_2)]_2$ ($\mathbf{8}_2\text{-P}_4\text{-}d_{54}$) were synthesized. The synthesis of these compounds is identical to that for $\mathbf{8}_2\text{-P}_4$; deuterated variants of $\mathbf{8}\text{-THF}$ were prepared in two steps from $\text{HN}[t\text{-Bu}]\text{Ar-}d_6$ ²¹ and $\text{HN}[t\text{-Bu}]\text{Ar-}d_9$.^{*,22} From the ^1H and ^2H NMR spectra of these

* $\text{HN}[t\text{-Bu}]\text{Ar-}d_9$ was synthesized from acetone- d_6 and $\text{H}_2\text{NAr-}d_3$ followed by addition of MeLi as described in Reference 20. The deuteration of the aniline $\text{H}_2\text{NAr-}d_3$ is described in Reference 21.

compounds, it was possible to determine that the solution structure of $\mathbf{8}_2\text{-P}_4$ includes three ligand environments in a 3:2:1 ratio. This is not the same ligand arrangement as in the crystal structure reported above, in which there are two ligands that have their aryl groups pointing toward the *cyclo*- P_4 unit and four other ligands that have approximately the opposite configuration. It was straightforward to assign the aryl methyl peaks since their integration did not change upon deuteration. At -11.7 ppm, there is a broadened singlet integrating to 6 hydrogen atoms; at -0.32 ppm, there is a broad singlet (with a shoulder on the upfield side of the peak, *vide infra*) integrating to 12 hydrogen atoms; at 0.53 ppm, there is a slightly broadened singlet integrating to 18 hydrogen atoms. It further appears from a combination of ^1H and ^2H NMR spectra that there are three *tert*-butyl environments in the molecule in a 3:2:1 ratio. At -9.6 ppm, there is a singlet integrating to 9 hydrogen atoms; a shoulder at approximately -0.33 ppm corresponds to 27 hydrogen atoms; at 10.7 ppm, there is a singlet integrating to 18 hydrogen atoms. Full assignments for $\mathbf{8}_2\text{-P}_4$ and its deuterated variants can be found in the Experimental Section.

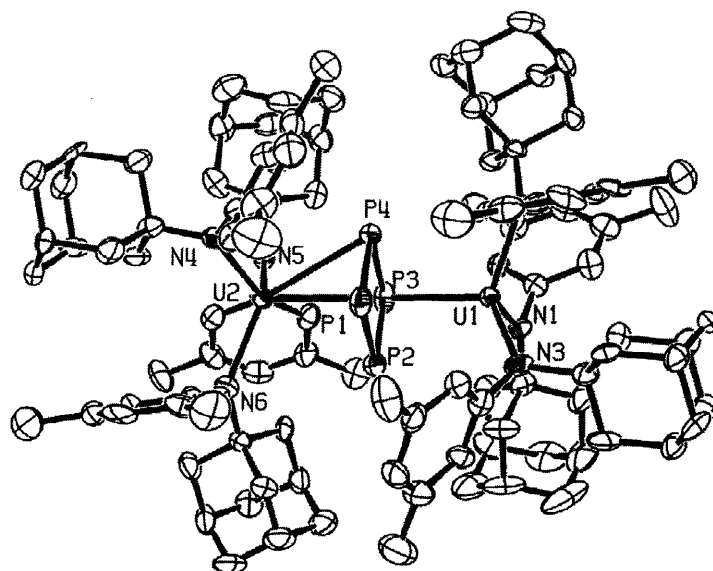


Figure 4.2: Molecular structure of $(\mu\text{-}\eta^4,\eta^4\text{-P}_4)[\text{U}(\text{N}[1\text{-Ad}]\text{Ar})_3]_2$ (35% thermal ellipsoids). Hydrogen atoms and a co-crystallized molecule of diethyl ether are omitted for clarity.

Table 4.2: Selected bond lengths and angles for $\mathbf{9}_2\text{-P}_4$.

<i>Bond Lengths (Å)</i>		<i>Bond Angles (deg)</i>	
P1–P2	2.138(6)	P2–P1–P4	90.2(2)
P2–P3	2.168(6)	P1–P2–P3	90.7(2)
P3–P4	2.171(5)	U1–P1–P2	66.19(14)
U1–P1	3.277(4)	U1–P1–P4	67.07(13)
U1–P2	3.107(4)	U2–P1–P2	67.76(14)
U1–P3	2.975(4)	U1–P1–U2	111.19(11)
U1–P4	3.138(4)	U1–P2–U2	119.18(12)

The analogous but more sterically hindered system $(\mu\text{-}\eta^4, \eta^4\text{-P}_4)[\text{U}(\text{N}[1\text{-Ad}]\text{Ar})_3]_2$ ($\mathbf{9}_2\text{-P}_4$) was also synthesized. Starting from $\text{UI}_3(\text{THF})_4$ ²³ and $\text{KN}[1\text{-Ad}]\text{Ar}$,^{5,24} the reactive black $(\text{THF})\text{U}(\text{N}[1\text{-Ad}]\text{Ar})_3$ ($\mathbf{9}\text{-THF}$) was synthesized.⁵ Dissolution of $\mathbf{9}\text{-THF}$ in toluene and cooling to $-35\text{ }^\circ\text{C}$, followed by addition of solid P_4 resulted in formation of the desired orange-brown product $\mathbf{9}_2\text{-P}_4$. It was recrystallized from cold toluene in *ca.* 55% overall yield as an orange-brown powder. This compound had an extremely broadened ^1H NMR spectrum at $20\text{ }^\circ\text{C}$. While it sharpened at temperatures above $30\text{ }^\circ\text{C}$, there appeared to be several ligand environments. Assignment of the high (*ca.* $60\text{ }^\circ\text{C}$) or low (*ca.* $-50\text{ }^\circ\text{C}$) temperature ^1H NMR spectra was not attempted, because efficient deuteration methods for the 1-adamantyl substituent have not been developed. Therefore, characterization of $\mathbf{9}_2\text{-P}_4$ was obtained primarily through the ^{31}P NMR shift at $\delta = 803$ ppm, which is within a few parts per million of the ^{31}P NMR shift of $\mathbf{8}_2\text{-P}_4$. An X-ray crystal structure of $\mathbf{9}_2\text{-P}_4$, which crystallized in the $P2_1/n$ space group, did not contain an inversion center at the *cyclo*- P_4 centroid (Figure 4.2). Its P–P and U–P distances were the same (within 3σ) as those in $\mathbf{8}_2\text{-P}_4$ (Table 4.2).

Reaction of $\mathbf{9}_2\text{-P}_4$ with iodine (I_2) was expected to result in formation of two equivalents of $\text{IU}(\text{N}[1\text{-Ad}]\text{Ar})_3$ ($\mathbf{9}\text{-I}$) and regeneration of P_4 . The latter could be detected using ^{31}P NMR, as it displays a signal at $\delta = -516$ ppm. Oxidation of $\mathbf{9}_2\text{-P}_4$ did occur upon addition of I_2 ; PI_3 was generated, consistent with reaction of P_4 with the remaining I_2 .²⁵ While $\mathbf{9}\text{-I}$ was one of the products generated, it was only one of the myriad of products present in the reaction mixture due to side reactions with PI_3 . A reagent such as 1,2-diiodoethane may be an appropriate oxidant since is not known to react with P_4 .

4.3 Theoretical Section

Computational actinide chemistry has made significant advances in the past decade. Theoretical studies of the electronic structure and reactions of actinides considerably augment the synthetic literature considering the radioactivity and scarcity of these elements.^{2a} Most chemists interested in computationally studying uranium complexes utilize density functional theory (DFT) to do so. DFT has several advantages over the other commonly used computational technique, Hartree-Fock self-consistent-field (HF-SCF) method. Primarily, these benefits are computational speed and incorporation of relativistic and spin-orbit effects. Both of these effects are important to include in calculations containing the *f* elements. Relativistic effects describe the significant expansion of the valence *d* and *f* orbitals due to shielding of the nucleus by contracted *s* and *p* orbitals. Spin orbit effects, which strongly depend on nuclear charge, are due to the spin angular momentum interacting with the total angular momentum of the orbital wavefunction.^{2a} The results reported herein were generated by DFT calculations.^{26,27}

The phenomenon of backbonding in uranium complexes is relatively recently documented. In 1986, the compound $\text{Cp}^{\text{Si}}_3\text{U}(\text{CO})$ ($\text{Cp}^{\text{Si}} = \text{C}_5\text{H}_4\text{SiMe}_3$) was characterized with a ν_{CO} approximately 170 cm^{-1} lower than free carbon monoxide.²⁸ This significant

lowering of the CO stretching frequency is analogous to transition metal carbonyl complexes, in which there is a strong π -backbonding interaction (Dewar-Chatt-Duncanson model).^{29,30} Compound $\text{Cp}^{\text{Si}}_3\text{U}(\text{CO})$ was shown by DFT to contain a similar interaction, with a σ bonding component from the HOMO of CO to the empty $6d_{z^2}$ orbital of uranium and a π -backbonding component from the filled uranium $5f$ orbitals to the LUMO of CO.^{2b} Examples of π -backbonding from uranium to side-on dinitrogen has since been published.^{31,32} In these cases, only the π -backbonding component of the Dewar-Chatt-Duncanson model of backbonding is noted; the σ component of the bond is not observed because the nitrogen molecular orbitals are too low in energy to effectively overlap with the appropriate uranium orbital.

Ferrocene analog $[\text{Ti}(\eta^5\text{-P}_5)_2]^{2-}$, published recently by Ellis *et al.*, displays a δ back-bonding interaction from a e_2' Ti orbital to the LUMO of the two P_5 fragments.^{33–35} As was shown recently by our group, low-valent uranium can engage in δ backbonding to the doubly degenerate LUMO of toluene or benzene. This strong interaction holds together dinuclear complexes of uranium with arene bridges in the case of amide³ or ketimide⁴ ligands. Here, in the cases of $\mathbf{8}_2\text{-P}_4$ and $\mathbf{9}_2\text{-P}_4$, there is a bridging tetraphosphorus moiety. The X-ray crystal structure of $\mathbf{8}_2\text{-P}_4$ revealed a square geometry for this bridge, indicating that its appropriate formulation is P_4^{2-} . This dianion is isolobal and isoelectronic with $[\text{C}_4\text{H}_4]^{2-}$, having six π electrons and a singly degenerate LUMO of δ symmetry.³⁶

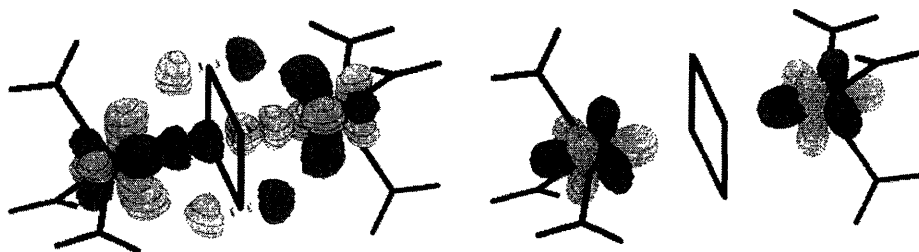


Figure 4.3: Orbital pictures generated by Molden for model compound $(\mu\text{-}\eta^4, \eta^4\text{-P}_4)[\text{U}(\text{NH}_2)_3]_2$. Left: HOMO–1, interaction between the LUMO of P_4^{2-} (δ symmetry) and uranium df hybrid orbitals; Right: HOMO, uranium f orbitals.

In order to understand the bonding between the uranium centers and the P_4 bridge in the compounds discussed above, a computational study on the model system $(\mu\text{-}\eta^4, \eta^4\text{-P}_4)[\text{U}(\text{NH}_2)_3]_2$ was undertaken.[†] Density functional theory (DFT) calculations show that the HOMO–1 orbital has δ symmetry but exhibits minimal overlap between bridge and metals (as compared to the strong δ backbonds of the aforementioned arene complexes)

[†] Thomas A. Baker and Christopher C. Cummins utilized *ADF 2.3.0* to complete this calculation.^{26,27} Relativistic corrections were incorporated using the Pauli scalar function with a frozen core approximation. Attempts to update these results using a more recent version of the software (*ADF 2000.02*) were unsuccessful; the calculations converged with non-Aufbau solutions.

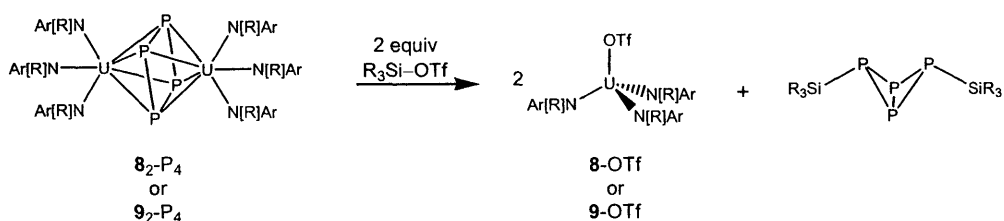
(Figure 4.3). Quite interestingly, no other orbitals show appreciable overlap between the uranium centers and the P_4 bridge. Therefore, we formulate this compound as an ionic compound supported by a weak δ bond. The formal oxidation state of both uranium centers is an often-observed^{2b} +4 (f^2) and the bridging unit is a formal P_4^{2-} .

The ionic nature of this system is further supported by the ^{31}P NMR data for these compounds. Both the *t*-Bu and 1-Ad derivatives exhibit resonances at $\delta = ca.$ 800 ppm, despite the paramagnetism of the complexes. The ^{31}P NMR shifts are observable due to the aforementioned limited orbital overlap. It is also seen from the DFT calculations that the unpaired electrons (HOMO) are localized in contracted *f* orbitals on the metals which have no contact with the orbitals on the bridge, further minimizing the signal broadening experienced by the phosphorus nuclei. These ^{31}P NMR signals are considerably further downfield than that observed for $\text{Cs}_2\text{P}_4 \cdot 2 \text{NH}_3$, which displays a singlet at 345.8 ppm (liquid ammonia, -60°C).¹⁹ This diamagnetic compound unambiguously consists of a P_4^{2-} unit supported by ammonia-complexed cesium cations. In diamagnetic compounds, the magnitude of the downfield shift of an NMR signal is primarily determined by the paramagnetic shielding component, which is related to the size of the HOMO-LUMO gap; a compound with a large HOMO-LUMO gap will have a signal that is upfield of a compound with a small HOMO-LUMO gap.

4.4 Future Work

Attempts to functionalize the P_4^{2-} unit of $\mathbf{8}_2\text{-P}_4$ and $\mathbf{9}_2\text{-P}_4$ are underway.¹ Addition of electrophiles like organosilyl triflates to these compounds may result in extrusion of two equivalents of $(\text{TfO})\text{U}(\text{N}[\text{R}]\text{Ar})_3$ ($\text{R} = t\text{-Bu}, 1\text{-Ad}$) with concomitant formation of a silylated P_4 unit. Silylated bicyclotetraphosphanes of this sort are rare molecules. The known example utilizes an extremely bulky R group, tri-*tert*-butylsilyl.³⁷ The compound 2,4-bis-(tri-*tert*-butylsilyl)-1,2,3,4-tetraphospha-bicyclo[1.1.0]butane ($\text{P}_4(\text{Si-}t\text{-Bu}_3)_2$) is synthesized during the reaction of hexa-*tert*-butyldisilane with white phosphorus at 100°C for 38 h. It can also be synthesized as one component of the product mixture when tri-*tert*-butylsilyl sodium is mixed with phosphorus trichloride in pentane for 5 h at 20°C . Compounds $\mathbf{8}_2\text{-P}_4$ and $\mathbf{9}_2\text{-P}_4$ allow the possibility of accessing similar bicyclotetraphosphanes via a mild route, directly from the element P_4 .

Scheme 4.2: Reaction of silyl triflates with $\mathbf{8}_2\text{-P}_4$ or $\mathbf{9}_2\text{-P}_4$.



To fully analyze the products of the reaction shown in Scheme 4.2, (TfO)U(N[*t*-Bu]Ar)₃ (**8**-OTf) was synthesized independently. Reaction of the uranium(IV) iodide **8**-I with silver triflate in tetrahydrofuran followed by removal of solvent and extraction with pentane allowed isolation of yellow **8**-OTf.³⁸ Synthesis of this compound may open an important door for synthetic recovery of the otherwise inert (μ-O)[U(N[*t*-Bu]Ar)₃]₂ (**8**₂-O). Treatment of **8**₂-O with one equivalent of triflic anhydride (Tf₂O) should form two equivalents of **8**-OTf.[†] The latter compound may be reduced³⁹ to a useful uranium(III) compound using sodium amalgam in a protocol similar to the preparation of **8**-THF from **8**-I.

4.5 Experimental Section

4.5.1 General Considerations: Synthesis and Characterization.

Unless stated otherwise, all operations were performed in a Vacuum Atmospheres drybox under an atmosphere of purified nitrogen or using Schlenk techniques under an argon atmosphere. Diethyl ether, toluene, benzene, *n*-pentane, and *n*-hexane were dried and deoxygenated by the method of Grubbs.⁴⁰ THF was distilled under nitrogen from purple sodium benzophenone ketyl. Benzene-*d*₆ was purchased from Cambridge Isotope Laboratory, was degassed, and was dried over 4 Å sieves. Alumina, Celite, and 4 Å sieves were dried *in vacuo* overnight at a temperature above 200 °C. UI₃(THF)₄, (THF)U(N[*t*-Bu]Ar)₃ and KN[1-Ad]Ar were synthesized according to literature procedures. Other chemicals were used as received. ¹H and ²H NMR spectra were recorded on Varian XL-300, Varian Mercury-300, or Varian INOVA-501 spectrometers at room temperature. Chemical shifts are reported with respect to internal residual benzene (7.15 and 128.38 (t) ppm) or external C₆D₆ in diethyl ether (7.16 ppm). C, H, and N analyses were performed by H. Kolbe Mikroanalytisches Laboratorium (Mülheim, Germany).

Synthesis of (μ-η^{4:4}-P₄)[U(N[*t*-Bu]Ar)₃]₂ (8**₂-P₄).** A hexane solution of (THF)U(N[*t*-Bu]Ar)₃ (0.119 g, 0.142 mmol) was chilled to -35 °C. To this solution was added solid P₄ (0.008 g, 0.066 mmol, 0.46 equiv) was added to this solution. The reaction mixture was stirred rapidly for 20 min, warming to room temperature. After this time, the solvent was removed *in vacuo*. The residue was extracted with pentane and the orange-brown, microcrystalline product was crystallized at -35 °C (0.025 g, 0.015 mmol, 10%). ¹H NMR (500 MHz, C₆D₆): δ = 16.73 (4H, *ortho*), 11.47 (6H, *ortho*), 10.50 (18H, *tert*-butyl), 5.05 (3H, *para*), 4.11 (2H, *para*), 0.53 (18H, aryl methyl), -0.33 (39H, overlapping aryl methyl and *tert*-butyl), -5.0 (2H, *ortho*), -6.86 (1H, *para*), -9.61 (9H, *tert*-butyl), -11.64 (6H, aryl methyl) ppm. ³¹P NMR (125 MHz, C₆D₆): δ = 794 ppm. Anal. Calcd. for C₇₂H₁₀₈N₆P₄U₂: C, 52.17; H, 6.57; N, 5.07. Found: C, 51.63; H, 5.90; N, 4.92.

(μ-η^{4:4}-P₄)[U(N[C(CH₃)(CD₃)₂]Ar)₃]₂ (**8**₂-P₄-*d*₃₆). ¹H NMR (500 MHz, C₆D₆): δ = 16.73 (4H, *ortho*), 11.47 (6H, *ortho*), 10.50 (6H, *tert*-butyl), 5.05 (3H, *para*), 4.11 (2H,

[†] Similar observations have been made for niobium *tris*-amides.³³

para), 0.53 (18H, aryl methyl), -0.33 (21H, overlapping aryl methyl and *tert*-butyl), -5.0 (2H, *ortho*), -6.86 (1H, *para*), -9.61 (3H, *tert*-butyl), -11.64 (6H, aryl methyl) ppm. ^2H NMR (77 MHz, C_6H_6): $\delta = 10.8, -0.3, -9.5$ ppm.

$(\mu\text{-}\eta^{4:4}\text{-P}_4)[\text{U}(\text{N}[\text{C}(\text{CH}_3)(\text{CD}_3)_2][3,5\text{-C}_6\text{Me}_2\text{D}_3])_3]_2$ (**8₂-P₄-d₅₄**). ^1H NMR (500 MHz, C_6D_6): $\delta = 10.50$ (6H, *tert*-butyl), 0.53 (18H, aryl methyl), -0.33 (21H, overlapping aryl methyl and *tert*-butyl), -9.61 (3H, *tert*-butyl), -11.64 (6H, aryl methyl) ppm. ^2H NMR (77 MHz, C_6H_6): $\delta = 11.5$ (*ortho*), 10.6 (*tert*-butyl), 6.0 (*para*), 4.1 (*para*), -0.3 (*tert*-butyl), -9.61 (*tert*-butyl) ppm.

Synthesis of $(\mu\text{-}\eta^{4:4}\text{-P}_4)[\text{U}(\text{N}[1\text{-Ad}]\text{Ar})_3]_2$ (9₂-P₄**).** A tetrahydrofuran solution of (THF) $\text{U}(\text{N}[1\text{-Ad}]\text{Ar})_3$ (0.439 g, 0.409 mmol) was chilled to $-35\text{ }^\circ\text{C}$. To this solution was added solid P_4 (0.050 g, 0.407 mmol, 1 equiv) was added to this solution. Vacuum was applied immediately to remove the solvent. The residue was extracted with pentane and the orange-brown, microcrystalline product was crystallized at $-35\text{ }^\circ\text{C}$ (0.369 g, 0.173 mmol, 42%). ^1H NMR (500 MHz, toluene-*d*₈): $\delta =$ very broad peaks between 6 and 0, -0.09, -2.5, -9.5 ppm. ^{31}P NMR (125 MHz, C_6D_6): $\delta = 803$ ppm. Anal. Calcd. for $\text{C}_{108}\text{H}_{144}\text{N}_6\text{P}_4\text{U}_2$: C, 61.01; H, 6.82; N, 3.95. Found: C, 60.25; H, 4.86; N, 3.70.

Synthesis of (TfO) $\text{U}(\text{N}[t\text{-Bu}]\text{Ar})_3$ (8-OTf**).** A THF solution of $\text{IU}(\text{N}[t\text{-Bu}]\text{Ar})_3$ (2.694 g, 3.2 mmol) was chilled to $-35\text{ }^\circ\text{C}$. This solution was added to solid silver triflate (0.827 g, 3.2 mmol) in a vial that had been chilled to $-35\text{ }^\circ\text{C}$. After 1.5 h, the reaction mixture was filtered to separate $\text{Ag}(0)$ and the solvent was removed from the filtrate *in vacuo*. The yellow-brown residue was dissolved in diethyl ether and the product was recrystallized. Yellow-green needles were isolated by crystallization (0.431 g, 0.500 mmol, 15%). ^1H NMR (C_6D_6 , 300 MHz): $\delta = 10.55$ (s, 27H, *tert*-butyl, $\Delta\nu_{1/2} = 17$ Hz), 6.59 (s, 6H, *ortho*, $\Delta\nu_{1/2} = 38$ Hz), -0.32 (s, 3H, *para*, $\Delta\nu_{1/2} = 4.6$ Hz), -4.18 (18H, aryl methyl, $\Delta\nu_{1/2} = 4$ Hz) ppm. ^{19}F NMR (Et_2O , 282 MHz): $\delta = -103$ ($\Delta\nu_{1/2} = 65$ Hz) ppm. Anal. Calcd. for $\text{C}_{37}\text{H}_{54}\text{F}_3\text{N}_3\text{O}_3\text{SU}$: C, 48.52; H, 5.94; N, 4.59. Found: C, 48.65; H, 5.83; N, 4.62.

4.5.2 Crystallographic Structure Determinations.

The X-ray data collections were carried out on a Siemens Platform three-circle diffractometer (Mo $\text{K}\alpha$, $\lambda = 0.71073\text{ \AA}$) mounted with a CCD detector and outfitted with a low-temperature, nitrogen-stream aperture (189 K). The structures were solved by direct methods, in conjunction with standard difference Fourier techniques and refined by full-matrix least-squares procedures. Selected bond distances and angles are supplied in Tables 4.1. A summary of crystallographic data is given in Table 4.3, with full details found in Appendix 2. The systematic absences in the diffraction data are uniquely consistent with the assigned space group of $P\bar{1}$ for **8₂-P₄** and $P2_1/n$ for **9₂-P₄**. This choice led to a chemically sensible and computationally stable refinement. An empirical absorption correction (ψ -scans) was applied to the data set. All software for diffraction data processing and crystal-structure solution and refinement are contained in the SHELXTL (v5.10) program suite (G. Sheldrick, Siemens XRD, Madison, WI).

Table 4.3: Crystallographic parameters for $\mathbf{8}_2\text{-P}_4$ and $\mathbf{9}_2\text{-P}_4$.

	$\mathbf{8}_2\text{-P}_4$	$\mathbf{9}_2\text{-P}_4$
formula	$\text{C}_{108}\text{H}_{144}\text{N}_6\text{P}_4\text{U}_2$	$\text{C}_{112}\text{H}_{144}\text{N}_6\text{OP}_4\text{U}_2$
fw	2126.29	2190.27
space group	$P\bar{1}$	$P2_1/n$
a, Å	11.9018(6)	15.6370(13)
b, Å	13.8947(8)	41.909(4)
c, Å	13.9991(8)	18.8439(16)
α , deg	77.7170(10)	90
β , deg	69.9770(10)	112.399(2)
γ , deg	67.3510(10)	90
V, Å ³	1998.6(2)	11417.4(17)
Z	1	4
cryst description	orange prism	orange-brown prism
D_{calcd} , g·cm ⁻³	1.449	1.274
F(000)	876	4440
GOF on F ²	1.035	1.138
$R(F)$, % ^a	0.0336	0.0980
$R_w(F)$, % ^a	0.0802	0.2141

^a Quantity minimized = $R_w(F^2) = \sum[w(F_o^2 - F_c^2)^2] / \sum[(wF_o^2)^2]^{1/2}$; $R = \sum\Delta / \sum(F_o)$, $\Delta = |(F_o - F_c)|$, $w = 1/[\sigma^2(F_o^2) + (aP)^2 + bP]$, $P = [2F_c^2 + \text{Max}(F_o, 0)]/3$.

4.6 References

1. Stephens, F. H.; Arnold, P. L.; Odom, A. L.; Baker, T. A.; Figueroa, J. S.; Diaconescu, P. L.; Cummins, C. C. Manuscript in preparation.
2. See the following references for a discussion of *f* orbitals in bonding: (a) Kaltsoyannis, N. *Chem. Soc. Rev.* **2003**, *32*, 9. (b) Bursten, B. E.; Strittmatter, R. J. *J. Am. Chem. Soc.* **1987**, *109*, 6606. (c) Dibella, S.; Gulino, A.; Lanza, G.; Fragala, I. L.; Marks, T. J. *J. Phys. Chem.* **1993**, *97*, 11673. (d) Bursten, B. E.; Strittmatter, R. J. *Angew. Chem. Int. Ed. Engl.* **1991**, *30*, 1069. (e) Cayton, R. H.; Novogradac, K. J.; Bursten, B. E. *Inorg. Chem.* **1991**, *30*, 2265.
3. Diaconescu, P. L.; Arnold, P. L.; Baker, T. A.; Mindiola, D. J.; Cummins, C. C. *J. Am. Chem. Soc.* **2000**, *122*, 6108.
4. Diaconescu, P. L.; Cummins, C. C. *J. Am. Chem. Soc.* **2002**, *124*, 7660.
5. Diaconescu, P. L. Ph.D. Thesis, Massachusetts Institute of Technology, 2002.
6. Odom, A. L.; Arnold, P. L.; Cummins, C. C. *J. Am. Chem. Soc.* **1998**, *120*, 5836.
7. Cherry, J.-P. F.; Stephens, F. H.; Johnson, M. J. A.; Diaconescu, P. L.; Cummins, C. C. *Inorg. Chem.* **2001**, *40*, 6860.
8. Stephens, F. H.; Figueroa, J. S.; Diaconescu, P. L.; Cummins, C. C. *J. Am. Chem. Soc.* **2003**, *125*, 9264.
9. (a) Bianchini, C.; DiVaira, M.; Meli, A.; Sacconi, L. *Angew. Chem. Int. Ed. Engl.* **1980**, *19*, 405. (b) Bianchini, C.; DiVaira, M.; Meli, A.; Sacconi, L. *J. Am. Chem. Soc.* **1981**, *103*, 1448. (c) Dapporto, P.; Sacconi, L.; Stoppioni, P.; Zanobini, F. *Inorg. Chem.* **1981**, *20*, 3834.
10. Scherer, O. J.; Werner, B.; Heckman, G.; Wolmershäuser, G. *Angew. Chem. Int. Ed. Engl.* **1991**, *30*, 553.
11. (a) Scherer, O. J.; Völmecke, T.; Wolmershäuser, G. *Eur. J. Inorg. Chem.* **1999**, 945. (b) Scherer, O. J.; Vondung, J.; Wolmershäuser, G. *Angew. Chem.* **1989**, *101*, 1395.
12. Greenwood, N. N.; Earnshaw, A. *Chemistry of the Elements*; New York: Pergamon Press, 1984.
13. Odom, A. L. Ph.D. Thesis, Massachusetts Institute of Technology, 1998.
14. Diaconescu, P. L.; Odom, A. L.; Agapie, T.; Cummins, C. C. *Organometallics* **2001**, *20*, 4993.
15. Kuznetsov, A. N.; Fässler, T. F. *Z. Anorg. Allg. Chem.* **2002**, *628*, 2537.
16. Critchlow, S. C.; Corbett, J. D. *Inorg. Chem.* **1984**, *23*, 770.

17. Kuznetsov, A. E.; Zhai, H.-J.; Wang, L.-S.; Boldyrev, A. I. *Inorg. Chem.* **2002**, *41*, 6062.
18. Korber, N.; Reil, M. *Chem. Commun.* **2002**, 84.
19. Kraus, F.; Aschenbrenner, J. C.; Korber, N. *Angew. Chem. Int. Ed.* **2003**, *42*, 4030.
20. La Mar, G. N.; Horrocks, W. D.; Holm, R. H. *NMR of Paramagnetic Molecules: Principles and Applications*, Academic Press: New York, 1973.
21. Laplaza, C. E.; Davis, W. M.; Cummins, C. C. *Organometallics* **1995**, *14*, 577.
22. Tsai, Y.-C.; Stephens, F. H.; Meyer, K.; Mendiratta, A.; Gheorghiu, M. D.; Cummins, C. C. *Organometallics* **2003**, *22*, 2902.
23. Sattleberger, A. P.; Clark, D. L. *Inorg. Synth.* **1989**, *28*, 1771.
24. (a) Ruppá, K. B. P.; Desmangles, N.; Gambarotta, S.; Yap, G.; Rheingold, A. L. *Inorg. Chem.* **1997**, *36*, 1194. (b) Johnson, A. R.; Cummins, C. C. *Inorg. Synth.* **1998**, *32*, 123.
25. (a) Germann, F. E. E.; Traxler, R. N. *J. Am. Chem. Soc.* **1927**, *49*, 307. (b) Blachnik, R.; Rabe, U. *Z. Anorg. Allg. Chem.* **1980**, *461*, 87. (c) Edwards, H. G. M. *J. Mol. Struct.* **1987**, *158*, 153. (d) Tattershall, B. W.; Kendall, N. L. *Polyhedron* **1994**, *13*, 1517.
26. Baerends, E. J.; Ellis, D. E.; Ros, P. *Chem. Phys.* **1973**, *2*, 41.
27. te Velde, G.; Baerends, E. J. *J. Comput. Phys.* **1992**, *99*, 84.
28. Brennan, J. G.; Andersen, R. A.; Robbins, J. L. *J. Am. Chem. Soc.* **1986**, *108*, 335.
29. (a) Mingos, D. M. P. *J. Organomet. Chem.* **2001**, *635*, 1. (b) Winterton, N. *Mod. Coord. Chem.* **2002**, 103.
30. (a) Frenking, G. *Mod. Coord. Chem.* **2002**, 111. (b) Pidun, U.; Frenking, G. *J. Organomet. Chem.* **1996**, *525*, 269. (c) Ehlers, A. W.; Dapprich, S.; Vyboishchikov, S. F.; Frenking, G. *Organometallics* **1996**, *15*, 105. (d) Pidun, U.; Frenking, G. *Organometallics* **1995**, *14*, 5325.
31. (a) Roussel, P.; Scott, P. *J. Am. Chem. Soc.* **1998**, *120*, 1070. (b) Kaltsoyannis, N.; Scott, P. *Chem. Commun.* **1998**, 1665. (c) Brown, K. L.; Kaltsoyannis, N. *Dalton* **1999**, 4425. (d) Roussel, P.; Errington, W. B.; Kaltsoyannis, N.; Scott, P. *J. Organomet. Chem.* **2001**, *635*, 69.
32. Cloke, F. G. N.; Hitchcock, P. B. *J. Am. Chem. Soc.* **2002**, *124*, 9352.
33. Urnéžius, E.; Brennessel, W. W.; Cramer, C. J.; Ellis, J. E.; Schleyer, P. v. R. *Science* **2002**, *295*, 832.

34. Lein, M.; Frunzke, J.; Frenking, G. *Inorg. Chem.* **2003**, *42*, 2504.
35. Cloke, F. G. N.; Green, J. C.; Hanks, J. R.; Nixon, J. F.; Suter, J. L. *Dalton* **2000**, 3534.
36. (a) Jung, Y.; Heine, T.; Schleyer, P. v. R.; Head-Gordon, M. *J. Am. Chem. Soc.* **2004**, *126*, 3132. (b) Kos, A. J.; Schleyer, P. v. R. *J. Am. Chem. Soc.* **1980**, *102*, 7928.
37. (a) Wiberg, N.; Wörner, A.; Lerner, H.-W.; Karaghiosoff, K. *Z. Naturforsch.* **2002**, *57B*, 1027. (b) Wiberg, N.; Wörner, A.; Lerner, H.-W.; Karaghiosoff, K.; Fenske, D.; Baum, G.; Dransfeld, A.; Schleyer, P. v. R. *Eur. J. Inorg. Chem.* **1998**, 833. (c) Wiberg, N.; Wörner, A.; Karaghiosoff, K. *Chem. Ber.* **1997**, *130*, 135. (d) Wiberg, N.; Wörner, A.; Nöth, H.; Karaghiosoff, K. in *Organosilicon Chemistry II* (Eds.: N. Auner, J. Weis) **1996**, Weinheim: VCH; 197. (e) Kovács, I.; Baum, G.; Fritz, G.; Fenske, D.; Wiberg, N.; Schuster, H.; Karaghiosoff, K. *Z. Anorg. Allg. Chem.* **1993**, *619*, 453.
38. Kiplinger, J. L.; John, K. J.; Morris, D. E.; Scott, B. L.; Burns, C. J. *Organometallics* **2002**, *21*, 4306.
39. Figueroa, J. S.; Cummins, C.C. Manuscript in preparation.
40. Pangborn, A. B.; Giardello, M. A.; Grubbs, R. H.; Rosen, R. K.; Timmers, F. J. *Organometallics* **1996**, *15*, 1518.

Appendix 1: Synthesis of MoCl₃(thf)₃

A modified version of the 1986 Dilworth preparation¹ of MoCl₃(thf)₃ has been utilized for several years by the Cummins group to make this important starting material on a 35 g or larger scale.² While this method generates large amounts of pure material (*ca.* 65% yield), the synthesis usually takes three days to perform: One for the preparation of MoCl₄(CH₃CN)₂, one for the preparation of MoCl₄(thf)₂, and one for the preparation of MoCl₃(thf)₃.

Recently Poli *et al.* published a new synthesis of MoCl₃(thf)₃.³ This small-scale synthesis (5 g or less) can be completed in a matter of several hours. With some modification of this published method, 30 g or more of pure MoCl₃(thf)₃ can be synthesized in several hours.⁴ The most important adjustments to the literature method are conscientious temperature and time control, as detailed below.

Approximately 300 mL of diethyl ether were chilled in a round-bottom flask using the cold well. To this cold solvent were added 29.71 g (10.8 mmol) of MoCl₅. This solution was stirred while the solid was added so that the solid was efficiently suspended. While the solution was still very cold, two equivalents of finely divided tin powder were added (25.7 g, 21.6 mmol, 1.98 equiv). Rapid stirring continued for 30 minutes during which time the deep brown suspension became orange. It must be ensured that the tin and unreacted MoCl₅ are stirring rapidly; this may involve scraping the sides of the flask to resuspend the solids. Over-reduction does not seem to be possible at this step, so the reaction time should be extended (up to 1 h) if the solids are not efficiently suspended.

After the suspension became orange, the reaction flask was placed back into the cold well while the solvent was pipetted away from the solids. The supernatant solvent was yellow, pale orange, or pale green, and it was discarded. To the cold solids were added approximately 200 mL tetrahydrofuran. The reaction mixture was rapidly stirred for *ca.* 15 min. During this time the supernatant became green and then blue. It is important to stop the reduction promptly at this point by filtering through a bed of Celite. (Carefully watch the color of the reaction! If the supernatant becomes purple or purple-red, the product will likely be over-reduced and unusable. The reaction can be stopped prematurely if the reduction appears to be proceeding more quickly than indicated.) The filtrate can be discarded after washing the mixture of product, tin, and tin chlorides with clean tetrahydrofuran.

To collect the product, the previously optimized procedure was followed.² Minimal methylene chloride was used to wash the solids, thereby extracting orange-red MoCl₃(thf)₃, into clean tetrahydrofuran. The volume of this orange-red solution was reduced under vacuum until orange MoCl₃(thf)₃ precipitated. The product was collected via vacuum filtration. Generally the first crop will be the purest (29.39 g, 7.0 mmol, 64.5 % yield); often, subsequent crops will have a pink or purple color. The impure batches of MoCl₃(thf)₃ appear to result in very greasy reaction products with lithium amides.

¹ Dilworth, J. R.; Zubieta, J. *Inorg. Synth.* **1986**, *24*, 193.

² Cherry, J.-P. F. Thesis, Massachusetts Institute of Technology, 2001.

³ Stoffelbach, F.; Saurenz, D.; Poli, R. *Eur. J. Inorg. Chem.* **2001**, 2699.

⁴ Dr. James Blackwell, Todd Ostomel, and Dr. John-Paul F. Cherry contributed to the optimization of this synthesis.

Appendix 2: Crystallographic Information and Tables

A2.1	X-ray crystal structure of $(\eta^2\text{-}(\text{D}_3\text{C})\text{C}=\text{NAr})\text{Mo}(\text{N}[i\text{-Pr-}d_6]\text{Ar})_3$ (2 - $(\eta^2\text{-imine})\text{-}d_{18}$).....	130
	Table A2.1.1. Atomic coordinates and equivalent isotropic displacement parameters for 2 - $(\eta^2\text{-imine})\text{-}d_{18}$	130
	Table A2.1.2. Bond lengths [\AA] and angles [$^\circ$] for 2 - $(\eta^2\text{-imine})\text{-}d_{18}$	131
	Table A2.1.3. Anisotropic displacement parameters for 2 - $(\eta^2\text{-imine})\text{-}d_{18}$	133
A2.2	X-ray crystal structure of $(t\text{-BuNC})\text{Mo}(\text{N}[i\text{-Pr}]\text{Ar})_3$ (3 - $t\text{-BuNC}$).....	135
	Table A2.2.1. Atomic coordinates and equivalent isotropic displacement parameters for 3 - $t\text{-BuNC}$	135
	Table A2.2.2. Bond lengths [\AA] and angles [$^\circ$] for 3 - $t\text{-BuNC}$	136
	Table A2.2.3. Anisotropic displacement parameters for 3 - $t\text{-BuNC}$	138
A2.3	X-ray Crystal Structure of $(1\text{-AdNC})_2\text{Mo}(\text{N}[i\text{-Pr}]\text{Ar})_3$ (2 - $(\text{AdNC})_2$).....	140
	Table A2.3.1. Atomic coordinates and equivalent isotropic displacement parameters for 2 - $(\text{AdNC})_2$	140
	Table A2.3.2. Bond lengths [\AA] and angles [$^\circ$] for 2 - $(\text{AdNC})_2$	142
	Table A2.3.3. Anisotropic displacement parameters for 2 - $(\text{AdNC})_2$	144
A2.4	X-ray crystal structure of $[\text{Na}(\text{THF})][(\mu\text{-P})\text{Mo}_2(\text{N}[i\text{-Pr}]\text{Ar})_6]$ $([\text{Na}(\text{THF})][\mathbf{2}_2\text{-}\mu\text{-P}])$	147
	Table A2.4.1. Atomic coordinates and equivalent isotropic displacement parameters for $[\text{Na}(\text{THF})][\mathbf{2}_2\text{-}\mu\text{-P}]$	147
	Table A2.4.2. Bond lengths [\AA] and angles [$^\circ$] for $[\text{Na}(\text{THF})][\mathbf{2}_2\text{-}\mu\text{-P}]$	149
	Table A2.4.3. Anisotropic displacement parameters for $[\text{Na}(\text{THF})][\mathbf{2}_2\text{-}\mu\text{-P}]$	152
A2.5	X-ray crystal structure of $\text{PMo}(\text{N}[i\text{-Pr}]\text{Ar})_3$ (2 -P).....	155
	Table A2.5.1. Atomic coordinates and equivalent isotropic displacement parameters for 2 -P.....	155
	Table A2.5.2. Bond lengths [\AA] and angles [$^\circ$] for 2 -P.....	157
	Table A2.5.3. Anisotropic displacement parameters for 2 -P.....	159
A2.6	X-ray Crystal Structure of $[\text{PMo}(\text{N}[i\text{-Pr}]\text{Ar})(\text{O-}2,6\text{-C}_6\text{H}_3\text{Me}_2)_2]_2$ (6 -P) $_2$).....	162
	Table A2.6.1. Atomic coordinates and equivalent isotropic displacement parameters for (6 -P) $_2$	162
	Table A2.6.2. Bond lengths [\AA] and angles [$^\circ$] for (6 -P) $_2$	163
	Table A2.6.3. Anisotropic displacement parameters for (6 -P) $_2$	165
A2.7	X-ray Crystal Structure of $\text{PMo}(\text{OMeCy})_3$ (4 -P).....	166
	Table A2.7.1. Atomic coordinates and equivalent isotropic displacement parameters for 4 -P.....	166
	Table A2.7.2. Bond lengths [\AA] and angles [$^\circ$] for 4 -P.....	166
	Table A2.7.3. Anisotropic displacement parameters for 4 -P.....	167

A2.8 X-ray Crystal Structure of (η^3 -P ₃)Mo(OCy) ₃ (HN[<i>i</i> -Pr]Ar) (7 -P ₃ -HN[<i>i</i> -Pr]Ar).....	168
Table A2.8.1. Atomic coordinates and equivalent isotropic displacement parameters for 7 -P ₃ -HN[<i>i</i> -Pr]Ar.	168
Table A2.8.2. Bond lengths [Å] and angles [°] for 7 -P ₃ -HN[<i>i</i> -Pr]Ar.....	169
Table A2.8.3. Anisotropic displacement parameters for 7 -P ₃ -HN[<i>i</i> -Pr]Ar.	171
A2.9 X-ray Crystal Structure of Mo ₂ (OCy) ₃ (N[<i>i</i> -Pr]Ar) ₃	172
Table A2.9.1. Atomic coordinates and equivalent isotropic displacement parameters for Mo ₂ (OCy) ₃ (N[<i>i</i> -Pr]Ar) ₃	172
Table A2.9.2. Bond lengths [Å] and angles [°] for Mo ₂ (OCy) ₃ (N[<i>i</i> -Pr]Ar) ₃	174
Table A2.9.3. Anisotropic displacement parameters for Mo ₂ (OCy) ₃ (N[<i>i</i> -Pr]Ar) ₃	176
A2.10 X-ray Crystal Structure of (μ - $\eta^{4:4}$ -P ₄)[U(N[<i>t</i> -Bu]Ar) ₃] ₂ (8 ₂ -P ₄).....	178
Table A2.10.1. Atomic coordinates and equivalent isotropic displacement parameters for 8 ₂ -P ₄	178
Table A2.10.2. Bond lengths [Å] and angles [°] for 8 ₂ -P ₄	179
Table A2.10.3. Anisotropic displacement parameters for 8 ₂ -P ₄	181
A2.11 X-ray Crystal Structure of (μ - $\eta^{4:4}$ -P ₄)[U(N[1-Ad]Ar) ₃] ₂ (9 ₂ -P ₄).....	183
Table A2.11.1: Atomic coordinates and equivalent isotropic displacement parameters for 9 ₂ -P ₄	183
Table A2.11.2: Bond lengths [Å] and angles [°] for 9 ₂ -P ₄	187
Table A2.11.3: Anisotropic displacement parameters for 9 ₂ -P ₄	194

A2.1 X-ray crystal structure of $(\eta^2\text{-}(\text{D}_3\text{C})\text{C}=\text{NAr})\text{Mo}(\text{N}[i\text{-Pr-}d_6]\text{Ar})_3$ (2- $(\eta^2\text{-imine})\text{-}d_{18}$).

Crystals grown from a concentrated diethyl ether solution at $-35\text{ }^\circ\text{C}$ were coated with Paratone N oil (Exxon) on a microscope slide. A green block was selected and mounted with wax on a glass fiber. A total of 14289 reflections ($-14 \leq h \leq 7$, $-16 \leq k \leq 14$, $-22 \leq l \leq 22$) were collected at 293(2) K in the θ range of 1.24 to 28.39 $^\circ$, of which 9914 were unique ($R_{\text{int}} = 0.1268$). All non-methyl hydrogen atoms were found in the difference map and refined isotropically. All methyl hydrogen atoms were placed in calculated ($d_{\text{CH}} = 0.96\text{ \AA}$) positions. The residual peak and hole electron density were 1.502 and $-1.450\text{ e}\cdot\text{\AA}^{-3}$, respectively. The least squares refinement converged normally with residuals of $R_1 = 0.0898$, $wR_2 = 0.1712$ based upon $I > 2\sigma I$, and GOF = 1.088 (based on F^2). Crystal and refinement data: Formula = $\text{C}_{44}\text{H}_{63}\text{MoN}_4$; space group, $\text{P}\bar{1}$; $a = 11.1241(15)\text{ \AA}$; $b = 12.0233(15)\text{ \AA}$; $c = 16.837(2)\text{ \AA}$; $\alpha = 78.988(3)\text{ }^\circ$; $\beta = 79.148(2)\text{ }^\circ$; $\gamma = 72.990(3)\text{ }^\circ$; $V = 2092.7(5)\text{ \AA}^3$; $Z = 2$; $D_{\text{calc}} = 1.181\text{ g}\cdot\text{cm}^{-3}$; $F(000) = 794$; R_1 (based on F) = 0.1159; wR_2 (based on F_2) = 0.1919.

Table A2.1.1. Atomic coordinates ($\times 10^4$) and equivalent isotropic displacement parameters ($\text{\AA}^2 \times 10^3$) for 2- $(\eta^2\text{-imine})\text{-}d_{18}$. U(eq) is defined as one third of the trace of the orthogonalized U^{ij} tensor.

	x	y	z	U(eq)
Mo(1)	7386(1)	-3752(1)	7509(1)	24(1)
N(1)	7780(5)	-2701(4)	6501(3)	34(1)
N(2)	5934(4)	-3075(4)	8291(3)	30(1)
N(3)	8911(5)	-4727(4)	7982(3)	34(1)
N(4)	6299(5)	-4339(4)	6981(3)	35(1)
C(11)	7816(6)	-1543(5)	6582(3)	33(1)
C(12)	8896(6)	-1308(5)	6715(4)	43(1)
C(13)	8883(7)	-182(6)	6835(5)	57(2)
C(14)	7784(7)	700(5)	6784(5)	52(2)
C(15)	6697(6)	524(5)	6636(4)	44(2)
C(16)	6715(6)	-618(5)	6537(4)	37(1)
C(17)	8057(7)	-2985(5)	5651(4)	42(1)
C(18)	9489(8)	-3382(7)	5385(5)	69(2)
C(19)	7426(8)	-2017(6)	5034(4)	54(2)
C(21)	6243(6)	-2536(5)	8901(3)	33(1)
C(22)	6388(6)	-3129(5)	9678(4)	38(1)
C(23)	6647(6)	-2612(6)	10278(4)	42(1)
C(24)	6756(7)	-1473(6)	10074(4)	50(2)
C(25)	6647(7)	-851(6)	9301(4)	50(2)
C(26)	6373(6)	-1384(5)	8708(4)	43(1)

C(27)	4553(6)	-3005(5)	8371(4)	36(1)
C(28)	3747(6)	-1732(6)	8239(4)	51(2)
C(29)	4040(6)	-3649(6)	9172(4)	45(2)
C(31)	9486(5)	-5939(5)	8229(3)	32(1)
C(32)	10489(5)	-6582(5)	7717(4)	34(1)
C(33)	11067(6)	-7760(5)	7956(4)	35(1)
C(34)	10634(6)	-8302(5)	8715(4)	39(1)
C(35)	9643(6)	-7686(5)	9238(4)	38(1)
C(36)	9088(6)	-6504(5)	8994(4)	40(1)
C(37)	9549(6)	-3891(5)	8143(4)	39(1)
C(38)	9689(7)	-4007(6)	9038(4)	53(2)
C(39)	10838(6)	-3956(6)	7601(4)	48(2)
C(41)	5301(5)	-4039(5)	6543(3)	32(1)
C(42)	4711(6)	-2865(5)	6292(3)	34(1)
C(43)	3703(6)	-2531(5)	5851(4)	40(1)
C(44)	3252(6)	-3392(5)	5659(4)	43(1)
C(45)	3803(6)	-4587(5)	5907(4)	39(1)
C(46)	4819(6)	-4899(5)	6343(4)	38(1)
C(47)	7104(5)	-5381(4)	7278(3)	31(1)
C(48)	8073(6)	-6074(5)	6669(4)	41(1)
C(49)	6553(6)	-6157(5)	7994(4)	44(2)
C(131)	10080(9)	24(8)	7028(8)	97(4)
C(151)	5513(7)	1520(6)	6561(6)	68(2)
C(231)	6802(8)	-3269(7)	11119(4)	61(2)
C(252)	6788(10)	389(7)	9082(6)	78(3)
C(331)	12182(6)	-8431(6)	7418(4)	49(2)
C(351)	9208(8)	-8296(6)	10071(4)	56(2)
C(431)	3115(8)	-1243(6)	5587(5)	61(2)
C(451)	3295(6)	-5512(6)	5696(4)	49(2)

Table A2.1.2. Bond lengths [\AA] and angles [$^\circ$] for **2**-(η^2 -imine)- d_{18} .

Mo(1)–N(3)	1.968(5)	N(3)–C(37)	1.477(7)
Mo(1)–N(4)	1.973(4)	N(4)–C(47)	1.376(7)
Mo(1)–N(2)	1.961(5)	N(4)–C(41)	1.370(7)
Mo(1)–N(1)	1.973(5)	C(11)–C(12)	1.378(8)
Mo(1)–C(47)	2.187(5)	C(11)–C(16)	1.396(8)
N(1)–C(11)	1.437(6)	C(12)–C(13)	1.402(8)
N(1)–C(17)	1.489(7)	C(13)–C(14)	1.368(10)
N(2)–C(21)	1.453(7)	C(13)–C(131)	1.526(10)
N(2)–C(27)	1.496(7)	C(14)–C(15)	1.361(9)
N(3)–C(31)	1.425(7)	C(15)–C(16)	1.408(7)

C(15)–C(151)	1.505(9)	C(11)–N(1)–C(17)	115.7(4)
C(17)–C(19)	1.503(9)	C(11)–N(1)–Mo(1)	117.6(3)
C(17)–C(18)	1.528(10)	C(17)–N(1)–Mo(1)	126.6(3)
C(21)–C(22)	1.378(8)	C(21)–N(2)–C(27)	113.7(4)
C(21)–C(26)	1.405(8)	C(21)–N(2)–Mo(1)	114.8(3)
C(22)–C(23)	1.394(8)	C(27)–N(2)–Mo(1)	131.5(3)
C(23)–C(24)	1.382(9)	C(31)–N(3)–C(37)	115.9(4)
C(23)–C(231)	1.498(9)	C(31)–N(3)–Mo(1)	138.4(3)
C(24)–C(25)	1.380(10)	C(37)–N(3)–Mo(1)	105.6(3)
C(25)–C(26)	1.405(8)	C(47)–N(4)–C(41)	134.8(4)
C(25)–C(252)	1.514(9)	C(47)–N(4)–Mo(1)	79.3(3)
C(27)–C(29)	1.521(8)	C(41)–N(4)–Mo(1)	145.8(4)
C(27)–C(28)	1.528(8)	C(12)–C(11)–C(16)	118.2(5)
C(31)–C(36)	1.395(8)	C(12)–C(11)–N(1)	122.5(5)
C(31)–C(32)	1.405(8)	C(16)–C(11)–N(1)	119.3(5)
C(32)–C(33)	1.389(8)	C(11)–C(12)–C(13)	121.1(6)
C(33)–C(34)	1.387(8)	C(14)–C(13)–C(12)	118.6(6)
C(33)–C(331)	1.509(8)	C(14)–C(13)–C(131)	121.9(6)
C(34)–C(35)	1.394(8)	C(12)–C(13)–C(131)	119.4(7)
C(35)–C(36)	1.388(8)	C(15)–C(14)–C(13)	122.7(6)
C(35)–C(351)	1.517(8)	C(14)–C(15)–C(16)	118.0(6)
C(37)–C(38)	1.521(9)	C(14)–C(15)–C(151)	121.4(6)
C(37)–C(39)	1.538(9)	C(16)–C(15)–C(151)	120.6(6)
C(41)–C(42)	1.392(7)	C(11)–C(16)–C(15)	121.2(6)
C(41)–C(46)	1.412(7)	N(1)–C(17)–C(19)	114.4(5)
C(42)–C(43)	1.379(8)	N(1)–C(17)–C(18)	110.5(5)
C(43)–C(44)	1.388(8)	C(19)–C(17)–C(18)	111.1(6)
C(43)–C(431)	1.509(8)	C(22)–C(21)–C(26)	119.0(5)
C(44)–C(45)	1.402(8)	C(22)–C(21)–N(2)	121.1(5)
C(45)–C(46)	1.384(8)	C(26)–C(21)–N(2)	119.9(5)
C(45)–C(451)	1.509(8)	C(21)–C(22)–C(23)	121.8(6)
C(47)–C(49)	1.525(8)	C(24)–C(23)–C(22)	118.0(6)
C(47)–C(48)	1.514(8)	C(24)–C(23)–C(231)	120.8(6)
		C(22)–C(23)–C(231)	121.1(6)
N(3)–Mo(1)–N(4)	125.21(18)	C(23)–C(24)–C(25)	122.4(6)
N(3)–Mo(1)–N(2)	115.81(19)	C(24)–C(25)–C(26)	118.6(6)
N(4)–Mo(1)–N(2)	91.3(2)	C(24)–C(25)–C(252)	121.9(6)
N(3)–Mo(1)–N(1)	113.0(2)	C(26)–C(25)–C(252)	119.5(7)
N(4)–Mo(1)–N(1)	91.80(19)	C(21)–C(26)–C(25)	120.1(6)
N(2)–Mo(1)–N(1)	116.57(18)	N(2)–C(27)–C(29)	114.0(5)
N(3)–Mo(1)–C(47)	87.22(19)	N(2)–C(27)–C(28)	111.7(5)
N(4)–Mo(1)–C(47)	38.20(18)	C(29)–C(27)–C(28)	110.2(5)
N(2)–Mo(1)–C(47)	107.08(19)	C(36)–C(31)–C(32)	118.6(5)
N(1)–Mo(1)–C(47)	113.32(19)	C(36)–C(31)–N(3)	120.6(5)

C(32)–C(31)–N(3)	120.8(5)	C(43)–C(42)–C(41)	122.3(5)
C(31)–C(32)–C(33)	121.2(5)	C(42)–C(43)–C(44)	119.0(5)
C(34)–C(33)–C(32)	118.7(5)	C(42)–C(43)–C(431)	119.8(6)
C(34)–C(33)–C(331)	120.3(5)	C(44)–C(43)–C(431)	121.2(6)
C(32)–C(33)–C(331)	121.0(6)	C(43)–C(44)–C(45)	120.9(5)
C(33)–C(34)–C(35)	121.4(5)	C(46)–C(45)–C(44)	118.9(5)
C(34)–C(35)–C(36)	119.2(5)	C(46)–C(45)–C(451)	120.9(5)
C(34)–C(35)–C(351)	120.1(5)	C(44)–C(45)–C(451)	120.2(5)
C(36)–C(35)–C(351)	120.7(6)	C(45)–C(46)–C(41)	121.3(5)
C(31)–C(36)–C(35)	120.9(6)	N(4)–C(47)–C(49)	117.6(5)
N(3)–C(37)–C(38)	113.4(5)	N(4)–C(47)–C(48)	118.0(5)
N(3)–C(37)–C(39)	112.5(5)	C(49)–C(47)–C(48)	113.2(5)
C(38)–C(37)–C(39)	110.5(5)	N(4)–C(47)–Mo(1)	62.5(3)
N(4)–C(41)–C(42)	120.7(5)	C(49)–C(47)–Mo(1)	118.3(4)
N(4)–C(41)–C(46)	121.7(5)	C(48)–C(47)–Mo(1)	118.5(4)
C(42)–C(41)–C(46)	117.5(5)		

Table A2.1.3. Anisotropic displacement parameters ($\text{\AA}^2 \times 10^3$) for **2**-(η^2 -imine)- d_{18} . The anisotropic displacement factor exponent takes the form: $-2\pi^2 [h^2 a^* U^{11} + \dots + 2 h k a^* b^* U^{12}]$

	U^{11}	U^{22}	U^{33}	U^{23}	U^{13}	U^{12}
Mo(1)	31(1)	14(1)	29(1)	-3(1)	-10(1)	-5(1)
N(1)	46(3)	24(2)	34(2)	-9(2)	-3(2)	-13(2)
N(2)	39(3)	23(2)	27(2)	-1(2)	-11(2)	-7(2)
N(3)	36(3)	31(2)	38(3)	-5(2)	-12(2)	-12(2)
N(4)	44(3)	18(2)	48(3)	1(2)	-26(2)	-6(2)
C(11)	44(3)	26(3)	29(3)	2(2)	-9(2)	-8(2)
C(12)	40(3)	27(3)	61(4)	-4(3)	-12(3)	-5(3)
C(13)	60(5)	44(4)	80(5)	-7(4)	-16(4)	-29(4)
C(14)	63(4)	25(3)	71(5)	-12(3)	-8(4)	-15(3)
C(15)	49(4)	25(3)	54(4)	-4(3)	-1(3)	-10(3)
C(16)	42(3)	25(3)	47(3)	-9(2)	-7(3)	-9(2)
C(17)	66(4)	25(3)	38(3)	-7(2)	-10(3)	-14(3)
C(18)	73(5)	69(5)	60(5)	-28(4)	7(4)	-11(4)
C(19)	94(6)	42(4)	29(3)	0(3)	-16(3)	-21(4)
C(21)	38(3)	28(3)	35(3)	-6(2)	-7(2)	-8(2)
C(22)	40(3)	34(3)	42(3)	-5(2)	-13(3)	-8(3)
C(23)	37(3)	46(4)	43(3)	-11(3)	-8(3)	-6(3)
C(24)	52(4)	52(4)	50(4)	-23(3)	-10(3)	-12(3)
C(25)	63(4)	39(3)	55(4)	-19(3)	-3(3)	-19(3)

C(26)	59(4)	32(3)	37(3)	-3(2)	-8(3)	-11(3)
C(27)	38(3)	35(3)	35(3)	-3(2)	-9(2)	-6(3)
C(28)	45(4)	42(4)	57(4)	-1(3)	-8(3)	0(3)
C(29)	47(4)	42(3)	44(4)	2(3)	-9(3)	-14(3)
C(31)	37(3)	27(3)	31(3)	3(2)	-14(2)	-9(2)
C(32)	36(3)	28(3)	38(3)	0(2)	-12(2)	-7(2)
C(33)	36(3)	31(3)	42(3)	-7(2)	-12(3)	-9(2)
C(34)	44(3)	22(3)	49(4)	-3(2)	-17(3)	-4(2)
C(35)	45(3)	24(3)	41(3)	5(2)	-13(3)	-6(2)
C(36)	41(3)	30(3)	44(3)	-7(2)	-3(3)	-6(3)
C(37)	47(4)	22(3)	47(3)	5(2)	-22(3)	-7(2)
C(38)	60(4)	51(4)	58(4)	-11(3)	-29(4)	-14(3)
C(39)	43(4)	36(3)	68(5)	-2(3)	-13(3)	-14(3)
C(41)	33(3)	25(3)	37(3)	-6(2)	-6(2)	-7(2)
C(42)	40(3)	26(3)	36(3)	-7(2)	-8(2)	-8(2)
C(43)	46(4)	31(3)	41(3)	-6(2)	-10(3)	-2(3)
C(44)	42(3)	43(3)	43(3)	-4(3)	-18(3)	-5(3)
C(45)	37(3)	40(3)	45(3)	-9(3)	-10(3)	-14(3)
C(46)	42(3)	25(3)	50(4)	-10(2)	-10(3)	-9(2)
C(47)	37(3)	20(2)	36(3)	2(2)	-14(2)	-7(2)
C(48)	47(4)	32(3)	51(4)	-16(3)	-8(3)	-12(3)
C(49)	51(4)	31(3)	54(4)	-3(3)	-13(3)	-16(3)
C(131)	80(7)	65(6)	172(11)	-32(7)	-40(7)	-33(5)
C(151)	57(5)	33(4)	107(7)	-17(4)	-5(5)	-3(3)
C(231)	77(5)	66(5)	48(4)	-3(3)	-30(4)	-22(4)
C(252)	118(8)	45(4)	89(6)	-18(4)	-14(6)	-41(5)
C(331)	44(4)	37(3)	62(4)	-14(3)	-5(3)	-5(3)
C(351)	76(5)	34(3)	51(4)	2(3)	-2(4)	-12(3)
C(431)	69(5)	37(4)	69(5)	2(3)	-32(4)	6(3)
C(451)	42(4)	53(4)	63(4)	-14(3)	-16(3)	-18(3)

A2.2 X-ray crystal structure of (*t*-BuNC)Mo(N[*i*-Pr]Ar)₃ (3-*t*-BuNC).

Crystals grown from a concentrated pentane solution at $-35\text{ }^{\circ}\text{C}$ were coated with Paratone N oil (Exxon) on a microscope slide. A brown–orange block was selected and mounted with wax on a glass fiber. A total of 14846 reflections ($-15 \leq h \leq 16$, $-14 \leq k \leq 9$, $-21 \leq l \leq 20$) were collected at 293(2) K in the θ range of 2.08 to 22.50 $^{\circ}$, of which 5247 were unique ($R_{\text{int}} = 0.0467$). All non–methyl hydrogen atoms were found in the difference map and refined isotropically. All methyl hydrogen atoms were placed in calculated ($d_{\text{CH}} = 0.96\text{ \AA}$) positions. The residual peak and hole electron density were 1.578 and $-0.704\text{ e}\cdot\text{\AA}^{-3}$, respectively. The least squares refinement converged normally with residuals of $R_1 = 0.0647$, $wR_2 = 0.1563$ based upon $I > 2\sigma I$, and GOF = 1.143 (based on F^2). Crystal and refinement data: Formula = $\text{C}_{41}\text{H}_{63}\text{MoN}_4$; space group, P2(1)/n; $a = 15.1350(14)\text{ \AA}$; $b = 13.5623(12)\text{ \AA}$; $c = 19.6178(18)\text{ \AA}$; $\alpha = 90\text{ }^{\circ}$; $\beta = 91.1720(10)\text{ }^{\circ}$; $\gamma = 90\text{ }^{\circ}$; $V = 4026.0(6)\text{ \AA}^3$; $Z = 4$; $D_{\text{calc}} = 1.168\text{ g}\cdot\text{cm}^{-3}$; $F(000) = 1516$; R_1 (based on F) = 0.0754; wR_2 (based on F_2) = 0.1605.

Table A2.2.1. Atomic coordinates ($\times 10^4$) and equivalent isotropic displacement parameters ($\text{\AA}^2 \times 10^3$) for 3-*t*-BuNC. U(eq) is defined as one third of the trace of the orthogonalized U^{ij} tensor.

	x	y	z	U(eq)
Mo(1)	2569(1)	2953(1)	231(1)	26(1)
N(1)	2404(3)	4120(4)	-357(2)	31(1)
N(2)	3758(3)	2348(4)	198(2)	34(1)
N(3)	1490(3)	2149(4)	277(3)	37(1)
N(4)	2709(5)	4052(5)	1624(3)	58(2)
C(11)	1935(4)	3833(5)	-971(3)	40(2)
C(12)	1012(5)	3948(5)	-1030(4)	46(2)
C(13)	550(5)	3647(6)	-1609(4)	48(2)
C(14)	1013(5)	3217(5)	-2132(4)	47(2)
C(15)	1930(5)	3102(5)	-2100(3)	44(2)
C(16)	2388(5)	3411(5)	-1513(3)	34(2)
C(17)	2542(5)	5215(5)	-252(3)	39(2)
C(18)	2557(7)	5755(6)	-928(4)	77(3)
C(19)	3415(5)	5374(6)	124(4)	55(2)
C(21)	4056(4)	2302(5)	-509(3)	36(2)
C(22)	3848(4)	1466(5)	-901(3)	39(2)
C(23)	4149(5)	1412(5)	-1571(4)	47(2)
C(24)	4646(5)	2167(6)	-1832(4)	52(2)
C(25)	4855(5)	3009(6)	-1448(4)	48(2)
C(26)	4558(4)	3057(5)	-783(3)	39(2)
C(27)	4437(4)	2088(6)	713(3)	48(2)
C(28)	5109(8)	1368(12)	438(5)	145(7)

C(29)	4893(7)	3010(8)	991(5)	95(4)
C(31)	1637(4)	1243(5)	-104(3)	38(2)
C(32)	2006(4)	419(5)	223(3)	40(2)
C(33)	2169(5)	-451(5)	-136(4)	46(2)
C(34)	1946(5)	-477(5)	-821(4)	53(2)
C(35)	1575(5)	340(6)	-1159(4)	53(2)
C(36)	1424(5)	1211(5)	-801(3)	44(2)
C(37)	626(4)	2199(5)	646(3)	40(2)
C(38)	525(5)	3243(5)	928(4)	52(2)
C(39)	581(5)	1455(6)	1218(4)	60(2)
C(41)	2659(4)	3588(4)	1114(3)	28(1)
C(42)	2690(6)	3867(6)	2375(3)	53(2)
C(43)	2311(6)	2871(7)	2529(4)	71(3)
C(44)	3643(7)	3940(8)	2657(4)	86(3)
C(45)	2167(10)	4674(9)	2672(5)	128(6)
C(110)	1816(6)	5629(6)	189(5)	68(2)
C(131)	-436(5)	3782(7)	-1660(4)	66(2)
C(151)	2417(5)	2637(6)	-2680(3)	52(2)
C(210)	3979(5)	1566(6)	1305(4)	54(2)
C(231)	3948(6)	502(6)	-1994(4)	62(2)
C(251)	5375(5)	3835(6)	-1740(4)	59(2)
C(310)	-135(5)	2012(7)	126(4)	65(2)
C(331)	2547(6)	-1344(5)	225(4)	62(2)
C(351)	1312(6)	307(6)	-1927(4)	66(2)

Table A2.2.2. Bond lengths [Å] and angles [°] for **3-*t*-BuNC**.

Mo(1)–C(41)	1.936(6)	C(13)–C(14)	1.384(10)
Mo(1)–N(1)	1.972(5)	C(13)–C(131)	1.506(10)
Mo(1)–N(3)	1.967(5)	C(14)–C(15)	1.396(10)
Mo(1)–N(2)	1.981(5)	C(15)–C(16)	1.398(9)
N(1)–C(11)	1.439(8)	C(15)–C(151)	1.505(10)
N(1)–C(17)	1.514(8)	C(17)–C(110)	1.521(10)
N(2)–C(27)	1.469(8)	C(17)–C(18)	1.515(9)
N(2)–C(21)	1.468(8)	C(17)–C(19)	1.515(10)
N(3)–C(31)	1.457(8)	C(21)–C(26)	1.389(9)
N(3)–C(37)	1.510(8)	C(21)–C(22)	1.402(9)
N(4)–C(41)	1.184(8)	C(22)–C(23)	1.401(9)
N(4)–C(42)	1.495(9)	C(23)–C(24)	1.377(10)
C(11)–C(12)	1.409(9)	C(23)–C(231)	1.514(10)
C(11)–C(16)	1.400(9)	C(24)–C(25)	1.400(10)
C(12)–C(13)	1.383(10)	C(25)–C(26)	1.391(9)

C(25)–C(251)	1.490(10)	C(14)–C(15)–C(151)	121.0(6)
C(27)–C(28)	1.517(12)	C(16)–C(15)–C(151)	120.4(7)
C(27)–C(29)	1.525(12)	C(11)–C(16)–C(15)	120.4(6)
C(27)–C(210)	1.537(10)	N(1)–C(17)–C(110)	109.9(6)
C(31)–C(32)	1.399(9)	N(1)–C(17)–C(18)	111.1(5)
C(31)–C(36)	1.400(9)	C(110)–C(17)–C(18)	110.1(7)
C(32)–C(33)	1.399(10)	N(1)–C(17)–C(19)	108.8(5)
C(33)–C(34)	1.379(10)	C(110)–C(17)–C(19)	107.7(6)
C(33)–C(331)	1.510(10)	C(18)–C(17)–C(19)	109.3(6)
C(34)–C(35)	1.403(11)	C(26)–C(21)–C(22)	120.2(6)
C(35)–C(36)	1.395(10)	C(26)–C(21)–N(2)	121.0(6)
C(35)–C(351)	1.551(10)	C(22)–C(21)–N(2)	118.9(6)
C(37)–C(39)	1.511(10)	C(21)–C(22)–C(23)	118.9(6)
C(37)–C(38)	1.529(10)	C(24)–C(23)–C(22)	120.0(7)
C(37)–C(310)	1.544(10)	C(24)–C(23)–C(231)	120.5(7)
C(42)–C(45)	1.476(12)	C(22)–C(23)–C(231)	119.4(7)
C(42)–C(43)	1.502(11)	C(23)–C(24)–C(25)	121.7(7)
C(42)–C(44)	1.537(12)	C(24)–C(25)–C(26)	118.0(7)
		C(24)–C(25)–C(251)	121.4(6)
C(41)–Mo(1)–N(1)	99.9(2)	C(26)–C(25)–C(251)	120.6(7)
C(41)–Mo(1)–N(3)	104.4(2)	C(21)–C(26)–C(25)	121.2(6)
N(1)–Mo(1)–N(3)	112.1(2)	N(2)–C(27)–C(28)	112.0(6)
C(41)–Mo(1)–N(2)	99.6(2)	N(2)–C(27)–C(29)	110.7(6)
N(1)–Mo(1)–N(2)	114.7(2)	C(28)–C(27)–C(29)	110.7(9)
N(3)–Mo(1)–N(2)	121.9(2)	N(2)–C(27)–C(210)	108.1(5)
C(11)–N(1)–C(17)	116.4(5)	C(28)–C(27)–C(210)	106.8(8)
C(11)–N(1)–Mo(1)	109.1(4)	C(29)–C(27)–C(210)	108.4(6)
C(17)–N(1)–Mo(1)	133.8(4)	C(32)–C(31)–C(36)	120.3(6)
C(27)–N(2)–C(21)	114.6(5)	C(32)–C(31)–N(3)	120.2(6)
C(27)–N(2)–Mo(1)	134.4(4)	C(36)–C(31)–N(3)	119.5(6)
C(21)–N(2)–Mo(1)	110.2(4)	C(31)–C(32)–C(33)	121.1(6)
C(31)–N(3)–C(37)	115.2(5)	C(34)–C(33)–C(32)	118.0(7)
C(31)–N(3)–Mo(1)	108.0(4)	C(34)–C(33)–C(331)	121.3(7)
C(37)–N(3)–Mo(1)	136.5(4)	C(32)–C(33)–C(331)	120.6(7)
C(41)–N(4)–C(42)	137.8(7)	C(33)–C(34)–C(35)	121.9(7)
C(12)–C(11)–C(16)	118.9(6)	C(34)–C(35)–C(36)	119.9(7)
C(12)–C(11)–N(1)	120.7(6)	C(34)–C(35)–C(351)	121.9(7)
C(16)–C(11)–N(1)	120.3(6)	C(36)–C(35)–C(351)	118.2(7)
C(11)–C(12)–C(13)	121.2(7)	C(31)–C(36)–C(35)	118.8(7)
C(12)–C(13)–C(14)	118.6(7)	N(3)–C(37)–C(39)	112.3(6)
C(12)–C(13)–C(131)	120.1(7)	N(3)–C(37)–C(38)	108.0(5)
C(14)–C(13)–C(131)	121.2(6)	C(39)–C(37)–C(38)	110.1(6)
C(15)–C(14)–C(13)	122.2(7)	N(3)–C(37)–C(310)	108.5(5)
C(14)–C(15)–C(16)	118.6(6)	C(39)–C(37)–C(310)	109.7(6)

C(38)–C(37)–C(310)	108.2(6)	N(4)–C(42)–C(43)	111.4(6)
N(4)–C(41)–Mo(1)	174.2(5)	C(45)–C(42)–C(44)	108.5(9)
C(45)–C(42)–N(4)	106.5(6)	N(4)–C(42)–C(44)	107.9(7)
C(45)–C(42)–C(43)	112.2(8)	C(43)–C(42)–C(44)	110.2(7)

Table A2.2.3. Anisotropic displacement parameters ($\text{\AA}^2 \times 10^3$) for **3-*t*-BuNC**.

	U ¹¹	U ²²	U ³³	U ²³	U ¹³	U ¹²
Mo(1)	34(1)	23(1)	22(1)	0(1)	-1(1)	-3(1)
N(1)	46(3)	22(3)	23(3)	-5(2)	-3(2)	-5(2)
N(2)	39(3)	35(3)	29(3)	2(2)	2(2)	2(2)
N(3)	40(3)	34(3)	36(3)	-5(3)	2(2)	-6(3)
N(4)	91(5)	41(4)	41(4)	2(3)	-3(3)	5(3)
C(11)	42(4)	36(4)	40(4)	6(3)	-3(3)	-4(3)
C(12)	48(4)	49(5)	40(4)	7(3)	-2(3)	9(4)
C(13)	47(4)	53(5)	44(4)	2(4)	-7(3)	3(4)
C(14)	58(5)	46(4)	36(4)	9(3)	-15(3)	-5(4)
C(15)	61(5)	35(4)	37(4)	6(3)	3(3)	-1(4)
C(16)	48(4)	28(3)	26(3)	2(3)	-1(3)	-1(3)
C(17)	60(5)	21(3)	35(4)	5(3)	-3(3)	-9(3)
C(18)	144(9)	38(5)	48(5)	18(4)	-19(5)	-23(5)
C(19)	70(5)	42(4)	53(5)	3(4)	-8(4)	-19(4)
C(21)	30(4)	41(4)	36(4)	1(3)	1(3)	2(3)
C(22)	45(4)	37(4)	34(4)	-5(3)	-2(3)	3(3)
C(23)	52(4)	44(4)	45(4)	-10(4)	4(3)	3(4)
C(24)	49(4)	65(5)	43(4)	-2(4)	10(3)	0(4)
C(25)	45(4)	55(5)	43(4)	-5(4)	8(3)	-9(4)
C(26)	37(4)	42(4)	37(4)	-8(3)	0(3)	-3(3)
C(27)	33(4)	70(5)	40(4)	10(4)	-1(3)	11(4)
C(28)	119(10)	253(18)	63(7)	8(9)	-1(6)	136(11)
C(29)	94(7)	128(9)	62(6)	31(6)	-37(5)	-58(7)
C(31)	39(4)	32(4)	42(4)	0(3)	1(3)	-10(3)
C(32)	51(4)	29(4)	39(4)	-1(3)	-4(3)	-3(3)
C(33)	53(5)	34(4)	51(5)	0(4)	6(4)	-10(3)
C(34)	64(5)	32(4)	62(5)	-7(4)	16(4)	-12(4)
C(35)	52(5)	60(5)	46(4)	-6(4)	4(4)	-25(4)
C(36)	56(4)	34(4)	43(4)	-6(3)	-2(3)	-16(3)
C(37)	34(4)	47(4)	40(4)	-2(3)	3(3)	-7(3)
C(38)	43(4)	50(5)	64(5)	0(4)	8(4)	5(4)
C(39)	59(5)	63(6)	59(5)	13(4)	21(4)	1(4)
C(41)	43(4)	26(3)	14(3)	1(3)	-4(3)	0(3)
C(42)	83(6)	46(5)	30(4)	6(3)	-1(4)	5(4)

C(43)	99(7)	75(6)	39(4)	4(4)	11(4)	-20(5)
C(44)	102(8)	100(8)	54(5)	6(5)	-15(5)	-37(6)
C(45)	236(16)	101(9)	46(6)	-12(6)	1(7)	86(10)
C(110)	77(6)	47(5)	80(6)	-5(5)	10(5)	3(4)
C(131)	61(5)	90(7)	47(5)	-11(5)	-17(4)	5(5)
C(151)	71(5)	56(5)	29(4)	-5(3)	4(4)	-6(4)
C(210)	61(5)	57(5)	43(4)	20(4)	-7(4)	-2(4)
C(231)	84(6)	55(5)	46(5)	-20(4)	6(4)	2(5)
C(251)	71(5)	66(5)	40(4)	5(4)	9(4)	-20(5)
C(310)	36(4)	81(6)	78(6)	-6(5)	-2(4)	-8(4)
C(331)	76(6)	32(4)	77(6)	-5(4)	0(4)	0(4)
C(351)	92(7)	61(5)	45(5)	-17(4)	6(4)	-24(5)

A2.3 X-ray Crystal Structure of (1-AdNC)₂Mo(N[*i*-Pr]Ar)₃ (2-(AdNC)₂).

Crystals grown from a concentrated pentane solution at $-35\text{ }^{\circ}\text{C}$ were coated with Paratone N oil (Exxon) on a microscope slide. A purple block ($0.15 \times 0.18 \times 0.24\text{ mm}^3$) was selected and mounted with wax on a glass fiber. A total of 10591 reflections ($-11 \leq h \leq 9$, $-11 \leq k \leq 11$, $-26 \leq l \leq 24$) were collected at 293(2) K in the θ range of 2.00 to 22.50°, of which 7199 were unique ($R_{\text{int}} = 0.0689$). All non-methyl hydrogen atoms were found in the difference map and refined isotropically. All methyl hydrogen atoms were placed in calculated ($d_{\text{CH}} = 0.96\text{ \AA}$) positions. The residual peak and hole electron density were 1.827 and $-1.450\text{ e}\cdot\text{\AA}^{-3}$, respectively. The high residual electron density values and final R values are attributed to poor crystal and data quality. Attempts to lower these values by application of a more thorough absorption correction (SADABS) did not lead to significant improvements. The possibility that these high values can be attributed to disordered and sub-stoichiometric solvent molecules of co-crystallization was checked by application of the SQUEEZE crystallographic routine to the diffraction data. The SQUEEZE output indicated a solvent accessible void space of no greater than 17.3 \AA^3 of a total volume of $2784.4(5)\text{ \AA}^3$, therefore obviating the possibility of solvent of co-crystallization. Furthermore, the position of the largest residual peak in the difference map leads to a chemically unreasonable assignment (1.1 Å from the periphery of the molecule). The least squares refinement on the original reflection data converged normally with residuals of $R_1 = 0.1077$, $wR_2 = 0.2495$ based upon $I > 2\sigma I$, and GOF = 1.219 (based on F^2). Crystal and refinement data: Formula = $\text{C}_{60}\text{H}_{90}\text{MoN}_5$; space group, P-1; $a = 10.6383(11)\text{ \AA}$; $b = 10.9340(11)\text{ \AA}$; $c = 24.980(3)\text{ \AA}$; $\alpha = 91.598(2)\text{ }^{\circ}$; $\beta = 101.624(2)\text{ }^{\circ}$; $\gamma = 101.257(2)\text{ }^{\circ}$; $V = 2784.4(5)\text{ \AA}^3$; $Z = 2$; $D_{\text{calc}} = 1.166\text{ g}\cdot\text{cm}^{-3}$; $F(000) = 1054$; R_1 (based on F) = 0.1238; wR_2 (based on F_2) = 0.2566.

Table A2.3.1. Atomic coordinates ($\times 10^4$) and equivalent isotropic displacement parameters ($\text{\AA}^2 \times 10^3$) for 2-(AdNC)₂. U(eq) is defined as one third of the trace of the orthogonalized U^{ij} tensor.

	x	y	z	U(eq)
Mo(1)	6525(1)	-4005(1)	7217(1)	26(1)
N(1)	7309(8)	-4256(8)	6519(3)	35(2)
N(2)	5448(7)	-2706(7)	7163(3)	32(2)
N(3)	6478(8)	-4904(7)	7897(3)	39(2)
N(4)	4063(8)	-6085(8)	6500(4)	45(2)
N(5)	9243(9)	-2171(9)	7821(4)	49(2)
C(11)	7400(9)	-5481(10)	6392(4)	38(2)
C(12)	7815(9)	-6200(10)	6818(4)	40(3)
C(13)	7895(10)	-7449(10)	6738(5)	45(3)
C(14)	7501(11)	-7983(11)	6202(5)	55(3)
C(15)	7105(10)	-7311(11)	5758(5)	48(3)
C(16)	7070(9)	-6077(10)	5857(4)	40(3)

C(17)	7354(10)	-3393(10)	6088(4)	42(3)
C(18)	8113(13)	-2097(10)	6328(5)	60(3)
C(19)	5989(12)	-3326(13)	5773(5)	63(4)
C(21)	4037(9)	-3115(9)	7064(4)	35(2)
C(22)	3446(10)	-3695(9)	7458(5)	42(3)
C(23)	2095(11)	-4178(10)	7359(5)	49(3)
C(24)	1333(11)	-4058(11)	6843(5)	52(3)
C(25)	1884(10)	-3470(10)	6439(5)	45(3)
C(26)	3248(10)	-2996(10)	6552(5)	47(3)
C(27)	5910(10)	-1372(9)	7357(5)	42(3)
C(28)	5808(12)	-1104(11)	7940(5)	60(3)
C(29)	5216(12)	-507(10)	6984(6)	68(4)
C(31)	7490(10)	-4578(9)	8398(4)	39(3)
C(32)	7413(12)	-3646(10)	8773(4)	49(3)
C(33)	8360(12)	-3328(10)	9257(4)	49(3)
C(34)	9372(12)	-3980(11)	9354(5)	52(3)
C(35)	9492(10)	-4903(10)	8997(4)	41(3)
C(36)	8532(10)	-5198(10)	8506(4)	39(2)
C(37)	5390(10)	-5979(9)	7953(4)	41(3)
C(38)	4989(11)	-5931(11)	8498(5)	53(3)
C(39)	5791(12)	-7244(10)	7858(6)	59(3)
C(41)	4895(10)	-5344(10)	6764(4)	36(2)
C(42)	3099(10)	-7097(9)	6206(4)	37(2)
C(43)	3697(13)	-8246(12)	6175(6)	73(4)
C(44)	1966(14)	-7337(14)	6499(7)	84(5)
C(45)	2622(16)	-6718(15)	5639(6)	85(4)
C(46)	2568(14)	-9411(14)	5836(6)	77(4)
C(47)	2221(15)	-8925(13)	5300(6)	73(4)
C(48)	1521(16)	-7888(15)	5304(6)	84(5)
C(49)	501(16)	-8013(17)	5624(8)	100(6)
C(51)	8258(10)	-2792(10)	7601(4)	39(3)
C(52)	10303(9)	-1186(9)	8112(4)	37(2)
C(53)	9735(12)	-386(12)	8469(6)	72(4)
C(54)	10918(15)	-344(13)	7705(5)	76(4)
C(55)	11336(13)	-1739(12)	8465(6)	78(4)
C(56)	10895(14)	639(13)	8810(6)	73(4)
C(57)	11910(15)	46(15)	9131(6)	85(5)
C(58)	12435(15)	-705(13)	8769(7)	85(5)
C(59)	13004(12)	133(14)	8364(7)	78(4)
C(61)	5600(20)	3550(30)	10462(10)	171(12)
C(62)	5500(20)	2630(20)	10008(8)	118(7)
C(63)	6704(14)	2517(17)	9848(6)	83(4)
C(64)	6645(16)	1454(17)	9467(7)	94(5)
C(65)	7840(17)	1329(17)	9293(7)	100(5)

C(131)	8413(12)	-8149(12)	7211(5)	63(3)
C(151)	6718(12)	-7899(12)	5196(5)	64(4)
C(231)	1500(13)	-4887(12)	7780(5)	63(3)
C(251)	1052(11)	-3382(14)	5888(6)	72(4)
C(331)	8243(14)	-2349(13)	9661(5)	75(4)
C(351)	10625(12)	-5574(13)	9106(5)	67(4)
C(410)	878(16)	-8496(16)	6151(7)	90(5)
C(411)	1527(16)	-9571(15)	6166(7)	88(5)
C(510)	11978(13)	697(13)	8025(6)	74(4)
C(511)	11368(17)	1453(13)	8410(6)	86(5)

Table A2.3.2. Bond lengths [\AA] and angles [$^\circ$] for 2-(AdNC)₂.

Mo(1)–N(2)	1.983(8)	C(23)–C(231)	1.494(16)
Mo(1)–N(3)	1.990(8)	C(24)–C(25)	1.380(16)
Mo(1)–C(51)	2.083(11)	C(25)–C(26)	1.410(15)
Mo(1)–N(1)	2.112(8)	C(25)–C(251)	1.495(16)
Mo(1)–C(41)	2.135(11)	C(27)–C(28)	1.507(16)
N(1)–C(11)	1.395(13)	C(27)–C(29)	1.533(15)
N(1)–C(17)	1.454(13)	C(31)–C(36)	1.394(14)
N(2)–C(21)	1.448(12)	C(31)–C(32)	1.389(15)
N(2)–C(27)	1.480(12)	C(32)–C(33)	1.396(15)
N(3)–C(31)	1.462(13)	C(33)–C(34)	1.389(16)
N(3)–C(37)	1.511(12)	C(33)–C(331)	1.490(17)
N(4)–C(41)	1.153(12)	C(34)–C(35)	1.370(16)
N(4)–C(42)	1.422(13)	C(35)–C(36)	1.414(14)
N(5)–C(51)	1.153(13)	C(35)–C(351)	1.513(16)
N(5)–C(52)	1.454(13)	C(37)–C(38)	1.509(15)
C(11)–C(12)	1.391(14)	C(37)–C(39)	1.550(15)
C(11)–C(16)	1.418(14)	C(42)–C(45)	1.504(17)
C(12)–C(13)	1.396(15)	C(42)–C(43)	1.522(16)
C(13)–C(14)	1.395(16)	C(42)–C(44)	1.516(17)
C(13)–C(131)	1.497(16)	C(43)–C(46)	1.648(19)
C(14)–C(15)	1.386(17)	C(44)–C(410)	1.63(2)
C(15)–C(16)	1.374(15)	C(45)–C(48)	1.63(2)
C(15)–C(151)	1.473(16)	C(46)–C(47)	1.46(2)
C(17)–C(18)	1.527(15)	C(46)–C(411)	1.50(2)
C(17)–C(19)	1.522(15)	C(47)–C(48)	1.47(2)
C(21)–C(22)	1.376(14)	C(48)–C(49)	1.46(2)
C(21)–C(26)	1.406(15)	C(49)–C(410)	1.44(2)
C(22)–C(23)	1.400(15)	C(52)–C(55)	1.500(16)
C(23)–C(24)	1.401(17)	C(52)–C(53)	1.519(17)

C(52)–C(54)	1.547(16)	C(13)–C(14)–C(15)	122.7(11)
C(53)–C(56)	1.577(17)	C(16)–C(15)–C(14)	118.2(11)
C(54)–C(510)	1.514(18)	C(16)–C(15)–C(151)	120.5(11)
C(55)–C(58)	1.517(17)	C(14)–C(15)–C(151)	121.3(11)
C(56)–C(57)	1.48(2)	C(15)–C(16)–C(11)	122.4(10)
C(56)–C(511)	1.46(2)	N(1)–C(17)–C(18)	110.1(9)
C(57)–C(58)	1.46(2)	N(1)–C(17)–C(19)	112.1(9)
C(58)–C(59)	1.52(2)	C(18)–C(17)–C(19)	110.6(10)
C(59)–C(510)	1.49(2)	C(22)–C(21)–C(26)	118.5(9)
C(61)–C(62)	1.47(3)	C(22)–C(21)–N(2)	120.7(9)
C(62)–C(63)	1.45(2)	C(26)–C(21)–N(2)	120.7(9)
C(63)–C(64)	1.46(2)	C(21)–C(22)–C(23)	121.8(10)
C(64)–C(65)	1.45(2)	C(22)–C(23)–C(24)	118.5(10)
C(410)–C(411)	1.47(2)	C(22)–C(23)–C(231)	120.4(11)
C(510)–C(511)	1.56(2)	C(24)–C(23)–C(231)	120.9(10)
		C(25)–C(24)–C(23)	121.5(10)
N(2)–Mo(1)–N(3)	111.6(3)	C(24)–C(25)–C(26)	118.5(10)
N(2)–Mo(1)–C(51)	94.7(4)	C(24)–C(25)–C(251)	120.3(10)
N(3)–Mo(1)–C(51)	90.8(4)	C(26)–C(25)–C(251)	121.1(11)
N(2)–Mo(1)–N(1)	114.1(3)	C(21)–C(26)–C(25)	121.1(10)
N(3)–Mo(1)–N(1)	133.9(3)	N(2)–C(27)–C(28)	113.4(9)
C(51)–Mo(1)–N(1)	90.7(4)	N(2)–C(27)–C(29)	112.7(9)
N(2)–Mo(1)–C(41)	90.7(3)	C(28)–C(27)–C(29)	109.5(10)
N(3)–Mo(1)–C(41)	91.6(4)	C(36)–C(31)–C(32)	119.6(10)
C(51)–Mo(1)–C(41)	172.8(4)	C(36)–C(31)–N(3)	120.6(9)
N(1)–Mo(1)–C(41)	82.7(3)	C(32)–C(31)–N(3)	119.9(10)
C(11)–N(1)–C(17)	117.3(8)	C(31)–C(32)–C(33)	120.9(11)
C(11)–N(1)–Mo(1)	115.0(6)	C(34)–C(33)–C(32)	117.9(11)
C(17)–N(1)–Mo(1)	124.6(7)	C(34)–C(33)–C(331)	122.0(11)
C(21)–N(2)–C(27)	113.5(8)	C(32)–C(33)–C(331)	120.1(12)
C(21)–N(2)–Mo(1)	117.9(6)	C(35)–C(34)–C(33)	123.4(11)
C(27)–N(2)–Mo(1)	126.5(6)	C(34)–C(35)–C(36)	117.8(10)
C(31)–N(3)–C(37)	113.0(8)	C(34)–C(35)–C(351)	122.2(10)
C(31)–N(3)–Mo(1)	123.2(6)	C(36)–C(35)–C(351)	120.0(10)
C(37)–N(3)–Mo(1)	123.8(6)	C(31)–C(36)–C(35)	120.5(10)
C(41)–N(4)–C(42)	173.9(11)	N(3)–C(37)–C(38)	113.5(8)
C(51)–N(5)–C(52)	167.1(11)	N(3)–C(37)–C(39)	110.3(8)
N(1)–C(11)–C(12)	118.6(9)	C(38)–C(37)–C(39)	109.5(9)
N(1)–C(11)–C(16)	124.9(9)	N(4)–C(41)–Mo(1)	175.9(9)
C(12)–C(11)–C(16)	116.5(10)	N(4)–C(42)–C(45)	108.4(10)
C(11)–C(12)–C(13)	123.2(10)	N(4)–C(42)–C(43)	109.7(9)
C(14)–C(13)–C(12)	116.8(10)	C(45)–C(42)–C(43)	110.1(10)
C(14)–C(13)–C(131)	122.7(11)	N(4)–C(42)–C(44)	108.0(9)
C(12)–C(13)–C(131)	120.4(11)	C(45)–C(42)–C(44)	109.2(11)

C(43)–C(42)–C(44)	111.4(11)	C(52)–C(55)–C(58)	109.9(11)
C(42)–C(43)–C(46)	109.1(10)	C(57)–C(56)–C(511)	113.6(13)
C(42)–C(44)–C(410)	106.8(11)	C(57)–C(56)–C(53)	110.5(12)
C(42)–C(45)–C(48)	107.9(11)	C(511)–C(56)–C(53)	105.5(12)
C(47)–C(46)–C(411)	115.6(14)	C(58)–C(57)–C(56)	110.6(13)
C(47)–C(46)–C(43)	102.3(12)	C(57)–C(58)–C(59)	108.9(12)
C(411)–C(46)–C(43)	103.4(12)	C(57)–C(58)–C(55)	109.0(14)
C(46)–C(47)–C(48)	113.7(12)	C(59)–C(58)–C(55)	110.1(12)
C(49)–C(48)–C(47)	117.0(15)	C(510)–C(59)–C(58)	110.8(11)
C(49)–C(48)–C(45)	102.3(13)	C(63)–C(62)–C(61)	117.0(18)
C(47)–C(48)–C(45)	104.7(12)	C(62)–C(63)–C(64)	117.0(16)
C(48)–C(49)–C(410)	113.2(13)	C(65)–C(64)–C(63)	118.0(15)
N(5)–C(51)–Mo(1)	176.7(10)	C(49)–C(410)–C(411)	117.1(15)
N(5)–C(52)–C(55)	110.3(9)	C(49)–C(410)–C(44)	103.4(14)
N(5)–C(52)–C(53)	108.1(8)	C(411)–C(410)–C(44)	106.1(14)
C(55)–C(52)–C(53)	109.6(11)	C(410)–C(411)–C(46)	112.3(13)
N(5)–C(52)–C(54)	110.7(9)	C(59)–C(510)–C(54)	108.6(12)
C(55)–C(52)–C(54)	109.8(11)	C(59)–C(510)–C(511)	109.1(12)
C(53)–C(52)–C(54)	108.3(10)	C(54)–C(510)–C(511)	109.1(12)
C(52)–C(53)–C(56)	108.2(10)	C(56)–C(511)–C(510)	109.2(11)
C(510)–C(54)–C(52)	109.0(10)		

Table A2.3.3. Anisotropic displacement parameters ($\text{\AA}^2 \times 10^3$) for 2-(AdNC)₂.

	U ¹¹	U ²²	U ³³	U ²³	U ¹³	U ¹²
Mo(1)	20(1)	22(1)	31(1)	2(1)	1(1)	–4(1)
N(1)	32(5)	42(5)	28(4)	7(4)	6(4)	–3(4)
N(2)	24(4)	27(4)	39(5)	8(4)	4(4)	–7(3)
N(3)	30(5)	34(5)	45(5)	4(4)	14(4)	–16(4)
N(4)	31(5)	44(5)	49(6)	–8(5)	–1(4)	–7(5)
N(5)	39(6)	53(6)	48(6)	–6(5)	9(5)	–10(5)
C(11)	30(6)	46(7)	35(6)	0(5)	7(5)	4(5)
C(12)	27(5)	48(7)	42(6)	9(5)	4(5)	6(5)
C(13)	37(6)	42(7)	57(8)	13(6)	8(5)	11(5)
C(14)	39(7)	47(7)	76(9)	1(7)	11(6)	6(6)
C(15)	29(6)	52(7)	59(8)	–9(6)	3(5)	4(5)
C(16)	23(5)	51(7)	45(7)	7(5)	1(5)	12(5)
C(17)	46(6)	45(6)	36(6)	11(5)	10(5)	5(5)
C(18)	83(9)	44(7)	60(8)	18(6)	42(7)	–3(6)
C(19)	56(8)	89(10)	54(8)	31(7)	15(6)	29(7)
C(21)	26(5)	33(6)	44(6)	–3(5)	5(5)	5(4)
C(22)	39(6)	35(6)	53(7)	6(5)	8(5)	6(5)

C(23)	39(7)	43(7)	64(8)	-1(6)	21(6)	-3(5)
C(24)	27(6)	53(7)	73(9)	5(6)	10(6)	2(5)
C(25)	28(6)	44(6)	61(7)	5(6)	3(5)	7(5)
C(26)	44(7)	37(6)	59(8)	17(5)	13(6)	2(5)
C(27)	35(6)	20(5)	66(8)	1(5)	9(5)	-1(4)
C(28)	61(8)	36(7)	72(9)	-22(6)	6(7)	-6(6)
C(29)	52(8)	33(7)	103(11)	4(7)	-13(7)	2(6)
C(31)	43(6)	37(6)	30(6)	7(5)	3(5)	-5(5)
C(32)	55(7)	40(6)	45(7)	2(5)	7(6)	-4(5)
C(33)	58(8)	43(7)	35(6)	5(5)	0(6)	-4(6)
C(34)	50(7)	60(8)	37(7)	10(6)	0(6)	-3(6)
C(35)	41(6)	41(6)	34(6)	15(5)	-3(5)	1(5)
C(36)	35(6)	39(6)	41(6)	6(5)	11(5)	2(5)
C(37)	32(6)	40(6)	42(6)	11(5)	7(5)	-13(5)
C(38)	53(7)	48(7)	51(7)	6(6)	15(6)	-8(6)
C(39)	55(8)	26(6)	87(10)	6(6)	11(7)	-8(5)
C(41)	25(6)	37(6)	44(6)	3(5)	6(5)	5(5)
C(42)	40(6)	35(6)	33(6)	-5(5)	4(5)	7(5)
C(43)	56(8)	56(8)	98(11)	12(8)	10(8)	-2(7)
C(44)	64(9)	67(9)	109(12)	-14(9)	28(9)	-25(7)
C(45)	92(11)	83(11)	70(10)	5(8)	6(8)	6(9)
C(46)	75(10)	75(10)	84(11)	-12(8)	19(8)	23(8)
C(47)	82(10)	75(10)	59(9)	-7(7)	17(8)	9(8)
C(48)	80(11)	97(12)	67(10)	13(9)	-10(8)	27(9)
C(49)	60(10)	94(13)	135(17)	-26(12)	-9(11)	25(9)
C(51)	32(6)	42(6)	42(6)	4(5)	9(5)	0(5)
C(52)	23(5)	32(6)	47(6)	0(5)	-1(5)	-10(4)
C(53)	48(8)	58(8)	93(11)	-16(7)	5(7)	-13(6)
C(54)	87(10)	71(9)	54(8)	16(7)	12(7)	-20(8)
C(55)	61(9)	55(8)	90(11)	12(7)	-25(8)	-11(7)
C(56)	63(9)	64(9)	78(10)	-23(8)	8(8)	-9(7)
C(57)	73(10)	79(11)	70(10)	11(8)	-19(8)	-30(8)
C(58)	71(10)	61(9)	91(11)	-9(9)	-46(9)	10(8)
C(59)	32(7)	78(10)	108(12)	-14(9)	14(8)	-20(7)
C(61)	89(15)	260(30)	150(20)	-90(20)	31(14)	32(17)
C(62)	108(16)	161(19)	82(13)	16(13)	15(11)	23(14)
C(63)	55(9)	115(13)	73(10)	10(10)	0(8)	14(9)
C(64)	72(11)	106(13)	91(12)	10(11)	0(9)	0(10)
C(65)	97(13)	117(14)	91(12)	11(10)	33(10)	20(11)
C(131)	52(8)	53(8)	82(9)	9(7)	6(7)	17(6)
C(151)	56(8)	68(9)	66(9)	-12(7)	1(7)	25(7)
C(231)	59(8)	65(8)	66(9)	8(7)	20(7)	1(7)
C(251)	31(7)	92(10)	83(10)	21(8)	-9(6)	9(7)
C(331)	78(10)	82(10)	58(8)	-19(7)	6(7)	13(8)

C(351)	54(8)	84(10)	61(8)	18(7)	3(7)	16(7)
C(410)	69(10)	101(13)	103(13)	4(10)	45(10)	0(9)
C(411)	90(12)	71(10)	104(13)	5(9)	39(10)	-1(9)
C(510)	58(9)	80(10)	65(9)	27(8)	12(7)	-35(8)
C(511)	120(13)	42(8)	88(11)	12(8)	4(10)	19(9)

A2.4 X-ray crystal structure of [Na(THF)][(μ-P)Mo₂(N[*i*-Pr]Ar)₆] ([Na(THF)][2₂-μ-P]).

Crystals of [Na(THF)][2₂-μ-P] grown from a concentrated pentane solution at -35 °C were coated with Paratone N oil (an Exxon product) on a microscope slide. A purple block of approximate dimensions 0.22 × 0.18 × 0.11 mm³ was selected and mounted with wax on a glass fiber. A total of 27959 reflections (-8 ≤ *h* ≤ 19, -19 ≤ *k* ≤ 19, -24 ≤ *l* ≤ 24) were collected at 183(2) K in the 2θ range of 2.28 to 23.29°, of which 10061 were unique (*R*_{int} = 0.0890). The structure was solved using the Patterson method (SHELXLT V5.1, G. M. Sheldrick and Siemens Industrial Automation, Inc., 1997) in conjunction with standard difference Fourier techniques. All non-hydrogen atoms were refined anisotropically and hydrogen atoms were placed in calculated (*d*_{CH} = 0.96 Å) positions. The residual peak and hole electron density were 1.143 and -1.027 e·Å⁻³, respectively. A semi-empirical absorption correction was applied based on pseudo-psi-scans with maximum and minimum transmission equal to 0.3094 and 0.2072, respectively. The least squares refinement converged normally with residuals of *R*₁ = 0.0845, *wR*₂ = 0.1659 based on *I* > 2σ and GOF = 1.213 (based on *F*²). The final values of *R*₁ and *wR*₂ may be explained if the *R*_{int} = 0.0890 value is taken into consideration. Also, the molecule contains a molecule of coordinated tetrahydrofuran that is slightly disordered. This thermal disorder has not been modeled. No extinction coefficient was applied to the refinement. Crystal and refinement data: formula = C₇₀H₁₀₄N₆Mo₂PNaO, space group *P*2₁/*c*, *a* = 17.724(4) Å, *b* = 17.853(4) Å, *c* = 22.301(5) Å, α = 90°, β = 96.392(5)°, γ = 90°, *Z* = 4, *V* = 7013(3) Å³, *D*_{calcd} = 1.223 g·cm⁻³, *F*(000) = 2736, *R* (based on *F*) = 0.1061, *wR* (based on *F*²) = 0.1745.

Table A2.4.1. Atomic coordinates [$\times 10^4$] and equivalent isotropic displacement parameters [$\text{\AA}^2 \times 10^3$] for [Na(THF)][2₂-μ-P]. *U*(eq) is defined as one third of the trace of the orthogonalized *U*_{ij} tensor.

	x	y	z	U(eq)
Mo(1)	2437(1)	9136(1)	8657(1)	23(1)
Mo(2)	2660(1)	6701(1)	8561(1)	25(1)
P	2585(1)	7929(1)	8569(1)	26(1)
N(1)	1400(3)	9171(3)	8984(2)	30(1)
N(2)	2483(3)	9482(3)	7800(2)	28(1)
N(5)	2083(3)	6557(3)	9304(3)	33(1)
C(52)	2741(5)	5564(4)	9931(3)	41(2)
C(53)	2746(6)	4862(5)	10208(4)	56(3)
C(24)	2275(5)	11839(4)	7761(3)	39(2)
N(3)	3317(3)	9379(3)	9244(3)	31(1)
C(59)	2590(6)	7339(5)	10198(4)	57(2)
C(21)	2401(4)	10276(3)	7741(3)	26(2)

N(6)	3766(3)	6615(3)	8596(3)	37(2)
C(45)	2295(7)	4582(5)	7015(4)	67(3)
C(51)	2093(5)	5824(4)	9580(3)	37(2)
C(23)	2661(5)	11499(4)	7336(3)	41(2)
C(11)	752(4)	8733(4)	8812(3)	31(2)
C(61)	4021(5)	5863(4)	8460(4)	44(2)
C(44)	2422(6)	4142(4)	7521(4)	58(3)
C(67)	4382(5)	7188(4)	8685(5)	54(2)
C(28)	2346(6)	9153(5)	6691(4)	64(3)
C(25)	1932(4)	11418(4)	8177(4)	37(2)
C(43)	2390(5)	4438(4)	8084(4)	47(2)
C(35)	3984(4)	11263(4)	8783(3)	37(2)
C(27)	2779(5)	9056(4)	7308(3)	42(2)
C(26)	1974(4)	10642(4)	8136(3)	32(2)
C(42)	2222(5)	5203(4)	8133(4)	45(2)
C(12)	265(4)	8460(4)	9214(4)	41(2)
C(33)	3332(4)	11414(4)	9683(4)	42(2)
C(36)	3849(4)	10496(4)	8804(3)	34(2)
C(41)	2136(5)	5680(4)	7631(3)	44(2)
C(15)	-115(5)	8218(5)	7993(4)	51(2)
C(22)	2745(5)	10723(4)	7328(3)	36(2)
C(34)	3725(5)	11710(4)	9223(4)	43(2)
C(66)	4221(5)	5343(4)	8911(4)	42(2)
C(351)	4424(5)	11593(5)	8302(4)	56(2)
C(16)	558(5)	8589(4)	8195(4)	42(2)
C(57)	1914(5)	7153(4)	9744(3)	39(2)
C(56)	1466(5)	5366(5)	9514(4)	53(2)
C(58)	1215(6)	6975(5)	10064(4)	59(3)
C(31)	3463(4)	10179(4)	9255(3)	32(2)
C(451)	2309(9)	4242(5)	6389(4)	103(5)
C(14)	-598(5)	7983(5)	8409(5)	56(3)
C(54)	2102(7)	4439(5)	10134(5)	67(3)
C(251)	1530(5)	11776(4)	8666(4)	48(2)
C(46)	2164(6)	5343(4)	7070(4)	63(3)
C(62)	4049(5)	5666(5)	7860(4)	49(2)
C(32)	3211(4)	10651(4)	9685(4)	35(2)
C(231)	3013(6)	11972(5)	6867(4)	61(3)
C(13)	-407(5)	8094(5)	9025(4)	51(2)
N(4)	2050(4)	6449(3)	7745(3)	40(2)
C(431)	2506(6)	3954(4)	8647(4)	53(3)
C(63)	4276(5)	4948(5)	7704(5)	59(3)
C(39)	4694(4)	9037(5)	9429(5)	59(3)
C(29)	3641(5)	9105(5)	7312(4)	62(3)
C(37)	3892(5)	8925(4)	9608(4)	44(2)
C(38)	3891(6)	9061(5)	10293(4)	68(3)
C(64)	4472(5)	4444(5)	8179(5)	62(3)

C(18)	596(5)	10193(5)	9358(5)	76(3)
C(17)	1335(5)	9747(5)	9455(4)	47(2)
C(55)	1460(7)	4660(5)	9783(5)	70(3)
C(331)	3047(5)	11923(5)	10147(5)	64(3)
C(47)	1883(7)	6968(5)	7221(4)	68(3)
C(631)	4310(7)	4731(6)	7054(5)	82(4)
C(49)	2599(8)	7094(5)	6895(4)	86(4)
C(531)	3460(7)	4601(6)	10592(5)	80(3)
C(65)	4454(5)	4629(5)	8772(5)	54(2)
C(151)	-360(6)	8118(6)	7324(4)	74(3)
C(19)	1512(6)	9454(6)	10095(4)	83(4)
C(651)	4667(6)	4059(5)	9267(5)	78(3)
C(131)	-925(6)	7831(6)	9474(5)	82(3)
C(69)	4947(7)	7019(6)	9231(6)	105(5)
C(68)	4790(7)	7301(6)	8123(7)	105(5)
C(551)	757(7)	4168(6)	9667(7)	115(5)
C(48)	1120(11)	6831(10)	6854(7)	171(8)
Na	966(2)	7085(2)	8491(2)	54(1)
O	82(5)	6204(5)	8226(5)	108(3)
C(3S)	-379(12)	5013(10)	8099(8)	144(7)
C(1S)	-601(9)	6081(9)	8489(11)	192(11)
C(4S)	116(11)	5585(16)	7784(11)	200(10)
C(2S)	-755(12)	5358(12)	8649(11)	193(9)

Table A2.4.2. Bond lengths [Å] and angles [°] for [Na(THF)]₂[2-μ-P].

Mo(1)-N(3)	1.970(6)	C(52)-C(51)	1.395(11)
Mo(1)-N(2)	2.017(5)	C(52)-C(53)	1.398(11)
Mo(1)-N(1)	2.051(6)	C(53)-C(54)	1.363(14)
Mo(1)-P	2.183(2)	C(53)-C(531)	1.519(13)
Mo(2)-N(6)	1.959(6)	C(24)-C(23)	1.373(11)
Mo(2)-N(5)	2.059(6)	C(24)-C(25)	1.386(11)
Mo(2)-N(4)	2.059(6)	N(3)-C(31)	1.450(9)
Mo(2)-P	2.197(2)	N(3)-C(37)	1.474(9)
Mo(2)-Na	3.066(3)	C(59)-C(57)	1.517(11)
P-Na	3.228(4)	C(21)-C(26)	1.388(10)
N(1)-C(11)	1.406(9)	C(21)-C(22)	1.408(10)
N(1)-C(17)	1.484(9)	N(6)-C(61)	1.461(9)
N(2)-C(21)	1.430(8)	N(6)-C(67)	1.494(10)
N(2)-C(27)	1.478(9)	C(45)-C(44)	1.374(12)
N(5)-C(51)	1.445(9)	C(45)-C(46)	1.386(12)
N(5)-C(57)	1.499(9)	C(45)-C(451)	1.525(12)
N(5)-Na	2.702(7)	C(51)-C(56)	1.375(11)

C(23)-C(22)	1.395(10)	C(37)-C(38)	1.547(12)
C(23)-C(231)	1.530(11)	C(64)-C(65)	1.368(13)
C(11)-C(12)	1.401(10)	C(18)-C(17)	1.526(12)
C(11)-C(16)	1.404(11)	C(17)-C(19)	1.521(13)
C(11)-Na	3.062(8)	C(55)-C(551)	1.522(15)
C(61)-C(66)	1.386(11)	C(47)-C(48)	1.52(2)
C(61)-C(62)	1.388(11)	C(47)-C(49)	1.55(2)
C(44)-C(43)	1.369(11)	C(65)-C(651)	1.518(12)
C(67)-C(69)	1.517(14)	Na-O	2.252(8)
C(67)-C(68)	1.529(14)	O-C(1S)	1.42(2)
C(28)-C(27)	1.511(11)	O-C(4S)	1.49(2)
C(25)-C(26)	1.391(10)	C(3S)-C(4S)	1.56(3)
C(25)-C(251)	1.510(11)	C(3S)-C(2S)	1.58(3)
C(43)-C(42)	1.404(11)	C(1S)-C(2S)	1.38(2)
C(43)-C(431)	1.518(11)		
C(35)-C(34)	1.383(11)	N(3)-Mo(1)-N(2)	116.7(2)
C(35)-C(36)	1.391(10)	N(3)-Mo(1)-N(1)	115.6(2)
C(35)-C(351)	1.516(11)	N(2)-Mo(1)-N(1)	117.3(2)
C(27)-C(29)	1.529(12)	N(3)-Mo(1)-P	100.6(2)
C(42)-C(41)	1.402(11)	N(2)-Mo(1)-P	101.5(2)
C(12)-C(13)	1.383(11)	N(1)-Mo(1)-P	100.6(2)
C(33)-C(32)	1.380(11)	N(6)-Mo(2)-N(5)	122.8(3)
C(33)-C(34)	1.406(11)	N(6)-Mo(2)-N(4)	116.3(3)
C(33)-C(331)	1.505(11)	N(5)-Mo(2)-N(4)	115.2(3)
C(36)-C(31)	1.399(10)	N(6)-Mo(2)-P	97.9(2)
C(41)-C(46)	1.392(11)	N(5)-Mo(2)-P	94.7(2)
C(41)-N(4)	1.409(9)	N(4)-Mo(2)-P	101.5(2)
C(15)-C(14)	1.395(13)	N(6)-Mo(2)-Na	171.5(2)
C(15)-C(16)	1.394(11)	N(5)-Mo(2)-Na	59.9(2)
C(15)-C(151)	1.517(12)	N(4)-Mo(2)-Na	65.8(2)
C(15)-Na	2.920(9)	P-Mo(2)-Na	73.59(8)
C(66)-C(65)	1.384(11)	Mo(1)-P-Mo(2)	173.87(10)
C(16)-Na	2.839(8)	Mo(1)-P-Na	110.51(9)
C(57)-C(58)	1.531(11)	Mo(2)-P-Na	65.66(8)
C(57)-Na	3.099(9)	C(11)-N(1)-C(17)	116.9(6)
C(56)-C(55)	1.397(12)	C(11)-N(1)-Mo(1)	128.5(4)
C(31)-C(32)	1.386(10)	C(17)-N(1)-Mo(1)	114.6(4)
C(14)-C(13)	1.393(13)	C(21)-N(2)-C(27)	118.8(5)
C(54)-C(55)	1.366(14)	C(21)-N(2)-Mo(1)	112.1(4)
C(62)-C(63)	1.399(12)	C(27)-N(2)-Mo(1)	126.9(4)
C(13)-C(131)	1.506(13)	C(51)-N(5)-C(57)	111.0(5)
N(4)-C(47)	1.494(10)	C(51)-N(5)-Mo(2)	118.2(4)
N(4)-Na	2.908(8)	C(57)-N(5)-Mo(2)	126.3(4)
C(63)-C(64)	1.402(13)	C(51)-N(5)-Na	125.1(5)
C(63)-C(631)	1.508(13)	C(57)-N(5)-Na	90.4(4)
C(39)-C(37)	1.532(11)	Mo(2)-N(5)-Na	78.9(2)

C(51)-C(52)-C(53)	120.7(8)	N(2)-C(27)-C(29)	113.8(7)
C(54)-C(53)-C(52)	118.6(9)	C(28)-C(27)-C(29)	113.8(8)
C(54)-C(53)-C(531)	122.2(9)	C(21)-C(26)-C(25)	123.2(7)
C(52)-C(53)-C(531)	119.2(10)	C(41)-C(42)-C(43)	122.3(8)
C(23)-C(24)-C(25)	120.9(7)	C(13)-C(12)-C(11)	122.7(8)
C(31)-N(3)-C(37)	114.9(5)	C(32)-C(33)-C(34)	117.6(7)
C(31)-N(3)-Mo(1)	110.8(4)	C(32)-C(33)-C(331)	122.0(8)
C(37)-N(3)-Mo(1)	133.9(5)	C(34)-C(33)-C(331)	120.4(7)
C(26)-C(21)-C(22)	117.1(6)	C(35)-C(36)-C(31)	121.4(7)
C(26)-C(21)-N(2)	117.7(6)	C(46)-C(41)-C(42)	116.3(7)
C(22)-C(21)-N(2)	125.1(6)	C(46)-C(41)-N(4)	126.8(7)
C(61)-N(6)-C(67)	114.7(6)	C(42)-C(41)-N(4)	116.9(7)
C(61)-N(6)-Mo(2)	113.3(5)	C(14)-C(15)-C(16)	119.6(8)
C(67)-N(6)-Mo(2)	131.8(5)	C(14)-C(15)-C(151)	119.3(8)
C(44)-C(45)-C(46)	120.0(8)	C(16)-C(15)-C(151)	121.0(9)
C(44)-C(45)-C(451)	120.5(8)	C(14)-C(15)-Na	87.9(5)
C(46)-C(45)-C(451)	119.5(8)	C(16)-C(15)-Na	72.8(5)
C(56)-C(51)-C(52)	117.9(7)	C(151)-C(15)-Na	113.3(6)
C(56)-C(51)-N(5)	121.4(7)	C(23)-C(22)-C(21)	120.0(7)
C(52)-C(51)-N(5)	120.7(7)	C(35)-C(34)-C(33)	122.0(7)
C(24)-C(23)-C(22)	120.7(7)	C(65)-C(66)-C(61)	120.9(9)
C(24)-C(23)-C(231)	120.1(7)	C(15)-C(16)-C(11)	120.8(8)
C(22)-C(23)-C(231)	119.2(7)	C(15)-C(16)-Na	79.3(5)
C(12)-C(11)-C(16)	117.5(7)	C(11)-C(16)-Na	85.3(4)
C(12)-C(11)-N(1)	124.2(7)	N(5)-C(57)-C(59)	113.1(7)
C(16)-C(11)-N(1)	118.2(7)	N(5)-C(57)-C(58)	112.9(7)
C(12)-C(11)-Na	85.2(4)	C(59)-C(57)-C(58)	110.8(7)
C(16)-C(11)-Na	67.5(4)	N(5)-C(57)-Na	60.7(4)
N(1)-C(11)-Na	118.6(4)	C(59)-C(57)-Na	156.8(5)
C(66)-C(61)-C(62)	119.8(8)	C(58)-C(57)-Na	91.5(5)
C(66)-C(61)-N(6)	121.6(7)	C(51)-C(56)-C(55)	122.4(9)
C(62)-C(61)-N(6)	118.6(7)	C(32)-C(31)-C(36)	118.2(7)
C(43)-C(44)-C(45)	121.0(8)	C(32)-C(31)-N(3)	122.6(7)
N(6)-C(67)-C(69)	112.1(7)	C(36)-C(31)-N(3)	119.1(6)
N(6)-C(67)-C(68)	112.7(8)	C(13)-C(14)-C(15)	121.0(8)
C(69)-C(67)-C(68)	110.7(10)	C(53)-C(54)-C(55)	123.0(8)
C(24)-C(25)-C(26)	117.8(7)	C(45)-C(46)-C(41)	121.8(8)
C(24)-C(25)-C(251)	122.1(6)	C(61)-C(62)-C(63)	120.8(8)
C(26)-C(25)-C(251)	120.1(7)	C(33)-C(32)-C(31)	122.4(8)
C(44)-C(43)-C(42)	118.4(7)	C(12)-C(13)-C(14)	118.3(8)
C(44)-C(43)-C(431)	121.6(7)	C(12)-C(13)-C(131)	120.8(9)
C(42)-C(43)-C(431)	120.0(7)	C(14)-C(13)-C(131)	120.9(9)
C(34)-C(35)-C(36)	118.3(7)	C(41)-N(4)-C(47)	118.6(6)
C(34)-C(35)-C(351)	121.0(7)	C(41)-N(4)-Mo(2)	108.4(4)
C(36)-C(35)-C(351)	120.7(7)	C(47)-N(4)-Mo(2)	126.5(5)
N(2)-C(27)-C(28)	115.5(7)	C(41)-N(4)-Na	125.1(5)

C(47)-N(4)-Na	96.9(6)	N(5)-Na-C(11)	106.2(2)
Mo(2)-N(4)-Na	74.0(2)	C(16)-Na-C(11)	27.2(2)
C(62)-C(63)-C(64)	117.0(9)	N(4)-Na-C(11)	128.0(2)
C(62)-C(63)-C(631)	121.2(9)	C(15)-Na-C(11)	47.9(2)
C(64)-C(63)-C(631)	121.8(8)	O-Na-Mo(2)	120.4(3)
N(3)-C(37)-C(39)	113.0(6)	N(5)-Na-Mo(2)	41.22(13)
N(3)-C(37)-C(38)	112.3(7)	C(16)-Na-Mo(2)	116.5(2)
C(39)-C(37)-C(38)	109.9(7)	N(4)-Na-Mo(2)	40.21(12)
C(65)-C(64)-C(63)	123.0(8)	C(15)-Na-Mo(2)	140.5(2)
N(1)-C(17)-C(19)	113.7(7)	C(11)-Na-Mo(2)	110.4(2)
N(1)-C(17)-C(18)	113.3(7)	O-Na-C(57)	123.7(3)
C(19)-C(17)-C(18)	113.4(8)	N(5)-Na-C(57)	28.9(2)
C(54)-C(55)-C(56)	117.4(9)	C(16)-Na-C(57)	105.7(2)
C(54)-C(55)-C(551)	123.0(9)	N(4)-Na-C(57)	101.8(2)
C(56)-C(55)-C(551)	119.6(10)	C(15)-Na-C(57)	125.6(2)
N(4)-C(47)-C(48)	114.1(10)	C(11)-Na-C(57)	79.7(2)
N(4)-C(47)-C(49)	110.9(8)	Mo(2)-Na-C(57)	62.2(2)
C(48)-C(47)-C(49)	119.9(10)	O-Na-P	158.2(3)
C(64)-C(65)-C(66)	118.5(9)	N(5)-Na-P	63.01(14)
C(64)-C(65)-C(651)	120.7(8)	C(16)-Na-P	76.9(2)
C(66)-C(65)-C(651)	120.8(9)	N(4)-Na-P	64.72(14)
O-Na-N(5)	111.6(3)	C(15)-Na-P	103.8(2)
O-Na-C(16)	116.6(3)	C(11)-Na-P	70.8(2)
N(5)-Na-C(16)	129.4(2)	Mo(2)-Na-P	40.75(6)
O-Na-N(4)	93.6(3)	C(57)-Na-P	62.8(2)
N(5)-Na-N(4)	76.5(2)	C(1S)-O-C(4S)	105.0(13)
C(16)-Na-N(4)	113.8(2)	C(1S)-O-Na	126.9(11)
O-Na-C(15)	88.7(3)	C(4S)-O-Na	127.9(11)
N(5)-Na-C(15)	153.9(2)	C(4S)-C(3S)-C(2S)	113.6(16)
C(16)-Na-C(15)	28.0(2)	C(2S)-C(1S)-O	117.0(18)
N(4)-Na-C(15)	120.0(2)	O-C(4S)-C(3S)	96.9(16)
O-Na-C(11)	129.2(3)	C(1S)-C(2S)-C(3S)	92.9(19)

Table A2.4.3. Anisotropic displacement parameters [$\text{\AA}^2 \times 10^3$] for $[\text{Na}(\text{THF})][\text{2}_2\text{-}\mu\text{-P}]$.

	U^{11}	U^{22}	U^{33}	U^{23}	U^{13}	U^{12}
Mo(1)	28(1)	17(1)	23(1)	-1(1)	1(1)	-3(1)
Mo(2)	35(1)	17(1)	23(1)	3(1)	1(1)	1(1)
P	32(1)	21(1)	25(1)	4(1)	3(1)	-1(1)
N(1)	36(4)	26(3)	29(3)	-1(3)	10(3)	1(3)
N(2)	43(4)	20(3)	20(3)	3(2)	-1(3)	0(3)
N(5)	46(4)	24(3)	28(3)	5(3)	8(3)	5(3)

C(52)	53(5)	38(5)	33(4)	6(4)	12(4)	6(4)
C(53)	82(7)	52(6)	39(5)	15(4)	26(5)	23(6)
C(24)	55(5)	16(4)	45(5)	-1(3)	5(4)	3(4)
N(3)	33(3)	27(3)	31(3)	2(3)	-6(3)	-4(3)
C(59)	86(7)	43(5)	40(5)	-1(4)	-2(5)	-11(5)
C(21)	33(4)	15(3)	30(4)	2(3)	-3(3)	-4(3)
N(6)	32(4)	29(3)	50(4)	5(3)	8(3)	1(3)
C(45)	135(10)	33(5)	30(5)	-5(4)	-4(6)	-16(5)
C(51)	51(5)	30(4)	34(4)	7(4)	17(4)	1(4)
C(23)	55(5)	27(4)	40(5)	4(4)	4(4)	0(4)
C(11)	27(4)	18(3)	46(5)	6(3)	-4(4)	6(3)
C(61)	42(5)	32(4)	59(6)	4(4)	19(4)	-1(4)
C(44)	102(8)	23(4)	47(5)	-7(4)	2(5)	-3(5)
C(67)	39(5)	28(4)	95(7)	-4(4)	7(5)	4(4)
C(28)	121(9)	35(5)	36(5)	-4(4)	0(5)	-4(5)
C(25)	37(5)	25(4)	49(5)	1(4)	3(4)	10(3)
C(43)	75(6)	20(4)	45(5)	3(4)	2(5)	-9(4)
C(35)	35(5)	34(4)	42(5)	3(4)	2(4)	-6(4)
C(27)	72(6)	22(4)	34(4)	3(3)	18(4)	11(4)
C(26)	40(5)	24(4)	33(4)	7(3)	5(4)	-1(3)
C(42)	66(6)	30(4)	38(5)	-2(4)	-4(4)	-9(4)
C(12)	40(5)	27(4)	56(5)	10(4)	7(4)	-3(4)
C(33)	34(5)	38(5)	52(5)	-9(4)	2(4)	-11(4)
C(36)	37(4)	31(4)	34(4)	-3(3)	4(4)	-1(4)
C(41)	72(6)	28(4)	30(4)	1(4)	-9(4)	-6(4)
C(15)	53(6)	40(5)	55(6)	-1(4)	-12(5)	-7(4)
C(22)	54(5)	22(4)	33(4)	3(3)	8(4)	5(4)
C(34)	48(5)	20(4)	59(5)	-1(4)	-6(4)	-7(4)
C(66)	45(5)	33(5)	49(6)	5(4)	6(4)	4(4)
C(351)	64(6)	49(5)	57(6)	12(5)	16(5)	-10(5)
C(16)	41(5)	32(4)	51(5)	-1(4)	-1(4)	-11(4)
C(57)	58(6)	33(4)	28(4)	8(3)	15(4)	12(4)
C(56)	56(6)	39(5)	65(6)	16(4)	13(5)	-7(4)
C(58)	84(7)	40(5)	59(6)	18(4)	32(5)	16(5)
C(31)	31(4)	28(4)	35(4)	-2(3)	-6(3)	-8(3)
C(451)	223(16)	30(5)	52(6)	-4(5)	-2(8)	15(7)
C(14)	31(5)	41(5)	91(8)	6(5)	-14(5)	-9(4)
C(54)	101(9)	39(5)	66(7)	30(5)	34(7)	12(6)
C(251)	61(6)	22(4)	61(6)	3(4)	13(5)	12(4)
C(46)	122(9)	27(5)	32(5)	-2(4)	-17(5)	-8(5)
C(62)	57(6)	40(5)	55(6)	7(4)	22(5)	10(4)
C(32)	35(5)	35(4)	34(4)	-1(4)	4(4)	-13(4)
C(231)	93(8)	31(5)	64(6)	17(4)	28(6)	1(5)
C(13)	34(5)	41(5)	76(7)	15(5)	8(5)	-8(4)
N(4)	67(5)	21(3)	25(3)	4(3)	-21(3)	2(3)
C(431)	98(7)	13(4)	46(5)	5(3)	-7(5)	-7(4)

C(63)	63(6)	43(5)	78(7)	-2(5)	39(5)	5(5)
C(39)	33(5)	45(5)	95(7)	12(5)	-15(5)	-6(4)
C(29)	72(7)	43(5)	75(7)	0(5)	36(6)	12(5)
C(37)	53(5)	26(4)	47(5)	4(4)	-14(4)	-13(4)
C(38)	85(7)	62(6)	50(6)	8(5)	-27(5)	-16(6)
C(64)	62(6)	29(5)	102(8)	-4(5)	38(6)	8(4)
C(18)	63(7)	36(5)	139(10)	-26(6)	58(7)	-7(5)
C(17)	43(5)	48(5)	54(6)	-19(4)	24(4)	-17(4)
C(55)	88(8)	42(6)	86(8)	31(5)	32(7)	-8(5)
C(331)	60(6)	53(6)	84(7)	-37(5)	24(6)	-18(5)
C(47)	116(9)	45(5)	35(5)	10(4)	-28(6)	-11(6)
C(631)	114(10)	58(6)	84(8)	-13(6)	50(7)	9(6)
C(49)	188(14)	31(5)	44(6)	1(4)	38(8)	15(6)
C(531)	110(9)	71(7)	62(7)	34(6)	15(6)	42(7)
C(65)	42(5)	36(5)	86(8)	3(5)	17(5)	7(4)
C(151)	74(7)	70(7)	70(7)	-9(5)	-24(6)	-12(6)
C(19)	99(8)	114(9)	41(6)	-36(6)	30(6)	-68(7)
C(651)	98(8)	39(5)	93(8)	19(5)	0(7)	24(6)
C(131)	60(7)	82(8)	108(9)	27(7)	20(7)	-12(6)
C(69)	76(8)	45(6)	178(14)	17(7)	-62(9)	-14(6)
C(68)	95(9)	64(7)	173(14)	-8(8)	87(10)	-24(7)
C(551)	115(11)	63(8)	168(14)	37(8)	18(10)	-38(7)
C(48)	251(23)	143(14)	96(11)	4(10)	-77(13)	52(15)
Na	42(2)	48(2)	69(2)	7(2)	-6(2)	-1(2)
O	62(5)	66(5)	188(10)	-25(6)	-15(6)	-16(4)
C(3S)	172(18)	112(13)	136(15)	-53(12)	-41(13)	32(13)
C(1S)	86(12)	90(11)	388(33)	88(16)	-27(15)	-45(9)
C(4S)	90(14)	266(30)	231(26)	-21(25)	-34(15)	-23(17)
C(2S)	168(19)	156(19)	251(27)	-19(19)	0(19)	-53(16)

A2.5 X-ray crystal structure of PMo(N[*i*-Pr]Ar)₃ (2-P).

Crystals of 2-P grown from a concentrated ether solution at $-35\text{ }^{\circ}\text{C}$ were coated with Paratone N oil (an Exxon product) on a microscope slide. A yellow block of approximate dimensions $0.89 \times 0.76 \times 0.50\text{ mm}^3$ was selected and mounted with wax on a glass fiber. A total of 26197 reflections ($-10 \leq h \leq 11$, $-12 \leq k \leq 10$, $-64 \leq l \leq 52$) were collected at 183(2) K in the θ range of 2.39 to 23.28° , of which 9645 were unique ($R_{\text{int}} = 0.0656$). The structure was solved by direct methods (SHELXTL V5.1, G. M. Sheldrick and Siemens Industrial Automation, Inc., 1997) in conjunction with standard difference Fourier techniques. 2-P crystallizes in a chiral space group. This fact could be a solely consequence of packing forces in the solid state. Since the chirality of this compound does not present an interest, a chiral flag was not set when solving the crystal structure. The unit cell contains two molecules. All non-hydrogen atoms were refined anisotropically except C61 and hydrogen atoms were placed in calculated ($d_{\text{CH}} = 0.96\text{ \AA}$) positions. The residual peak and hole electron density were 1.120 and $-1.621\text{ e}\cdot\text{\AA}^{-3}$, respectively. A semi-empirical absorption correction was applied based on pseudo-psi-scans with maximum and minimum transmission equal to 0.2860 and 0.2100, respectively. The least squares refinement converged normally with residuals of $R_1 = 0.0900$, $wR_2 = 0.2065$ based on $I > 2\sigma I$ and $\text{GOF} = 1.325$ (based on F^2). The somewhat high values of R_1 and wR_2 could be attributed to the fact that there are two independent molecules in the unit cell. No significant extinction coefficient was applied to the refinement. Crystal and refinement data: formula = $\text{C}_{33}\text{H}_{48}\text{N}_3\text{MoP}$, space group $P2_12_12_1$, $a = 10.493(4)\text{ \AA}$, $b = 10.985(4)\text{ \AA}$, $c = 58.45(2)\text{ \AA}$, $\alpha = 90^{\circ}$, $\beta = 90^{\circ}$, $\gamma = 90^{\circ}$, $Z = 8$, $V = 6737(4)\text{ \AA}^3$, $D_{\text{calcd}} = 1.210\text{ g}\cdot\text{cm}^{-3}$, $F(000) = 2592$, R (based on F) = 0.0909, wR (based on F^2) = 0.2070.

Table A2.5.1. Atomic coordinates [$\times 10^4$] and equivalent isotropic displacement parameters [$\text{\AA}^2 \times 10^3$] for 2-P. $U(\text{eq})$ is defined as one third of the trace of the orthogonalized U_{ij} tensor.

	x	y	z	U(eq)
Mo(2)	6176(1)	5297(1)	1952(1)	33(1)
P(2)	4362(3)	5972(4)	2042(1)	47(1)
C(42)	8979(10)	7393(10)	1949(2)	34(3)
C(51)	7908(10)	3931(14)	2230(2)	39(3)
C(61)	6742(11)	3566(10)	1589(2)	32(3)
C(65)	8646(11)	2425(12)	1510(2)	45(3)
C(451)	11061(13)	5293(14)	1472(2)	56(4)
C(62)	6745(12)	4066(12)	1380(2)	49(3)
C(46)	9024(10)	6004(11)	1638(2)	33(3)
C(45)	10369(12)	6023(12)	1646(2)	43(3)
C(55)	8510(12)	1841(11)	2295(2)	43(3)

C(63)	7713(12)	3740(14)	1223(2)	52(4)
C(52)	9148(10)	4202(11)	2151(2)	35(3)
N(5)	6966(9)	4915(9)	2247(2)	34(2)
C(44)	10957(11)	6748(11)	1807(2)	31(3)
C(43)	10307(12)	7437(11)	1958(2)	39(3)
C(67)	4556(11)	3183(13)	1746(2)	41(3)
N(4)	6938(8)	6652(10)	1789(2)	40(3)
C(56)	7616(10)	2742(11)	2303(2)	29(3)
C(41)	8361(10)	6708(10)	1785(2)	33(3)
C(54)	9744(11)	2104(12)	2216(2)	37(3)
C(66)	7691(11)	2739(11)	1672(2)	43(3)
C(551)	8202(15)	570(13)	2377(3)	69(5)
C(53)	10049(12)	3245(13)	2139(2)	46(3)
C(64)	8628(12)	2934(12)	1290(2)	43(3)
C(59)	6694(16)	6678(15)	2497(3)	66(4)
C(57)	6737(12)	5319(13)	2483(2)	42(3)
C(69)	4016(12)	3114(14)	1515(2)	58(4)
C(651)	9670(14)	1511(15)	1578(3)	66(5)
C(68)	4780(16)	1919(15)	1847(3)	72(5)
C(631)	7728(16)	4313(15)	986(3)	66(4)
C(58)	5599(14)	4710(16)	2596(2)	68(5)
C(48)	6423(27)	8852(19)	1775(5)	141(11)
C(431)	10974(14)	8232(15)	2132(3)	63(4)
C(47)	6297(16)	7672(13)	1666(2)	60(4)
Mo(1)	3727(1)	1088(1)	580(1)	33(1)
C(37)	1272(15)	2460(13)	769(3)	61(4)
P(1)	4453(4)	2846(3)	510(1)	49(1)
C(32)	895(11)	-485(11)	861(2)	37(3)
N(1)	3379(8)	412(8)	280(2)	30(2)
C(21)	5200(11)	-989(12)	739(2)	35(3)
C(31)	1787(10)	400(11)	916(2)	29(2)
N(2)	5158(9)	327(9)	747(2)	36(2)
C(11)	2373(11)	-506(10)	272(2)	31(3)
C(12)	1152(11)	-230(11)	183(2)	40(3)
C(25)	4505(14)	-2876(12)	900(2)	46(3)
C(36)	2297(11)	391(11)	1133(2)	37(3)
C(35)	1925(12)	-496(12)	1292(2)	45(3)
C(22)	5907(10)	-1591(12)	576(2)	40(3)
C(34)	982(12)	-1311(12)	1222(2)	49(3)
C(15)	1612(12)	-2495(13)	372(2)	44(3)
C(13)	191(12)	-1094(14)	182(2)	46(3)
C(23)	5909(10)	-2873(12)	569(2)	45(3)
N(3)	2162(9)	1368(9)	759(2)	35(2)
C(151)	1799(15)	-3755(14)	478(3)	61(4)
C(17)	3816(14)	705(11)	45(2)	42(3)
C(14)	395(13)	-2186(13)	277(2)	45(3)

C(39)	1833(13)	3441(12)	918(2)	48(3)
C(24)	5207(12)	-3500(13)	742(2)	48(3)
C(131)	-1096(14)	-793(17)	68(3)	88(6)
C(251)	3758(18)	-3611(13)	1080(3)	69(4)
C(27)	6285(15)	926(14)	854(3)	68(4)
C(351)	2469(17)	-554(15)	1526(3)	69(5)
C(33)	506(11)	-1336(10)	1006(2)	34(3)
C(19)	3345(16)	1897(16)	-49(2)	70(5)
C(38)	866(15)	2886(13)	547(3)	62(4)
C(26)	4508(11)	-1608(11)	900(2)	35(3)
C(231)	6689(14)	-3556(15)	398(3)	66(5)
C(18)	5272(13)	613(16)	27(3)	62(4)
N(6)	5768(8)	3896(9)	1758(2)	31(2)
C(531)	11394(13)	3556(14)	2063(3)	63(4)
C(16)	2566(12)	-1601(12)	374(2)	41(3)
C(331)	-487(17)	-2256(16)	931(4)	87(6)
C(29)	6476(22)	495(19)	1093(3)	115(9)
C(28)	7422(14)	918(17)	699(3)	87(7)
C(49)	6704(29)	7681(27)	1423(4)	159(13)

Table A2.5.2. Bond lengths [\AA] and angles [$^\circ$] for 2-P.

Mo(2)-N(4)	1.939(10)	C(55)-C(56)	1.36(2)
Mo(2)-N(5)	1.954(9)	C(55)-C(54)	1.41(2)
Mo(2)-N(6)	1.962(9)	C(55)-C(551)	1.51(2)
Mo(2)-P(2)	2.109(3)	C(63)-C(64)	1.36(2)
C(42)-C(41)	1.38(2)	C(63)-C(631)	1.52(2)
C(42)-C(43)	1.40(2)	C(52)-C(53)	1.42(2)
C(51)-C(56)	1.41(2)	N(5)-C(57)	1.469(15)
C(51)-C(52)	1.41(2)	C(44)-C(43)	1.35(2)
C(51)-N(5)	1.47(2)	C(43)-C(431)	1.51(2)
C(61)-C(62)	1.34(2)	C(67)-C(69)	1.46(2)
C(61)-C(66)	1.43(2)	C(67)-N(6)	1.495(15)
C(61)-N(6)	1.466(14)	C(67)-C(68)	1.53(2)
C(65)-C(64)	1.40(2)	N(4)-C(47)	1.49(2)
C(65)-C(66)	1.42(2)	N(4)-C(41)	1.495(13)
C(65)-C(651)	1.52(2)	C(54)-C(53)	1.37(2)
C(451)-C(45)	1.48(2)	C(53)-C(531)	1.52(2)
C(62)-C(63)	1.42(2)	C(59)-C(57)	1.50(2)
C(46)-C(41)	1.35(2)	C(57)-C(58)	1.52(2)
C(46)-C(45)	1.41(2)	C(48)-C(47)	1.45(2)
C(45)-C(44)	1.38(2)	C(47)-C(49)	1.48(3)

Mo(1)-N(1)	1.935(9)	C(41)-C(42)-C(43)	121.0(11)
Mo(1)-N(3)	1.971(10)	C(56)-C(51)-C(52)	19.7(11)
Mo(1)-N(2)	1.978(10)	C(56)-C(51)-N(5)	121.1(9)
Mo(1)-P(1)	2.116(3)	C(52)-C(51)-N(5)	119.2(11)
C(37)-C(38)	1.44(2)	C(62)-C(61)-C(66)	124.7(12)
C(37)-C(39)	1.50(2)	C(62)-C(61)-N(6)	120.9(11)
C(37)-N(3)	1.52(2)	C(66)-C(61)-N(6)	114.4(10)
C(32)-C(33)	1.33(2)	C(64)-C(65)-C(66)	120.3(12)
C(32)-C(31)	1.39(2)	C(64)-C(65)-C(651)	121.0(12)
N(1)-C(11)	1.461(14)	C(66)-C(65)-C(651)	118.7(13)
N(1)-C(17)	1.483(14)	C(61)-C(62)-C(63)	119.3(13)
C(21)-C(26)	1.37(2)	C(41)-C(46)-C(45)	119.0(11)
C(21)-C(22)	1.38(2)	C(44)-C(45)-C(46)	118.6(12)
C(21)-N(2)	1.45(2)	C(44)-C(45)-C(451)	124.0(12)
C(31)-C(36)	1.38(2)	C(46)-C(45)-C(451)	117.3(12)
C(31)-N(3)	1.460(15)	C(56)-C(55)-C(54)	119.6(11)
N(2)-C(27)	1.49(2)	C(56)-C(55)-C(551)	120.9(11)
C(11)-C(16)	1.36(2)	C(54)-C(55)-C(551)	119.5(12)
C(11)-C(12)	1.42(2)	C(64)-C(63)-C(62)	118.8(14)
C(12)-C(13)	1.38(2)	C(64)-C(63)-C(631)	121.6(12)
C(25)-C(24)	1.37(2)	C(62)-C(63)-C(631)	119.6(13)
C(25)-C(26)	1.39(2)	C(51)-C(52)-C(53)	118.4(12)
C(25)-C(251)	1.54(2)	C(51)-N(5)-C(57)	113.2(10)
C(36)-C(35)	1.40(2)	C(51)-N(5)-Mo(2)	112.7(7)
C(35)-C(34)	1.40(2)	C(57)-N(5)-Mo(2)	133.8(8)
C(35)-C(351)	1.48(2)	C(43)-C(44)-C(45)	123.0(11)
C(22)-C(23)	1.41(2)	C(44)-C(43)-C(42)	117.4(11)
C(34)-C(33)	1.36(2)	C(44)-C(43)-C(431)	122.0(12)
C(15)-C(16)	1.40(2)	C(42)-C(43)-C(431)	120.6(12)
C(15)-C(14)	1.43(2)	C(69)-C(67)-N(6)	113.5(10)
C(15)-C(151)	1.53(2)	C(69)-C(67)-C(68)	111.6(12)
C(13)-C(14)	1.34(2)	N(6)-C(67)-C(68)	109.1(11)
C(13)-C(131)	1.54(2)	C(47)-N(4)-C(41)	114.3(11)
C(23)-C(24)	1.43(2)	C(47)-N(4)-Mo(2)	128.9(9)
C(23)-C(231)	1.50(2)	C(41)-N(4)-Mo(2)	116.8(7)
C(17)-C(19)	1.50(2)	C(55)-C(56)-C(51)	120.9(10)
C(17)-C(18)	1.53(2)	C(46)-C(41)-C(42)	120.8(10)
C(27)-C(29)	1.49(2)	C(46)-C(41)-N(4)	120.2(10)
C(27)-C(28)	1.50(2)	C(42)-C(41)-N(4)	118.6(11)
C(33)-C(331)	1.52(2)	C(53)-C(54)-C(55)	120.8(12)
N(4)-Mo(2)-N(5)	115.0(4)	C(65)-C(66)-C(61)	114.6(13)
N(4)-Mo(2)-N(6)	114.0(5)	C(54)-C(53)-C(52)	120.4(12)
N(5)-Mo(2)-N(6)	115.7(4)	C(54)-C(53)-C(531)	121.2(12)
N(4)-Mo(2)-P(2)	102.9(3)	C(52)-C(53)-C(531)	118.0(12)
N(5)-Mo(2)-P(2)	103.9(3)	C(63)-C(64)-C(65)	122.3(11)
N(6)-Mo(2)-P(2)	102.8(3)	N(5)-C(57)-C(59)	111.1(11)

N(5)-C(57)-C(58)	113.8(11)	C(31)-C(36)-C(35)	120.6(11)
C(59)-C(57)-C(58)	113.0(13)	C(34)-C(35)-C(36)	116.5(12)
C(48)-C(47)-C(49)	112.8(20)	C(34)-C(35)-C(351)	121.1(14)
C(48)-C(47)-N(4)	114.7(14)	C(36)-C(35)-C(351)	122.4(13)
C(49)-C(47)-N(4)	109.7(15)	C(21)-C(22)-C(23)	120.0(12)
N(1)-Mo(1)-N(3)	112.5(4)	C(33)-C(34)-C(35)	123.2(13)
N(1)-Mo(1)-N(2)	115.4(4)	C(16)-C(15)-C(14)	118.3(12)
N(3)-Mo(1)-N(2)	115.8(4)	C(16)-C(15)-C(151)	122.5(12)
N(1)-Mo(1)-P(1)	104.1(3)	C(14)-C(15)-C(151)	119.0(12)
N(3)-Mo(1)-P(1)	105.1(3)	C(14)-C(13)-C(12)	119.7(11)
N(2)-Mo(1)-P(1)	102.0(3)	C(14)-C(13)-C(131)	120.7(13)
C(38)-C(37)-C(39)	113.8(12)	C(12)-C(13)-C(131)	119.6(13)
C(38)-C(37)-N(3)	113.6(12)	C(22)-C(23)-C(24)	117.5(11)
C(39)-C(37)-N(3)	110.3(12)	C(22)-C(23)-C(231)	121.3(13)
C(33)-C(32)-C(31)	123.7(11)	C(24)-C(23)-C(231)	121.0(12)
C(11)-N(1)-C(17)	110.0(9)	C(31)-N(3)-C(37)	112.5(10)
C(11)-N(1)-Mo(1)	115.5(7)	C(31)-N(3)-Mo(1)	116.4(7)
C(17)-N(1)-Mo(1)	134.1(8)	C(37)-N(3)-Mo(1)	131.0(9)
C(26)-C(21)-C(22)	121.5(12)	N(1)-C(17)-C(19)	115.3(11)
C(26)-C(21)-N(2)	117.1(11)	N(1)-C(17)-C(18)	111.0(11)
C(22)-C(21)-N(2)	121.3(11)	C(19)-C(17)-C(18)	111.0(12)
C(36)-C(31)-C(32)	118.0(11)	C(13)-C(14)-C(15)	121.0(12)
C(36)-C(31)-N(3)	118.7(10)	C(25)-C(24)-C(23)	121.1(12)
C(32)-C(31)-N(3)	123.2(10)	C(29)-C(27)-N(2)	111.0(13)
C(21)-N(2)-C(27)	115.5(11)	C(29)-C(27)-C(28)	117.2(16)
C(21)-N(2)-Mo(1)	115.4(7)	N(2)-C(27)-C(28)	112.2(13)
C(27)-N(2)-Mo(1)	128.6(9)	C(32)-C(33)-C(34)	117.8(11)
C(16)-C(11)-C(12)	119.1(11)	C(32)-C(33)-C(331)	119.7(13)
C(16)-C(11)-N(1)	119.3(10)	C(34)-C(33)-C(331)	122.5(13)
C(12)-C(11)-N(1)	121.2(10)	C(21)-C(26)-C(25)	119.8(12)
C(13)-C(12)-C(11)	120.9(11)	C(61)-N(6)-C(67)	115.6(9)
C(24)-C(25)-C(26)	120.0(12)	C(61)-N(6)-Mo(2)	115.6(7)
C(24)-C(25)-C(251)	118.3(12)	C(67)-N(6)-Mo(2)	128.6(7)
C(26)-C(25)-C(251)	121.7(12)	C(11)-C(16)-C(15)	120.6(12)

Table A2.5.3. Anisotropic displacement parameters [$\text{\AA}^2 \times 10^3$] for 2-P.

	U^{11}	U^{22}	U^{33}	U^{23}	U^{13}	U^{12}
Mo(2)	18(1)	41(1)	39(1)	-8(1)	-1(1)	6(1)
P(2)	23(1)	59(2)	58(2)	-16(2)	-2(1)	10(2)

C(42)	23(6)	41(6)	38(6)	3(5)	6(5)	7(5)
C(51)	17(5)	58(8)	43(7)	23(7)	3(5)	7(6)
C(65)	19(6)	47(7)	68(9)	-16(6)	-13(6)	4(6)
C(451)	41(7)	70(9)	58(8)	-12(8)	20(7)	0(8)
C(62)	43(7)	36(7)	66(9)	0(7)	2(6)	-11(6)
C(46)	23(6)	38(6)	37(6)	-17(6)	-7(5)	3(5)
C(45)	42(7)	31(7)	57(8)	6(7)	10(6)	-2(6)
C(55)	41(8)	30(6)	58(8)	-1(6)	10(6)	-3(6)
C(63)	34(7)	58(9)	64(9)	-25(8)	12(6)	-1(7)
C(52)	34(7)	32(7)	39(7)	15(5)	-19(5)	6(5)
N(5)	32(5)	32(6)	39(6)	-1(5)	0(4)	1(4)
C(44)	30(6)	37(6)	27(6)	-2(5)	3(5)	2(6)
C(43)	50(7)	30(6)	37(7)	-9(6)	3(6)	-6(6)
C(67)	21(6)	63(9)	40(7)	-22(7)	8(5)	-13(6)
N(4)	16(5)	45(6)	60(7)	22(5)	1(5)	9(5)
C(56)	16(5)	45(7)	26(6)	13(5)	8(4)	-8(5)
C(41)	17(5)	26(6)	54(7)	-9(6)	-9(5)	-6(5)
C(54)	31(6)	45(8)	35(7)	9(6)	-8(5)	8(6)
C(66)	22(6)	39(7)	67(9)	-38(7)	0(6)	5(5)
C(551)	64(10)	45(9)	99(13)	16(9)	22(9)	1(8)
C(53)	33(7)	49(8)	57(9)	16(7)	0(6)	15(6)
C(64)	31(7)	62(8)	37(7)	-28(6)	13(6)	-1(7)
C(59)	69(11)	68(10)	61(10)	-16(8)	1(8)	3(9)
C(57)	50(7)	49(8)	27(6)	0(6)	-3(5)	-8(7)
C(69)	34(8)	71(10)	68(9)	17(8)	-25(7)	-21(7)
C(651)	60(9)	83(12)	54(9)	-24(8)	3(7)	37(9)
C(68)	67(10)	64(11)	86(12)	40(9)	-25(9)	-40(9)
C(631)	75(10)	70(11)	54(9)	-9(8)	20(8)	-7(9)
C(58)	75(10)	84(11)	44(8)	-18(8)	43(8)	-15(10)
C(48)	165(24)	64(12)	195(26)	-31(15)	-84(22)	37(17)
C(431)	43(9)	70(10)	76(10)	-7(8)	-24(8)	-3(8)
C(47)	56(9)	64(9)	59(9)	3(7)	-24(8)	15(9)
Mo(1)	34(1)	27(1)	37(1)	-2(1)	1(1)	-5(1)
C(37)	38(7)	50(8)	97(11)	-13(8)	2(9)	9(8)
P(1)	52(2)	29(2)	68(3)	5(2)	1(2)	-11(2)
N(1)	31(5)	22(5)	38(5)	3(4)	10(4)	4(4)
C(21)	33(6)	43(7)	29(6)	-1(6)	-13(5)	-9(6)
C(31)	27(5)	36(6)	24(6)	-8(5)	-1(4)	11(5)
N(2)	39(5)	17(5)	51(6)	1(5)	-4(5)	-11(4)
C(11)	37(6)	27(6)	30(6)	-6(5)	-4(5)	-4(5)
C(12)	30(6)	40(6)	49(7)	-4(6)	-3(6)	9(7)
C(25)	66(9)	39(7)	32(7)	8(6)	8(7)	-8(7)
C(36)	32(6)	20(6)	60(8)	-12(6)	0(6)	-4(5)
C(35)	42(7)	41(8)	50(8)	-8(6)	10(6)	26(6)

C(22)	30(7)	52(7)	38(6)	-11(6)	0(5)	2(5)
C(34)	40(8)	40(7)	67(9)	-7(6)	15(7)	4(6)
C(15)	44(8)	62(9)	25(6)	6(6)	-6(5)	-11(7)
C(13)	38(7)	52(8)	48(8)	-9(7)	-16(6)	4(7)
C(23)	27(7)	51(8)	56(8)	-29(7)	-9(6)	11(5)
N(3)	32(5)	29(5)	43(6)	-2(5)	-2(5)	-5(4)
C(151)	66(9)	54(9)	63(9)	22(8)	7(7)	-20(8)
C(17)	49(7)	41(7)	37(6)	0(5)	7(7)	-10(7)
C(14)	42(8)	47(8)	46(8)	6(7)	0(6)	-22(6)
C(39)	58(8)	49(8)	38(7)	10(6)	-4(6)	8(7)
C(24)	45(8)	45(8)	53(8)	-12(7)	-6(7)	6(6)
C(131)	31(8)	96(14)	139(17)	0(12)	-36(10)	-23(9)
C(251)	73(10)	52(9)	82(11)	7(8)	19(10)	-2(9)
C(27)	53(9)	58(9)	95(11)	-19(8)	-12(9)	-40(9)
C(351)	94(12)	58(10)	56(9)	15(8)	-7(9)	9(9)
C(33)	45(7)	25(6)	31(6)	-4(5)	14(6)	-18(5)
C(19)	76(12)	94(13)	40(8)	30(8)	15(7)	17(10)
C(38)	77(11)	46(8)	63(9)	-1(7)	-23(8)	25(7)
C(26)	39(7)	45(7)	22(6)	-3(5)	-7(5)	-4(6)
C(231)	54(9)	68(11)	77(11)	-24(9)	13(8)	20(8)
C(18)	46(8)	85(12)	55(9)	13(8)	-3(7)	-1(8)
N(6)	25(5)	36(5)	33(5)	-10(5)	8(4)	5(4)
C(531)	33(7)	75(10)	80(10)	27(8)	29(7)	11(7)
C(16)	34(7)	54(8)	34(7)	6(6)	-8(5)	-9(6)
C(331)	76(12)	64(11)	123(17)	-26(11)	13(12)	-24(10)
C(29)	134(19)	103(16)	107(15)	26(13)	-73(15)	-67(15)
C(28)	43(9)	79(12)	140(17)	49(13)	-25(10)	-30(9)
C(49)	215(34)	165(26)	97(18)	71(18)	-37(19)	58(25)

A2.6 X-ray Crystal Structure of [PMo(N[*i*-Pr]Ar)(O-2,6-C₆H₃Me₂)₂]₂ ((6-P)₂).

Crystals grown from a concentrated diethyl ether solution at $-35\text{ }^{\circ}\text{C}$ were coated with Paratone N oil (Exxon) on a microscope slide. A green-brown needle of approximate dimensions $0.16 \times 0.07 \times 0.05\text{ mm}^3$ was selected and mounted with wax on a glass fiber. A total of 22054 reflections ($-20 \leq h \leq 16$, $-18 \leq k \leq 17$, $-16 \leq l \leq 20$) were collected at 183(2) K in the θ range of 1.98 to 23.28 $^{\circ}$, of which 4095 were unique ($R_{\text{int}} = 0.0665$). The radiation used was Mo-K α ($\lambda = 0.71073\text{ \AA}$, $\mu = 0.465\text{ mm}^{-1}$). The structure was solved by direct methods (SHELXTL V5.0, G. M. Sheldrick and Siemens Industrial Automation, Inc., 1995) in conjunction with standard difference Fourier techniques. All non-hydrogen atoms were refined anisotropically and the hydrogen atoms were placed in calculated ($d_{\text{CH}} = 0.96\text{ \AA}$) positions. The residual peak and hole electron density were 0.676 and $-0.517\text{ e}\cdot\text{\AA}^{-3}$, respectively. The least squares refinement converged normally with residuals of $R_1 = 0.0400$, $wR_2 = 0.0895$ based upon $I > 2\sigma I$, and GOF = 1.046 (based on F^2). No significant extinction coefficient was applied to the refinement (0.00006(6)). Crystal and refinement data: Formula = C₅₉H₇₅Mo₂N₂O₄P₂; space group, Pccn; $a = 18.7073(8)\text{ \AA}$; $b = 16.8765(7)\text{ \AA}$; $c = 18.0139(7)\text{ \AA}$; $\alpha = 90\text{ }^{\circ}$; $\beta = 90\text{ }^{\circ}$; $\gamma = 90\text{ }^{\circ}$; $V = 5687.2(4)\text{ \AA}^3$; $Z = 4$; $D_{\text{calc}} = 1.320\text{ g}\cdot\text{cm}^{-3}$; $F(000) = 2356$; R_1 (based on F) = 0.0536; wR_2 (based on F^2) = 0.0955.

Table A2.6.1. Atomic coordinates ($\times 10^4$) and equivalent isotropic displacement parameters ($\text{\AA}^2 \times 10^3$) for (6-P)₂. U(eq) is defined as one third of the trace of the orthogonalized U^{ij} tensor.

	x	y	z	U(eq)
C(2S)	7032(8)	2163(9)	1704(8)	216(7)
C(1S)	6475(6)	1760(6)	1294(6)	148(4)
C(3S)	7500	2500	1351(8)	123(5)
Mo	2721(1)	1738(1)	632(1)	21(1)
P	3014(1)	2741(1)	-340(1)	30(1)
O(3)	3166(1)	2570(2)	1277(1)	23(1)
C(31)	3721(2)	2561(2)	1783(2)	24(1)
C(26)	1592(2)	-168(3)	22(3)	34(1)
O(2)	2132(2)	819(2)	812(2)	28(1)
N(1)	3531(2)	1158(2)	235(2)	27(1)
C(12)	3377(2)	-245(3)	581(3)	33(1)
C(21)	1752(2)	142(2)	724(3)	29(1)
C(22)	1542(2)	-255(3)	1378(3)	34(1)
C(24)	975(3)	-1255(3)	622(3)	54(2)
C(34)	4821(3)	2573(3)	2808(3)	40(1)
C(35)	4200(3)	2171(3)	2959(3)	33(1)
C(36)	3636(2)	2148(2)	2455(2)	26(1)
C(13)	3452(2)	-862(3)	1085(3)	35(1)
C(15)	4180(2)	-12(3)	1865(2)	33(1)

C(11)	3679(2)	493(2)	719(2)	28(1)
C(23)	1152(3)	-945(3)	1311(3)	49(1)
C(16)	4090(2)	599(3)	1358(3)	31(1)
C(32)	4350(2)	2959(3)	1613(3)	30(1)
C(14)	3853(3)	-730(3)	1721(3)	38(1)
C(25)	1201(3)	-870(3)	-5(3)	49(1)
C(33)	4898(3)	2947(3)	2132(3)	40(1)
C(151)	4622(4)	135(4)	2559(4)	59(2)
C(361)	2994(3)	1646(3)	2615(3)	33(1)
C(321)	4463(3)	3362(4)	878(3)	43(1)
C(17)	4038(3)	1243(3)	-401(3)	36(1)
C(261)	1809(4)	229(4)	-688(3)	50(2)
C(221)	1744(4)	80(4)	2113(3)	47(1)
C(131)	3094(4)	-1648(4)	965(5)	63(2)
C(19)	3962(4)	578(6)	-957(4)	71(2)
C(18)	4841(5)	1307(9)	-117(8)	85(4)

Table A2.6.2. Bond lengths [Å] and angles [°] for (6-P)₂.

C(2S)-C(3S)	1.222(14)	C(22)-C(23)	1.381(7)
C(2S)-C(1S)	1.448(15)	C(22)-C(221)	1.488(7)
C(3S)-C(2S)#1	1.222(14)	C(24)-C(25)	1.370(8)
Mo-O(2)	1.930(3)	C(24)-C(23)	1.387(8)
Mo-N(1)	1.940(3)	C(34)-C(35)	1.372(7)
Mo-O(3)	2.005(3)	C(34)-C(33)	1.379(7)
Mo-O(3)#2	2.339(3)	C(35)-C(36)	1.391(6)
Mo-P#2	2.3926(12)	C(36)-C(361)	1.497(6)
Mo-P	2.4951(12)	C(13)-C(14)	1.387(7)
Mo-Mo#2	2.7021(7)	C(13)-C(131)	1.502(8)
P-P#2	2.086(2)	C(15)-C(14)	1.382(7)
P-Mo#2	2.3926(12)	C(15)-C(16)	1.388(7)
O(3)-C(31)	1.380(5)	C(15)-C(151)	1.519(8)
O(3)-Mo#2	2.339(3)	C(11)-C(16)	1.396(6)
C(31)-C(32)	1.389(6)	C(32)-C(33)	1.387(6)
C(31)-C(36)	1.407(6)	C(32)-C(321)	1.504(7)
C(26)-C(25)	1.393(7)	C(17)-C(19)	1.512(8)
C(26)-C(21)	1.400(6)	C(17)-C(18)	1.590(11)
C(26)-C(261)	1.501(7)		
O(2)-C(21)	1.355(5)	C(3S)-C(2S)-C(1S)	117.9(14)
N(1)-C(11)	1.449(5)	C(2S)#1-C(3S)-C(2S)	117(2)
N(1)-C(17)	1.494(5)	O(2)-Mo-N(1)	95.89(13)
C(12)-C(13)	1.389(7)	O(2)-Mo-O(3)	134.63(11)
C(12)-C(11)	1.390(6)	N(1)-Mo-O(3)	104.04(13)
C(21)-C(22)	1.412(6)	O(2)-Mo-O(3)#2	84.97(11)

N(1)-Mo-O(3)#2	171.58(12)	C(13)-C(12)-C(11)	120.9(5)
O(3)-Mo-O(3)#2	69.94(13)	O(2)-C(21)-C(26)	122.3(4)
O(2)-Mo-P#2	95.21(9)	O(2)-C(21)-C(22)	116.5(4)
N(1)-Mo-P#2	111.37(11)	C(26)-C(21)-C(22)	121.1(4)
O(3)-Mo-P#2	113.90(8)	C(23)-C(22)-C(21)	118.3(5)
O(3)#2-Mo-P#2	76.83(7)	C(23)-C(22)-C(221)	122.2(5)
O(2)-Mo-P	142.05(9)	C(21)-C(22)-C(221)	119.5(4)
N(1)-Mo-P	84.96(10)	C(25)-C(24)-C(23)	119.1(5)
O(3)-Mo-P	80.81(8)	C(35)-C(34)-C(33)	119.4(5)
O(3)#2-Mo-P	99.53(7)	C(34)-C(35)-C(36)	121.7(5)
P#2-Mo-P	50.49(6)	C(35)-C(36)-C(31)	117.5(4)
O(2)-Mo-Mo#2	126.18(9)	C(35)-C(36)-C(361)	119.9(4)
N(1)-Mo-Mo#2	135.98(10)	C(31)-C(36)-C(361)	122.4(4)
O(3)-Mo-Mo#2	57.33(8)	C(14)-C(13)-C(12)	118.3(4)
O(3)#2-Mo-Mo#2	46.17(6)	C(14)-C(13)-C(131)	120.1(5)
P#2-Mo-Mo#2	58.27(3)	C(12)-C(13)-C(131)	121.5(5)
P-Mo-Mo#2	54.65(3)	C(14)-C(15)-C(16)	118.3(4)
P#2-P-Mo#2	67.30(4)	C(14)-C(15)-C(151)	122.6(5)
P#2-P-Mo	62.21(4)	C(16)-C(15)-C(151)	119.0(5)
Mo#2-P-Mo	67.08(3)	C(12)-C(11)-C(16)	119.2(4)
C(31)-O(3)-Mo	133.4(2)	C(12)-C(11)-N(1)	120.6(4)
C(31)-O(3)-Mo#2	150.1(2)	C(16)-C(11)-N(1)	120.1(4)
Mo-O(3)-Mo#2	76.50(9)	C(22)-C(23)-C(24)	121.5(5)
O(3)-C(31)-C(32)	119.1(4)	C(15)-C(16)-C(11)	120.9(5)
O(3)-C(31)-C(36)	119.3(4)	C(33)-C(32)-C(31)	118.1(4)
C(32)-C(31)-C(36)	121.6(4)	C(33)-C(32)-C(321)	119.7(4)
C(25)-C(26)-C(21)	117.6(5)	C(31)-C(32)-C(321)	122.1(4)
C(25)-C(26)-C(261)	119.4(5)	C(15)-C(14)-C(13)	122.4(5)
C(21)-C(26)-C(261)	123.0(4)	C(24)-C(25)-C(26)	122.4(5)
C(21)-O(2)-Mo	163.2(3)	C(34)-C(33)-C(32)	121.6(5)
C(11)-N(1)-C(17)	114.5(3)	N(1)-C(17)-C(19)	112.1(5)
C(11)-N(1)-Mo	108.6(3)	N(1)-C(17)-C(18)	111.1(6)
C(17)-N(1)-Mo	136.9(3)	C(19)-C(17)-C(18)	110.6(7)

Symmetry transformations used to generate equivalent atoms:

#1 $-x + 3/2, -y + 1/2, z$

#2 $-x + 1/2, -y + 1/2, z$

Table A2.6.3. Anisotropic displacement parameters ($\text{\AA}^2 \times 10^3$) for $(6\text{-P})_2$. The anisotropic displacement factor exponent takes the form: $-2\pi^2[h^2 a^{*2}U^{11} + \dots + 2 h k a^* b^* U^{12}]$

	U^{11}	U^{22}	U^{33}	U^{23}	U^{13}	U^{12}
Mo	21(1)	22(1)	19(1)	1(1)	0(1)	-1(1)
P	36(1)	30(1)	23(1)	5(1)	9(1)	7(1)
O(3)	21(2)	24(2)	23(2)	-3(1)	-2(1)	-1(1)
C(31)	20(2)	25(2)	28(2)	-7(2)	-6(2)	4(2)
C(26)	33(3)	31(3)	38(3)	3(2)	-6(2)	-4(2)
O(2)	30(2)	26(2)	27(2)	1(1)	-3(1)	-5(1)
N(1)	27(2)	25(2)	28(2)	3(2)	1(2)	5(2)
C(12)	31(3)	31(3)	38(3)	-1(2)	-5(2)	6(2)
C(21)	22(2)	24(2)	42(3)	1(2)	-1(2)	-3(2)
C(22)	32(3)	31(3)	39(3)	2(2)	5(2)	-5(2)
C(24)	56(4)	39(3)	68(4)	-1(3)	-6(3)	-22(3)
C(34)	35(3)	43(3)	43(3)	-13(3)	-21(3)	5(2)
C(35)	37(3)	37(3)	26(3)	-3(2)	-4(2)	6(2)
C(36)	26(2)	25(2)	26(2)	-7(2)	2(2)	4(2)
C(13)	28(3)	28(3)	50(3)	3(2)	2(2)	7(2)
C(15)	31(3)	37(3)	32(3)	1(2)	2(2)	14(2)
C(11)	25(2)	25(2)	33(3)	1(2)	5(2)	8(2)
C(23)	53(3)	40(3)	54(4)	14(3)	5(3)	-12(3)
C(16)	27(3)	29(3)	38(3)	-8(2)	1(2)	5(2)
C(32)	23(2)	28(2)	38(3)	-4(2)	-1(2)	2(2)
C(14)	40(3)	34(3)	39(3)	13(3)	4(2)	15(2)
C(25)	57(4)	42(3)	49(4)	-6(3)	-19(3)	-15(3)
C(33)	25(3)	38(3)	55(4)	-7(3)	-5(3)	-5(2)
C(151)	66(5)	60(4)	51(4)	-8(3)	-22(3)	38(4)
C(361)	37(3)	38(3)	25(3)	7(2)	-3(2)	-1(2)
C(321)	28(3)	48(4)	53(4)	9(3)	5(3)	-8(3)
C(17)	35(3)	38(3)	36(3)	9(2)	10(2)	13(2)
C(261)	66(4)	50(4)	34(3)	-2(3)	-12(3)	-11(3)
C(221)	63(4)	40(4)	37(3)	8(3)	8(3)	-15(3)
C(131)	52(4)	29(3)	107(6)	3(3)	-18(4)	1(3)
C(19)	68(5)	101(6)	43(4)	-19(4)	20(4)	-10(4)
C(18)	30(6)	133(10)	93(8)	-1(6)	15(6)	-9(6)

A2.7 X-ray Crystal Structure of PMo(OMeCy)₃ (4-P).

Crystals grown from a concentrated pentane solution at $-35\text{ }^{\circ}\text{C}$ were coated with Paratone N oil (Exxon) on a microscope slide. A yellow block was selected and mounted with wax on a glass fiber. A total of 8573 reflections ($-11 \leq h \leq 12$, $-12 \leq k \leq 5$, $-76 \leq l \leq 76$) were collected at 293(2) K in the θ range of 2.47 to 23.27 $^{\circ}$, of which 1127 were unique ($R_{\text{int}} = 0.0879$). The radiation used was Mo-K α ($\lambda = 0.71073\text{ \AA}$, $\mu = 0.465\text{ mm}^{-1}$). The structure was solved by direct methods (SHELXTL V5.0, G. M. Sheldrick and Siemens Industrial Automation, Inc., 1995) in conjunction with standard difference Fourier techniques. All non-hydrogen atoms were refined anisotropically. All non-methyl hydrogen atoms were found in the difference map and refined isotropically. All methyl hydrogen atoms were placed in calculated ($d_{\text{CH}} = 0.96\text{ \AA}$) positions. The residual peak and hole electron density were 0.646 and $-0.744\text{ e}\cdot\text{\AA}^{-3}$, respectively. The least squares refinement converged normally with residuals of $R_1 = 0.0357$, $wR_2 = 0.0958$ based upon $I > 2\sigma I$, and GOF = 1.092 (based on F^2). Crystal and refinement data: Formula = C₂₁H₃₉MoO₃P; space group, R-3c; $a = 10.8130(4)\text{ \AA}$; $b = 10.8130(4)\text{ \AA}$; $c = 69.271(3)\text{ \AA}$; $\alpha = 90\text{ }^{\circ}$; $\beta = 90\text{ }^{\circ}$; $\gamma = 120\text{ }^{\circ}$; $V = 7014.2(5)\text{ \AA}^3$; $Z = 12$; $D_{\text{calc}} = 1.325\text{ g}\cdot\text{cm}^{-3}$; $F(000) = 2952$; R_1 (based on F) = 0.0394; wR_2 (based on F_2) = 0.0986.

Table A2.7.1. Atomic coordinates ($\times 10^4$) and equivalent isotropic displacement parameters ($\text{\AA}^2 \times 10^3$) for 4-P. U(eq) is defined as one third of the trace of the orthogonalized U^{ij} tensor.

	x	y	z	U(eq)
Mo(1)	3333	6667	471(1)	26(1)
P(1)	3333	6667	776(1)	44(1)
O(1)	4495(2)	8536(2)	389(1)	29(1)
C(11)	5536(3)	9949(3)	460(1)	32(1)
C(12)	6027(4)	10905(4)	283(1)	39(1)
C(13)	6798(4)	10494(4)	137(1)	43(1)
C(14)	8045(4)	10440(4)	229(1)	48(1)
C(15)	7557(4)	9448(4)	401(1)	42(1)
C(16)	6779(3)	9855(4)	548(1)	36(1)
C(17)	4824(4)	10427(4)	606(1)	47(1)

Table A2.7.2. Bond lengths [\AA] and angles [$^{\circ}$] for 4-P.

Mo(1)–O(1)#1	1.857(2)	C(11)–C(17)	1.514(4)
Mo(1)–O(1)	1.857(2)	C(11)–C(12)	1.517(4)
Mo(1)–O(1)#2	1.857(2)	C(11)–C(16)	1.525(4)
Mo(1)–P(1)	2.1144(16)	C(12)–C(13)	1.511(5)
O(1)–C(11)	1.456(3)	C(13)–C(14)	1.520(5)

C(14)–C(15)	1.510(5)	O(1)–C(11)–C(12)	105.5(2)
C(15)–C(16)	1.517(4)	C(17)–C(11)–C(12)	111.9(3)
O(1)#1–Mo(1)–O(1)	111.10(5)	O(1)–C(11)–C(16)	108.0(2)
O(1)#1–Mo(1)–O(1)#2	111.10(5)	C(17)–C(11)–C(16)	111.7(3)
O(1)–Mo(1)–O(1)#2	111.10(5)	C(12)–C(11)–C(16)	110.4(3)
O(1)#1–Mo(1)–P(1)	107.79(6)	C(13)–C(12)–C(11)	113.3(3)
O(1)–Mo(1)–P(1)	107.79(6)	C(12)–C(13)–C(14)	111.2(3)
O(1)#2–Mo(1)–P(1)	107.79(6)	C(15)–C(14)–C(13)	110.9(3)
C(11)–O(1)–Mo(1)	141.92(16)	C(14)–C(15)–C(16)	111.6(3)
O(1)–C(11)–C(17)	108.9(2)	C(15)–C(16)–C(11)	112.7(3)

Symmetry transformations used to generate equivalent atoms:

#1 $-y + 1, x - y + 1, z$

#2 $-x + y, -x + 1, z$

Table A2.7.3. Anisotropic displacement parameters ($\text{\AA}^2 \times 10^3$) for 4-P. The anisotropic displacement factor exponent takes the form: $-2\pi^2[h^2 a^*^2 U^{11} + \dots + 2 h k a^* b^* U^{12}]$

	U^{11}	U^{22}	U^{33}	U^{23}	U^{13}	U^{12}
Mo(1)	25(1)	25(1)	30(1)	0	0	12(1)
P(1)	49(1)	49(1)	33(1)	0	0	25(1)
O(1)	26(1)	25(1)	35(1)	-1(1)	-3(1)	11(1)
C(11)	27(2)	24(2)	41(2)	-9(1)	-6(1)	11(1)
C(12)	35(2)	23(2)	53(2)	-3(2)	-14(2)	10(2)
C(13)	42(2)	33(2)	38(2)	2(2)	-2(2)	6(2)
C(14)	34(2)	48(2)	51(2)	-7(2)	6(2)	13(2)
C(15)	30(2)	45(2)	54(2)	-6(2)	-7(2)	21(2)
C(16)	36(2)	33(2)	36(2)	-6(2)	-10(1)	15(2)
C(17)	44(2)	37(2)	60(2)	-14(2)	2(2)	21(2)

A2.8 X-ray Crystal Structure of (η^3 -P₃)Mo(OCy)₃(HN[*i*-Pr]Ar) (7-P₃-HN[*i*-Pr]Ar).

Crystals grown from a concentrated diethyl ether solution at $-35\text{ }^\circ\text{C}$ were coated with Paratone N oil (Exxon) on a microscope slide. A yellow prism of approximate dimensions $0.24 \times 0.24 \times 0.16\text{ mm}^3$ was selected and mounted with wax on a glass fiber. A total of 13129 reflections ($-12 \leq h \leq 12$, $-16 \leq k \leq 14$, $-22 \leq l \leq 20$) were collected at 183(2) K in the θ range of 2.28 to 23.28 $^\circ$, of which 4798 were unique ($R_{\text{int}} = 0.0364$). The radiation used was Mo-K α ($\lambda = 0.71073\text{ \AA}$, $\mu = 0.465\text{ mm}^{-1}$). The structure was solved by direct methods (SHELXTL V5.0, G. M. Sheldrick and Siemens Industrial Automation, Inc., 1995) in conjunction with standard difference Fourier techniques. All non-hydrogen atoms were refined anisotropically and the hydrogen atoms were placed in calculated ($d_{\text{CH}} = 0.96\text{ \AA}$) positions. The residual peak and hole electron density were 0.449 and $-0.583\text{ e}\cdot\text{\AA}^{-3}$, respectively. A semi-empirical absorption correction was applied based on pseudo-psi-scans with maximum and minimum transmission equal to 0.3025 and 0.2334, respectively. The least squares refinement converged normally with residuals of $R_1 = 0.0555$, $wR_2 = 0.1022$ based upon $I > 2\sigma I$, and GOF = 1.344 (based on F^2). No significant extinction coefficient was applied to the refinement. Crystal and refinement data: Formula = C₅₈H₉₈Mo₂N₂O₆P₆; space group, $P2_1/n$; $a = 11.087(2)\text{ \AA}$; $b = 15.273(3)\text{ \AA}$; $c = 19.948(4)\text{ \AA}$; $\alpha = 90\text{ }^\circ$; $\beta = 97.973(3)\text{ }^\circ$; $\gamma = 90\text{ }^\circ$; $V = 3345.5(11)\text{ \AA}^3$; $Z = 2$; $D_{\text{calc}} = 1.288\text{ g}\cdot\text{cm}^{-3}$; $F(000) = 1364$; R_1 (based on F) = 0.0604; wR_2 (based on F^2) = 0.1037.

Table A2.8.1. Atomic coordinates ($\times 10^4$) and equivalent isotropic displacement parameters ($\text{\AA}^2 \times 10^3$) for 7-P₃-HN[*i*-Pr]Ar. U(eq) is defined as one third of the trace of the orthogonalized U^{ij} tensor.

	x	y	z	U(eq)
Mo	2068(1)	6579(1)	2291(1)	29(1)
P(3)	2377(1)	7231(1)	3454(1)	42(1)
P(2)	2260(1)	8143(1)	2634(1)	42(1)
P(1)	653(1)	7496(1)	2868(1)	43(1)
O(3)	3782(3)	6524(2)	2358(2)	36(1)
O(2)	1471(3)	5565(2)	2688(2)	35(1)
O(1)	1188(3)	6958(2)	1455(2)	35(1)
N(4)	2371(3)	5401(2)	1486(2)	30(1)
C(31)	4835(4)	6876(4)	2756(2)	43(1)
C(47)	1312(4)	5157(3)	964(2)	34(1)
C(41)	3492(4)	5527(3)	1200(2)	32(1)
C(49)	1622(5)	4417(3)	506(2)	46(1)
C(11)	388(5)	7652(3)	1220(3)	48(1)
C(46)	4522(4)	5046(3)	1450(3)	40(1)
C(21)	979(5)	5346(3)	3287(2)	42(1)
C(42)	3548(5)	6137(3)	694(2)	39(1)

C(43)	4626(5)	6270(4)	431(3)	49(1)
C(48)	217(4)	4904(4)	1300(3)	47(1)
C(22)	-164(6)	4803(5)	3096(3)	69(2)
C(26)	1901(6)	4861(4)	3766(3)	59(2)
C(45)	5612(5)	5187(4)	1200(3)	53(2)
C(32)	5712(5)	7206(4)	2305(3)	48(1)
C(44)	5644(5)	5790(4)	694(3)	59(2)
C(34)	7443(5)	6892(6)	3206(3)	83(2)
C(35)	6551(5)	6542(6)	3659(3)	94(3)
C(451)	6742(5)	4685(5)	1492(4)	87(2)
C(25)	1363(7)	4591(4)	4405(3)	75(2)
C(23)	-698(7)	4550(6)	3734(4)	93(3)
C(16)	734(8)	7998(4)	563(3)	88(2)
C(36)	5406(5)	6179(5)	3235(3)	66(2)
C(33)	6862(5)	7564(5)	2723(3)	71(2)
C(15)	-143(12)	8752(6)	303(4)	146(5)
C(24)	206(8)	4068(4)	4222(3)	87(3)
C(431)	4693(7)	6919(4)	-137(3)	75(2)
C(14)	-1474(12)	8457(8)	265(5)	175(7)
C(13)	-1772(8)	8094(7)	901(5)	134(4)
C(12)	-913(5)	7343(5)	1144(4)	81(2)

Table A2.8.2. Bond lengths [\AA] and angles [$^\circ$] for 7-P₃-HN[*i*-Pr]Ar.

Mo-O(3)	1.888(3)	C(41)-C(42)	1.382(6)
Mo-O(2)	1.900(3)	C(41)-C(46)	1.390(6)
Mo-O(1)	1.903(3)	C(11)-C(12)	1.506(8)
Mo-N(4)	2.467(3)	C(11)-C(16)	1.511(8)
Mo-P(2)	2.4868(14)	C(46)-C(45)	1.387(7)
Mo-P(1)	2.5002(14)	C(21)-C(26)	1.496(7)
Mo-P(3)	2.5028(14)	C(21)-C(22)	1.518(7)
P(3)-P(1)	2.136(2)	C(42)-C(43)	1.385(7)
P(3)-P(2)	2.138(2)	C(43)-C(44)	1.386(8)
P(2)-P(1)	2.145(2)	C(43)-C(431)	1.516(8)
O(3)-C(31)	1.424(5)	C(22)-C(23)	1.526(8)
O(2)-C(21)	1.421(5)	C(26)-C(25)	1.537(7)
O(1)-C(11)	1.420(5)	C(45)-C(44)	1.371(8)
N(4)-C(41)	1.450(5)	C(45)-C(451)	1.515(8)
N(4)-C(47)	1.504(5)	C(32)-C(33)	1.526(7)
C(31)-C(32)	1.500(7)	C(34)-C(33)	1.492(9)
C(31)-C(36)	1.510(8)	C(34)-C(35)	1.526(9)
C(47)-C(48)	1.516(6)	C(35)-C(36)	1.529(8)
C(47)-C(49)	1.522(6)	C(25)-C(24)	1.513(9)

C(23)-C(24)	1.491(10)	C(47)-N(4)-Mo	117.9(2)
C(16)-C(15)	1.550(9)	O(3)-C(31)-C(32)	109.9(4)
C(15)-C(14)	1.53(2)	O(3)-C(31)-C(36)	109.0(4)
C(14)-C(13)	1.46(2)	C(32)-C(31)-C(36)	111.5(4)
C(13)-C(12)	1.525(9)	N(4)-C(47)-C(48)	110.7(4)
		N(4)-C(47)-C(49)	112.3(4)
O(3)-Mo-O(2)	109.91(14)	C(48)-C(47)-C(49)	109.7(4)
O(3)-Mo-O(1)	117.62(13)	C(42)-C(41)-C(46)	120.1(4)
O(2)-Mo-O(1)	116.56(13)	C(42)-C(41)-N(4)	120.3(4)
O(3)-Mo-N(4)	77.68(12)	C(46)-C(41)-N(4)	119.6(4)
O(2)-Mo-N(4)	76.30(12)	O(1)-C(11)-C(12)	110.2(5)
O(1)-Mo-N(4)	75.54(12)	O(1)-C(11)-C(16)	109.0(4)
O(3)-Mo-P(2)	88.64(10)	C(12)-C(11)-C(16)	112.1(5)
O(2)-Mo-P(2)	133.67(9)	C(45)-C(46)-C(41)	120.1(5)
O(1)-Mo-P(2)	87.87(10)	O(2)-C(21)-C(26)	110.2(4)
N(4)-Mo-P(2)	150.02(9)	O(2)-C(21)-C(22)	108.8(4)
O(3)-Mo-P(1)	133.03(10)	C(26)-C(21)-C(22)	111.2(5)
O(2)-Mo-P(1)	89.31(10)	C(41)-C(42)-C(43)	120.2(5)
O(1)-Mo-P(1)	87.41(10)	C(42)-C(43)-C(44)	118.7(5)
N(4)-Mo-P(1)	149.28(9)	C(42)-C(43)-C(431)	120.9(5)
P(2)-Mo-P(1)	50.96(5)	C(44)-C(43)-C(431)	120.4(5)
O(3)-Mo-P(3)	86.89(10)	C(21)-C(22)-C(23)	109.6(5)
O(2)-Mo-P(3)	87.12(9)	C(21)-C(26)-C(25)	110.7(5)
O(1)-Mo-P(3)	132.76(10)	C(44)-C(45)-C(46)	118.8(5)
N(4)-Mo-P(3)	151.69(9)	C(44)-C(45)-C(451)	121.3(5)
P(2)-Mo-P(3)	50.75(4)	C(46)-C(45)-C(451)	119.9(6)
P(1)-Mo-P(3)	50.55(5)	C(31)-C(32)-C(33)	110.7(4)
P(1)-P(3)-P(2)	60.25(6)	C(45)-C(44)-C(43)	122.1(5)
P(1)-P(3)-Mo	64.66(5)	C(33)-C(34)-C(35)	111.5(6)
P(2)-P(3)-Mo	64.24(5)	C(34)-C(35)-C(36)	110.8(5)
P(3)-P(2)-P(1)	59.83(6)	C(24)-C(25)-C(26)	110.8(5)
P(3)-P(2)-Mo	65.01(5)	C(24)-C(23)-C(22)	111.5(6)
P(1)-P(2)-Mo	64.84(5)	C(11)-C(16)-C(15)	109.1(6)
P(3)-P(1)-P(2)	59.92(6)	C(31)-C(36)-C(35)	109.7(6)
P(3)-P(1)-Mo	64.79(5)	C(34)-C(33)-C(32)	111.1(5)
P(2)-P(1)-Mo	64.20(5)	C(14)-C(15)-C(16)	110.7(9)
C(31)-O(3)-Mo	139.6(3)	C(23)-C(24)-C(25)	111.6(5)
C(21)-O(2)-Mo	137.6(3)	C(13)-C(14)-C(15)	113.6(7)
C(11)-O(1)-Mo	137.5(3)	C(14)-C(13)-C(12)	110.7(7)
C(41)-N(4)-C(47)	113.0(3)	C(11)-C(12)-C(13)	110.1(7)
C(41)-N(4)-Mo	111.1(3)		

Table A2.8.3. Anisotropic displacement parameters [$\text{\AA}^2 \times 10^3$] for 7-P₃-HN[*i*-Pr]Ar. The anisotropic displacement factor exponent takes the form: $-2\pi^2[h^2 a^{*2}U^{11} + \dots + 2 h k a^* b^* U^{12}]$

	U ¹¹	U ²²	U ³³	U ²³	U ¹³	U ¹²
Mo	28(1)	30(1)	27(1)	-2(1)	4(1)	-1(1)
P(3)	54(1)	42(1)	31(1)	-6(1)	4(1)	-4(1)
P(2)	53(1)	33(1)	39(1)	-5(1)	8(1)	-4(1)
P(1)	43(1)	44(1)	45(1)	-11(1)	13(1)	1(1)
O(3)	27(2)	45(2)	36(2)	-7(2)	1(1)	-2(2)
O(2)	39(2)	35(2)	32(2)	-2(1)	11(1)	-8(2)
O(1)	36(2)	35(2)	33(2)	-3(1)	1(1)	7(1)
N(4)	28(2)	34(2)	26(2)	3(2)	0(2)	3(2)
C(31)	31(3)	60(3)	38(3)	-12(2)	-1(2)	-9(2)
C(47)	32(2)	38(3)	31(2)	-4(2)	0(2)	3(2)
C(41)	32(2)	33(3)	33(3)	-7(2)	8(2)	-2(2)
C(49)	48(3)	45(3)	42(3)	-9(2)	0(2)	0(2)
C(11)	54(3)	49(3)	38(3)	-5(2)	-5(2)	26(3)
C(46)	34(3)	34(3)	51(3)	-4(2)	5(2)	3(2)
C(21)	55(3)	36(3)	38(3)	-6(2)	23(2)	-8(2)
C(42)	49(3)	36(3)	35(3)	-1(2)	12(2)	-3(2)
C(43)	57(4)	47(3)	47(3)	-15(3)	24(3)	-13(3)
C(48)	36(3)	60(4)	44(3)	-11(3)	2(2)	-8(3)
C(22)	63(4)	84(5)	64(4)	8(3)	21(3)	-23(3)
C(26)	75(4)	69(4)	36(3)	4(3)	17(3)	3(3)
C(45)	34(3)	49(3)	77(4)	-24(3)	14(3)	2(3)
C(32)	44(3)	51(3)	48(3)	-3(3)	3(2)	-13(3)
C(44)	47(3)	62(4)	74(4)	-28(3)	36(3)	-20(3)
C(34)	38(3)	146(7)	63(4)	-15(5)	-3(3)	-16(4)
C(35)	45(4)	173(8)	57(4)	15(5)	-15(3)	-8(5)
C(451)	35(3)	92(5)	134(7)	-18(5)	11(4)	15(3)
C(25)	118(6)	70(5)	42(3)	5(3)	30(4)	9(4)
C(23)	89(5)	112(6)	86(5)	9(5)	40(5)	-46(5)
C(16)	140(7)	69(4)	56(4)	18(3)	13(4)	58(5)
C(36)	41(3)	103(5)	50(3)	17(3)	-4(3)	-7(3)
C(33)	51(4)	93(5)	71(4)	-22(4)	12(3)	-28(4)
C(15)	277(14)	107(7)	57(5)	29(5)	35(7)	122(9)
C(24)	161(8)	48(4)	65(4)	-5(3)	62(5)	-27(5)
C(431)	106(5)	68(4)	59(4)	-7(3)	42(4)	-30(4)
C(14)	209(13)	207(13)	82(7)	-34(7)	-72(8)	164(11)
C(13)	101(6)	154(9)	126(8)	-61(7)	-59(6)	86(6)
C(12)	50(4)	95(5)	90(5)	-38(4)	-16(3)	35(4)

A2.9 X-ray Crystal Structure of Mo₂(OCy)₃(N[*i*-Pr]Ar)₃.

Crystals grown from a concentrated pentane solution at $-35\text{ }^{\circ}\text{C}$ were coated with Paratone N oil (Exxon) on a microscope slide. A yellow prism was selected and mounted with wax on a glass fiber. A total of 15119 reflections ($-14 \leq h \leq 15$, $-14 \leq k \leq 17$, $-18 \leq l \leq 18$) were collected at 183(2) K in the θ range of 1.28 to 24.00 $^{\circ}$, of which 9618 were unique ($R_{\text{int}} = 0.0335$). The radiation used was Mo-K α ($\lambda = 0.71073\text{ \AA}$, $\mu = 0.465\text{ mm}^{-1}$). The structure was solved by direct methods (SHELXTL V5.0, G. M. Sheldrick and Siemens Industrial Automation, Inc., 1995) in conjunction with standard difference Fourier techniques. All non-hydrogen atoms were refined anisotropically and the hydrogen atoms were placed in calculated ($d_{\text{CH}} = 0.96\text{ \AA}$) positions. The residual peak and hole electron density were 1.441 and $-0.834\text{ e}\cdot\text{\AA}^{-3}$, respectively. An empirical absorption correction was applied based on pseudo-psi-scans with maximum and minimum transmission equal to 0.4858 and 0.3432, respectively. The least squares refinement converged normally with residuals of $R_1 = 0.0405$, $wR_2 = 0.1171$ based upon $I > 2\sigma I$, and GOF = 1.039 (based on F^2). No significant extinction coefficient was applied to the refinement. Crystal and refinement data: Formula = C₅₆H₉₃Mo₂N₃O₃; space group, $P\bar{1}$; $a = 13.2354(14)\text{ \AA}$; $b = 15.5273(16)\text{ \AA}$; $c = 16.2423(17)\text{ \AA}$; $\alpha = 90.147(2)\text{ }^{\circ}$; $\beta = 100.121(2)\text{ }^{\circ}$; $\gamma = 109.650(2)\text{ }^{\circ}$; $V = 3087.8(6)\text{ \AA}^3$; $Z = 2$; $D_{\text{calc}} = 1.127\text{ g}\cdot\text{cm}^{-3}$; $F(000) = 1116$; R_1 (based on F) = 0.0450; wR_2 (based on F^2) = 0.1209.

Table A2.9.1. Atomic coordinates ($\times 10^4$) and equivalent isotropic displacement parameters ($\text{\AA}^2 \times 10^3$) for Mo₂(OCy)₃(N[*i*-Pr]Ar)₃. U(eq) is defined as one third of the trace of the orthogonalized U^{ij} tensor.

	x	y	z	U(eq)
Mo(1)	6731(1)	7745(1)	7530(1)	34(1)
N(1)	5337(2)	6819(2)	7722(2)	41(1)
N(2)	6634(2)	8147(2)	6394(2)	38(1)
Mo(2)	7812(1)	6913(1)	7509(1)	35(1)
O(3)	7638(2)	8645(2)	8411(2)	59(1)
N(4)	7917(2)	6482(2)	8633(2)	41(1)
O(5)	7028(2)	5995(2)	6609(1)	45(1)
O(6)	9145(2)	7729(1)	7288(1)	44(1)
C(11)	4492(3)	7198(2)	7702(2)	43(1)
C(12)	4766(3)	8074(2)	8074(2)	48(1)
C(13)	4020(3)	8533(3)	8028(2)	55(1)
C(14)	2948(3)	8071(3)	7646(2)	60(1)
C(15)	2627(3)	7184(3)	7296(2)	57(1)
C(16)	3397(3)	6761(3)	7308(2)	52(1)
C(17)	5051(3)	5808(2)	7743(2)	49(1)
C(18)	4372(3)	5410(3)	8410(3)	69(1)

C(19)	4552(3)	5279(3)	6882(3)	66(1)
C(21)	5983(3)	8734(2)	6286(2)	41(1)
C(22)	6465(3)	9662(2)	6548(2)	49(1)
C(23)	5864(3)	10247(2)	6481(2)	57(1)
C(24)	4762(3)	9891(3)	6127(2)	59(1)
C(25)	4250(3)	8973(3)	5851(2)	52(1)
C(26)	4867(3)	8398(2)	5939(2)	44(1)
C(27)	6994(3)	7904(2)	5635(2)	45(1)
C(28)	6080(3)	7158(3)	5062(2)	61(1)
C(29)	7484(3)	8750(3)	5168(2)	60(1)
C(31)	7636(4)	9463(3)	8677(3)	67(1)
C(32)	8705(3)	10242(2)	8602(3)	66(1)
C(33)	8585(5)	11114(4)	8865(3)	89(2)
C(34)	8452(5)	11121(4)	9767(3)	101(2)
C(35)	7512(5)	10338(5)	9911(3)	108(2)
C(36)	7568(5)	9442(3)	9633(3)	103(2)
C(41)	8609(3)	5927(2)	8713(2)	42(1)
C(42)	8147(3)	4973(2)	8565(2)	53(1)
C(43)	8803(4)	4433(3)	8618(2)	62(1)
C(44)	9930(4)	4860(3)	8827(2)	67(1)
C(45)	10415(3)	5806(3)	8968(2)	56(1)
C(46)	9744(3)	6331(2)	8909(2)	47(1)
C(47)	7548(3)	6663(2)	9406(2)	51(1)
C(48)	8476(4)	7329(3)	10017(3)	79(1)
C(49)	7008(4)	5786(3)	9815(3)	70(1)
C(51)	7560(3)	5386(2)	6380(2)	55(1)
C(52)	6796(4)	4462(3)	6211(4)	85(1)
C(53)	7341(5)	3794(3)	5939(4)	103(2)
C(54)	7891(5)	4142(3)	5188(3)	96(2)
C(55)	8667(5)	5075(4)	5379(4)	109(2)
C(56)	8102(5)	5736(3)	5636(4)	92(2)
C(61)	9647(3)	8663(2)	7121(2)	43(1)
C(62)	10141(3)	8691(2)	6341(2)	49(1)
C(63)	10752(3)	9677(3)	6166(2)	62(1)
C(64)	11621(3)	10170(3)	6912(3)	69(1)
C(65)	11139(3)	10143(3)	7695(3)	67(1)
C(66)	10508(3)	9150(2)	7869(2)	51(1)
C(71)	4447(9)	7951(8)	10321(6)	196(4)
C(72)	4884(14)	7284(8)	10393(7)	225(7)
C(73)	5744(14)	7534(13)	11473(17)	343(14)
C(74)	5024(13)	7339(14)	11769(12)	295(10)
C(75)	5710(8)	7480(6)	12790(5)	180(4)
C(131)	4370(4)	9502(3)	8404(3)	75(1)
C(151)	1446(3)	6672(3)	6897(3)	76(1)
C(231)	6387(4)	11245(3)	6794(3)	84(1)
C(251)	3051(3)	8607(3)	5479(3)	70(1)

C(431)	8307(5)	3408(3)	8446(4)	96(2)
C(451)	11637(4)	6246(4)	9193(3)	79(1)

Table A2.9.2. Bond lengths [Å] and angles [°] for Mo₂(OCy)₃(N[*i*-Pr]Ar)₃.

Mo(1)-O(3)	1.923(2)	C(33)-C(34)	1.506(7)
Mo(1)-N(2)	1.946(2)	C(34)-C(35)	1.471(8)
Mo(1)-N(1)	1.998(3)	C(35)-C(36)	1.492(7)
Mo(1)-Mo(2)	2.2315(4)	C(41)-C(46)	1.396(5)
N(1)-C(11)	1.424(4)	C(41)-C(42)	1.401(5)
N(1)-C(17)	1.487(4)	C(42)-C(43)	1.389(5)
N(2)-C(21)	1.442(4)	C(43)-C(44)	1.391(6)
N(2)-C(27)	1.488(4)	C(43)-C(431)	1.508(6)
Mo(2)-O(6)	1.888(2)	C(44)-C(45)	1.391(6)
Mo(2)-O(5)	1.925(2)	C(45)-C(46)	1.385(5)
Mo(2)-N(4)	1.943(2)	C(45)-C(451)	1.505(6)
O(3)-C(31)	1.342(4)	C(47)-C(48)	1.509(6)
N(4)-C(41)	1.445(4)	C(47)-C(49)	1.524(5)
N(4)-C(47)	1.483(4)	C(51)-C(52)	1.442(6)
O(5)-C(51)	1.438(4)	C(51)-C(56)	1.521(6)
O(6)-C(61)	1.427(4)	C(52)-C(53)	1.550(6)
C(11)-C(12)	1.392(5)	C(53)-C(54)	1.537(7)
C(11)-C(16)	1.408(5)	C(54)-C(55)	1.462(8)
C(12)-C(13)	1.390(5)	C(55)-C(56)	1.553(6)
C(13)-C(14)	1.385(5)	C(61)-C(66)	1.508(5)
C(13)-C(131)	1.511(5)	C(61)-C(62)	1.519(4)
C(14)-C(15)	1.384(6)	C(62)-C(63)	1.527(5)
C(15)-C(16)	1.383(5)	C(63)-C(64)	1.513(6)
C(15)-C(151)	1.517(5)	C(64)-C(65)	1.514(6)
C(17)-C(18)	1.529(5)	C(65)-C(66)	1.541(5)
C(17)-C(19)	1.540(5)	C(71)-C(72)	1.342(12)
C(21)-C(22)	1.396(5)	C(72)-C(73)	1.88(2)
C(21)-C(26)	1.399(5)	C(73)-C(74)	1.095(19)
C(22)-C(23)	1.388(5)	C(74)-C(75)	1.72(2)
C(23)-C(24)	1.388(6)		
C(23)-C(231)	1.513(5)	O(3)-Mo(1)-N(2)	116.83(10)
C(24)-C(25)	1.390(6)	O(3)-Mo(1)-N(1)	120.13(11)
C(25)-C(26)	1.391(5)	N(2)-Mo(1)-N(1)	112.82(11)
C(25)-C(251)	1.503(5)	O(3)-Mo(1)-Mo(2)	98.52(8)
C(27)-C(28)	1.525(5)	N(2)-Mo(1)-Mo(2)	100.99(7)
C(27)-C(29)	1.525(5)	N(1)-Mo(1)-Mo(2)	102.83(7)
C(31)-C(32)	1.546(6)	C(11)-N(1)-C(17)	118.6(2)
C(31)-C(36)	1.571(6)	C(11)-N(1)-Mo(1)	112.4(2)
C(32)-C(33)	1.484(6)	C(17)-N(1)-Mo(1)	128.30(19)

C(21)-N(2)-C(27)	116.7(2)	C(28)-C(27)-C(29)	111.9(3)
C(21)-N(2)-Mo(1)	109.68(18)	O(3)-C(31)-C(32)	111.8(3)
C(27)-N(2)-Mo(1)	133.34(19)	O(3)-C(31)-C(36)	108.5(4)
O(6)-Mo(2)-O(5)	113.19(10)	C(32)-C(31)-C(36)	106.6(4)
O(6)-Mo(2)-N(4)	113.84(10)	C(33)-C(32)-C(31)	107.0(4)
O(5)-Mo(2)-N(4)	116.25(10)	C(32)-C(33)-C(34)	110.9(4)
O(6)-Mo(2)-Mo(1)	105.89(6)	C(35)-C(34)-C(33)	111.6(5)
O(5)-Mo(2)-Mo(1)	103.42(6)	C(34)-C(35)-C(36)	112.5(4)
N(4)-Mo(2)-Mo(1)	102.41(7)	C(35)-C(36)-C(31)	108.0(4)
C(31)-O(3)-Mo(1)	133.7(3)	C(46)-C(41)-C(42)	119.0(3)
C(41)-N(4)-C(47)	116.0(2)	C(46)-C(41)-N(4)	120.8(3)
C(41)-N(4)-Mo(2)	108.60(18)	C(42)-C(41)-N(4)	120.1(3)
C(47)-N(4)-Mo(2)	135.1(2)	C(43)-C(42)-C(41)	120.8(4)
C(51)-O(5)-Mo(2)	117.5(2)	C(44)-C(43)-C(42)	118.5(4)
C(61)-O(6)-Mo(2)	140.92(18)	C(44)-C(43)-C(431)	120.7(4)
C(12)-C(11)-C(16)	117.1(3)	C(42)-C(43)-C(431)	120.8(4)
C(12)-C(11)-N(1)	118.2(3)	C(43)-C(44)-C(45)	122.1(3)
C(16)-C(11)-N(1)	124.7(3)	C(46)-C(45)-C(44)	118.3(4)
C(13)-C(12)-C(11)	122.5(3)	C(46)-C(45)-C(451)	120.9(4)
C(14)-C(13)-C(12)	118.3(3)	C(44)-C(45)-C(451)	120.8(3)
C(14)-C(13)-C(131)	121.1(3)	C(45)-C(46)-C(41)	121.3(3)
C(12)-C(13)-C(131)	120.6(3)	N(4)-C(47)-C(48)	111.0(3)
C(13)-C(14)-C(15)	121.2(3)	N(4)-C(47)-C(49)	112.5(3)
C(14)-C(15)-C(16)	119.5(3)	C(48)-C(47)-C(49)	111.2(3)
C(14)-C(15)-C(151)	121.0(3)	O(5)-C(51)-C(52)	110.7(3)
C(16)-C(15)-C(151)	119.5(4)	O(5)-C(51)-C(56)	109.5(3)
C(15)-C(16)-C(11)	121.3(3)	C(52)-C(51)-C(56)	112.1(4)
N(1)-C(17)-C(18)	112.7(3)	C(51)-C(52)-C(53)	111.8(4)
N(1)-C(17)-C(19)	114.4(3)	C(54)-C(53)-C(52)	110.5(4)
C(18)-C(17)-C(19)	112.3(3)	C(55)-C(54)-C(53)	110.7(4)
C(22)-C(21)-C(26)	118.4(3)	C(54)-C(55)-C(56)	111.2(5)
C(22)-C(21)-N(2)	119.6(3)	C(51)-C(56)-C(55)	109.9(4)
C(26)-C(21)-N(2)	122.0(3)	O(6)-C(61)-C(66)	109.2(3)
C(23)-C(22)-C(21)	121.7(3)	O(6)-C(61)-C(62)	108.7(3)
C(24)-C(23)-C(22)	118.3(3)	C(66)-C(61)-C(62)	111.1(3)
C(24)-C(23)-C(231)	120.6(3)	C(61)-C(62)-C(63)	110.9(3)
C(22)-C(23)-C(231)	121.2(4)	C(64)-C(63)-C(62)	111.3(3)
C(23)-C(24)-C(25)	122.0(3)	C(63)-C(64)-C(65)	111.3(3)
C(24)-C(25)-C(26)	118.5(3)	C(64)-C(65)-C(66)	111.1(3)
C(24)-C(25)-C(251)	120.7(3)	C(61)-C(66)-C(65)	111.3(3)
C(26)-C(25)-C(251)	120.8(3)	C(71)-C(72)-C(73)	103.4(10)
C(25)-C(26)-C(21)	121.1(3)	C(74)-C(73)-C(72)	92(2)
N(2)-C(27)-C(28)	112.0(3)	C(73)-C(74)-C(75)	97(2)
N(2)-C(27)-C(29)	111.4(3)		

Table A2.9.3. Anisotropic displacement parameters ($\text{\AA}^2 \times 10^3$) for $\text{Mo}_2(\text{OCy})_3(\text{N}[i\text{-Pr]Ar})_3$. The anisotropic displacement factor exponent takes the form: $-2\pi^2[h^2 a^{*2}U^{11} + \dots + 2 h k a^* b^* U^{12}]$

	U11	U22	U33	U23	U13	U12
Mo(1)	35(1)	32(1)	40(1)	9(1)	13(1)	16(1)
N(1)	39(1)	42(2)	49(2)	11(1)	19(1)	18(1)
N(2)	38(1)	39(1)	43(1)	11(1)	13(1)	17(1)
Mo(2)	36(1)	34(1)	44(1)	12(1)	15(1)	17(1)
O(3)	76(2)	40(1)	49(1)	3(1)	8(1)	7(1)
N(4)	47(2)	39(1)	45(1)	14(1)	17(1)	22(1)
O(5)	47(1)	45(1)	52(1)	6(1)	17(1)	22(1)
O(6)	40(1)	40(1)	62(1)	18(1)	21(1)	20(1)
C(11)	40(2)	49(2)	50(2)	15(2)	22(1)	20(2)
C(12)	44(2)	56(2)	51(2)	7(2)	19(2)	20(2)
C(13)	55(2)	62(2)	59(2)	8(2)	25(2)	30(2)
C(14)	54(2)	72(3)	71(2)	13(2)	25(2)	38(2)
C(15)	40(2)	71(3)	64(2)	14(2)	18(2)	23(2)
C(16)	46(2)	55(2)	60(2)	9(2)	18(2)	20(2)
C(17)	43(2)	39(2)	70(2)	14(2)	18(2)	15(2)
C(18)	61(2)	62(2)	92(3)	32(2)	37(2)	21(2)
C(19)	53(2)	51(2)	98(3)	-5(2)	24(2)	18(2)
C(21)	49(2)	41(2)	38(2)	14(1)	14(1)	21(2)
C(22)	51(2)	44(2)	51(2)	9(2)	10(2)	17(2)
C(23)	78(3)	45(2)	57(2)	12(2)	15(2)	33(2)
C(24)	74(3)	64(2)	56(2)	11(2)	14(2)	46(2)
C(25)	57(2)	66(2)	47(2)	10(2)	10(2)	36(2)
C(26)	42(2)	51(2)	45(2)	7(2)	8(1)	23(2)
C(27)	47(2)	56(2)	43(2)	15(2)	17(1)	27(2)
C(28)	66(2)	72(3)	51(2)	-3(2)	13(2)	31(2)
C(29)	62(2)	73(3)	59(2)	30(2)	28(2)	35(2)
C(31)	73(3)	71(3)	65(2)	3(2)	19(2)	34(2)
C(32)	71(3)	46(2)	75(3)	-5(2)	26(2)	5(2)
C(33)	106(4)	89(3)	83(3)	-4(3)	3(3)	54(3)
C(34)	136(5)	88(4)	96(4)	-18(3)	16(3)	66(4)
C(35)	84(4)	188(7)	64(3)	-42(4)	5(3)	64(4)
C(36)	135(5)	74(3)	84(3)	-10(3)	64(3)	-5(3)
C(41)	56(2)	44(2)	39(2)	16(1)	15(1)	28(2)
C(42)	70(2)	42(2)	55(2)	15(2)	22(2)	25(2)
C(43)	98(3)	47(2)	61(2)	20(2)	32(2)	42(2)
C(44)	97(3)	78(3)	63(2)	27(2)	34(2)	66(3)
C(45)	66(2)	73(3)	49(2)	20(2)	20(2)	46(2)
C(46)	56(2)	49(2)	46(2)	11(2)	14(2)	28(2)
C(47)	62(2)	58(2)	50(2)	18(2)	25(2)	35(2)

C(48)	82(3)	93(3)	68(3)	-17(2)	15(2)	39(3)
C(49)	89(3)	79(3)	66(2)	39(2)	40(2)	48(2)
C(51)	73(2)	55(2)	52(2)	1(2)	15(2)	38(2)
C(52)	80(3)	61(3)	119(4)	-1(3)	39(3)	20(2)
C(53)	132(5)	57(3)	136(5)	-1(3)	64(4)	33(3)
C(54)	155(5)	81(3)	74(3)	-11(3)	34(3)	65(4)
C(55)	129(5)	95(4)	137(5)	6(4)	81(4)	53(4)
C(56)	114(4)	70(3)	117(4)	14(3)	71(3)	38(3)
C(61)	38(2)	40(2)	58(2)	18(2)	20(1)	17(1)
C(62)	44(2)	51(2)	54(2)	14(2)	16(2)	15(2)
C(63)	56(2)	67(2)	63(2)	26(2)	24(2)	16(2)
C(64)	55(2)	59(2)	84(3)	22(2)	23(2)	1(2)
C(65)	63(2)	54(2)	74(3)	3(2)	8(2)	11(2)
C(66)	52(2)	54(2)	52(2)	12(2)	18(2)	22(2)
C(71)	192(10)	219(12)	167(9)	23(9)	83(7)	31(9)
C(72)	380(20)	178(11)	194(10)	59(9)	131(12)	160(13)
C(73)	194(17)	320(20)	590(40)	190(20)	100(20)	164(16)
C(74)	190(15)	420(30)	340(20)	35(18)	116(16)	152(17)
C(75)	201(10)	155(8)	152(7)	36(6)	-9(7)	42(7)
C(131)	75(3)	72(3)	95(3)	-6(2)	28(2)	40(2)
C(151)	47(2)	90(3)	95(3)	7(3)	11(2)	29(2)
C(231)	107(4)	47(2)	103(3)	6(2)	16(3)	37(2)
C(251)	58(2)	99(3)	66(2)	9(2)	3(2)	48(2)
C(431)	147(5)	50(3)	114(4)	19(3)	49(4)	50(3)
C(451)	67(3)	118(4)	75(3)	18(3)	14(2)	60(3)

A2.10 X-ray Crystal Structure of $(\mu\text{-}\eta^{4:4}\text{-P}_4)[\text{U}(\text{N}[\textit{t}\text{-Bu}]\text{Ar})_3]_2$ ($\mathbf{8}_2\text{-P}_4$).

Crystals grown from a concentrated pentane solution at $-35\text{ }^\circ\text{C}$ were coated with Paratone N oil (Exxon) on a microscope slide. An orange prism was selected and mounted with wax on a glass fiber. A total of 8224 reflections ($-10 \leq h \leq 13$, $-15 \leq k \leq 13$, $-15 \leq l \leq 15$) were collected at 183(2) K in the θ range of 2.12 to 23.27°, of which 5642 were unique ($R_{\text{int}} = 0.0368$). The radiation used was Mo-K α ($\lambda = 0.71073\text{ \AA}$, $\mu = 0.465\text{ mm}^{-1}$). The structure was solved by direct methods (SHELXTL V5.0, G. M. Sheldrick and Siemens Industrial Automation, Inc., 1995) in conjunction with standard difference Fourier techniques. All non-hydrogen atoms were refined anisotropically and the hydrogen atoms were placed in calculated ($d_{\text{CH}} = 0.96\text{ \AA}$) positions. The residual peak and hole electron density were 1.441 and $-0.834\text{ e}\cdot\text{\AA}^{-3}$, respectively. A semi-empirical absorption correction was applied based on pseudo-psi-scans with maximum and minimum transmission equal to 0.6887 and 0.3767, respectively. The least squares refinement converged normally with residuals of $R_1 = 0.0336$, $wR_2 = 0.0802$ based upon $I > 2\sigma I$, and GOF = 1.035 (based on F^2). No significant extinction coefficient was applied to the refinement. Crystal and refinement data: Formula = $\text{C}_{78}\text{H}_{122}\text{N}_6\text{P}_4\text{U}_2$; space group, $P\bar{4}$; $a = 11.9018(6)\text{ \AA}$; $b = 13.8947(8)\text{ \AA}$; $c = 13.9991(8)\text{ \AA}$; $\alpha = 77.7170(10)^\circ$; $\beta = 69.9770(10)^\circ$; $\gamma = 67.3510(10)^\circ$; $V = 1998.6(2)\text{ \AA}^3$; $Z = 1$; $D_{\text{calc}} = 1.449\text{ g}\cdot\text{cm}^{-3}$; $F(000) = 876$; R_1 (based on F) = 0.0426; wR_2 (based on F^2) = 0.0843.

Table A2.10.1. Atomic coordinates [$\times 10^4$] and equivalent isotropic displacement parameters [$\text{\AA}^2 \times 10^3$] for $\mathbf{8}_2\text{-P}_4$.

	x	y	z	U(eq)
U	4670(1)	8625(1)	1695(1)	32(1)
N(2)	6623(4)	7636(4)	1806(4)	35(1)
N(3)	3456(4)	7834(4)	1490(4)	35(1)
N(1)	3743(5)	9165(5)	3264(4)	52(2)
C(27)	7616(6)	7869(5)	2058(5)	40(2)
C(36)	1460(6)	9285(5)	1461(5)	38(1)
C(26)	6717(6)	5802(5)	2191(6)	47(2)
C(31)	2143(6)	8382(5)	1960(5)	38(1)
C(37)	3629(6)	6990(5)	867(5)	43(2)
C(13)	1480(7)	11853(7)	2863(5)	59(2)
C(23)	8207(6)	5366(5)	198(5)	46(2)
C(22)	7782(6)	6373(5)	505(5)	40(2)
C(35)	180(6)	9832(5)	1906(5)	42(2)
C(251)	6732(8)	3945(6)	2673(7)	70(2)
C(25)	7134(7)	4790(5)	1905(6)	51(2)
C(33)	220(6)	8560(5)	3385(5)	43(2)
C(210)	6964(6)	8890(5)	2567(6)	50(2)
C(21)	7066(5)	6596(4)	1491(5)	37(1)
C(32)	1486(6)	8036(5)	2919(5)	44(2)

C(16)	3877(7)	10922(6)	3122(5)	53(2)
C(351)	-552(6)	10778(6)	1324(6)	61(2)
C(15)	3401(7)	12003(6)	2936(5)	56(2)
C(34)	-415(6)	9474(5)	2865(5)	43(2)
C(24)	7873(6)	4590(5)	929(6)	49(2)
C(12)	1965(7)	10770(7)	3044(5)	56(2)
C(29)	8682(6)	8006(6)	1100(6)	52(2)
C(331)	-466(7)	8165(6)	4426(5)	63(2)
C(310)	5023(6)	6603(5)	242(5)	48(2)
C(17)	3524(7)	8657(6)	4344(6)	58(2)
C(11)	3179(7)	10286(6)	3164(5)	51(2)
C(39)	2836(7)	7404(6)	130(7)	65(2)
C(38)	3297(8)	6079(6)	1569(6)	68(2)
C(231)	8963(7)	5136(6)	-890(6)	58(2)
C(19)	2106(8)	8855(7)	4881(6)	77(3)
C(18)	4045(8)	9064(7)	4974(6)	66(2)
C(14)	2203(8)	12448(7)	2815(5)	63(2)
C(28)	8200(7)	7011(6)	2803(6)	57(2)
C(151)	4209(8)	12645(7)	2854(8)	80(3)
C(131)	158(8)	12390(8)	2704(7)	90(3)
C(110)	4255(9)	7476(7)	4264(7)	84(3)
C(3S)	399(16)	5097(12)	5254(13)	149(6)
C(1S)	2470(24)	5221(14)	4944(15)	222(11)
P(1)	6345(2)	9257(1)	-465(1)	41(1)
P(2)	5528(2)	10492(1)	540(1)	41(1)
C(2S)	1592(19)	4996(13)	4592(16)	174(7)

Table A2.10.2. Bond lengths [Å] and angles [°] for 8₂-P₄.

U-N(2)	2.238(5)	N(3)-C(37)	1.519(8)
U-N(3)	2.240(5)	N(1)-C(11)	1.436(9)
U-N(1)	2.238(5)	N(1)-C(17)	1.507(9)
U-C(11)	3.011(7)	C(27)-C(28)	1.524(9)
U-C(31)	3.044(6)	C(27)-C(210)	1.525(9)
U-P(2)	3.084(2)	C(27)-C(29)	1.534(9)
U-P(1)#1	3.101(2)	C(36)-C(35)	1.395(9)
U-P(1)	3.158(2)	C(36)-C(31)	1.397(9)
U-P(2)#1	3.162(2)	C(26)-C(25)	1.396(10)
N(2)-C(21)	1.445(7)	C(26)-C(21)	1.401(9)
N(2)-C(27)	1.502(8)	C(31)-C(32)	1.393(9)
N(3)-C(31)	1.431(8)	C(37)-C(39)	1.511(10)

C(37)-C(38)	1.521(10)	C(11)-U-P(2)	77.39(14)
C(37)-C(310)	1.525(9)	C(31)-U-P(2)	126.39(12)
C(13)-C(14)	1.383(11)	N(2)-U-P(1)#1	132.43(12)
C(13)-C(12)	1.389(11)	N(3)-U-P(1)#1	97.66(13)
C(13)-C(131)	1.531(10)	N(1)-U-P(1)#1	98.3(2)
C(23)-C(24)	1.397(10)	C(11)-U-P(1)#1	71.61(14)
C(23)-C(22)	1.400(9)	C(31)-U-P(1)#1	85.57(12)
C(23)-C(231)	1.510(10)	P(2)-U-P(1)#1	40.81(5)
C(22)-C(21)	1.378(9)	N(2)-U-P(1)	79.42(13)
C(35)-C(34)	1.374(9)	N(3)-U-P(1)	109.48(13)
C(35)-C(351)	1.516(9)	N(1)-U-P(1)	139.9(2)
C(251)-C(25)	1.518(10)	C(11)-U-P(1)	117.66(14)
C(25)-C(24)	1.366(10)	C(31)-U-P(1)	121.61(12)
C(33)-C(32)	1.382(9)	P(2)-U-P(1)	40.50(4)
C(33)-C(34)	1.400(9)	P(1)#1-U-P(1)	58.68(5)
C(33)-C(331)	1.511(9)	N(2)-U-P(2)#1	115.50(13)
C(16)-C(15)	1.387(10)	N(3)-U-P(2)#1	77.50(13)
C(16)-C(11)	1.409(10)	N(1)-U-P(2)#1	137.3(2)
C(15)-C(14)	1.374(10)	C(11)-U-P(2)#1	111.54(14)
C(15)-C(151)	1.508(11)	C(31)-U-P(2)#1	82.49(12)
C(12)-C(11)	1.392(10)	P(2)-U-P(2)#1	58.23(5)
C(17)-C(18)	1.530(10)	P(1)#1-U-P(2)#1	40.37(4)
C(17)-C(19)	1.533(10)	P(1)-U-P(2)#1	39.90(4)
C(17)-C(110)	1.541(11)	C(21)-N(2)-C(27)	113.0(4)
C(3S)-C(2S)	1.38(2)	C(21)-N(2)-U	114.2(3)
C(3S)-C(3S)#2	1.49(3)	C(27)-N(2)-U	132.5(4)
C(1S)-C(2S)	1.45(2)	C(31)-N(3)-C(37)	112.0(4)
P(1)-P(2)#1	2.156(2)	C(31)-N(3)-U	110.1(3)
P(1)-P(2)	2.162(2)	C(37)-N(3)-U	137.1(4)
P(1)-U#1	3.101(2)	C(11)-N(1)-C(17)	115.3(5)
P(2)-P(1)#1	2.157(2)	C(11)-N(1)-U	108.1(4)
P(2)-U#1	3.162(2)	C(17)-N(1)-U	136.6(5)
		N(2)-C(27)-C(28)	111.4(5)
N(2)-U-N(3)	118.2(2)	N(2)-C(27)-C(210)	107.6(5)
N(2)-U-N(1)	100.6(2)	C(28)-C(27)-C(210)	108.2(6)
N(3)-U-N(1)	105.6(2)	N(2)-C(27)-C(29)	112.1(5)
N(2)-U-C(11)	116.0(2)	C(28)-C(27)-C(29)	109.0(5)
N(3)-U-C(11)	112.3(2)	C(210)-C(27)-C(29)	108.6(5)
N(1)-U-C(11)	27.0(2)	C(35)-C(36)-C(31)	121.8(6)
N(2)-U-C(31)	139.3(2)	C(25)-C(26)-C(21)	120.4(7)
N(3)-U-C(31)	26.2(2)	C(32)-C(31)-C(36)	117.2(6)
N(1)-U-C(31)	84.5(2)	C(32)-C(31)-N(3)	121.9(6)
C(11)-U-C(31)	86.4(2)	C(36)-C(31)-N(3)	120.9(5)
N(2)-U-P(2)	92.80(12)	C(32)-C(31)-U	119.0(4)
N(3)-U-P(2)	134.24(13)	C(36)-C(31)-U	106.1(4)
N(1)-U-P(2)	100.1(2)	N(3)-C(31)-U	43.7(3)

C(39)-C(37)-N(3)	112.1(5)	C(35)-C(34)-C(33)	121.5(6)
C(39)-C(37)-C(38)	109.7(6)	C(25)-C(24)-C(23)	122.4(6)
N(3)-C(37)-C(38)	110.3(5)	C(13)-C(12)-C(11)	120.2(7)
C(39)-C(37)-C(310)	107.7(6)	N(1)-C(17)-C(18)	111.4(6)
N(3)-C(37)-C(310)	107.7(5)	N(1)-C(17)-C(19)	111.5(7)
C(38)-C(37)-C(310)	109.2(6)	C(18)-C(17)-C(19)	108.3(6)
C(14)-C(13)-C(12)	119.6(7)	N(1)-C(17)-C(110)	106.0(6)
C(14)-C(13)-C(131)	119.9(8)	C(18)-C(17)-C(110)	109.2(7)
C(12)-C(13)-C(131)	120.5(7)	C(19)-C(17)-C(110)	110.5(7)
C(24)-C(23)-C(22)	117.5(6)	C(12)-C(11)-C(16)	118.3(7)
C(24)-C(23)-C(231)	121.3(6)	C(12)-C(11)-N(1)	121.1(6)
C(22)-C(23)-C(231)	121.3(6)	C(16)-C(11)-N(1)	120.4(6)
C(21)-C(22)-C(23)	121.6(6)	C(12)-C(11)-U	108.4(4)
C(34)-C(35)-C(36)	118.8(6)	C(16)-C(11)-U	111.6(4)
C(34)-C(35)-C(351)	120.7(6)	N(1)-C(11)-U	44.9(3)
C(36)-C(35)-C(351)	120.5(6)	C(15)-C(14)-C(13)	122.1(8)
C(24)-C(25)-C(26)	119.0(6)	C(2S)-C(3S)-C(3S)#2	110(2)
C(24)-C(25)-C(251)	121.5(7)	P(2)#1-P(1)-P(2)	89.48(9)
C(26)-C(25)-C(251)	119.5(7)	P(2)#1-P(1)-U#1	69.16(6)
C(32)-C(33)-C(34)	118.1(6)	P(2)-P(1)-U#1	71.34(6)
C(32)-C(33)-C(331)	121.4(6)	P(2)#1-P(1)-U	70.14(6)
C(34)-C(33)-C(331)	120.5(6)	P(2)-P(1)-U	67.89(6)
C(22)-C(21)-C(26)	119.0(6)	U#1-P(1)-U	121.32(5)
C(22)-C(21)-N(2)	121.6(5)	P(1)#1-P(2)-P(1)	90.52(8)
C(26)-C(21)-N(2)	119.3(6)	P(1)#1-P(2)-U	70.03(6)
C(33)-C(32)-C(31)	122.6(6)	P(1)-P(2)-U	71.61(6)
C(15)-C(16)-C(11)	121.8(7)	P(1)#1-P(2)-U#1	69.96(6)
C(14)-C(15)-C(16)	117.9(7)	P(1)-P(2)-U#1	68.29(6)
C(14)-C(15)-C(151)	122.4(7)	U-P(2)-U#1	121.77(5)
C(16)-C(15)-C(151)	119.7(7)	C(3S)-C(2S)-C(1S)	118(2)

Symmetry transformations used to generate equivalent atoms:

#1 $-x + 1, -y + 2, -z$

#2 $-x, -y + 1, -z + 1$

Table A2.10.3. Anisotropic displacement parameters [$\text{\AA}^2 \times 10^3$] for $\mathbf{8}_2\text{-P}_4$.

	U^{11}	U^{22}	U^{33}	U^{23}	U^{13}	U^{12}
U	33(1)	34(1)	29(1)	0(1)	-12(1)	-12(1)
N(2)	34(3)	33(3)	40(3)	3(2)	-17(2)	-11(2)
N(3)	32(3)	39(3)	36(3)	-7(2)	-9(2)	-14(2)
N(1)	46(3)	70(4)	47(3)	-21(3)	-4(3)	-27(3)
C(27)	41(4)	33(3)	47(4)	3(3)	-20(3)	-12(3)

C(36)	41(4)	40(3)	37(3)	-1(3)	-11(3)	-18(3)
C(26)	45(4)	52(4)	54(4)	7(3)	-26(3)	-21(3)
C(31)	40(4)	42(3)	42(4)	-7(3)	-15(3)	-19(3)
C(37)	36(4)	44(4)	50(4)	-18(3)	-10(3)	-11(3)
C(13)	50(4)	96(6)	32(4)	4(4)	-13(3)	-29(4)
C(23)	38(4)	46(4)	58(4)	-4(3)	-26(3)	-10(3)
C(22)	37(3)	38(3)	51(4)	2(3)	-20(3)	-15(3)
C(35)	37(4)	49(4)	48(4)	-11(3)	-18(3)	-16(3)
C(251)	89(6)	50(4)	79(6)	12(4)	-31(5)	-36(4)
C(25)	56(4)	44(4)	64(5)	8(3)	-30(4)	-26(3)
C(33)	44(4)	51(4)	35(3)	-14(3)	-4(3)	-18(3)
C(210)	50(4)	46(4)	60(4)	-5(3)	-22(4)	-18(3)
C(21)	27(3)	34(3)	51(4)	-2(3)	-18(3)	-7(3)
C(32)	50(4)	43(4)	41(4)	-3(3)	-15(3)	-16(3)
C(16)	48(4)	74(5)	40(4)	-17(4)	-9(3)	-22(4)
C(351)	40(4)	68(5)	60(5)	-2(4)	-19(4)	0(4)
C(15)	58(5)	69(5)	45(4)	-2(4)	-14(4)	-29(4)
C(34)	32(3)	52(4)	49(4)	-18(3)	-8(3)	-13(3)
C(24)	43(4)	37(4)	79(5)	-9(4)	-34(4)	-9(3)
C(12)	47(4)	98(6)	33(4)	-10(4)	-14(3)	-32(4)
C(29)	37(4)	59(4)	61(5)	-5(4)	-12(3)	-21(3)
C(331)	59(5)	76(5)	43(4)	-7(4)	-2(4)	-22(4)
C(310)	46(4)	48(4)	55(4)	-15(3)	-20(3)	-12(3)
C(17)	63(5)	69(5)	45(4)	-17(4)	-2(4)	-31(4)
C(11)	57(4)	81(5)	28(3)	-20(3)	-8(3)	-32(4)
C(39)	47(4)	75(5)	90(6)	-38(5)	-35(4)	-7(4)
C(38)	83(6)	54(4)	67(5)	-19(4)	2(4)	-36(4)
C(231)	50(4)	53(4)	71(5)	-19(4)	-19(4)	-10(3)
C(19)	81(6)	112(7)	55(5)	-31(5)	10(4)	-65(5)
C(18)	85(6)	87(6)	43(4)	-7(4)	-17(4)	-47(5)
C(14)	66(5)	76(5)	41(4)	9(4)	-15(4)	-27(4)
C(28)	57(5)	59(4)	65(5)	7(4)	-38(4)	-19(4)
C(151)	81(6)	73(6)	96(7)	0(5)	-33(5)	-33(5)
C(131)	65(6)	123(8)	79(6)	25(6)	-34(5)	-35(6)
C(110)	94(7)	76(6)	73(6)	-17(5)	-3(5)	-33(5)
C(3S)	170(17)	106(10)	147(16)	68(10)	-68(11)	-45(11)
C(1S)	393(34)	142(15)	208(21)	56(14)	-183(23)	-127(19)
P(1)	41(1)	41(1)	32(1)	0(1)	-9(1)	-8(1)
P(2)	51(1)	44(1)	32(1)	0(1)	-15(1)	-21(1)
C(2S)	208(20)	107(11)	208(22)	-1(12)	-89(17)	-36(13)

A2.11 X-ray Crystal Structure of $(\mu\text{-}\eta^{4:4}\text{-P}_4)[\text{U}(\text{N}[\text{1-Ad}]\text{Ar})_3]_2$ ($\mathbf{9}_2\text{-P}_4$).

Crystals grown from a concentrated diethyl ether solution at $-35\text{ }^\circ\text{C}$ were coated with Paratone N oil (Exxon) on a microscope slide. An orange-brown prism was selected and mounted with wax on a glass fiber. A total of 57712 reflections ($-18 \leq h \leq 18$, $-31 \leq k \leq 49$, $-22 \leq l \leq 22$) were collected at 183(2) K in the θ range of 1.41 to 25.00 $^\circ$, of which 19955 were unique ($R_{\text{int}} = 0.0678$). The radiation used was Mo-K α ($\lambda = 0.71073\text{ \AA}$, $\mu = 0.465\text{ mm}^{-1}$). The structure was solved by direct methods (SHELXTL V5.0, G. M. Sheldrick and Siemens Industrial Automation, Inc., 1995) in conjunction with standard difference Fourier techniques. Carbon atoms C140 and C141 were refined isotropically with hydrogen atoms as idealized riding contributions. All other non-hydrogen atoms were refined anisotropically and the hydrogen atoms were placed in calculated ($d_{\text{CH}} = 0.96\text{ \AA}$) positions. The structure was found to contain severely disordered diethyl ether molecules of solvation that could not be reasonably modeled as discrete molecules. The crystallographic routine SQUEEZE was implemented to obtain the total residual electron density in the void area of the structure, corresponding to a value of 370 electrons in an area of 2098.3 \AA^{-3} (18.3% of the total volume of the unit cell). Assignment of this electron density to diethyl ether of solvation (42 electrons) resulted in an average of 2.2 equiv of solvent per molecule of $\mathbf{9}_2\text{-P}_4$. The final stages of refinement were performed against solvent-free modified structure factors obtained from SQUEEZE. The residual peak and hole electron density were 1.732 and $-16.061\text{ e}\cdot\text{\AA}^{-3}$, respectively. An empirical absorption correction (SADABS) was applied to the reflection data. The least squares refinement converged normally with residuals of $R_1 = 0.0980$, $wR_2 = 0.2141$ based upon $I > 2\sigma I$, and GOF = 1.138 (based on F^2). No significant extinction coefficient was applied to the refinement. Crystal and refinement data: Formula = $\text{C}_{112}\text{H}_{144}\text{N}_6\text{O}_4\text{P}_4\text{U}_2$; space group, $P2_1/n$; $a = 15.6370(13)\text{ \AA}$; $b = 41.909(4)\text{ \AA}$; $c = 18.8439(16)\text{ \AA}$; $\alpha = 90\text{ }^\circ$; $\beta = 112.399(2)\text{ }^\circ$; $\gamma = 90\text{ }^\circ$; $V = 11417.4(17)\text{ \AA}^3$; $Z = 4$; $D_{\text{calc}} = 1.274\text{ g}\cdot\text{cm}^{-3}$; $F(000) = 4440$; R_1 (based on F) = 0.1117; wR_2 (based on F^2) = 0.2207.

Table A2.11.11: Atomic coordinates [$\times 10^4$] and equivalent isotropic displacement parameters [$\text{\AA}^2 \times 10^3$] for $\mathbf{9}_2\text{-P}_4$.

	x	y	z	U(eq)
U(1)	13009(1)	1503(1)	3337(1)	22(1)
P(1)	10940(2)	1482(1)	1976(2)	36(1)
N(1)	13528(8)	1394(2)	4591(6)	28(2)
O(1)	11410(30)	1404(11)	7840(30)	250(20)
U(2)	9667(1)	922(1)	2298(1)	23(1)
P(2)	10934(3)	1511(1)	3107(2)	41(1)

N(2)	13884(7)	1316(2)	2698(6)	25(2)
P(3)	11578(3)	1045(1)	3384(2)	38(1)
C(3)	13748(9)	2242(3)	3569(7)	31(3)
N(3)	12889(8)	2036(2)	3270(7)	35(3)
P(4)	11576(2)	1023(1)	2232(2)	33(1)
C(4)	10783(10)	911(4)	-15(9)	48(4)
N(4)	9190(7)	833(2)	1022(6)	28(2)
N(5)	10031(7)	446(2)	2859(6)	29(2)
C(6)	13336(10)	1526(3)	5266(8)	33(3)
N(6)	8614(8)	1220(3)	2548(7)	33(3)
C(9)	14751(10)	1708(3)	2239(8)	32(3)
C(13)	9311(10)	1358(4)	4701(8)	42(4)
C(14)	13952(9)	2406(3)	2914(8)	30(3)
C(16)	8543(9)	1358(3)	3259(8)	30(3)
C(17)	14575(9)	2023(3)	4016(8)	35(3)
C(19)	9637(10)	964(3)	526(8)	37(3)
C(22)	13922(10)	1558(3)	2168(8)	32(3)
C(23)	15482(10)	2217(3)	4330(9)	40(4)
C(24)	8318(9)	648(3)	606(7)	29(3)
C(25)	10464(10)	138(3)	2726(7)	31(3)
C(26)	13999(10)	763(3)	3110(8)	35(3)
C(27)	10349(10)	796(3)	431(7)	37(3)
C(28)	9841(10)	433(3)	3554(8)	32(3)
C(30)	14200(9)	997(3)	2567(8)	27(3)
C(32)	15672(9)	2370(4)	3687(9)	44(4)
C(33)	9774(10)	-143(4)	2492(9)	45(4)
C(34)	10507(10)	504(3)	4261(8)	36(3)
C(35)	14000(11)	553(4)	1617(9)	46(4)
C(36)	15101(10)	1160(4)	4998(8)	39(3)
C(38)	13128(10)	1650(3)	1530(9)	38(3)
C(39)	12637(12)	1803(4)	4949(9)	46(4)
C(40)	15540(9)	643(4)	2647(10)	43(4)
C(41)	11522(10)	2304(3)	3335(9)	34(3)
C(42)	12055(10)	2214(3)	2913(8)	34(3)
C(43)	9343(9)	1226(3)	3968(7)	31(3)
C(44)	15324(12)	609(4)	5272(9)	46(4)

C(45)	10778(11)	196(3)	2058(8)	39(3)
C(46)	9807(13)	1375(4)	-292(10)	52(4)
C(47)	9377(11)	1262(4)	171(8)	43(4)
C(48)	15314(10)	411(3)	3164(9)	40(3)
C(49)	13717(10)	882(3)	1728(8)	34(3)
C(50)	13150(11)	1882(4)	1029(8)	43(4)
C(51)	14388(11)	560(4)	5085(9)	42(4)
C(54)	11056(12)	581(4)	5694(9)	54(4)
C(55)	13767(10)	316(4)	2138(10)	45(4)
C(56)	11700(10)	2274(4)	2150(9)	39(3)
C(57)	14134(9)	1124(3)	4803(7)	31(3)
C(59)	13797(9)	821(3)	4849(7)	31(3)
C(60)	7640(10)	1264(4)	3351(9)	45(4)
C(62)	12088(11)	-198(4)	2584(10)	47(4)
C(63)	14272(9)	417(3)	2980(8)	34(3)
C(64)	9386(12)	1718(4)	4703(9)	50(4)
C(66)	10228(11)	-444(4)	2349(10)	49(4)
C(67)	15397(11)	2483(4)	4872(9)	43(4)
C(68)	9421(12)	415(4)	4861(10)	48(4)
C(69)	12415(15)	1952(4)	5590(11)	65(5)
C(70)	15243(9)	982(3)	2762(9)	35(3)
C(73)	15697(11)	2096(4)	1812(10)	50(4)
C(74)	7687(13)	1779(4)	4096(12)	62(5)
C(77)	15047(12)	543(4)	1827(10)	50(4)
C(79)	8946(10)	352(3)	3496(8)	37(3)
C(80)	15692(11)	905(4)	5240(9)	46(4)
C(81)	14596(10)	2699(4)	4431(8)	37(3)
C(82)	11327(10)	40(4)	3422(8)	37(3)
C(83)	11782(10)	-256(4)	3259(9)	44(4)
C(84)	13680(11)	2512(3)	4113(9)	41(4)
C(85)	10349(10)	2509(4)	2213(11)	49(4)
C(86)	8571(12)	1854(4)	4019(10)	52(4)
C(89)	13976(11)	2015(3)	1132(10)	44(4)
C(90)	10305(10)	498(4)	4915(8)	37(3)
C(91)	8602(10)	1731(3)	3279(9)	38(3)
C(92)	11095(12)	-531(4)	3052(10)	50(4)

C(94)	12261(14)	1974(5)	368(10)	70(6)
C(95)	8747(10)	342(4)	4174(9)	44(4)
C(96)	13534(16)	1570(6)	6867(9)	75(6)
C(98)	14805(10)	1927(3)	1723(9)	35(3)
C(100)	10520(12)	1211(5)	-373(9)	55(5)
C(101)	8400(11)	1265(5)	4771(9)	60(5)
C(102)	14861(10)	2586(3)	3233(8)	35(3)
C(103)	14795(12)	2857(3)	3765(8)	42(4)
C(109)	12892(11)	1287(4)	5616(9)	41(4)
C(115)	11999(16)	1713(5)	5947(12)	73(6)
C(118)	7588(10)	1409(4)	4081(8)	47(4)
C(122)	10849(10)	2419(3)	1765(9)	38(3)
C(124)	12656(12)	1448(5)	6265(10)	55(4)
C(125)	11586(11)	737(4)	-111(11)	55(4)
C(126)	6845(11)	385(4)	-785(9)	53(4)
C(127)	6668(9)	663(4)	-334(8)	42(4)
C(128)	5436(12)	1368(4)	506(10)	60(5)
C(129)	6334(10)	543(4)	279(9)	45(4)
C(130)	10665(11)	2456(4)	2990(10)	48(4)
C(131)	7276(11)	44(4)	389(9)	47(4)
C(132)	7740(11)	1773(3)	862(9)	39(3)
C(133)	7561(10)	856(3)	45(9)	39(3)
C(134)	8490(10)	362(4)	153(8)	41(3)
C(135)	6822(11)	1680(3)	560(9)	44(4)
C(136)	7091(11)	325(4)	827(9)	42(4)
C(137)	7977(10)	516(3)	1207(8)	35(3)
C(138)	8307(10)	1619(3)	1512(8)	33(3)
C(139)	7046(8)	1301(3)	1544(7)	24(3)
C(140)	6457(9)	1444(3)	884(8)	31(3)
C(141)	7986(8)	1376(3)	1866(7)	21(2)
C(142)	14216(12)	1653(5)	5888(9)	56(5)
C(143)	13998(13)	235(4)	5132(11)	55(4)
C(144)	7588(11)	174(3)	-237(9)	44(4)
C(145)	13310(20)	2085(5)	6178(13)	93(9)
C(146)	9534(16)	1701(4)	-652(13)	75(6)
C(147)	10110(14)	2543(5)	3462(12)	70(6)

C(148)	13967(15)	1809(6)	6517(10)	72(6)
C(149)	8076(15)	2042(4)	503(12)	67(5)
C(150)	16719(12)	961(5)	5457(14)	78(7)
C(151)	7776(11)	258(5)	4116(11)	59(5)
C(152)	10504(14)	-379(4)	1673(11)	60(5)
C(153)	10471(12)	2491(5)	938(10)	60(5)
C(154)	11224(12)	-106(4)	1880(10)	50(4)
C(201)	12890(30)	1506(12)	8900(20)	148(15)
C(202)	11910(50)	1655(10)	8240(40)	190(30)
C(203)	10400(30)	1520(15)	7170(30)	220(30)
C(204)	9720(40)	1440(15)	7210(30)	220(20)

Table A2.11.2: Bond lengths [Å] and angles [°] for **9₂-P₄**.

U(1)–N(1)	2.233(11)	U(2)–P(2)	3.166(4)
U(1)–N(3)	2.241(10)	P(2)–P(3)	2.168(6)
U(1)–N(2)	2.278(10)	N(2)–C(22)	1.440(16)
U(1)–P(3)	2.975(4)	N(2)–C(30)	1.479(16)
U(1)–C(22)	3.055(13)	P(3)–P(4)	2.171(5)
U(1)–P(2)	3.107(4)	C(3)–N(3)	1.515(17)
U(1)–P(4)	3.138(4)	C(3)–C(17)	1.55(2)
U(1)–P(1)	3.277(4)	C(3)–C(14)	1.546(18)
P(1)–P(4)	2.137(5)	C(3)–C(84)	1.555(18)
P(1)–P(2)	2.138(6)	N(3)–C(42)	1.427(18)
P(1)–U(2)	3.281(4)	C(4)–C(27)	1.35(2)
N(1)–C(57)	1.432(17)	C(4)–C(100)	1.41(3)
N(1)–C(6)	1.518(17)	C(4)–C(125)	1.52(2)
O(1)–C(202)	1.36(6)	N(4)–C(19)	1.469(18)
O(1)–C(203)	1.67(6)	N(4)–C(24)	1.504(17)
U(2)–N(5)	2.229(10)	N(5)–C(28)	1.451(17)
U(2)–N(4)	2.260(11)	N(5)–C(25)	1.520(16)
U(2)–N(6)	2.256(11)	C(6)–C(109)	1.506(18)
U(2)–P(3)	2.953(4)	C(6)–C(39)	1.55(2)
U(2)–C(28)	3.065(13)	C(6)–C(142)	1.52(2)
U(2)–P(4)	3.064(3)	N(6)–C(141)	1.443(16)

N(6)–C(16)	1.501(17)	C(38)–C(50)	1.37(2)
C(9)–C(98)	1.362(18)	C(39)–C(69)	1.51(2)
C(9)–C(22)	1.402(19)	C(40)–C(77)	1.50(2)
C(13)–C(43)	1.507(19)	C(40)–C(48)	1.51(2)
C(13)–C(64)	1.51(2)	C(40)–C(70)	1.536(19)
C(13)–C(101)	1.53(2)	C(41)–C(42)	1.406(19)
C(14)–C(102)	1.518(19)	C(41)–C(130)	1.40(2)
C(16)–C(43)	1.543(19)	C(42)–C(56)	1.35(2)
C(16)–C(60)	1.536(18)	C(44)–C(80)	1.38(2)
C(16)–C(91)	1.567(19)	C(44)–C(51)	1.38(2)
C(17)–C(23)	1.544(19)	C(45)–C(154)	1.54(2)
C(19)–C(27)	1.39(2)	C(46)–C(100)	1.37(2)
C(19)–C(47)	1.40(2)	C(46)–C(47)	1.37(2)
C(22)–C(38)	1.41(2)	C(46)–C(146)	1.51(2)
C(23)–C(32)	1.50(2)	C(48)–C(63)	1.532(19)
C(23)–C(67)	1.55(2)	C(50)–C(89)	1.35(2)
C(24)–C(133)	1.526(18)	C(50)–C(94)	1.52(2)
C(24)–C(137)	1.527(19)	C(51)–C(59)	1.39(2)
C(24)–C(134)	1.554(18)	C(51)–C(143)	1.51(2)
C(25)–C(82)	1.537(18)	C(54)–C(90)	1.53(2)
C(25)–C(45)	1.535(19)	C(55)–C(63)	1.54(2)
C(25)–C(33)	1.54(2)	C(56)–C(122)	1.39(2)
C(26)–C(30)	1.532(18)	C(57)–C(59)	1.390(19)
C(26)–C(63)	1.559(18)	C(60)–C(118)	1.53(2)
C(28)–C(34)	1.374(19)	C(62)–C(83)	1.54(2)
C(28)–C(79)	1.40(2)	C(62)–C(154)	1.54(2)
C(30)–C(70)	1.530(17)	C(64)–C(86)	1.54(2)
C(30)–C(49)	1.545(19)	C(66)–C(152)	1.52(2)
C(32)–C(102)	1.53(2)	C(66)–C(92)	1.54(2)
C(33)–C(66)	1.52(2)	C(67)–C(81)	1.51(2)
C(34)–C(90)	1.39(2)	C(68)–C(95)	1.36(2)
C(35)–C(49)	1.49(2)	C(68)–C(90)	1.39(2)
C(35)–C(77)	1.53(2)	C(69)–C(115)	1.49(3)
C(35)–C(55)	1.54(2)	C(69)–C(145)	1.52(3)
C(36)–C(80)	1.37(2)	C(73)–C(98)	1.515(19)
C(36)–C(57)	1.421(19)	C(74)–C(86)	1.48(3)

C(74)–C(118)	1.56(2)	C(139)–C(141)	1.395(16)
C(79)–C(95)	1.43(2)	C(142)–C(148)	1.53(2)
C(80)–C(150)	1.52(2)	C(145)–C(148)	1.52(3)
C(81)–C(103)	1.55(2)	C(152)–C(154)	1.55(2)
C(81)–C(84)	1.54(2)	C(201)–C(202)	1.67(7)
C(82)–C(83)	1.52(2)	C(203)–C(204)	1.15(5)
C(83)–C(92)	1.52(2)		
C(85)–C(130)	1.37(2)	N(1)–U(1)–N(3)	104.6(4)
C(85)–C(122)	1.40(2)	N(1)–U(1)–N(2)	116.1(4)
C(86)–C(91)	1.51(2)	N(3)–U(1)–N(2)	111.5(4)
C(89)–C(98)	1.40(2)	N(1)–U(1)–P(3)	79.1(3)
C(95)–C(151)	1.52(2)	N(3)–U(1)–P(3)	126.6(3)
C(96)–C(124)	1.50(3)	N(2)–U(1)–P(3)	113.8(3)
C(96)–C(148)	1.50(3)	N(1)–U(1)–C(22)	134.2(4)
C(101)–C(118)	1.55(2)	N(3)–U(1)–C(22)	86.3(4)
C(102)–C(103)	1.542(19)	N(2)–U(1)–C(22)	26.6(3)
C(109)–C(124)	1.56(2)	P(3)–U(1)–C(22)	129.3(3)
C(115)–C(124)	1.48(3)	N(1)–U(1)–P(2)	95.1(3)
C(122)–C(153)	1.47(2)	N(3)–U(1)–P(2)	85.5(3)
C(126)–C(144)	1.51(2)	N(2)–U(1)–P(2)	137.3(3)
C(126)–C(127)	1.53(2)	P(3)–U(1)–P(2)	41.69(11)
C(127)–C(129)	1.53(2)	C(22)–U(1)–P(2)	130.4(3)
C(127)–C(133)	1.53(2)	N(1)–U(1)–P(4)	116.8(3)
C(128)–C(140)	1.51(2)	N(3)–U(1)–P(4)	125.3(3)
C(129)–C(136)	1.54(2)	N(2)–U(1)–P(4)	81.3(3)
C(130)–C(147)	1.51(2)	P(3)–U(1)–P(4)	41.50(10)
C(131)–C(136)	1.53(2)	C(22)–U(1)–P(4)	88.9(3)
C(131)–C(144)	1.54(2)	P(2)–U(1)–P(4)	58.00(9)
C(132)–C(138)	1.37(2)	N(1)–U(1)–P(1)	132.5(3)
C(132)–C(135)	1.39(2)	N(3)–U(1)–P(1)	86.8(3)
C(132)–C(149)	1.51(2)	N(2)–U(1)–P(1)	101.0(3)
C(134)–C(144)	1.54(2)	P(3)–U(1)–P(1)	58.43(10)
C(135)–C(140)	1.39(2)	C(22)–U(1)–P(1)	91.8(3)
C(136)–C(137)	1.52(2)	P(2)–U(1)–P(1)	39.03(11)
C(138)–C(141)	1.412(18)	P(4)–U(1)–P(1)	38.84(10)
C(139)–C(140)	1.369(18)	P(4)–P(1)–P(2)	90.2(2)

P(4)-P(1)-U(1)	67.07(13)	P(2)-U(2)-P(1)	38.69(10)
P(2)-P(1)-U(1)	66.19(14)	P(1)-P(2)-P(3)	90.7(2)
P(4)-P(1)-U(2)	64.94(13)	P(1)-P(2)-U(1)	74.78(14)
P(2)-P(1)-U(2)	67.76(14)	P(3)-P(2)-U(1)	65.90(14)
U(1)-P(1)-U(2)	111.19(11)	P(1)-P(2)-U(2)	73.54(14)
C(57)-N(1)-C(6)	112.0(10)	P(3)-P(2)-U(2)	64.05(14)
C(57)-N(1)-U(1)	113.0(8)	U(1)-P(2)-U(2)	119.18(12)
C(6)-N(1)-U(1)	134.8(8)	C(22)-N(2)-C(30)	114.6(10)
C(202)-O(1)-C(203)	112(5)	C(22)-N(2)-U(1)	108.4(8)
N(5)-U(2)-N(4)	106.2(4)	C(30)-N(2)-U(1)	134.9(8)
N(5)-U(2)-N(6)	118.1(4)	P(2)-P(3)-P(4)	88.5(2)
N(4)-U(2)-N(6)	110.0(4)	P(2)-P(3)-U(2)	74.64(15)
N(5)-U(2)-P(3)	79.6(3)	P(4)-P(3)-U(2)	71.62(14)
N(4)-U(2)-P(3)	127.1(3)	P(2)-P(3)-U(1)	72.41(14)
N(6)-U(2)-P(3)	112.7(3)	P(4)-P(3)-U(1)	73.27(14)
N(5)-U(2)-C(28)	26.2(4)	U(2)-P(3)-U(1)	131.76(13)
N(4)-U(2)-C(28)	127.4(4)	N(3)-C(3)-C(17)	107.6(11)
N(6)-U(2)-C(28)	93.7(4)	N(3)-C(3)-C(14)	112.3(11)
P(3)-U(2)-C(28)	79.2(3)	C(17)-C(3)-C(14)	108.3(10)
N(5)-U(2)-P(4)	93.8(3)	N(3)-C(3)-C(84)	112.7(11)
N(4)-U(2)-P(4)	84.9(3)	C(17)-C(3)-C(84)	109.0(11)
N(6)-U(2)-P(4)	137.1(3)	C(14)-C(3)-C(84)	106.9(11)
P(3)-U(2)-P(4)	42.25(10)	C(42)-N(3)-C(3)	113.5(10)
C(28)-U(2)-P(4)	108.8(3)	C(42)-N(3)-U(1)	126.1(9)
N(5)-U(2)-P(2)	118.0(3)	C(3)-N(3)-U(1)	120.3(8)
N(4)-U(2)-P(2)	122.2(3)	P(1)-P(4)-P(3)	90.6(2)
N(6)-U(2)-P(2)	80.8(3)	P(1)-P(4)-U(2)	75.89(14)
P(3)-U(2)-P(2)	41.31(11)	P(3)-P(4)-U(2)	66.13(13)
C(28)-U(2)-P(2)	107.1(3)	P(1)-P(4)-U(1)	74.09(14)
P(4)-U(2)-P(2)	58.12(9)	P(3)-P(4)-U(1)	65.23(13)
N(5)-U(2)-P(1)	131.8(3)	U(2)-P(4)-U(1)	121.45(11)
N(4)-U(2)-P(1)	84.2(3)	C(27)-C(4)-C(100)	119.4(15)
N(6)-U(2)-P(1)	100.7(3)	C(27)-C(4)-C(125)	122.3(16)
P(3)-U(2)-P(1)	58.58(10)	C(100)-C(4)-C(125)	118.2(15)
C(28)-U(2)-P(1)	137.8(3)	C(19)-N(4)-C(24)	114.7(10)
P(4)-U(2)-P(1)	39.18(10)	C(19)-N(4)-U(2)	124.8(8)

C(24)–N(4)–U(2)	120.4(8)	C(17)–C(23)–C(67)	109.5(13)
C(28)–N(5)–C(25)	112.0(10)	N(4)–C(24)–C(133)	112.0(11)
C(28)–N(5)–U(2)	111.0(8)	N(4)–C(24)–C(137)	107.7(10)
C(25)–N(5)–U(2)	136.9(8)	C(133)–C(24)–C(137)	108.9(12)
N(1)–C(6)–C(109)	113.4(11)	N(4)–C(24)–C(134)	111.9(11)
N(1)–C(6)–C(39)	106.6(11)	C(133)–C(24)–C(134)	108.1(11)
C(109)–C(6)–C(39)	107.0(12)	C(137)–C(24)–C(134)	108.2(11)
N(1)–C(6)–C(142)	111.2(11)	N(5)–C(25)–C(82)	112.8(11)
C(109)–C(6)–C(142)	109.0(13)	N(5)–C(25)–C(45)	107.6(10)
C(39)–C(6)–C(142)	109.4(13)	C(82)–C(25)–C(45)	106.9(11)
C(141)–N(6)–C(16)	111.3(10)	N(5)–C(25)–C(33)	112.8(11)
C(141)–N(6)–U(2)	111.6(8)	C(82)–C(25)–C(33)	109.3(11)
C(16)–N(6)–U(2)	135.1(8)	C(45)–C(25)–C(33)	107.1(11)
C(98)–C(9)–C(22)	122.8(14)	C(30)–C(26)–C(63)	110.6(11)
C(43)–C(13)–C(64)	109.8(13)	C(19)–C(27)–C(4)	121.1(14)
C(43)–C(13)–C(101)	110.0(11)	C(34)–C(28)–C(79)	119.6(13)
C(64)–C(13)–C(101)	109.2(14)	C(34)–C(28)–N(5)	121.7(13)
C(102)–C(14)–C(3)	110.6(11)	C(79)–C(28)–N(5)	118.7(12)
N(6)–C(16)–C(43)	108.9(10)	C(34)–C(28)–U(2)	114.5(9)
N(6)–C(16)–C(60)	112.7(11)	C(79)–C(28)–U(2)	108.0(9)
C(43)–C(16)–C(60)	106.7(11)	N(5)–C(28)–U(2)	42.7(5)
N(6)–C(16)–C(91)	112.4(11)	N(2)–C(30)–C(26)	107.4(10)
C(43)–C(16)–C(91)	108.4(11)	N(2)–C(30)–C(70)	112.9(10)
C(60)–C(16)–C(91)	107.5(11)	C(26)–C(30)–C(70)	106.5(11)
C(23)–C(17)–C(3)	110.5(11)	N(2)–C(30)–C(49)	112.8(11)
C(27)–C(19)–C(47)	119.4(14)	C(26)–C(30)–C(49)	109.9(11)
C(27)–C(19)–N(4)	119.6(13)	C(70)–C(30)–C(49)	107.1(11)
C(47)–C(19)–N(4)	121.0(13)	C(23)–C(32)–C(102)	109.2(11)
C(38)–C(22)–C(9)	116.1(12)	C(66)–C(33)–C(25)	111.2(12)
C(38)–C(22)–N(2)	121.8(12)	C(28)–C(34)–C(90)	120.9(14)
C(9)–C(22)–N(2)	122.1(12)	C(49)–C(35)–C(77)	109.7(13)
C(38)–C(22)–U(1)	97.7(9)	C(49)–C(35)–C(55)	110.7(12)
C(9)–C(22)–U(1)	129.4(9)	C(77)–C(35)–C(55)	107.9(13)
N(2)–C(22)–U(1)	45.0(6)	C(80)–C(36)–C(57)	121.3(14)
C(32)–C(23)–C(17)	110.6(12)	C(50)–C(38)–C(22)	122.4(14)
C(32)–C(23)–C(67)	108.5(12)	C(69)–C(39)–C(6)	110.1(13)

C(77)–C(40)–C(48)	109.3(13)	C(33)–C(66)–C(92)	111.2(14)
C(77)–C(40)–C(70)	109.9(13)	C(81)–C(67)–C(23)	109.2(12)
C(48)–C(40)–C(70)	110.3(12)	C(95)–C(68)–C(90)	121.1(14)
C(42)–C(41)–C(130)	122.0(14)	C(115)–C(69)–C(39)	111.0(15)
C(56)–C(42)–C(41)	117.3(13)	C(115)–C(69)–C(145)	110.9(17)
C(56)–C(42)–N(3)	121.9(13)	C(39)–C(69)–C(145)	107.9(17)
C(41)–C(42)–N(3)	120.5(12)	C(40)–C(70)–C(30)	110.8(10)
C(13)–C(43)–C(16)	111.3(11)	C(86)–C(74)–C(118)	107.4(13)
C(80)–C(44)–C(51)	122.6(14)	C(40)–C(77)–C(35)	109.7(12)
C(25)–C(45)–C(154)	111.1(12)	C(28)–C(79)–C(95)	119.2(13)
C(100)–C(46)–C(47)	121.0(16)	C(44)–C(80)–C(36)	118.4(15)
C(100)–C(46)–C(146)	120.4(16)	C(44)–C(80)–C(150)	122.9(15)
C(47)–C(46)–C(146)	118.3(17)	C(36)–C(80)–C(150)	118.7(15)
C(46)–C(47)–C(19)	119.2(15)	C(67)–C(81)–C(103)	108.7(12)
C(40)–C(48)–C(63)	109.5(12)	C(67)–C(81)–C(84)	111.2(12)
C(35)–C(49)–C(30)	112.1(12)	C(103)–C(81)–C(84)	110.2(11)
C(89)–C(50)–C(38)	118.0(14)	C(83)–C(82)–C(25)	111.9(12)
C(89)–C(50)–C(94)	122.6(15)	C(82)–C(83)–C(92)	109.4(12)
C(38)–C(50)–C(94)	119.4(16)	C(82)–C(83)–C(62)	110.9(12)
C(44)–C(51)–C(59)	118.4(14)	C(92)–C(83)–C(62)	108.6(13)
C(44)–C(51)–C(143)	122.0(14)	C(81)–C(84)–C(3)	109.8(11)
C(59)–C(51)–C(143)	119.6(14)	C(130)–C(85)–C(122)	122.8(14)
C(35)–C(55)–C(63)	109.1(12)	C(74)–C(86)–C(91)	112.4(14)
C(42)–C(56)–C(122)	124.0(14)	C(74)–C(86)–C(64)	110.3(16)
C(59)–C(57)–C(36)	118.1(12)	C(91)–C(86)–C(64)	110.0(13)
C(59)–C(57)–N(1)	120.9(12)	C(50)–C(89)–C(98)	123.4(13)
C(36)–C(57)–N(1)	121.0(12)	C(34)–C(90)–C(68)	119.7(13)
C(51)–C(59)–C(57)	121.1(13)	C(34)–C(90)–C(54)	119.9(14)
C(118)–C(60)–C(16)	111.4(12)	C(68)–C(90)–C(54)	120.4(14)
C(83)–C(62)–C(154)	107.6(12)	C(86)–C(91)–C(16)	109.9(12)
C(48)–C(63)–C(55)	108.3(12)	C(83)–C(92)–C(66)	110.1(12)
C(48)–C(63)–C(26)	108.1(12)	C(68)–C(95)–C(79)	119.5(14)
C(55)–C(63)–C(26)	110.8(11)	C(68)–C(95)–C(151)	120.8(14)
C(13)–C(64)–C(86)	109.1(13)	C(79)–C(95)–C(151)	119.7(15)
C(152)–C(66)–C(33)	107.6(13)	C(124)–C(96)–C(148)	109.4(14)
C(152)–C(66)–C(92)	109.1(14)	C(9)–C(98)–C(89)	117.1(13)

C(9)–C(98)–C(73)	122.7(15)	C(135)–C(132)–C(149)	120.7(14)
C(89)–C(98)–C(73)	120.0(12)	C(24)–C(133)–C(127)	110.5(12)
C(46)–C(100)–C(4)	119.7(15)	C(144)–C(134)–C(24)	109.7(12)
C(13)–C(101)–C(118)	108.6(14)	C(132)–C(135)–C(140)	123.6(13)
C(14)–C(102)–C(32)	112.2(11)	C(131)–C(136)–C(137)	109.5(12)
C(14)–C(102)–C(103)	109.9(11)	C(131)–C(136)–C(129)	110.6(13)
C(32)–C(102)–C(103)	108.6(12)	C(137)–C(136)–C(129)	109.5(12)
C(102)–C(103)–C(81)	107.3(11)	C(24)–C(137)–C(136)	110.7(12)
C(6)–C(109)–C(124)	110.1(13)	C(132)–C(138)–C(141)	122.5(13)
C(124)–C(115)–C(69)	109.5(17)	C(140)–C(139)–C(141)	122.0(11)
C(60)–C(118)–C(101)	107.0(13)	C(139)–C(140)–C(135)	117.5(12)
C(60)–C(118)–C(74)	111.8(14)	C(139)–C(140)–C(128)	123.9(13)
C(101)–C(118)–C(74)	109.2(14)	C(135)–C(140)–C(128)	118.5(13)
C(56)–C(122)–C(85)	116.5(14)	C(139)–C(141)–C(138)	117.5(11)
C(56)–C(122)–C(153)	124.1(15)	C(139)–C(141)–N(6)	122.2(11)
C(85)–C(122)–C(153)	119.4(15)	C(138)–C(141)–N(6)	120.3(11)
C(115)–C(124)–C(96)	110.2(18)	C(148)–C(142)–C(6)	108.9(14)
C(115)–C(124)–C(109)	110.0(14)	C(126)–C(144)–C(134)	110.7(13)
C(96)–C(124)–C(109)	108.6(14)	C(126)–C(144)–C(131)	110.3(14)
C(144)–C(126)–C(127)	108.6(12)	C(134)–C(144)–C(131)	108.5(12)
C(126)–C(127)–C(129)	110.9(14)	C(148)–C(145)–C(69)	108.2(16)
C(126)–C(127)–C(133)	109.6(12)	C(145)–C(148)–C(96)	110.2(19)
C(129)–C(127)–C(133)	109.6(11)	C(145)–C(148)–C(142)	109.5(16)
C(127)–C(129)–C(136)	107.8(12)	C(96)–C(148)–C(142)	110.2(17)
C(85)–C(130)–C(41)	117.5(14)	C(66)–C(152)–C(154)	109.5(14)
C(85)–C(130)–C(147)	122.4(16)	C(45)–C(154)–C(152)	108.5(13)
C(41)–C(130)–C(147)	120.1(16)	C(45)–C(154)–C(62)	109.9(13)
C(136)–C(131)–C(144)	108.8(13)	C(152)–C(154)–C(62)	110.3(14)
C(138)–C(132)–C(135)	116.8(14)	O(1)–C(202)–C(201)	107(4)
C(138)–C(132)–C(149)	122.4(15)	C(204)–C(203)–O(1)	120(4)

Table A2.11.3: Anisotropic displacement parameters ($\text{\AA}^2 \times 10^3$) for $\mathbf{9}_2\text{-P}_4$.

	U^{11}	U^{22}	U^{33}	U^{23}	U^{13}	U^{12}
U(1)	22(1)	22(1)	24(1)	-1(1)	10(1)	-1(1)
P(1)	29(2)	32(2)	41(2)	4(2)	8(2)	-6(2)
N(1)	37(6)	17(5)	32(6)	-3(4)	14(5)	1(5)
O(1)	320(50)	250(50)	270(50)	90(40)	230(40)	40(40)
U(2)	21(1)	24(1)	24(1)	0(1)	9(1)	0(1)
P(2)	33(2)	42(2)	56(2)	-19(2)	25(2)	-12(2)
N(2)	23(5)	23(5)	28(6)	-2(4)	9(4)	-4(4)
P(3)	31(2)	42(2)	36(2)	8(2)	6(2)	-11(2)
C(3)	36(7)	34(8)	27(7)	-4(6)	16(6)	-4(6)
N(3)	49(7)	17(5)	45(7)	-1(5)	25(6)	-1(5)
P(4)	27(2)	31(2)	43(2)	-11(2)	15(2)	-2(1)
C(4)	33(8)	74(12)	33(8)	-8(8)	8(7)	-11(8)
N(4)	28(6)	26(6)	33(6)	-1(5)	14(5)	2(5)
N(5)	26(6)	20(5)	37(6)	3(5)	7(5)	2(4)
C(6)	47(8)	21(7)	37(8)	2(6)	24(7)	-8(6)
N(6)	29(6)	32(6)	38(6)	-3(5)	12(5)	5(5)
C(9)	45(8)	18(6)	40(8)	-4(6)	25(7)	-3(6)
C(13)	26(7)	59(10)	34(8)	-9(7)	5(6)	-4(7)
C(14)	41(8)	14(6)	35(7)	-1(5)	15(6)	7(5)
C(16)	28(7)	29(7)	38(8)	-7(6)	17(6)	-2(6)
C(17)	38(8)	39(8)	31(7)	5(6)	16(6)	-9(6)
C(19)	39(8)	34(8)	35(8)	-11(6)	12(6)	2(6)
C(22)	47(8)	19(6)	34(7)	-2(5)	21(6)	-2(6)
C(23)	41(8)	26(7)	41(8)	4(6)	0(7)	2(6)
C(24)	37(7)	24(7)	23(6)	2(5)	7(6)	10(6)
C(25)	41(8)	22(7)	29(7)	7(5)	13(6)	7(6)
C(26)	44(8)	21(7)	46(8)	-6(6)	25(7)	-3(6)
C(27)	51(9)	36(8)	21(7)	6(6)	10(6)	10(7)
C(28)	39(8)	25(7)	35(7)	9(6)	14(6)	7(6)
C(30)	28(7)	26(7)	37(7)	-3(5)	22(6)	-1(5)
C(32)	21(7)	57(10)	54(9)	-33(8)	14(7)	-6(7)

C(33)	37(8)	48(9)	52(10)	22(7)	20(7)	9(7)
C(34)	35(8)	34(8)	30(7)	3(6)	4(6)	0(6)
C(35)	54(10)	42(9)	43(9)	-7(7)	21(8)	6(7)
C(36)	35(8)	36(8)	41(8)	17(7)	8(6)	4(6)
C(38)	41(8)	26(7)	56(9)	-14(7)	30(7)	0(6)
C(39)	70(11)	38(9)	36(8)	4(7)	27(8)	22(8)
C(40)	21(7)	38(8)	77(12)	-3(8)	26(7)	-3(6)
C(41)	38(8)	24(7)	44(8)	3(6)	20(7)	6(6)
C(42)	35(8)	28(7)	35(8)	3(6)	8(6)	0(6)
C(43)	24(7)	37(8)	31(7)	-2(6)	10(6)	-11(6)
C(44)	58(10)	36(9)	49(9)	14(7)	25(8)	14(7)
C(45)	50(9)	28(7)	40(8)	-1(6)	18(7)	-5(7)
C(46)	67(11)	40(9)	51(10)	8(8)	25(9)	-5(8)
C(47)	55(10)	40(9)	35(8)	0(7)	18(7)	-6(7)
C(48)	41(8)	33(8)	53(9)	0(7)	27(7)	6(6)
C(49)	41(8)	27(7)	38(8)	-2(6)	20(6)	-5(6)
C(50)	59(10)	44(9)	24(7)	2(6)	15(7)	13(8)
C(51)	48(9)	32(8)	45(9)	5(7)	16(7)	4(7)
C(54)	58(11)	53(11)	46(10)	9(8)	13(8)	-2(8)
C(55)	36(8)	31(8)	72(11)	-10(7)	25(8)	4(6)
C(56)	36(8)	40(8)	43(9)	-5(7)	18(7)	-5(6)
C(57)	33(7)	37(8)	23(7)	4(6)	10(6)	3(6)
C(59)	30(7)	34(8)	27(7)	1(6)	7(6)	0(6)
C(60)	25(7)	72(11)	41(9)	-8(8)	17(7)	-5(7)
C(62)	42(9)	38(9)	64(11)	1(8)	25(8)	3(7)
C(63)	36(8)	30(7)	37(8)	10(6)	14(6)	5(6)
C(64)	48(9)	52(10)	41(9)	-11(7)	6(7)	9(8)
C(66)	46(9)	27(8)	72(12)	1(7)	18(8)	-6(7)
C(67)	48(9)	46(9)	36(8)	-5(7)	17(7)	-11(7)
C(68)	62(11)	42(9)	49(10)	2(7)	32(9)	8(8)
C(69)	102(16)	46(10)	63(12)	-11(9)	50(12)	21(10)
C(70)	28(7)	24(7)	60(9)	-5(6)	23(7)	-6(6)
C(73)	51(10)	55(10)	60(11)	-3(8)	38(9)	-19(8)
C(74)	62(11)	47(10)	74(13)	-22(9)	23(10)	20(9)
C(77)	72(12)	32(8)	68(11)	0(8)	51(10)	12(8)
C(79)	38(8)	34(8)	33(7)	3(6)	8(6)	2(6)

C(80)	46(9)	42(9)	50(9)	9(7)	18(8)	12(7)
C(81)	40(8)	42(8)	30(7)	-11(6)	14(6)	-10(7)
C(82)	40(8)	43(8)	27(7)	8(6)	12(6)	-10(7)
C(83)	32(8)	52(10)	41(8)	8(7)	4(7)	9(7)
C(84)	62(10)	34(8)	44(9)	-5(7)	39(8)	5(7)
C(85)	29(8)	34(8)	78(12)	-5(8)	14(8)	8(6)
C(86)	59(11)	34(9)	58(10)	-7(7)	16(9)	16(8)
C(89)	65(11)	34(8)	65(11)	16(7)	61(9)	8(7)
C(90)	39(8)	44(9)	23(7)	2(6)	5(6)	2(7)
C(91)	35(8)	38(8)	44(8)	-5(7)	18(7)	7(6)
C(92)	76(12)	24(8)	58(10)	-2(7)	35(9)	2(8)
C(94)	69(13)	87(15)	45(10)	5(10)	11(9)	27(11)
C(95)	37(8)	50(9)	56(10)	11(8)	30(8)	-2(7)
C(96)	101(16)	106(17)	19(8)	0(9)	22(9)	26(13)
C(98)	52(9)	19(6)	58(9)	4(6)	50(8)	4(6)
C(100)	52(10)	82(13)	34(9)	-1(8)	19(8)	-7(9)
C(101)	47(10)	110(16)	38(9)	-33(10)	34(8)	-15(10)
C(102)	40(8)	33(8)	36(8)	-3(6)	19(6)	-10(6)
C(103)	58(10)	21(7)	42(8)	-12(6)	15(7)	-14(7)
C(109)	48(9)	38(8)	42(9)	2(7)	22(7)	-6(7)
C(115)	102(16)	72(14)	71(13)	-25(11)	62(13)	-13(12)
C(118)	25(7)	87(13)	29(8)	-16(8)	12(6)	-15(8)
C(122)	36(8)	30(8)	44(8)	-6(6)	8(7)	-7(6)
C(124)	59(11)	66(12)	55(11)	11(9)	37(9)	9(9)
C(125)	44(9)	62(11)	64(11)	-9(9)	26(9)	-3(8)
C(126)	43(9)	70(12)	35(8)	-22(8)	2(7)	-7(8)
C(127)	25(7)	61(10)	22(7)	-16(7)	-9(6)	9(7)
C(128)	55(11)	53(11)	51(10)	6(8)	-2(8)	19(9)
C(129)	25(7)	61(10)	46(9)	-26(8)	10(7)	-11(7)
C(130)	48(9)	47(10)	57(11)	-11(8)	31(8)	0(8)
C(131)	46(9)	43(9)	40(9)	-5(7)	3(7)	-1(7)
C(132)	48(9)	32(8)	43(8)	13(6)	26(7)	18(7)
C(133)	43(8)	24(7)	42(8)	-1(6)	10(7)	5(6)
C(134)	45(9)	38(8)	35(8)	-10(6)	11(7)	1(7)
C(135)	50(9)	32(8)	46(9)	3(7)	12(7)	33(7)
C(136)	52(9)	34(8)	54(9)	-10(7)	35(8)	3(7)

C(137)	42(8)	30(7)	40(8)	-8(6)	23(7)	4(6)
C(138)	44(8)	25(7)	35(7)	-9(6)	21(6)	-5(6)
C(139)	20(6)	15(6)	35(7)	8(5)	11(5)	0(5)
C(142)	61(11)	66(12)	40(9)	-23(8)	17(8)	-22(9)
C(143)	61(11)	35(9)	69(12)	11(8)	26(9)	8(8)
C(144)	51(9)	31(8)	43(9)	-30(7)	10(7)	-9(7)
C(145)	180(30)	55(13)	73(15)	-35(12)	84(17)	-43(16)
C(146)	101(16)	36(10)	99(16)	28(10)	52(14)	12(10)
C(147)	65(12)	70(13)	87(15)	-5(11)	44(11)	12(10)
C(148)	87(15)	97(17)	30(9)	-27(10)	20(9)	-33(13)
C(149)	81(14)	41(10)	75(13)	14(9)	26(11)	0(9)
C(150)	35(10)	74(14)	127(19)	30(13)	32(11)	7(9)
C(151)	31(9)	82(14)	71(12)	5(10)	28(9)	-5(8)
C(152)	81(13)	38(9)	56(11)	-6(8)	19(10)	5(9)
C(153)	41(9)	70(12)	60(11)	29(9)	9(8)	-2(9)
C(154)	71(11)	41(9)	57(10)	-7(8)	46(9)	1(8)
C(201)	110(20)	200(40)	140(30)	-40(30)	50(20)	-20(30)
C(202)	320(80)	90(30)	230(60)	20(30)	190(60)	0(40)
C(203)	120(30)	350(70)	220(50)	210(50)	80(30)	70(40)
C(204)	150(40)	280(70)	220(60)	80(50)	80(40)	0(40)

Appendix 3: Protocol for use of uranium (^{238}U) in the Cummins group

After a member of the Cummins group successfully completes their departmental safety training, they must also complete a training session with the Environmental Health and Safety (EHS) office if they wish to work with or near uranium; if a student works in lab 6-327 daily, they must have EHS training. Below is listed the protocol for training, use, and disposal of uranium in the Cummins lab 6-327.

1. Training
 - a. After the group's safety officer has trained the new group member in general safety protocol, the group member must contact the EHS office to schedule radiation safety training. The Cummins group contact in EHS is Dr. William B. McCarthy, who can be contacted at (617) 253-0346 or via email at wbm@mit.edu
 - b. The radiation safety training session lasts for approximately one hour. During this time, the group member will be trained in safe use and disposal practices including the use of a Geiger counter.
2. Use
 - a. Use of uranium must be limited to the glovebox and hoods in lab 6-327.
 - b. Transportation of, for example, NMR tubes containing solutions of uranium compounds must take place in secondary containment. No restrictions exist for use of sealed containers of uranium compounds in the department's spectroscopy lab.
 - c. If samples of a uranium compound must be sent for elemental analysis, H. Kolbe Mikroanalytisches Laboratorium in Mülheim, Germany can process the samples. A letter to this company must be included describing the elements present in the samples and giving them the option of sending the excess material back to MIT for disposal.
 - d. Detailed rules of use as described by EHS can be found on the MIT website: http://web.mit.edu/environment/pdf/MIT_Reqd.pdf
 - e. If any spills occur, see list of important contact information below. When the spill is small, remove any contaminated clothing and wash any exposed skin following the protocol for any chemical spill. Isolate the spill so it does not spread on anyone's shoes, etc., and clean it up appropriately. If the spill is large, immediately contact EHS for assistance (see 4b).
3. Disposal
 - a. Solid wastes that are contaminated with uranium must be disposed in the large, cardboard waste container in lab 6-327. *No other radioactive isotopes can be disposed in this container!* All paper, glass, chemical, and other contaminated waste should go into this container. When this container is full, the EHS technician assigned to the Cummins group must be contacted for removal. Currently, this technician is Steve Greenlaw (x3-3674, greenlaw@mit.edu).

- b. Uranium-contaminated mercury must be disposed separately. Steve Greenlaw should be contacted for the appropriate paperwork.
 - c. Solution waste containing uranium must have the solvent removed prior to disposal. This must be done either evaporatively or by addition of a “clotting” agent (available in the stockroom). The solid residue can then be disposed in the cardboard container mentioned above.
 - d. Periodic (once per month) evaluations of the laboratory take place. An EHS technician will do wipe tests of the floor near the doors and hoods and will check the lab with a sensitive Geiger counter. If there is contamination detected outside of the hoods and glovebox, the lab members will be contacted by EHS.
4. Useful contact information
- a. The MIT EHS office’s website:
<http://web.mit.edu/environment/index.html>
 - b. In emergencies, call the Radiation Protection Program office at x2-3477 (during business hours). On weekends or after business hours, dial the MIT-wide emergency number x100 from any MIT phone.
 - c. For detailed information on radioactive spill protocol:
http://web.mit.edu/environment/ehs/radiation_spill.html

Acknowledgements

I would like first to acknowledge the important contributions that my labmates have made to my education at MIT, both professionally and personally. While I cannot list everyone here, I need particularly to thank Josh Figueroa and Arjun Mendiratta. While you are a year behind me academically, I think you're years ahead of me in your understanding of chemistry. It's appropriate for me to acknowledge you here for the many helpful discussions we've had. Furthermore, what a source of entertainment you've both been! Josh is certainly the only person I know that can somehow get away with giving *himself* nicknames, and Arjun has one of the wittiest senses of humor I've encountered. Both of you have been important friends and coworkers.

I would also like to thank my glovebox-mates Chris Clough, Qing-Hao Chen, Paula Diaconescu, Víctor Durà-Vilà, Karsten Meyer, and Han Sen Soo. I especially want to thank Paula for several years of invaluable guidance in glovebox use and synthetic protocol, and Chris for a being a breath of fresh air... so to speak. It is always nice to have a lab buddy for going to have some lunch or some gossip. And you can't beat a labmate who brings in a whole book full of Led Zeppelin CDs! (On that note, I should also thank James Blackwell for reintroducing me to rock and roll! I was beginning to think it might be dead after all.)

I'm certainly indebted to Kit Cummins for the education and generous research opportunities (and leeway) he's provided me as my thesis advisor. Probably I should first thank him for putting up with my sass. I'd like to think it did us both some good, but I shouldn't go as far as to say that in public. (How insubordinate!) I have been in a unique position to see many changes in this research group over the past five years. While the group is smaller (and certainly less of a raucous fraternity) than when I joined, I think everyone now involved is friendlier and more productive. Certainly that is largely due to the guidance and friendship we've received from Kit.

For their help scientifically, I'd like to thank the staff of the MIT Department of Chemistry Instrumentation Facility (DCIF). The DCIF is a great place to gather data and gossip from Mark Wall and David Bray. The former director of that facility, Jeff Simpson, trained me in the use of various instruments and techniques that proved invaluable to my thesis research. Finally, Li Li, the mass spectroscopist at the DCIF, collected one of the most important pieces of verification for the identification of $\text{PMo}(\text{OMeCy})_3$ as a monomeric terminal phosphide. For that I'm grateful!

My science teachers during my early education deserve thanks as well. I suppose if I can even *remember* a teacher from my childhood, they must have made a positive impact. Those people include Mrs. Sullivan, my fifth grade teacher, who had a penchant for biology. In her class, we dissected cows' eyes, certainly convincing me that I didn't want to be a biologist. In high school, I had a series of wonderful math teachers, culminating in advanced math classes from Mr. Huebner. He was the most energetic person I'd met until then, and it carried over into his exciting teaching. That's saying a lot for advanced algebra!

During college at the University of St. Thomas, I had several important mentors. Thanks to Tom Ippoliti and David Boyd for introducing me to research. Teaching research skills to undergraduates who have almost no laboratory experience takes a lot of patience, I've come to realize. Drs. Ippoliti and Boyd have tremendous patience and gifts

for teaching that exceed most. I would particularly like to thank Dr. Boyd for always being extremely supportive and encouraging, and for taking the time to discuss my options for my future. I would like to thank Dr. Ippoliti for being the first of many chemistry professors who bought my labmates and me some drinks and then proceeded to get really drunk in front of us. Maybe that's what really made me want to go to graduate school...

I want to acknowledge the importance of the friendships I've had during the time I've been at MIT. My friends have been my second family. Importantly, I would like to thank Abi Haka, Aaron Skaggs, Todd Ostomel, Josh Brown, Hector Hernandez, Mary O'Reilly, Peter Rye, Dan Mindiola, Susan Brighton, and my other labmates for their friendship. Just as important are my friends from the University of St. Thomas who lent their support to me even when their own lives were getting busier and busier. Thanks to Sara Freund, Mary Fischer, Elizabeth Eggert, and Julie Piasecki particularly. While I was an undergraduate, I went to England for a semester. There I met some people who are very important to me, and deserve thanks for being supportive during my time at MIT: Darren Noble, Miriam Spering, Laurent Phelép, and Fred Jean. Last, I would like to thank the friends I have had since high school, including Monisha Kannan, Amy Niemczyk, Eric Lorbach, and Matt Schwartz. You four are some of the most important people in my life, and I hope we continue to be friends for a long, long time. Matt deserves special thanks for many reasons; I'll try to tell you one reason every day for the next 100 years, Matt!

Fifteen or twenty years ago, when Grandma and Grandpa Stephens still had their cabin near Deerwood, MN, my dad and I went walking around the dirt roads up there. It may not have seemed to Dad that I was interested in the mini-geochemistry lectures that he gave me when we found a piece of jasper or agate. However, I am privileged to have a father who is smart, resourceful, and willing to share both qualities with me, since those moments at the cabin introduced me to my career in chemistry. Equally important in my achievements was my mom. Although all parents are supposed to encourage their children, Mom told me things like, "You are smart enough to do anything you want, so you just need to decide what you like best." I feel lucky to have had such unwavering support over the years.

Frances H. Stephens

Department of Chemistry, Room 6-327
Massachusetts Institute of Technology
Cambridge, MA 02139

Phone (617) 452-2528
Fax (617) 258-5700
E-mail stephens@mit.edu

Education

1995 - 1999 **University of St. Thomas, St. Paul, MN** **B.S. Chemistry**

- Graduated *summa cum laude* from the Aquinas Scholars honors program. Completed a minor in mathematics. Completed a six-month study abroad program at the University of Exeter, England.
- Completed one year of organic chemistry research in conjunction with H. B. Fuller Company in powder coatings development. Completed two years of organometallic chemistry research in photochromic complexes of group VIII transition metals. Presented latter results at the National Conference for Undergraduate Research (1999).
- Worked as both a mathematics tutor and an advanced undergraduate teaching assistant for the general chemistry course (laboratory and lecture).

1999 - present **Massachusetts Institute of Technology** **Ph.D. Inorganic Chemistry**

- Awarded Department of Chemistry teaching fellowship (3 semesters) and research fellowship (3 years). Graduation date (anticipated): June, 2004.
- Completed coursework in descriptive, practical, and theoretical inorganic chemistry including the following: Group theory, physical methods for inorganic chemists, physical organic chemistry, organometallic chemistry, bioinorganic chemistry, and main group chemistry.
- Completed research in the areas of early metal and actinide activation of small molecules. Experienced in the handling of air- and moisture-sensitive and radioactive compounds by Schlenk and glovebox techniques. Experienced in various nuclear magnetic resonance techniques for the observation of various nuclei and of both diamagnetic and paramagnetic species. Experienced in the use of Amsterdam Density Functional Theory (2002), including geometry optimization, single point, and NMR shift calculations. Competent at the use of Linux-based file generation and the use of Molden and Molekel orbital visualization programs. Tentative thesis title: "The activation of white phosphorus using *tris*-amide complexes of molybdenum and uranium."
- Worked as a teaching assistant for a senior-level undergraduate laboratory course. Revised and updated laboratory teaching manual for content and clarity. Implemented a new protocol for the synthesis of $\text{MoCl}_3(\text{THF})_3$. Trained new teaching assistants in both synthetic and teaching methods.
- Worked as a teaching assistant for an introductory inorganic chemistry course where recitations were provided for approximately 30 students on the following topics: Organometallic chemistry, ligand field theory, symmetry and introductory group theory, and various current topics. Worked as a grader and informal teaching assistant for a main group chemistry course.

Publications

- Stephens, F. H.; Figueroa, J. S.; Cummins, C. C.; Kryatova, O. P.; Kryatov, S. V.; Rybak-Akimova, E. V.; McDonough, J. E.; Hoff, C. D. "Investigating the reversible β -hydrogen elimination process in molybdaziridine-hydride: Reactions of $\text{Mo}(\text{H})(\eta^5\text{-Me}_2\text{C}=\text{NAr})(\text{N}[i\text{-Pr}]\text{Ar})_3$ and $\text{Mo}(\text{N}[t\text{-Bu}]\text{Ar})_3$ with isocyanides," *Organometallics* **2004**, ASAP.
- Stephens, F. H.; Figueroa, J. S.; Diaconescu, P. L.; Cummins, C. C. "Molybdenum-phosphorus triple bond stabilization by ancillary alkoxides ligation: Synthesis and structure of a terminal phosphide *tris*-1-methylcyclohexanoxide complex," *J. Am. Chem. Soc.* **2003**, *125*, 9264.
- Blackwell, J. M.; Figueroa, J. S.; Stephens, F. H.; Cummins, C. C. "Eneidyne via sequential acetylide

reductive coupling and alkyne metathesis: Easy access to well-defined molybdenum initiators for alkyne metathesis,” *Organometallics* **2003**, *22*, 3351.

- Tsai, Y.-C.; Stephens, F. H.; Meyer, K.; Mendiratta, A.; Gheorghiu, M. D.; Cummins, C. C. “Reactions of organic nitriles with a three-coordinate molybdenum(III) complex and with a related molybdaziridine-hydride,” *Organometallics* **2003**, *22*, 2902.
- Cherry, J.-P. F.; Stephens, F. H.; Johnson, M. J. A.; Diaconescu, P. L.; Cummins, C. C. “Terminal phosphide and dinitrogen molybdenum compounds obtained from pnictide-bridged precursors,” *Inorg. Chem.* **2001**, *40*, 6860. This article was featured on the journal’s cover.

Conferences

- Stephens, F. H.; Figueroa, J. S.; Cummins, C. C.; Kryatova, O. P.; Kryatov, S. V.; Rybak-Akimova, E. V.; McDonough, J. E.; Hoff, C. D. “Investigating the reversible β -hydrogen elimination process in molybdaziridine-hydride: Reactions of $\text{Mo}(\text{H})(\eta^2\text{-Me}_2\text{C}=\text{NAr})(\text{N}[i\text{-Pr}]\text{Ar})_3$ and $\text{Mo}(\text{N}[t\text{-Bu}]\text{Ar})_3$ with isocyanides,” *Gordon Research Conference (Organometallics)*, **2003**.
- Stephens, F. H.; Diaconescu, P. L.; Cummins, C. C. “Synthesis of new terminal phosphides of molybdenum,” *224th American Chemical Society Meeting*, **2002**, 601-INOR.
- Stephens, F. H.; Diaconescu, P. L.; Cummins, C. C. “Trialkoxy molybdenum(VI) phosphido complexes,” *221st American Chemical Society Meeting*, **2001**, 33-INOR. The Massachusetts Institute of Technology Graduate Student Council Travel Fund provided a travel grant.
- Stephens, F. H.; Arnold, P. L.; Diaconescu, P. L.; Cummins, C. C. “Novel uranium-phosphorus chemistry,” *220th American Chemical Society Meeting*, **2000**, 18-INOR.

Relevant professional skills

Student leadership. Served for one year as the MIT Department of Chemistry representative to the Graduate Student Council. Served for four years as a committee member and treasurer for the Chemistry Graduate Student Committee (CGSC). As a CGSC member, responsibilities included organizing social events for the department, being a liaison between students and faculty in matters of education, teaching, and research, and planning prospective student weekends.

Education development. Trained new Chemistry Department teaching assistants in undergraduate education methods. Served as the graduate student liaison for the MIT Teaching and Learning Lab, an organization that fosters good teaching skills and methods in teaching assistants and faculty.

Professional affiliations

- Member of the American Chemical Society, Inorganic Division